1969

Study Of Heat Flow In The Lower Troposphere By Laboratory Simulation

Fouad Kwam Fanaki

CANADA

NATIONAL LIBRARY OF CANADA

CANADIAN THESES

ON MICROFILM

BIBLIOTHÈQUE NATIONALE DU CANADA

THÈSES CANADIENNES

SUR MICROFILM

NL-101(1/66)

STUDY OF HEAT FLOW IN THE LOWER TROPOSPHERE BY LABORATORY SIMULATION

by

Fouad H. Fanaki

Department of Physics

Submitted in partial fulfillment

of the requirements for the degree of

Doctor of Philosophy

Faculty of Graduate Studies

The University of Western Ontario

London, Canada.

November 1967

ABSTRACT

A laboratory simulation of the troposphere has been constructed in which details of heat flow above the ground in the lowest kilometer may be observed. The scaling criteria, which are derived from the governing equations with a number of approximations, are based upon invariance of the Froude number, Reynolds number, Peclet number, and Grashof number. In this study the troposphere is assumed dry and under adiabatic or isothermal conditons with a residual heat flux from below. Mechanical turbulence is considered a second order perturbation in free and natural convection, and radiative flux divergence is assumed important only in the lowest few meters of the atmosphere. The simulation has scaling factors of 10^4 for length, 200 for velocity and 0.2 for temperature; water is the simulating fluid. The laboratory simulation is a closed circuit water-tunnel in which general horizontal flow is introduced to represent the wind. A set of electrically heated aluminum plates simulates the ground as heated by insolation. The isothermal region above them simulates an isothermal or adiabatic troposphere. Fine structure of the temperature distribution is measured by moving arrays of calibrated thermistors; velocity profiles are indicated by streak photography of illuminated aluminum particles in suspension; and the fluid isotherms are observed by shadowgraph photography. All observations are confined to conditions in natural and free convection.

The validity of the simulation is examined by comparing the temperature and velocity profiles within the prototype and the simulation, for similar boundary conditions. This includes the relationship between vertical temperature gradient and standard deviation of temperature, the profiles of temperature fluctuation along a horizontal line, the isotherm contours in horizontal planes, and the dependence of wind shear upon the Richardson number. All show that the simulation is a good representation of the lower troposphere at heights between 50 and 1000 meters.

This laboratory simulation has provided information on the process of heat transfer in the lower troposphere. It is found that the vertical transfer of warm air is along cylindrical columns, which take on different forms in natural and in free convection. In the former, they carry heat aloft into caps which rise at some 0.6 meter per second, or which may merge with neighboring columns to continue upwards to heights of several hundred meters. If an elevated temperature-inversion layer is present, these convective columns perturb it into horizontally travelling waves. But in free convection, the columns are inclined downwind, with their upper extremities extending almost horizontally; the cap is absent but the wave-like tail may be separated and move across the fluid independently of its parent. It is assumed that these convective columns are present in addition to mechanical turbulence, which is a commonly observed feature of the lower troposphere. The dynamics of these columns may be examined through the theory of smoke plumes emitted by stacks.

ACKNOWLEDGEMENTS

The author wishes to thank Dr. P.A. Forsyth, former Head of the Physics Department, and Dr. P.A. Fraser, Acting Head of the Physics Department, for the use of the facilities of the Department of Physics.

He is greatly indebted to the members of his Advisory Committee and in particular to Dr. D.R. Hay for his supervision, advice and assistance throughout the work of the thesis. His thanks are due to the Tropospheric Physics Group and in particular to Dr. K. Naito and Dr. H.C. Martin for friendly advice.

Particular thanks are extended to Dr. J.F. Hart for the use of the facilities of the University of Western Ontario Computing Centre.

The author wishes to express his gratitude to the government of the United Arab Republic for the scholarship held by him during the period from 1962 to 1965, to the Defence Research Board of Canada and to the United States Air Force for their financial support.

He is grateful for the help given in technical matters by Mr. J. Radema, Mr. K. Jeffries and Mr. W. Wood.

The author wishes to express his thanks to Mrs. A. Armstrong for her great care and attention to detail in typing this thesis.

This investigation was supported by a grant from the Defence Research Board of Canada, for which the author wishes to express his gratitude.

TABLE OF CONTENTS

LIST OF ILLUSTRATIONS

LIST OF TABLES

CHAPTER I

INTRODUCTION

During the past twenty years there has been a growing interest in the interaction between short radio waves and the troposphere*. Air refractivity provides the essential link between these and, within the troposphere, the radio refractive index is governed by temperature, pressure and humidity. The complex motions of the air carry heat and water vapour between the ground and the air above it, by processes which, as yet are poorly understood. Thus, although many experiments have demonstrated that the clear air in the lower troposphere is capable of reflecting, refracting and scattering radio waves, the physical nature of these refracting inhomogeneities is obscure.

Small-scale fluctuations of temperature are of interest to both the radio physicist and the micrometeorologist. The elementary theory of refraction indicates that radio waves are reflected or scattered predominantly by inhomogeneities with dimensions of the order of the radio wavelength. In the present context, short radio waves have wavelengths of less than one meter; hence, we are concerned here with temperature and humidity fluctuations over distances less than a few

---

* The troposphere is that part of the earth's atmosphere which extends from the ground upwards to some 12 kilometers.

meters.

Information on the small-scale changes of refractivity in the troposphere is available through several experimental techniques. One is the radio refractometer, whose rapid response and high spatial resolution make it especially suited for direct probing of the atmosphere. However, in practice the examination is limited to a very small volume. An alternative involves the study of radar angels*, in which a relatively large volume of the atmosphere is observed continuously with a sensitive radar. As an example, the interpretation of radar echoes has suggested that the reflecting inhomogeneities in air refractivity are horizontal laminas only a few centimeters in vertical depth but extending several meters in the horizontal (Hay and Reid 1962; Bell, Hay and Johnston 1964). The refractivity in these laminas may differ by only a few parts per million from that of the environment, and hence, they may be produced by adiabatic transfer and erosion of air parcels at the boundary of a convective cell. The reflecting strata are persistent and most commonly observed when the underlying ground is very damp. Furthermore, periodicity in the incidence of these reflecting centres suggests a possible association with internal gravity waves. The writer also has established a laboratory technique for measuring the reflection coefficient of a dielectric lamina with arbitrary curvature and refractivity profile (Fanaki 1962; Hay and Fanaki 1963).

The lack of information on the air motion and heat and

---

* A radar angel is an anomalous radar echo from clear air presumably due to radio reflection at an irregularity in the air refractivity (Plank 1956).

humidity profiles, which accompany the refractivity centres in the air, has hampered the interpretation of radar angels. Indeed, the interpretation has remained controversial for over twenty years.

One approach to clarifying this problem is to study the physical processes by which heat is transferred between the ground and the atmosphere above it. Again, direct probing with anemometers and thermometers may be helpful to this end, but the significance of such measurements requires further study. Chapter II presents a review of the present concepts of heat transfer in the lower troposphere; it will be noted that supporting evidence and details of the models are generally lacking. An alternative is to begin with a study of the models, preferably in a controlled environment. It is this technique which the writer has followed, in the present investigation.

A laboratory simulation* of the lower troposphere has been devised through the appropriate scaling criteria. Here, the region of interest extends from a few meters above the ground upwards to one kilometer. No attempt has been made to include humidity in the simulation, and hence, the observations apply to a dry troposphere. Many studies of the atmosphere using laboratory simulation have been reported previously; a summary of these is given in Chapter IV. It will be seen that all are incomplete in various details and especially, in providing for horizontal flow (wind).

Chapter III presents the general requirements for laboratory

---

* This designation is used in place of the more common "laboratory model" to avoid confusion with physical "models" of heat transfer.

scaling of the atmosphere. The conditions for the present laboratory simulation and the mechanical and electrical details of this method are given in Chapter V. The techniques of experimental observation employed in this study are described in Chapter VI. An extensive series of observations with this simulation has been made with controlled boundary conditions; these are given in Chapter VII. The validity of this laboratory simulation is examined in Chapter VIII by referring to experimental studies of the full-scale troposphere. An extension of the present concepts (or models) of heat transfer in the troposphere, through interpretation of the laboratory measurements, is described in Chapter IX. This concluding Chapter also provides comments on the interpretation and capabilities of this laboratory simulation for further study.

CHAPTER II

PRESENT CONCEPTS OF HEAT TRANSFER IN THE LOWER TROPOSPHERE

Solar radiation reaching the earth's surface is the primary source of tropospheric heat. Only about 1% is contributed by other sources and this will be neglected in the following discussion (see, e.g. Haltiner and Martin, 1957 p. 87).

For purposes of heat transfer, the sun appears as a black body radiator with temperature 6,000°K. Its radiant energy is confined chiefly to wavelengths between 0.15 and 4.0 microns (short wave radiation), with maximum energy at 0.5 micron. Absorption by ozone in the earth's atmosphere at levels between 20 to 50 kilometers prevents wavelengths of less than 0.29 micron from reaching the earth's surface (Brunt 1934, p. 149 and Munn 1966, p. 10). In clear skies most of the remaining energy passes to the earth's surface while being subjected to relatively weak absorption by carbon dioxide and water vapour in the air.

The earth absorbs and reflects this incident energy also as a black-body. In this case the effective black-body temperature of the earth is 300°K on the average, with the wavelengths of reradiated energy confined essentially to the range 4 to 80 microns (long wave

radiation). The maximum energy is at a wavelength of 10 microns. Local changes in the surface temperature of the earth will be governed by the diurnal cycle, topography, cloud cover and season.

The transfer of heat during the day through the air from the earth's surface occurs generally by four distinct processes. These are radiation, conduction, convection and advection. Radiation describes the transfer of heat energy by electromagnetic waves; no intervening medium is required. Conduction implies the transfer of heat through the elastic impact of air molecules; no net transfer of the air molecules is necessary. On the other hand, convection and advection describe the transfer of heat by the net translation of aggregates of air molecules. If the motion is predominantly along the vertical the transfer is by convection; if it is predominantly along the horizontal, the transfer is by advection. Advection and convection usually are closely related in the atmosphere. All of these processes of heat transfer may occur simultaneously in the troposphere to varying degrees.

Two indicators of the process of heat transfer are the air temperature and the air motion. Little is known about the relevant details of air temperature but some general statements may be made on the forces governing the air motion. In general, the horizontal air flow over the earth's surface is subject to pressure gradient force, Coriolis force*, and the force of friction at the surface (see e.g.

---

* A particle moving in a rotating frame of reference is subject to a Coriolis force per unit mass equal to $-2\,\vec{\Omega} \times \vec{V}$. Here $\vec{\Omega}$ is the angular velocity of the rotating frame and $\vec{V}$ is the velocity of the particle relative to the rotating frame of reference.

Haltiner and Martin 1957, p. 158). The relative importance of these forces, and consequently the pattern of air motion, varies with height above the surface. At heights above 1000 meters the frictional force is negligible, and steady motion is the resultant of pressure gradient forces and Coriolis forces. Below this region, the frictional force becomes increasingly prominent with the approach to the surface. The transition height between these two regions varies widely. Many models have been proposed to describe the mechanism of heat transfer in the lower division of the troposphere. The essential details of these models are reviewed in the remainder of this Chapter.

2.1 Transfer by Radiation

The primary components in this process are short-wave radiation from the sun and long-wave radiation from the earth. The former is absorbed weakly by atmospheric water vapor and carbon dioxide, to the extent that it causes a change in air temperature ranging from 0.1°C to 0.7°C on the average per day (Fritz 1951 and Martin 1957, p. 102), depending upon the amount of water vapor present.

The long-wave radiation is absorbed more strongly by carbon dioxide and water vapor in the air. While it is expected that these longer wavelengths may contribute substantially to the heating of the air, yet experimental measurements on the relative effects of these two types of radiation are scarce because of limitations in the measuring techniques and the theory of radiation absorption (Moller 1951, Sutton 1953, p. 167 and Munn 1966, p. 17). Robinson (1950) has estimated local heat transfer by long-wave radiation* is comparable

---

* The term "radiative flux divergence" is used in meteorology texts to indicate local heating by the absorption of radiation.

to that by the other modes of transfer in the day-time only in the lowest one or two meters above the ground. Experimental observations by Funk (1960) have indicated that, at night, the effect of long-wave radiation is important to heights well above that.

2.2 Transfer by Conduction

Heat transfer by conduction is the predominant mode in the air layer within a few millimeters of the earth's surface. Convection and advection are suppressed in this layer because of the proximity of the boundary (Geiger 1959, p. 51). A large height-change (lapse rate) of temperature which may reach a value of hundred of times larger than the dry adiabatic lapse rate (e.g. 5°C per meter (Geiger 1959, p. 83) is observed generally in this region.

In the atmosphere, the height interval through which conduction is important remains uncertain. Sutton (1953, p. 124) suggests that this interval is less than 1 centimeter, but observations on temperature fluctuations presented by Geiger (1959, p. 53) indicate that it should be no greater than 1 millimeter.

Some insight into the physical nature of the conduction layer may be derived from laboratory experiments. Observations on the air above a heated plate were made by Rayleigh (1882), Aitken (1884), Lodge and Clarke (1884), Malurkar and Ramadas (1931), Ramadas and Malurkar (1932) and Ramadas (1953). These indicated a "dust-free" layer just above the heated boundary. The upper surface of this thin layer (less than 1 millimeter in depth) is undulating; as the temperature of the plate increases, a thin, shimmering layer forms directly above the "dust-free" layer in which tongue-like columns rise and descend

alternately (Fig. 2.1). These phenomena are similar to those observed

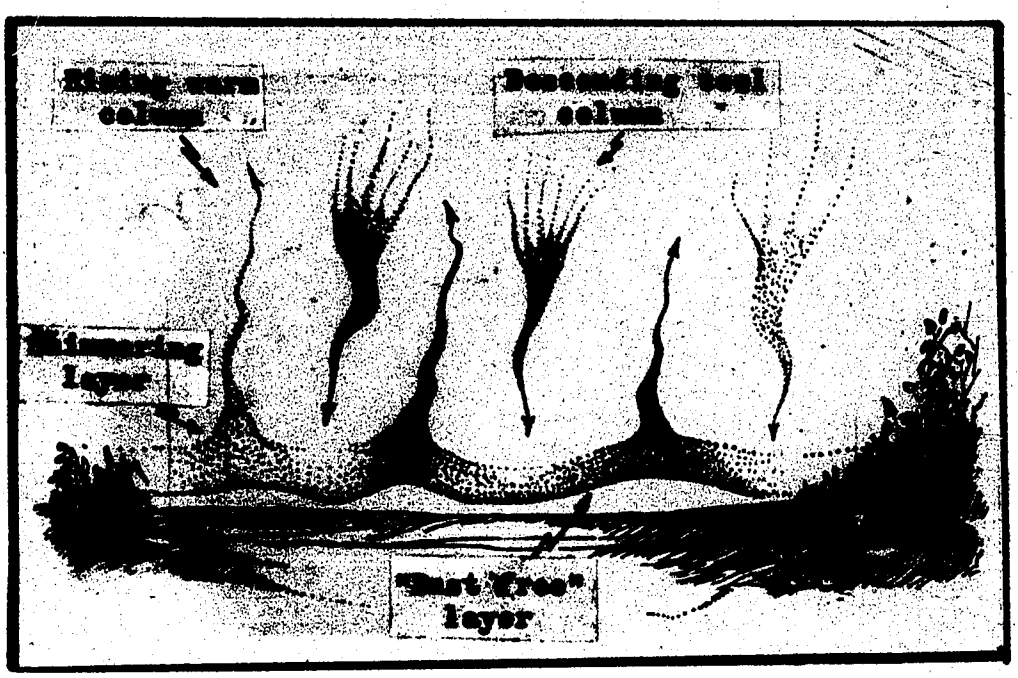

Figure 2.1 Details of Fluid Motion Above Heated Ground.

by Geiger (1959, p. 53) above hot barren soild during the summer. This type of air instability accompanies the high lapse-rate of temperature at the ground, but the relationship between the laboratory studies and Geiger's field observations requires further clarification.

2.3 Transfer by Convection

The earth's surface supplies heat to the thin air layer adjacent to it so rapidly that a third mechanism of heat transfer becomes important. If conduction was the only process of transfer, the maximum air temperature a few meters above the ground would occur in late evening of each day and the highest seasonal temperature would not be reached until the beginning of winter (Geiger 1959, p. 36).

Furthermore, it should be noted that the super adiabatic lapse rates of temperature described in the previous section result in strong instability of the air in this thin layer. Taylor (1915), through his studies of heat transfer in the first thousand meters above a water surface, suggested that convection is the predominant mechanism at levels more than a few meters above the surface; heat transfer by convection was several orders of magnitude greater than that by conduction.

Convection is divided, for convenience, into three categories which depend on the magnitude of the wind. Forced convection occurs when a strong wind blows across a rough surface; the resulting turbulence provides an agent for transferring heat upwards. Free convection is present when the wind speed is low and buoyancy forces predominate. In the absence of wind, buoyancy forces alone are present and the regime of natural convection occurs. Some authors question the existence of natural convection near the ground (see e.g. Priestley, 1960 and Townsend, 1962).

The present concepts or models of convection are based upon simple experiments in the laboratory and isolated observations in the field. Description of the convection patterns through the solution of the governing equations is impractical at the present time, because knowledge of the forces involved is incomplete. It is clear that many details of the models are lacking, including their dependence upon the convective regime, and that experimental studies in the field are desirable. In the following sections, a review is presented on the geometrical patterns of convection as proposed by authors elsewhere;

for simplicity, these patterns are subdivided into cellular models and parcel models.

2.3.1 Cellular Models

The concept of cellular patterns in atmospheric convection originated from experiments by Bénard in 1900. If a shallow layer of fluid is bounded above and below by two conductors at different temperatures, convective patterns will first appear in the form of hexagonal cells with fluid ascending at the center and descending at the edges of each cell (Fig. 2.2 a). Rayleigh (1916) termed these

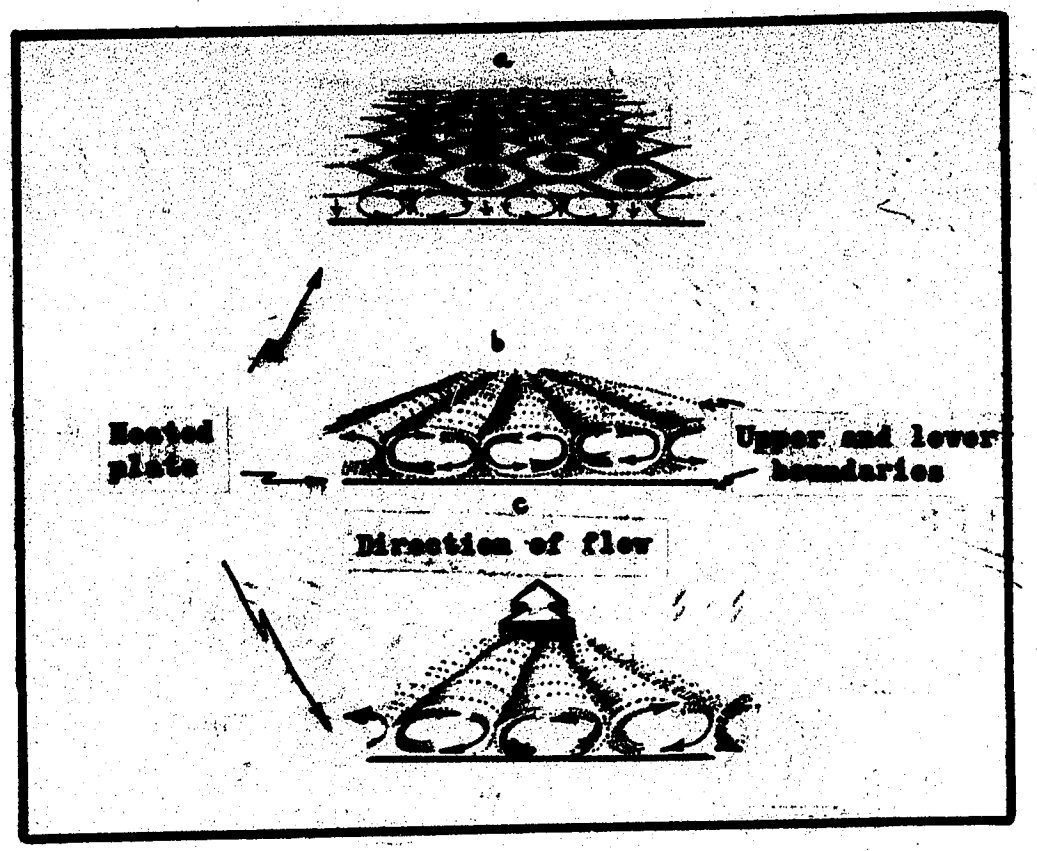

Figure 2.2 Convective Motion of a Fluid Heated from Below.

for simplicity, these patterns are subdivided into cellular models and parcel models.

2.3.1 Cellular Models

The concept of cellular patterns in atmospheric convection originated from experiments by Bénard in 1900. If a shallow layer of fluid is bounded above and below by two conductors at different temperatures, convective patterns will first appear in the form of hexagonal cells with fluid ascending at the center and descending at the edges of each cell (Fig. 2.2 a). Rayleigh (1916) termed these

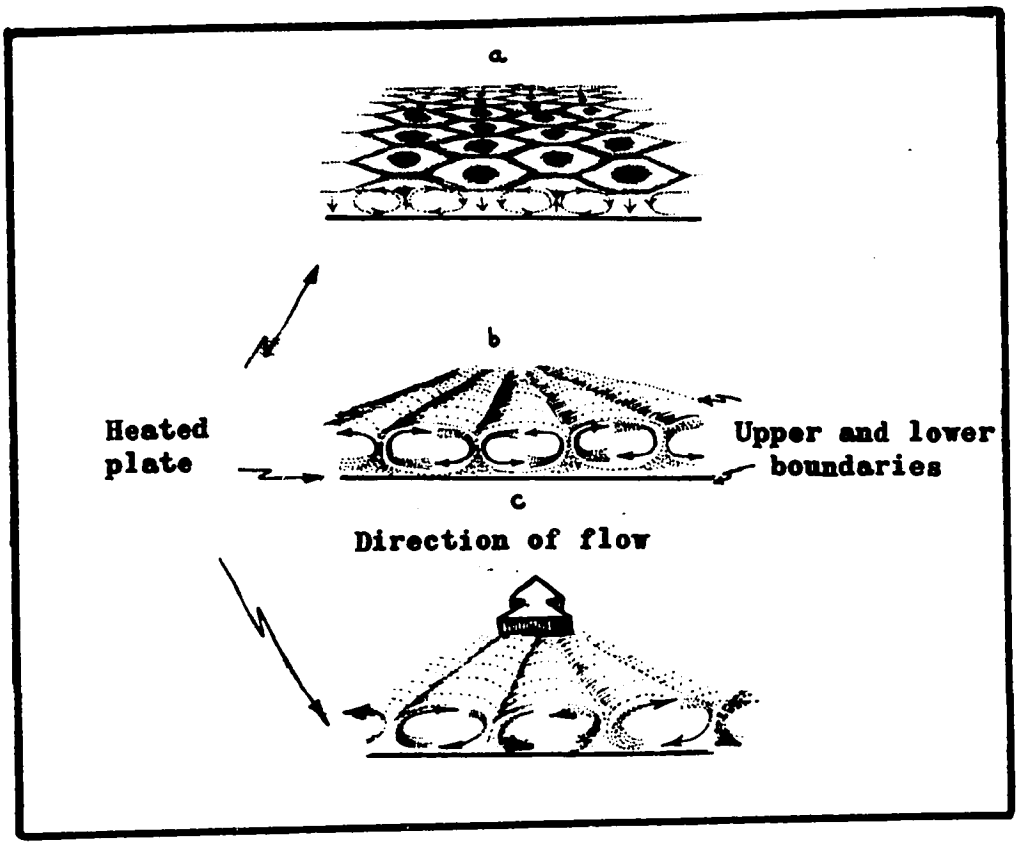

Figure 2.2 Convective Motion of a Fluid Heated from Below.

Bénard cells. With a further increase in the temperature difference between the fluid boundaries, the convective cells changed into convective columns as in Figure 2.2 b. If the fluid moved laterally between the boundaries, all columnar cells would rotate in the same sense as in Figure 2.2 c. Rayleigh (1916) extended the Benard concepts by examining the flow equation for conditions of convective instability. He found that the onset of thermal convection is governed by the temperature gradient (β) and depth of the fluid (h) through the non-dimensional Rayleigh number,

$$Ra = \frac{g \alpha \beta h^4}{\kappa \nu} \qquad 2.1$$

where g is the gravitational acceleration

α is the coefficient of thermal expansion

κ is the thermal diffusivity

ν is the kinematic viscosity.

When Ra exceeds a critical value, buoyancy forces prevail over viscous forces and heat is transferred by convection rather than by conduction. Several values of the critical Rayleigh number have been suggested by various authors as based upon theoretical studies (e.g. Rayleigh 1916, Jeffreys 1926 and 1928, Low 1929 and Pellow and Southwell 1940); these range from 657 to 1708 for different boundary conditions in the fluid.

In this classical theory, Stommel (1947) has shown that the ratio of the cell diameter to the cell height is independent of the physical properties of the fluid. The ratio is 3 for boundary conditions similar to that of the troposphere, i.e. a fluid bounded by a horizontal rigid surface at the bottom and by a free surface at

the top.

Several authors have suggested that the convective cells of Bénard and Rayleigh are found on a larger scale in the troposphere. According to Walker (1931 and 1932), Brunt (1951), Sutton (1953, p. 58) and Ludlam and Scorer (1953), the growth, movement and decay of cumulus clouds are subject to circulation in the hexagonal and columnar cells described above (see Fig. 2.3). Photographs of the

Figure 2.3 Roll and Vertical Motion within Cumulus Clouds.

tops of cloud layers by the meteorological satellite (Tiros I) showed regular cellular patterns (Krueger and Fritz 1961). Woodcock (1940) and Scorer (1954) have observed the flight patterns of soaring birds to suggest that convection occurs along vertical planes which extend

the top.

Several authors have suggested that the convective cells of Bénard and Rayleigh are found on a larger scale in the troposphere. According to Walker (1931 and 1932), Brunt (1951), Sutton (1953, p. 58) and Ludlam and Scorer (1953), the growth, movement and decay of cumulus clouds are subject to circulation in the hexagonal and columnar cells described above (see Fig. 2.3). Photographs of the

Figure 2.3 Roll and Vertical Motion within Cumulus Clouds.

tops of cloud layers by the meteorological satellite (Tiros I) showed regular cellular patterns (Krueger and Fritz 1961). Woodcock (1940) and Scorer (1954) have observed the flight patterns of soaring birds to suggest that convection occurs along vertical planes which extend

along the wind direction. By observing the deformation of horizontal and vertical smoke trails over a tropical ocean, Woodcock and Wyman (1947) concluded that the air circulation was similar to that of Bénard cells and that the ratio of height to diameter was similar to that observed by Bénard* in the laboratory. An example of single-cell convection has been suggested by Defant (1951), who examined the development of land and sea breezes; he considered the local wind and heat circulation to be in the form of a single rectangular cell and his analysis predicted a system of land and sea breezes that are in essential agreement with the observations.

It is clear that the models of fluid convection suggested by Bénard, Rayleigh and others have received very limited application to the convective patterns of the troposphere. Many difficulties arise in applying these classical concepts to the troposphere; Rayleigh's analysis requires a constant temperature gradient in the vertical, a condition generally not found in the lower troposphere (Sutton 1953, p. 124); the lower boundary which is uniformly heated in the classical theory is subject to non-uniformity of albedo** in

---

* It is believed now, that Bénard cells may be induced by either heating of the lower boundary or by surface tension (see e.g. Pearson, 1958 and Nield 1964).

** The surface albedo is the ratio of the intensity of the solar radiation reflected and scattered by the surface to the intensity of incident radiation (Munn 1966, p. 14).

practice; the question remains as to what are the upper and lower boundaries of the fluid, when Rayleigh's theory is applied to the troposphere. Priestley (1962) has noted that the dimensions of the cellular cloud patterns observed by the Tiros satellite are not predicted by the classical theory; he suggests that this discrepancy is related to Stommel's (1947) classical prediction that the geometry of Bénard cells is independent of the physical constants of the fluid. Further, the classical theory assumes laminar motion of the fluid, whereas the motion of the air in the troposphere is generally turbulent at levels below 200 meters (Hay and Naito 1965). It appears then that cellular convection as Bénard cells cannot exist in the atmosphere. However, Kuettner (1959) and Kuo (1961 and 1963) suggest that Bénard-like convection is possible, in which the initiation and maintenance are associated with wind shear.

2.3.2 Parcel Models*

An alternative model of convection in the troposphere involves the transfer of heat by isolated parcels of air. Here, the air parcel is somewhat like a large balloon (with a nebulous membrane), and the path followed by the ascending parcel from the ground into the troposphere is specified by the model. However, the return of air from aloft to replace the displaced parcel is assumed so diffuse and widespread, relative to the volume occupied by the ascending parcel, that the return path from aloft is usually not included in the model description.

---

* In the recent literature, the term "parcel model" is replaced by "fluid element".

Two types of air parcels have been suggested by various authors. One is a local volume of air which retains its identity as it rises and entrains its environment; this is called a closed parcel. The other is an open parcel, which may be described as the vertical flow of air (whether turbulent or laminar) within a column or envelope. These will be reviewed in separate sections below. It should be noted that both models may contain eddies which tend to move in an organized pattern.

2.3.2a Closed Parcels (Thermals)

The concept of closed parcels is based upon laboratory studies on bubbles of air rising through liquid, by Davis and Taylor (1950). The top of the bubble has a clearly defined curved surface, but the bottom of the bubble is relatively flat and merging into a turbulent wake. Scorer and Ronne (1956) showed that erosion of the bubble occurs only at its leading edge when the density of the water decreases upwards. If the water density is uniform, the diameter of the air bubble increases as it rises while entraining environmental fluid into the bubble. In a theoretical analysis, Scorer (1957) assumed that the bubble preserved its shape and showed that the radius of its leading edge (R) is related to its height above the source (z) by

$$z = 4.0\ R \qquad 2.2$$

The upward velocity (w) of the leading edge is related to R and to the average buoyancy force $\bar{B}$ of the bubble by

$$w = 1.2\ (g\bar{B}R)^{\frac{1}{2}} \qquad 2.3$$

where g is the gravitational acceleration.

Woodward (1959) examined the motion in and around a rising bubble by observing suspended particles in the water. She found that the bubble mixes with its environment, instead of eroding as had been suggested earlier. Mixing occurs over the leading edge and at the rear of the bubble. The core of the bubble rises faster than the periphery, so that the bubble resembles a spherical vortex as in Figure 2.4 a.

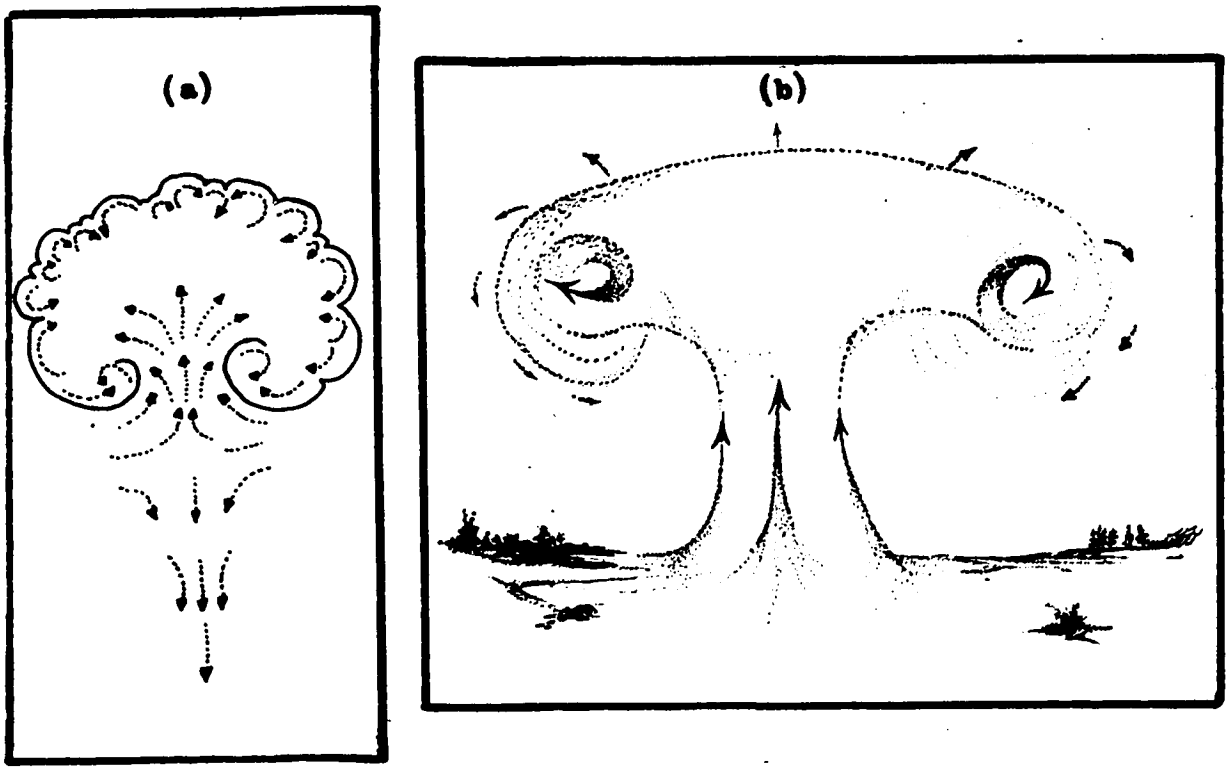

Figure 2.4 Thermals in Vortex Form Assumed by Bubble in a Fluid.

If the bubble source is continuous, the bubble resembles a column with a vortex ring at the top as in Figure 2.4 b. (Woodward 1960). In experiments similar to those of Woodward, Turner (1963a, 1963b and 1964) found that turbulent mixing occurred chiefly at the envelope of the thermal.

The above model of convection has been applied to the troposphere. Because of changes in topography and albedo of the earth's surface. local sources of heat will occur with definite boundaries. Woodward (1960) suggests that the air immediately above these warm areas will form into closed buoyant parcels to rise through the troposphere like bubbles in water (Fig. 2.5).

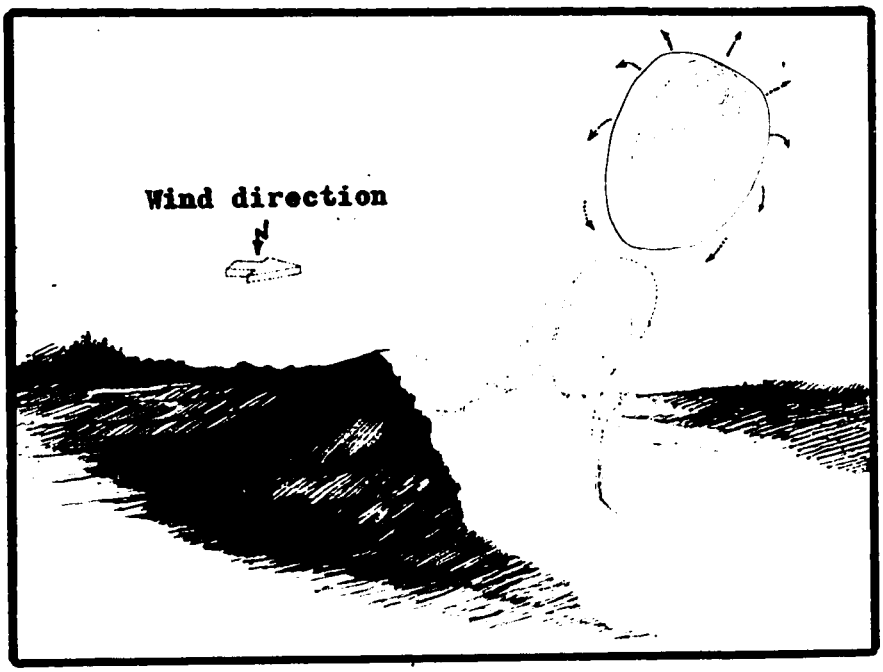

Figure 2.5 Rise of a Thermal Due to Local Heating of the Earth's Surface by the Sun, under the Effect of Light Wind.

Yates (1953), from his gliding observations, described the thermal as a rising bubble with a spherical leading edge, in which the bubble was a few degrees warmer than its environment (Fig. 2.6 a); the wind causes the bubble to ascend obliquely, as in Figure 2.6 b. Through studies of cloud patterns, Scorer and Ludlam (1953) suggested that the parcel shape was similar to that described by Yates but that

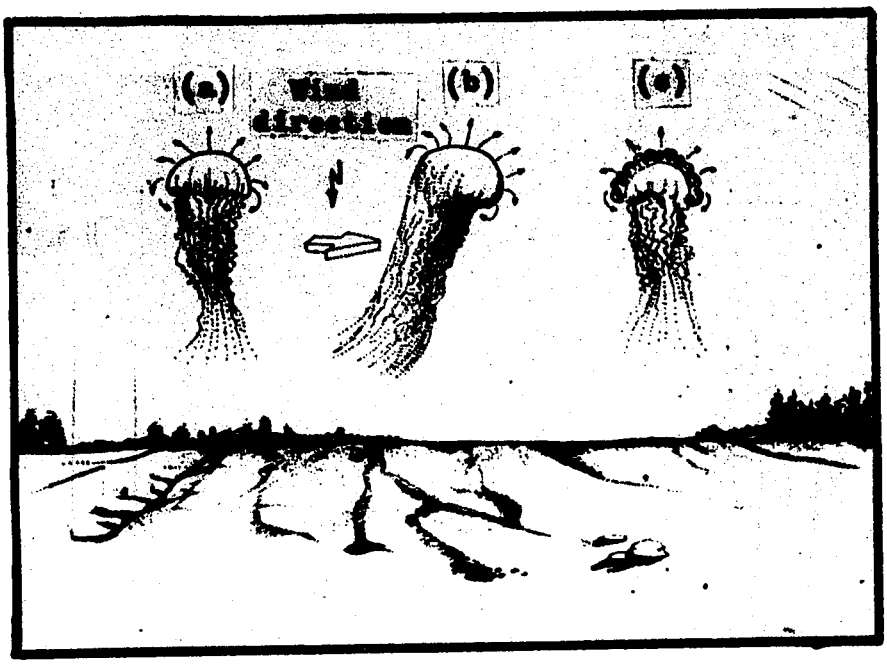

Figure 2.6 Rising Thermal in the Form of a Bubble with Spherical Leading Edge.

its bottom surface was very disturbed as in Figure 2.6 c. Malkus and Scorer (1954) suggested further, from examination of the erosion of cumulus clouds, that the rising parcel formed a trailing wake which moved slowly relative to the leading edge.

2.3.2b Open Parcels (Eddies and Plumes)

An alternative to the bubble theory of convection assumes that heat is transferred through open parcels or streaming filaments. This concept of convection is more complex than the former one, in that the filaments generally are in the form of turbulent eddies in the lower part of the troposphere and in the form of columns or plumes at higher levels. The theory and concepts of turbulence have been investigated for many years; Reynolds provided a substantial impetus in his treatment of water flow in pipes (Reynold 1883).

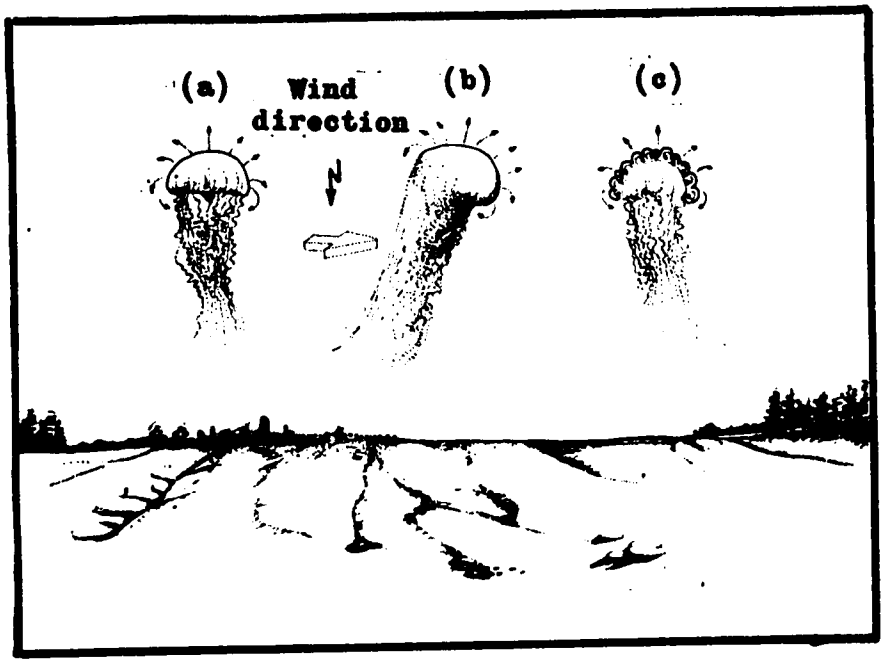

Figure 2.6 Rising Thermal in the Form of a Bubble with Spherical Leading Edge.

its bottom surface was very disturbed as in Figure 2.6 c. Malkus and Scorer (1954) suggested further, from examination of the erosion of cumulus clouds, that the rising parcel formed a trailing wake which moved slowly relative to the leading edge.

2.3.2b Open Parcels (Eddies and Plumes)

An alternative to the bubble theory of convection assumes that heat is transferred through open parcels or streaming filaments. This concept of convection is more complex than the former one, in that the filaments generally are in the form of turbulent eddies in the lower part of the troposphere and in the form of columns or plumes at higher levels. The theory and concepts of turbulence have been investigated for many years; Reynolds provided a substantial impetus in his treatment of water flow in pipes (Reynold 1883).

Recent theoretical studies of energy transfer by eddies have served to develop the eddy model. Their primary aim is to examine the relationship between the eddy fluxes of heat and momentum and the average properties of the air. The transfer by eddies is treated analogously to molecular transfer, with the exception that the molecular transfer coefficients are replaced by their turbulent counterparts which are of several orders of magnitude greater than the molecular coefficients. Since the vertical eddy flux generally is far greater than the horizontal flux (see, e.g. Swinbank, 1955), the latter normally is neglected. A review of the theoretical studies of turbulent heat flux is desirable at this point to obtain insight into the nature and behavior of these eddies.

Taylor (1915) was the first to analyze the relationship between the upward turbulent heat flux (H) and the average vertical potential temperature gradient $(\frac{\partial \bar{\theta}}{\partial z})$* for steady state condition. The suggested relationship is:

$$H = \rho c_p \kappa \frac{\partial \bar{\theta}}{\partial z} \qquad 2.4$$

where ρ is density of air, c_p is specific heat at constant pressure, κ is turbulent thermal diffusivity, θ is the potential temperature and z is vertical height.

It will be noted that the above relation is similar to the Fourier law of heat conduction . Usually κ is taken as a variable which may be negative or positive (see, e.g. Deissler, 1968) but some workers treat this coefficient as positive constant (see, e.g. Defant

---

* The overbar indicates the temporal average.

1951, Priestley 1953 and 1954, Kuo 1961 and Lilly 1964). However, much current research is directed towards a better understanding of how κ varies with height, stability and type of flow (see, e.g. Munn 1966, p. 84).

Taylor's analysis was modified later for a more general treatment of temperature gradient (see, e.g. Brunt 1929). Here, the equation of heat flux is written

$$H = -\rho c_p \kappa \left(\frac{\partial \bar{T}}{\partial z} + \beta\right) \qquad 2.5$$

where $\frac{\partial \bar{T}}{\partial z}$ is the mean temperature gradient in the vertical, and β is a constant. Formerly, it was believed that β was the adiabatic lapse-rate of temperature, $1^{\circ}C/100$ m., as in Eq. 2.4. But Budyko and Yudin in 1948 (see, e.g. Orlenko 1967) suggested that $\beta = 0.6^{\circ}C/100$ m. Yudin (1966), Orlenko (1967) and others have observed temperature gradient during vanishing heat flux, they indicated that these observations confirmed the inequality of β and the adiabatic lapse rate. The magnitude of β is still open to question.

An important extension to the theory of turbulence was presented by Kolmogorov (see, e.g. Munn 1966, p. 71). He suggested that the energy of larger turbulent eddies (diameter of the order of a few kilometers) is passed on to other eddies of successively smaller diameter in a cascade process, until it reaches the smallest possible eddies (diameter of the order of a few millimeters) where it is dissipated by viscosity into heating of the air. It has been suggested by Townsend (1956, p. 98) that large eddies which derive their energy from the mean shear flow in the unstable boundary layer, tend to predominate in strong winds and the eddy viscosity transfers the energy to smaller scales. This process

is important to heat transfer in the absence of natural convection, since it provides a means of vertical transfer through the surface boundary layer.

The relationship between the vertical gradient of temperature and the direction of heat transfer is open to further investigation. Bunker (1956), in observing the heat flow above a warm sea, found that the direction of flow was up the environmental temperature gradient at heights between 150 and 550 meters. Telford and Warner (1964) found a similar condition above the ground at heights between 150 and 1250 meters. In another study Webb (1958) noted that vertical heat transfer continued through a vanishing temperature gradient at a height of about 25 meters. It appears then that the theory of turbulent transfer by eddies alone (Eq. 2.5) fails to describe the actual flow of heat at heights more than a few tens of meters above ground in some environments.

The concept of the plume as a form of convection in the troposphere was incorporated into the eddy model. It originated with the study of smoke rising from fires and stacks and has received considerable attention in the diffusion of pollutants in the atmosphere (see, e.g. Priestley, McCormick and Pasquill 1958). At the present time, the "open parcel" model assumes that both turbulent eddies and convective plumes exist simultaneously in the troposphere with turbulence predominating at the lower levels and plumes at the higher levels.

Evidence of a transition from turbulent flow in the lower troposphere to quasi-laminar flow at higher levels has been provided by several authors. From observations on chimney smoke, Townsend

(1962) and Webb (1962 and 1964) have suggested that the motion was a composite of turbulent and laminar flow, with the amount of mechanical turbulence decreasing as height above the ground increases. A similar conclusion was reached through examination of rocket smoke trails (Lester and Tolefson 1964; Hay and Naito 1965), where it was noted that the transition from turbulent to laminar flow occurred at about 200 meters and that thin turbulent layers sometimes appeared in the laminar flow at a mean wind speed of some 5 m. sec^{-1}.

Townsend, Priestley and Webb have related the amount of turbulent and laminar flow with the amount of forced and free convection*. From field measurements, Priestley (1959, p. 39) and Webb (1958) found that the Richardson number (Ri)** was between -0.03 and -1 for composite convection, with more negative values in forced

---

* Several names have been given for this type of convection. Webb (1962 and 1964) calls it "composite convection" while the names "mixed convection" and "quasi-free convection" have been suggested by Townsend (1962) and Priestley (1962) respectively.

** If $\frac{\partial \bar{\theta}}{\partial z}$ and $\frac{\partial \bar{u}}{\partial z}$ are the vertical gradient of the mean potential temperature and the wind speed respectively, Ri is given as

$$Ri = \frac{g}{T} \frac{(\partial \bar{\theta} / \partial z)}{(\frac{\partial \bar{u}}{\partial z})^2} \qquad 2.6$$

Here, g is the gravitational acceleration and $\bar{\theta}$ is the mean potential temperature related to the actual temperature T at pressure P by the equation

$$\theta = T(\frac{1000}{P})^{\frac{\gamma-1}{\gamma}} \qquad 2.7$$

where γ is the ratio of specific heats.

convection and more positive values in free convection.

The open-parcel model of convective plumes has developed from analysis of smoke columns rising into the troposphere. Priestley (1953) introduced the plume as a column of turbulent air, in which heat mixes gradually with the environment until it is dissipated a plume may rise to a few hundred meters in the troposphere and it may exist in both forced and free convection. His analysis (see Priestley 1959, p. 73) indicated that the plume motion may have three modes: that due to absolute buoyancy, oscillatory motion and asymptotic motion. These are governed by the environmental temperature and the diameter of the plume, so that two plumes of different diameters may behave differently in the same environment. Later, Priestley (1954) related the upward heat flux to the temperature fluctuations of the plume, through the environmental lapse rate and diameter of the plume.

Priestley and Ball (1955) considered a plume of circularly symmetric form with a gaussian distribution of temperature and velocity in the horizontal (Fig. 2.7 a). Their analysis suggested that the

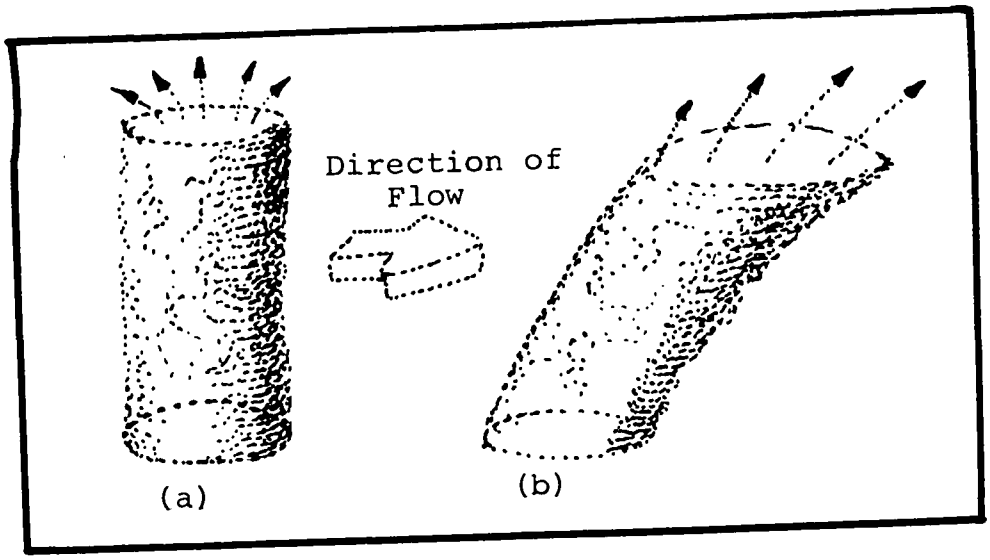

Figure 2.7 The Changing of a Rising Plume from Circular to an Oval Cross-Section under the Effect of Wind.

plume spreads its temperature excess radially outward from its core during ascent. Priestley (1956) extended this study to allow for wind effects; a light wind will incline the plume to the vertical and restrict its height (Fig. 2.7 b). The warm core of the plume rises faster than the cooler circumference, and consequently the former is displaced a shorter distance downwind than the circumference. As a result, the circular cross-section (Fig. 2.7 a) changes to an oval cross-section which is elongated downwind (Fig. 2.7 b). For strong winds, Ball (1958) observed that buoyant smoke plumes deteriorate into well-developed turbulence.

Only a few experiments have been reported in which the buoyant plume model of convection, described above, has been related to heat flow and temperature in the clear troposphere. Morton (1957) was the first to apply the buoyant plume concept to suggest that a small cloud will form at the top of a clear-air plume if the plume ceases to rise just below the freezing level. Priestley (1959, p. 66) has found that observed fluctuations of velocity and temperature within a few tens of meters of the ground are consistent with the plume concept. Observations by James (1954) and Vul'fson (1961), Telford (1966), and Warner and Telford (1967), favor a model in which the plume has a constant cross-section and a diameter between 200 and 300 meters. The horizontal distance between plumes is slightly greater than their diameter. On the other hand, Grant (1965) reported that the plume diameter changes during ascent, increasing with height up to 600 meters above ground and decreasing with further ascent. Martin's (1966) observations on temperature and humidity within 3 meters of the ground also were explained by the model of composite convection, with buoyant

plumes superimposed upon well-developed turbulence. The distribution of the isotherms and the characteristic fluctuations of temperature, as observed by Warner and Telford (1963) at heights up to a few hundred meters, give further support to this model of convection.

2.4 Statement of the Present Problem

The review in the preceding sections of this Chapter shows clearly that the present understanding of heat transfer in the lower troposphere is very immature. The daytime transfer by direct radiative flux divergence from the ground is probably important only in the lowest few meters, but field measurements to confirm this require improved instrumentation. The transfer by conduction apparently is even more limited, being confined to the lowest few millimeters; again, instrumentation difficulties have hampered studies of this physical process. Above the conducting layer, horizontal flow or advection near the ground sets up turbulence, which may predominate up to a height of some 200 meters. Generally, the flow at higher levels (at least up to 1 or 2 kilometers) is a mixture of laminar and turbulent flow where thin turbulent layers are embedded in the laminar flow.

The physical nature of convection associated with turbulent and laminar flow also is open to question. Simple laboratory experiments on fluids, not necessarily pertinent to the physical conditions in the troposphere, have suggested that convection is in the form of large cells or rising bubbles; a very limited amount of experimental evidence has been offered in support of each model. Further, the behaviour of smoke rising from a finite source has been used to suggest the plume model of convection for heat in clear air; again, the experimental support is very limited.

There is an obvious need for an experimental study of models of heat transfer in the lower troposphere, with adequate control over the boundary conditions. The present work is directed towards this end, through the use of laboratory simulation. For practical reasons, scaling of length by a factor of about 10,000 is necessary; thus observation of the details of heat transfer in the lowest few meters of the troposphere is not feasible in the simulation. Instead, attention is confined to patterns or models of convection in the troposphere between a few meters and 1 or 2 kilometers above ground, with control over advection and heating of the underlying surface. Water vapor in the air will affect the patterns of convection through its ability to absorb radiation and to store latent heat. For the present study, this factor will be neglected and the air in the troposphere will be assumed dry.

The aim of the present investigation is threefold: to examine the possibility of setting up a laboratory simulation of the lower troposphere, to ascertain the boundary conditions under which this simulation represents the lower troposphere, and to study the models of convection which are indicated by the simulation.

CHAPTER III

REQUIREMENTS FOR TROPOSPHERIC SIMULATION

This chapter reviews the governing equations which apply to the transfer of heat in the lower troposphere, with a view towards deriving the scaling criteria. The present interest is in daytime conditions when the profile of temperature in the vertical is adiabatic or isothermal, for heights extending from a few meters to one kilometer above the earth's surface. For simplicity in the first study, the air will be assumed dry. It was noted in the previous chapter that daytime heating of this part of the troposphere is essentially by convective flux divergence from the earth's surface. No attempt will be made here to examine the lowest few meters where heat transfer is also by radiative flux divergence and conduction; presumably, these additional factors will alter only the effective temperature of the underlying surface as it appears to the air at higher levels.

3.1 Governing Equations

The air of the dry troposphere is generally a non-ionized, compressible fluid of constant composition and varying density. This fluid is subject to the gravitational force of attraction, to pressure gradient forces related to internal pressure differences, to the Coriolis force because it moves in a rotating reference frame and to

frictional forces in the region of the solid underlying surface. For the range of pressures and temperatures normally found in the troposphere, the air behaves as a perfect gas (Haltiner and Martin 1957, p. 9).

The balance of these forces on a unit mass of the fluid is specified by the Navier-Stokes equation. (See, e.g. Sutton 1953, p. 14, Haltiner and Martin 1957, p. 158, Bird et al. 1960, p. 322 and Lumley and Panofsky 1964, p. 59).

$$\frac{D\vec{V}}{Dt} = -2\,\vec{\Omega} \times \vec{V} + \vec{g} - \frac{1}{\rho}\nabla p + \frac{1}{\rho}\,\vec{S} \qquad 3.1$$

where the term on the left represents the inertial force and the terms on the right represent, in order, the Coriolis force, the gravitational force, the force due to a pressure gradient, and the frictional force*. Here the frictional force depends on the coefficient of viscosity (μ) and on the spatial variation of the velocity ($\vec{V}$, relative to a point on the earth's surface) in the following manner

$$\vec{S} = \nabla \cdot (\mu \nabla \vec{V}) + \nabla \vec{V} \cdot \nabla \mu + \frac{1}{3}\mu \nabla (\nabla \cdot \vec{V}) - \frac{2}{3}(\nabla \cdot \vec{V})\nabla \mu \qquad 3.3$$

---

* The explanation of symbols in equations used in this thesis is given in Appendix I.

The total derivative, $\frac{D}{Dt}$, is a total time derivative as seen by an observer following the motion of the fluid. It is given by:

$$\frac{D}{Dt} = \frac{\partial}{\partial t} + \vec{V} \cdot \nabla \qquad 3.2$$

The components of $\overrightarrow{\overline{S}}$ represent normal and tangential stresses on the surfaces of a fluid element.

The conservation of mass in the fluid is represented by the equation of continuity,

$$\frac{1}{\rho}\frac{D\rho}{Dt} + \nabla.\vec{V} = 0 \qquad 3.4$$

The dependence of pressure and volume upon temperature in the fluid is given by the equation of state,

$$p = \rho RT \qquad 3.5$$

Finally, the principle of the conservation of energy is stated as

$$\frac{D}{Dt}(c_p T) = \frac{1}{\rho}\nabla.K\nabla T + \frac{1}{\rho}\frac{DP}{Dt} + \frac{\mu}{\rho}\Phi \qquad 3.6$$

The term on the left represents the rate of increase of heat per unit mass. The first term on the right indicates the rate of transfer of heat energy into the unit mass by conduction where K includes the molecular as well as the turbulent conduction (see, e.g. Haltiner and Martin 1957, p. 131). The second term represents the rate of transfer of heat energy by compression in a unit mass and the third term is the rate of increase of heat energy in unit mass that is due to viscous dissipation. Here, the dissipation function (Φ) in rectangular coordinates is

$$\Phi = 2\left[\left(\frac{\partial u}{\partial x}\right)^2 + \left(\frac{\partial u}{\partial y}\right)^2 + \left(\frac{\partial w}{\partial z}\right)^2\right]$$

$$+ \left(\frac{\partial v}{\partial x} + \frac{\partial u}{\partial y}\right)^2 + \left(\frac{\partial w}{\partial y} + \frac{\partial v}{\partial z}\right)^2 \left(\frac{\partial u}{\partial z} + \frac{\partial w}{\partial x}\right)^2$$

$$- \frac{2}{3}\left(\frac{\partial u}{\partial x} + \frac{\partial v}{\partial y} + \frac{\partial w}{\partial z}\right)^2 \qquad 3.7$$

It should be noted that Eq. 3.5 was used in the derivation of Eq. 3.6.

In Appendix II it is shown that the magnitude of the last term in Eq. 3.6 is negligible relative to the others, since heating of the air by friction is insignificant in comparison with heating by convection (see, e.g. Sutton 1953, p. 108, Lumley and Panofsky 1964, p. 61 and Munn 1966, p. 58).

A comment on the initial conditions should be introduced here. During the daytime, insolation of the ground creates a negative temperature gradient in the vertical within several tens of meters of the ground. This is associated with an upward heat flux from the ground into the air. But at night, lack of direct insolation of the ground results in a reversed of the vertical heat flux and consequently a positive temperature gradient in the vertical (see, e.g. Munn 1966, p. 45). The transition between these conditions occurs during the 20 minutes after sunrise or sunset. At this time, the vertical profile of temperature near the ground is approximately isothermal (see, e.g. Geiger 1959, p. 68). The environmental temperature T_o, in this case is given by

$$T_o = \text{constant} \qquad 3.8$$

Alternatively, the profile of air temperature near the

ground is approximately adiabatic, when the air is well mixed by strong winds and rough grounds. This condition occurs commonly in the daytime when the sky is overcast and advection is well developed. The air in this case is thermally neutral and the vertical gradient of temperature is (see, e.g. Eckart 1960, p. 12)

$$\frac{\partial \bar{T}_o}{\partial z} = -\frac{g \alpha \bar{T}_o}{c_p} \qquad 3.9$$

where α is the coefficient of thermal expansion ($\alpha \approx \frac{1}{\bar{T}_o}$ for air) and $\bar{T}_o$ is the parcel air temperature which differs infinitesimally from that of the environment.

3.2 Simplification of the Governing Equations

Terms describing the transfer of heat and momentum introduce non-linearity into the governing equations. This non-linearity leads to unnecessary complication in proceeding towards the conditions of simulation and consequently, a number of simplifying approximations will first be introduced. These approximations apply when the fluid is the lower atmosphere and when the volume of interest extends only a few kilometers in each direction.

3.2.1 Viscosity, Thermal Conductivity and Specific Heat

μ and K are independent of density and their variations with temperature are given by (see, e.g. Jeans, p. 285 and 291),

$$\mu = \mu_o \left(\frac{T}{273}\right)^{\frac{3}{2}} \left(\frac{273 + 113}{113 + T}\right) \qquad 3.10$$

where μ_o is the viscosity of air at 0°C, and

$$K = K_o \left(\frac{T}{273}\right)^{\frac{3}{2}} \left(\frac{273 + 113}{113 + T}\right) \qquad 3.11$$

where K_o is the thermal conductivity of the air at 0^oC. Temperature gradients as great as 1^oC per meter rarely are observed in dry air in the region of interest here. Then the maximum gradient to be expected in μ and K is 0.08%, relative to the respective viscosity $1.813\ 10^{-4}$ gm. cm^{-1} sec^{-1} and thermal conductivity $0.6\ 10^{-4}$ cal. cm^{-1} sec^{-1} $^oC^{-1}$.

Different models have been proposed to describe the dependence of μ and K upon the conditions of the environment and height above ground. The present state of knowledge, however, is such that no model can be used accurately and universally to describe the behaviour of the eddy coefficients (see, e.g. Munn 1966, p. 84). Following other workers (see Chapter II), the writer has chosen μ and K as constants for the present study, with the acknowledgement that it is a first approximation to be re-examined in future work.

By definition, the specific heat at constant pressure (c_p) represents the quantity of heat required to raise the air temperature by one degree, and consequently, it should not depend upon the type of heat transfer. Moreover, c_p may be considered to be independent of temperature for the range of temperature observed in the troposphere (Haltiner and Martin 1957, p. 13).

Appendix II examines the relative magnitudes of the various terms and factors in the governing equations, as they apply to the present problem. There, it will be noted that the above limitations

on μ and K permit the following simplifications, to a very good approximation:

Eq. (3.3) becomes:

$$\vec{S} = \mu \nabla \cdot \nabla \vec{V} + \frac{1}{3} \mu \nabla (\nabla \cdot \vec{V}) \qquad 3.12$$

and Eq. (3.6) reduces to

$$\frac{DT}{Dt} = \frac{K}{\rho c_p} \nabla^2 T + \frac{1}{\rho c_p} \frac{DP}{Dt} \qquad 3.13$$

3.2.2 Gravitational Force

The gravitational force is the resultant of two forces. One is the Newtonian attraction between the earth and the air mass which results in a force $\vec{g}_a$ per unit mass. The other is the centrifugal force $\Omega^2 \vec{R}$ which arises because the atmosphere is moving at about the same speed as the surface below it, around the earth's axis (see Fig. 3.1). It will be seen that the resultant gravitational force, $\vec{g}$, depends upon latitude (ϕ) and altitude (z); its magnitude is given by the empirical formula (Haltiner and Martin 1957, p. 47):

$$g = 9.806 \, (1 - 0.00259 \cos 2\phi)(1 - 3.14 \times 10^{-7} z) \qquad 3.14$$

where z is measured in meters.

Eq. (3.14) shows that the magnitude of g changes by less than 0.03% about its nominal value of 9.80 m. sec^{-2} throughout the region of present interest in the atmosphere* In Appendix II, the magnitudes of the terms in the Navier-Stokes equation (3.1) are compared for this application. There it is demonstrated that the

---

* This Figure applies to mid-latitudes at heights up to one kilometer.

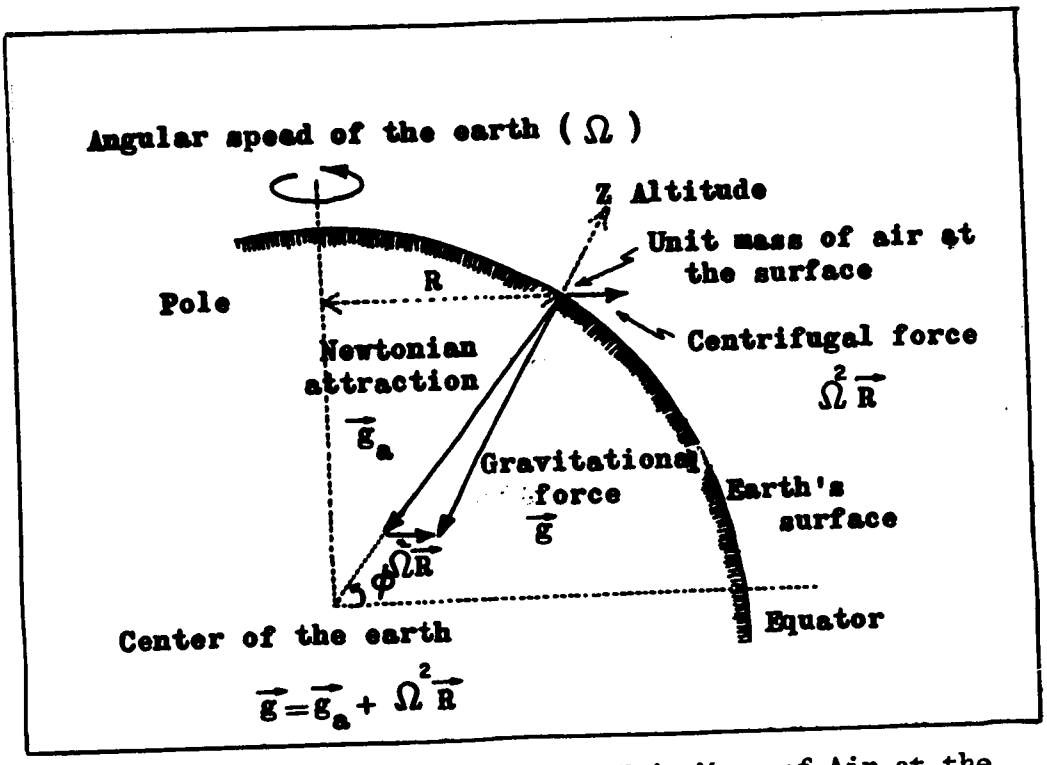

Figure 3.1 Gravitational Force Acting on Unit Mass of Air at the Earth's Surface.

gravitational, pressure gradient and frictional terms are the only important ones and that all are of the same order of magnitude. Then, the 0.03% change in $\vec{g}$, within the lower atmosphere, represents a higher order perturbation; this will be ignored and $\vec{g}$ will be assumed constant in the Navier-Stokes equation.

3.2.3 Coriolis Force

The Coriolis force is a fictitious force as seen by an observer in a moving reference frame. To the observer studying a limited region of the atmosphere from the ground, this force on a unit mass of air is normal to the air velocity and the angular velocity of the earth, as given by $-2\ \vec{\Omega} \times \vec{V}$ in the Navier-Stokes equation. Since $\vec{V}$ is the particle velocity relative to a point on the

earth's surface, its magnitude will rarely exceed 10 meters per second in the lower atmosphere. The accompanying Coriolis forces will be relatively small, and hence they will be neglected in the design of the present laboratory simulation (Appendix II). However, a detailed analysis in Appendix VII takes the Coriolis forces into account to show that their principal effect is a distortion of the observed convective structure into a partial spiral.

3.2.4 Compressibility of the Air

Local compression or expansion of a moving air parcel may be associated with local convergence or divergence of the air velocity. Since velocity divergence is included in the terms of the governing equations, it is of interest to enquire about the importance of this factor in the present problem.

A pressure perturbation dp is related to the density perturbation $d\rho$ of the air (as in a sound wave) by (see, e.g. Schlichting 1960, p. 8)

$$dp = c^2 d\rho \quad , \tag{3.15}$$

where c is the velocity of sound in the environment, as governed by the bulk modulus of elasticity and the density of the air.

Now typical pressure perturbations have magnitudes which are given by the hydrostatic equation

$$dp = - g \rho_o \, dz \quad , \tag{3.16}$$

where dz is an increment of height and ρ_o is the mean density at the region of interest. From these equations, we note that

$$d\rho = - \frac{g \rho_o}{c^2} \, dz \quad . \tag{3.17}$$

The substantial derivative of ρ is found by combining Eq. (3.17) and Eq. (3.2) to give

$$\frac{D\rho}{Dt} = - \frac{2g\rho_o}{c^2} w \qquad 3.18$$

where w is the air velocity along the direction of the density gradient (in this example). It will be noted that for w = 10 meter sec^{-1}, which is a very large value for the lower atmosphere, the right-hand side of Eq. (3.18) is of the order -10^{-6}. Thus, $\nabla.\vec{V}$ in Eq. 3.4 must be generally less than 10^{-3} (for $\rho = 10^{-3}$ gm. $cm.^{-3}$). As noted in Appendix II, this makes terms involving $\nabla.\vec{V}$ negligible in the governing equations and Eqs. (3.4) and (3.12) reduce to:

$$\nabla.\vec{V} = 0 \qquad 3.19$$

$$\vec{S} = \mu \nabla.\nabla\vec{V} \qquad 3.20$$

3.2.5 Method of Perturbation

The method of perturbation is introduced here according to Landau and Lifshitz (1959, p. 212) and Lumley and Panofsky (1964, p. 60). This technique permits further simplification of the governing equations, when the variables in these equations each have a large steady component and a relatively small fluctuating component.

Consider temperature (T), pressure (P) and density (ρ) of the atmosphere as found in the governing equations. Common observations in the lower troposphere show that short-term fluctuations in air temperature are of the order 1^o about the mean 300^oK, in air pressure are of the order 1 mb. about the mean of 1000 mb. and in density are of the order 10^{-6} about the mean 10^{-3} gm. cm^{-3}. Then temperature,

pressure and density can be represented by $T_o + T'$, $P_o + P'$ and $\rho_o + \rho'$ respectively, where the primed quantities are small perturbations about the steady components (represented by zero subscripts). In turn, the departure of the perturbed temperature from the initial (unperturbed) temperature, (T'), may be assumed to have an average component and a fluctuating component, in which the latter has a vanishing mean. In the following, the perturbations will be assumed sufficiently small that their products and squares are negligible.

We begin with the hydrostatic equation as it applies to the steady components of pressure and density:

$$-\frac{1}{\rho_o} \nabla P_o + \vec{g} = 0 \qquad 3.21$$

Next, we note that the volume of a unit mass of air (V) which is subjected to a temperature perturbation T' becomes

$$V = V_o (1 + \alpha T') = \frac{1}{\rho} \qquad 3.22$$

Here α is the thermal-expansion coefficient of air. If ρ is replaced by $\rho_o + \rho'$, and products of perturbation quantities are neglected, then to a good approximation

$$\rho' \approx -\rho_o \alpha T' \qquad 3.23$$

Then we expand $\frac{\nabla P}{\rho}$ by substituting $(P_o + P')$ and $(\rho_o + \rho')$ for P and ρ respectively, multiply numerator and denominator by $(\rho_o - \rho')$ and eliminate terms involving second-order perturbations to obtain

$$\frac{1}{\rho} \nabla P \approx \frac{\nabla P_o}{\rho_o} + \frac{\nabla P'}{\rho_o} - \frac{\rho'}{\rho_o^2} \nabla P_o \qquad 3.24$$

Substituting Eq. (3.21) and Eq. (3.23) into Eq. (3.24) yields

$$\frac{1}{\rho} \nabla P = \vec{g} + \frac{1}{\rho_o} \nabla P' + \alpha T' \vec{g} \qquad 3.25$$

Finally, combining Eq. (3.25) with the Navier-Stokes Eq. (3.1) gives

$$\frac{D\vec{V}}{Dt} = -\frac{1}{\rho_o}\nabla p' - \alpha T'\vec{g} + \nu \nabla \cdot \nabla \vec{V} \qquad 3.26$$

Here $\nu = \frac{\mu}{\rho_o}$, is the kinematic viscosity.

We next examine the conservation of energy (Eq. 3.13). Combining Eq. 3.13 and Eq. 3.21 while neglecting higher order perturbations gives

$$\frac{DT'}{Dt} = -\vec{V} \cdot \nabla T_o + \kappa \nabla^2 T' + \kappa \nabla^2 T_o + \frac{1}{c_p \rho_o}\frac{DP'}{Dt} - \frac{1}{c_p}\vec{V}.\vec{g} \qquad 3.27$$

Here, $\kappa = \frac{K}{\rho c_p}$ is the thermal diffusivity. It is shown in Appendix II that Eq. 3.27 reduces to

$$\frac{DT'}{Dt} = \kappa \nabla^2 T' \qquad 3.29$$

3.3 Principle of Similarity

The present interest is in defining the conditions under which a laboratory simulation will reproduce faithfully the models of heat flow which occur in the lower troposphere. Three types of simulation are possible in general: geometric, in which only the physical dimensions are scaled; kinematic, in which physical dimensions and velocities are scaled; and dynamic, in which the physical dimensions, velocities and forces are scaled. It is the latter which is required for the present study.

Birkhoff (1950), Fultz (1961) and others have reviewed the principles of similitude. Two approaches are available, depending upon the nature of the governing equations. If the governing equations

are linear, the variables in the prototype, $A_{i,p}$, (e.g. temperature, pressure in the atmosphere) are related to the corresponding variables in the simulation, $A_{i,s}$, by a set of transformations

$$A_{i,p} = \alpha_i A_{i,s}$$

where α_i is the appropriate scaling factor. These transformations are substituted systematically in the governing equations and the initial conditions. The requirement that the coefficients of corresponding terms in the governing equations and the initial conditions be numerically identical for the prototype and simulation leads to a set of equations in α_i which may be solved for the scaling factors. This method is used frequently in electromagnetic problems involving Maxwell's equations (see, e.g. Haller 1942; Sinclair et al 1947 and 1948; and Gjessing and Irgens 1964).

The second approach is useful when the governing equations are non-linear. This is the case in the present investigation. For this purpose, the governing equations together with the initial conditions are transformed into non-dimensional form by dividing each term with a suitable combination of variables. Hence, the coefficients of the terms in the transformed equations must be invariant in proceeding from the prototype to the simulation and these invariant coefficients provide the desired scaling factors. The remainder of this section will illustrate this approach by applying it to the reduced governing equations and initial conditions given in the previous section.

The first step towards normalizing the governing equations and the initial conditions is to select three variables which are readily measured or observed in the prototype and simulation. The choice of representative

length (L) representative velocity (U) and representative unit of temperature change (ΔT) is suitable; for the special case of natural convection, in which horizontal flow is absent, (U) is replaced by $(\frac{\kappa}{L})$.

In the next step, the variables in the governing equations are made non-dimensional (letters with an astrisk) through the use of these normalizing factors.

$$\nabla^* = L\nabla \quad , \quad \nabla^{*2} = L^2 \nabla^2 \quad , \quad \left(\frac{D}{Dt}\right)^* = \frac{L}{U}\frac{D}{Dt} \quad ,$$

$$T^* = \frac{T}{\Delta T} \quad , \quad \vec{V}^* = \frac{\vec{V}}{U} \quad , \quad p^* = \frac{p}{\rho_o U^2} \text{ and } t^* = \frac{tU}{L}$$

For the special case of natural convection, the last three normalizations are replaced by

$$\vec{V}^* = \frac{\vec{V}L}{\kappa} \quad , \quad p^* = \frac{pL^2}{\rho_o \kappa^2} \text{ and } t^* = \frac{tL^2}{\kappa}$$

Substitution of the above into the reduced governing equations yields:

$$\frac{D\vec{V}^*}{Dt^*} = -\nabla^* p^{*\prime} + \frac{\vec{g}\,\alpha\,\Delta TL}{U^2} T^{*\prime} + \frac{\nu}{UL} \nabla^* . \nabla^* \vec{V}^* \qquad 3.29$$

$$\nabla^* . \vec{V}^* = 0 \qquad 3.30$$

$$\frac{DT^{*\prime}}{Dt^*} = \frac{\kappa}{UL} \nabla^{*2} T^{*\prime} \qquad 3.31$$

and for natural convection:

$$\frac{D\vec{V}^*}{Dt^*} = -\nabla^* P'^* + \frac{\vec{g}\,\alpha\,\Delta T L^3}{\kappa^2} T'^* + \frac{\nu}{\kappa}\,\nabla^* \cdot \nabla^* \vec{V} \qquad 3.32$$

$$\nabla^* \cdot \vec{V}^* = 0 \qquad 3.33$$

$$\frac{DT'^*}{Dt^*} = \nabla^{*2}\, T'^* \qquad 3.34$$

We consider next the initial conditions. Substitution of the above representative quantities into Eq. 3.8, yields for an isothermal atmosphere:

$$T_o^* = \frac{T_o}{\Delta T} = \text{constant} \qquad 3.35$$

On the other hand, Eq. 3.9 is used to specify an adiabatic lapse rate of temperature. It will be useful in this case to obtain a scaling factor for temperature gradient. Consequently, the term

$$\left[\frac{\text{representative temperature}}{\text{representative length}}\right]$$

is replaced in this case by a representative temperature gradient $(\frac{\partial \bar{T}}{\partial z})_o$ for normalizing Eq. 3.9 (see, e.g. Batchelor, 1954). It will be noted that $(\frac{\partial \bar{T}}{\partial z})_o$ is constant in both the prototype and the simulation. Substitution of $(\frac{\partial \bar{T}}{\partial z})_o$ into Eq. 3.9 yields:

$$(\frac{\partial T_o}{\partial z}) = -\frac{g\,\alpha\,\Delta T}{c_p\,(\frac{\partial \bar{T}}{\partial z})_o}\, T^* \qquad 3.36$$

Finally, it is noted that dynamical similitude will be achieved if the following coefficients of the above equations are maintained invariant in transferring between the prototype and the simulation:

$$\frac{g\,\alpha\,\Delta TL}{U^2}\ ,\quad \frac{\nu}{UL}\ ,\quad \frac{\kappa}{UL}\ ,\quad \frac{g\,\alpha\,\Delta TL^3}{\kappa 2}\ \text{and}\ \frac{\nu}{\kappa}\ .$$

The first term is the reciprocal of the square of Froude number (Fr.). The second term is the reciprocal of Reynolds number (Re). $\frac{\kappa}{UL}$ is the reciprocal of Peclet number (Pe.). The last term is Prandtl number (Pr.). The fourth term can be written as

$$\frac{g\,\alpha\,\Delta TL^3}{\kappa^2} = \frac{g\,\alpha\,\Delta\,TL^3}{\nu^2}\ .\ \frac{\nu^2}{k^2} = Gr\ .\ Pr^2.$$

where Gr. is theGrashof number. No additional scaling parameter is introduced by the initial condition on the isothermal atmosphere (eq. 3.35). But the initial condition on the adiabatic atmosphere require, in addition to the above, that

$$-\frac{g\,\alpha\,\Delta T}{c_p\,(\frac{\partial \bar{T}}{\partial z})_o}$$

be invariant between the two systems.

CHAPTER IV

PRINCIPLES OF SIMULATION OF THE LOWER TROPOSPHERE AS APPLIED ELSEWHERE

It will be instructive at this stage to review the techniques of laboratory simulation used by other authors to study the lower troposphere. The aim of this review is twofold: to describe briefly the experimental methods of simulation with a view towards application to the present problem, and to note the limited extent to which the scaling criteria involving geometry, velocities and forces have been applied.

4.1 Approaches to Simulation

The requirement for large scaling factors of length, to represent a significant volume of the troposphere in a laboratory simulation, generally leads to difficulties in preserving the similarity parameters and in particular those connected with diffusion effects (e.g. the Reynolds number and the Peclet number). However, many simulation studies have led to detailed and useful comparisons of a qualitative type. An excellent summary of these methods and principles of simulation has been published by Fultz (1961) and more recently by Hidy (1967).

There are three general approaches to similarity. One assumes that the phenomenon to be examined is governed chiefly by one or two scaling conditions and that the other conditions may be ignored. In the second

approach, turbulent transfer in the lower troposphere is represented by laminar flow (molecular transfer) in the simulation. In this case, molecular diffusion coefficients (kinematic viscosity (ν) and thermal diffusivity (κ)) play the role of the corresponding eddy coefficients in the prototype. The first approach usually permits precise application of the one or two scaling conditions, but it raises the question of the consequences of neglect of the other scaling conditions on the phenomena being studied, In both approaches, no attempt is made to satisfy all scaling conditions simultaneously.

A third approach arises from the problem of solving the nonlinear governing equations. This has led to the use of mathematical models for wind and temperature profiles to assist in studying the lower troposphere.

In the first approach considerable care must be taken in choosing the appropriate similarity parameters. This generally requires some prior knowledge of the relative importance of the various physical processes involved in the problem. A difficulty in the second approach arises from the practical requirement that eddy coefficients in the atmosphere be represented by molecular coefficients in the simulation; the former depend upon position in the fluid and type of air motion, while the latter are physical constants of the simulation fluid. The implications of this relationship between the prototype and simulation are under investigation (see e.g. Willis and Deardorff 1965, and Plate 1966). The use of empirical equations to circumvent non-linearities in the governing equations (third approach) also raises questions of validity, which require further study.

4.2 Investigations using Selected Scaling Criteria

Some early simulations were designed to illustrate large-scale

motions of the whole atmosphere. These included rotating boundaries to represent the motion of the earth's surface and to introduce Coriolis forces into the fluid. The chief interest was in the nature of general circulation and how it is disturbed by cyclones, mountains and waves. Figure 4.1 shows

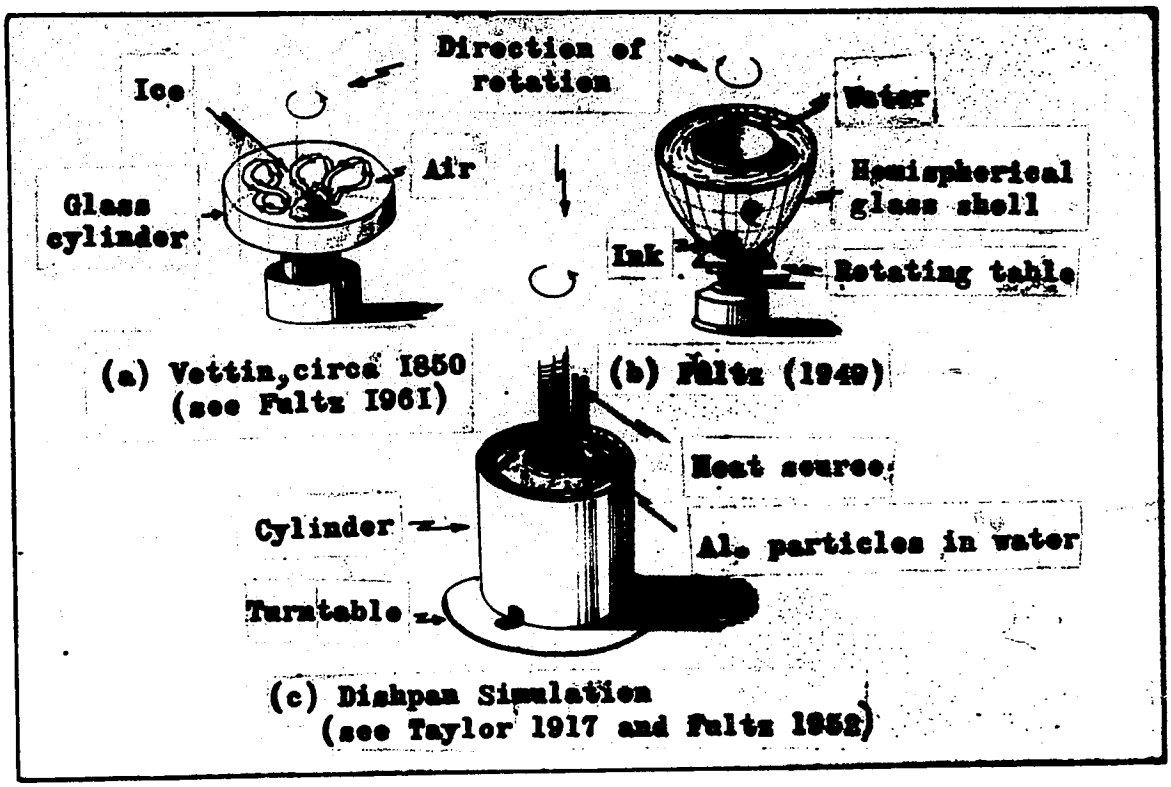

Figure 4.1 Laboratory Simulation of Large-Scale Motion of the Atmosphere.

three examples of these simulations. In each case, the fluid (atmosphere) is contained between an inner and an outer shell or boundary, to represent the earth's surface and the outer "limit" of the atmosphere. Motion of the fluid is shown by a visible indicator, such as metallic particles in suspension or liquid dye. A temperature gradient is introduced into the fluid by placing a cold or warm solid at the centre (Fig. 4.1 (a) and (c)) or by heating the cups at the pole (Fig. 4.1 (b)). In some work (see e.g. Fultz 1961), the hemispherical simulation of Fig. 4.1 (b) has been changed

motions of the whole atmosphere. These included rotating boundaries to represent the motion of the earth's surface and to introduce Coriolis forces into the fluid. The chief interest was in the nature of general circulation and how it is disturbed by cyclones, mountains and waves. Figure 4.1 shows

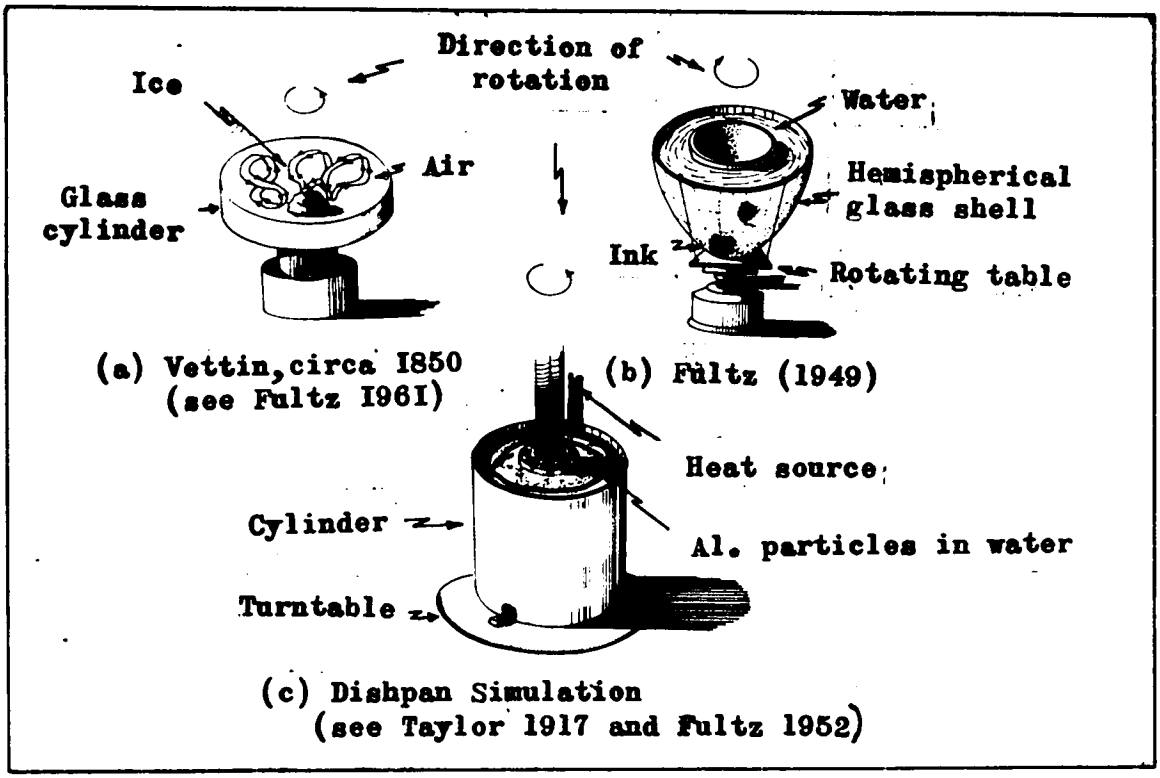

Figure 4.1 Laboratory Simulation of Large-Scale Motion of the Atmosphere.

three examples of these simulations. In each case, the fluid (atmosphere) is contained between an inner and an outer shell or boundary, to represent the earth's surface and the outer "limit" of the atmosphere. Motion of the fluid is shown by a visible indicator, such as metallic particles in suspension or liquid dye. A temperature gradient is introduced into the fluid by placing a cold or warm solid at the centre (Fig. 4.1 (a) and (c)) or by heating the cups at the pole (Fig. 4.1 (b)). In some work (see e.g. Fultz 1961), the hemispherical simulation of Fig. 4.1 (b) has been changed

by filling the space between the shells with two immiscible liquids of different densities; the two liquids represent air masses separated by a frontal surface discontinuity.

The scaling in this work called for preservation of the Rossby number (Ro), the Froude number (Fr) and the Reynolds number (Re). Although scaling of these numbers was imperfect, yet the observed flow patterns in the simulation were remarkably similar to those in the atmosphere. The authors rationalize that imperfection in the scaling conditions is not important either because the phenomena under study is not dependent upon the variables in the scaling criteria, or because the combination of these variables in each of the scaling criteria is unsensitive to changes in the magnitude of that criterion. (e.g. Prandtl number $Pr = \frac{\nu}{\kappa}$ is 0.7 for the atmosphere but 3.6 for the simulation).

Other investigators have studied thermal convection in the laboratory, to suggest details on the physical process in the atmosphere. Townsend (1964) has examined natural convection in a laboratory tank which is cooled from below while Croft (1958), Elder (1965 (a and b), 1967 (a and b)) and Deardorff and Willis (1967a) have considered the corresponding case of heating from below. Studies of turbulent convection in the air between two horizontal flat plates at different temperatures have been undertaken by Willis and Deardorff (1965) and Deardorff and Willis (1967b). Ingersoll (1966) examined the additional factor of shear through rotation of one of the metal plates. In these investigations, preservation of the Rayleigh number and Prandtl number were considered the dominant scaling criteria.

4.3 Investigations Using Laminar Flow to Simulate Turbulent Transfer

Many laboratory simulations have used wind tunnels of varying

complexity to represent turbulent transfer above the ground. Since only a small region of the atmosphere is considered, the surface representing the earth is flat with scaled topography superimposed as required. The upper surface of the fluid is free.

Of interest here are the scaling conditions that are used in the design of these simulations. Abé, in 1941, achieved similarity in the gross mean turbulent flow about Mount Fuji by observing laminar flow in a low-speed tunnel (Fultz 1961). The simulation of mean turbulent flow in mountain waves was carried out successfully by Long in a study of laminar flow within a water tank (Fultz 1961). Faller (1963 and 1964) has examined the stability of the turbulent Ekman layer through the use of a laboratory simulation. He used a cylindrical rotating tank of water, in which the Ekman flow was was produced by withdrawing water from the centre and introducing it at the rim. A symmetrical vortex in the laminar flow at the bottom of the tank was interpreted as the large eddies in the Ekman layer that were described by Townsend (1956) (see Chapter II).

Cermak's work with wind tunnels supports this approach to simulation when the Froude number is maintained invariant (Cermak et al 1966). The common practice of replacing the eddy Reynolds number in the prototype by the molecular Reynolds number in the simulation (for constant Froude number) has been commented upon by Fultz (1961), Cermak et al (1966)Hidy (1967) and others. They point out that the value of the Reynolds number is significant only in the transition region between laminar and turbulent flow. At heights in the atmosphere greater than a few meters above the ground, Re is always much greater than the transition value and its numerical value may vary over wide limits without altering its significance as a scaling criterion.

4.4 Investigations using Mathematical Models

Sutton (1953, p. 14) has suggested that motion observed in a wind tunnel above a flat smooth surface is an idealization of the flow over a small region of the earth's surface. A more realistic representation of the earth's surface has roughness which introduces turbulence into the otherwise laminar flow. Davenport (1961) points out that turbulence which is due to thermal convection is small compared to that arising from surface roughness and that the natural wind can be simulated in the wind tunnel by introducing appropriate roughness into the underlying boundary.

Priestley (1954) has examined patterns of thermal convection by observing the dispersion of smoke from chimneys, in the presence of wind. His analysis of these observations indicates that the full-scale patterns are simulated in a wind tunnel if $\frac{2C}{3}$ Fr. is preserved in scaling, where C is a spreading coefficient as determined experimentally from the smoke plumes.

Nemoto (1961 a) has derived a single scaling criterion for simulation of the structure of local wind and turbulence in the lower troposphere. By assuming that molecular viscosity is negligible in comparison with the eddy viscosity, that the air is incompressible and that pressure-gradient and Coriolis forces can be neglected, he found that an isothermal troposphere may be simulated in the laboratory if

$$\frac{U_{prototype}}{U_{simulation}} = \left[\frac{L_{prototype}}{L_{simulation}}\right]^{\frac{1}{3}} \qquad 4.1$$

where U and L have the same meaning as in the Reynolds number.

CHAPTER V

LABORATORY SIMULATION FOR THE PRESENT STUDY

The material of Chapter II and III provides a guide for a laboratory simulation of convection in the lower troposphere. Daytime heating of the earth's surface will be assumed and the actual temperature of the surface will be replaced by an effective temperature which is the air temperature at a height of a few meters and which results from conduction, radiation and convection below this level. The region of interest extends one kilometer in the vertical and only a few kilometers horizontally, where the flow is generally turbulent or a composite of laminar and turbulent. The complications of local heating or cooling by latent heat transfer will be avoided in this initial study by assuming that the atmosphere is essentially dry. Eddy conductivity and eddy viscosity in the lower troposphere will be considered constant throughout the region of interest. Either natural or free convection may be present.

An atmosphere which satisfies this description may be simulated through the conditions stated at the end of Chapter III. There it was noted that invariance of the coefficients in the governing equations is required in passing from the atmosphere (prototype) to the simulation. The present chapter will examine the magnitudes of these invariant coefficients in the prototype and then use them to specify the

nature of the laboratory simulation. The remainder of the chapter will describe the mechanical details of the simulation, including the provision for general horizontal flow and heating of the underlying surface.

5.1 Specifications for the Simulation

Five coefficients of the governing equations must be invariant for the simulation of convection. These involve the Froude number, Reynolds number, Peclet number, Grashof number, Prandtl number and a coefficient that contains the vertical gradient of temperature. Inspection shows that the Grashof number contains the Froude number and the Peclet number and hence, the former may be omitted from further consideration here. Table 5.1 lists these coefficients in the first column. The second column gives the numerical values of these coefficients for the lower troposphere. The representative quantities L, U, Δ T and $(\frac{\partial \bar{T}}{\partial z})_o$ have been assigned magnitudes arbitrarily as follows:

$$L = 10^5 \text{ cms.}$$

$$U = 10^2 \text{ cms.sec}^{-1}$$

$$\Delta T = 1^o \text{ (C or K)}$$

$$(\frac{\partial \bar{T}}{\partial z})_o = 10^{-4} \ ^o\text{(C or K)}$$

and the physical constants of the air are (Sutton 1953, p. 115 and Haltiner and Martin 1957, p. 12 and 253):

coefficient of thermal expansion (α) = $3 \times 10^{-3} \ ^oK^{-1}$

eddy kinematic viscosity (ν) = 10^4 cm.^{2} sec^{-1}

eddy thermal conductivity (κ) = 10^4 cm.^{2} sec^{-1}

Only approximate magnitudes are of interest here.

TABLE 5.1

Invariant Coefficients for Convection

Coefficient	Magnitude in Prototype	Magnitude in Simulation
$\frac{g \alpha \Delta TL}{U^2}$	40	$0.2 \frac{\Delta TL}{U^2}$
$\frac{\nu}{UL}$	10^{-3}	$10^{-2} \times \frac{1}{UL}$
$\frac{\kappa}{UL}$	10^{-3}	$1.5 \times 10^{-3} \times \frac{1}{UL}$
$\frac{\nu}{\kappa}$	≈ 1	7
$-\frac{g \quad \Delta T}{c_p (\frac{\partial \bar{T}}{\partial z})_o}$	$3.1 \quad 10^{-3}$	$-4.7 \quad 10^{-9} \quad \frac{\Delta T}{(\frac{\partial \bar{T}}{\partial z})_o}$

It should be noted that the values of ν and κ provide a compromise between the strong turbulence near the surface and the composite turbulence at higher levels.

The condition of the simulation may now be deduced from the requirement for invariance of the coefficients. Inspection of the physical constants of various fluids suggests that water will permit a convenient choice of scaling parameters. If the motion of the water is maintained laminar, its physical constants at a temperature of about 20°C are (Bird et al 1960, p. 8 and 248):

coefficient of thermal expansion (α) = 2×10^{-4} $^{o}K^{-1}$

molecular kinematic viscosity (ν) = 10^{-2} $cm.^2$ sec^{-1}

molecular thermal diffusivity (κ) = 1.5×10^{-3} $cm.^2$ sec^{-1}

Then, the magnitudes of the coefficients in the simulation are as listed in the third column of Table 5.1. Equating the coefficients in the

second and third columns leads to the following for the representative quantities in the simulation:

$$\begin{aligned} \frac{\Delta T\, L}{U^2} &= 200 \\ UL &= 10 \\ UL &= 1.5 \end{aligned} \qquad 5.1$$

The discrepancy between the second and the third equations is due, in part, to the assumed equality of ν and κ in turbulent air. In fact, the values of the coefficients for turbulent or semi-turbulent air may vary over a few orders of magnitude and the value of $\frac{\nu}{\kappa}$, in the second column, is intended only to suggest that they are of about the same order of magnitude. Then, the last two equations may be replaced by the compromise:

$$UL = 5$$

Finally, we let L take the value 10 cm. for a laboratory simulation of convenient dimensions and through solving of these equations we find the following relations between the representative quantities in the prototype and laboratory simulation:

$$\begin{aligned} L_{Prototype} &= 10^4\, L_{Simulation} \\ U_{Prototype} &= 200\, U_{Simulation} \\ \Delta T_{Prototype} &= 0.2\, \Delta T_{Simulation} \end{aligned} \qquad 5.2$$

5.2 Simulation of Initial Conditions

The significance of the initial conditions in the simulation may be implied through an heuristic approach. Here, we refer to the vertical gradient of temperature in the lowest 10 cms. of the simulation, before the application of heating from below. After thermal equilibrium between the fluid and its environment has been reached and horizontal flow is absent, the fluid is isothermal and the vertical temperature gradient vanishes. In this case, there is no net heat transfer in the vertical. When horizontal flow is introduced, some mixing of the fluid elements will occur adiabatically and the vertical gradient of temperature will approach the adiabatic lapse rate. For water, the adiabatic lapse rate is approximately -10^{-6} ^{o}C cm^{-1} (see, e.g. Munn 1966, p. 167). Then it is clear that the initial (unperturbed) temperature profiles in the simulation are isothermal either with or without horizontal flow, within the precision of the temperature measurement ($\pm$ 0.2 ^{o}C).

The corresponding conditions in the atmosphere (prototype) must also be associated with isothermal and adiabatic temperature profiles, respectively. This may be seen by considering the direction of heat flux divergence. In the absence of wind and excess heating from below (i.e. absence of temperature perturbations), only an isothermal profile of temperature will accompany no net transfer of heat in the vertical. The introduction of wind will again introduce adiabatic mixing, causing the vertical gradient of temperature to approach the adiabatic lapse rate (-10^{-4} ^{o}C cm^{-1} in air). From the previous section it will be noted that the appropriate scaling of temperature gradient converts this prototype value into -7×10^{-6} ^{o}C cm^{-1} in the simulation, which is very close to

the figure given above.

Thus, initial conditions with isothermal and adiabatic temperature profiles in the atmosphere are represented by initial conditions with an isothermal profile in the simulation. Subsequent perturbation of this profile, through the introduction of excess heating from below, is represented by the observations in the simulation of the present study.

5.3 Construction of the Fluid Housing

The physical housing of the laboratory simulation is shown in the photograph of Figure 5.1. It is essentially a closed-circuit water tunnel mounted on a laboratory table. Water is circulated in it about a rectangular path in the horizontal plane. Further details of construction are given in Figure 5.2.

The housing is of wood in the form of a rectangular box with a hollow centre. Turning vanes at the corners, a smooth varnished surface on the walls, and a contraction cone with a flow straightener

Illumination for metal particles in fluid

Temperature probe carriage

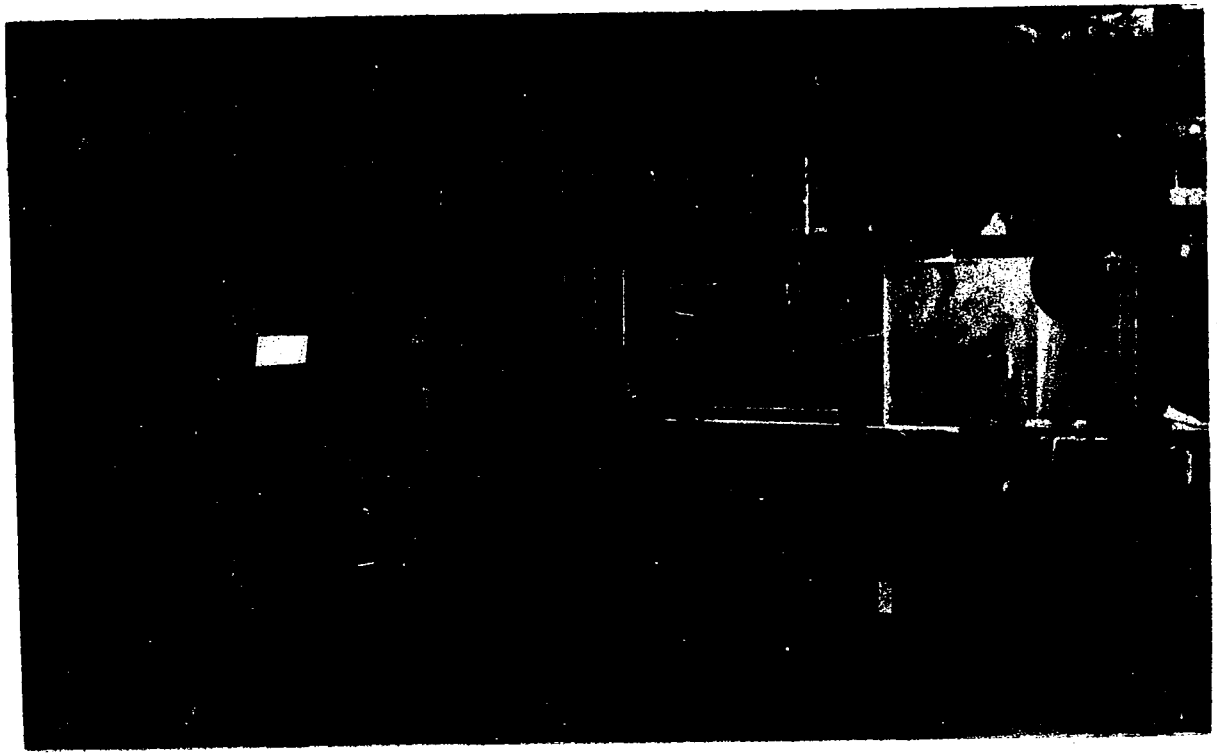

Water tunnel

Temperature recording system

Shadowgraph system

Figure 5.1 Laboratory Simulation (Water Tunnel) with the Associated Observing Equipments.

Temperature probe
carriage

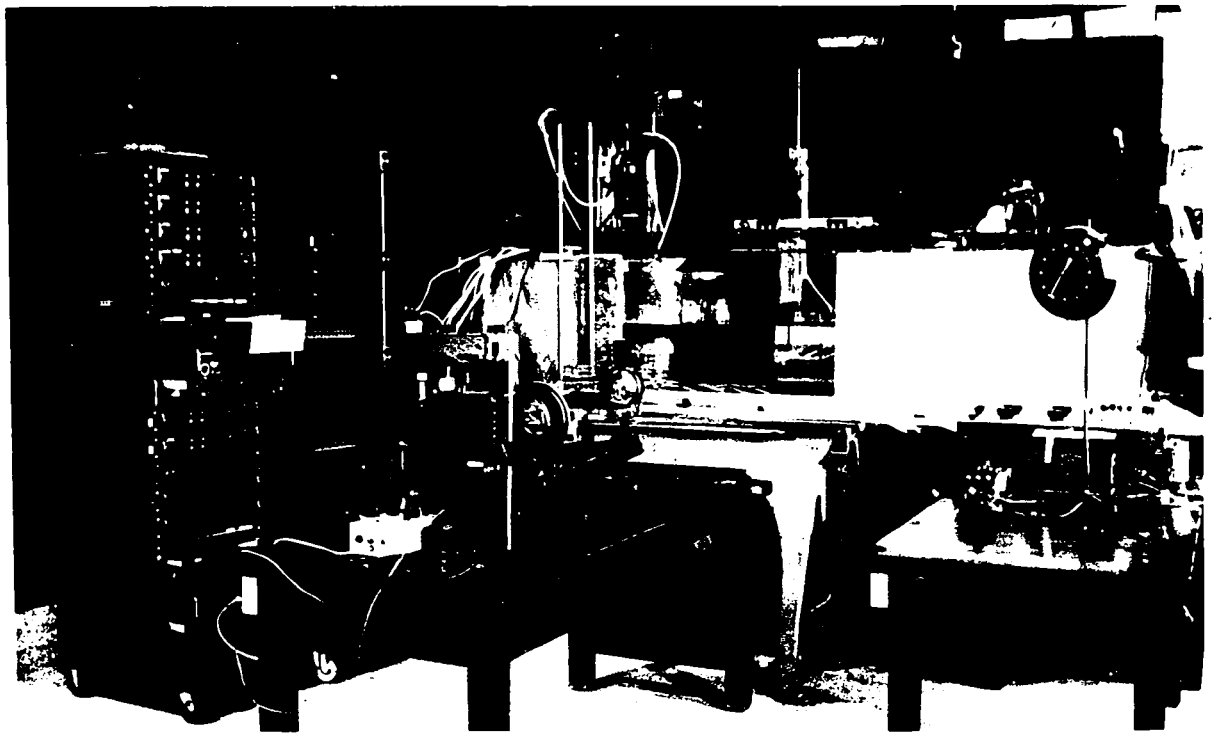

Water
tunnel

Temperature recording system

Shadowgraph system

Figure 5.1 Laboratory Simulation (Water Tunnel) with the Associated Observing Equipments.

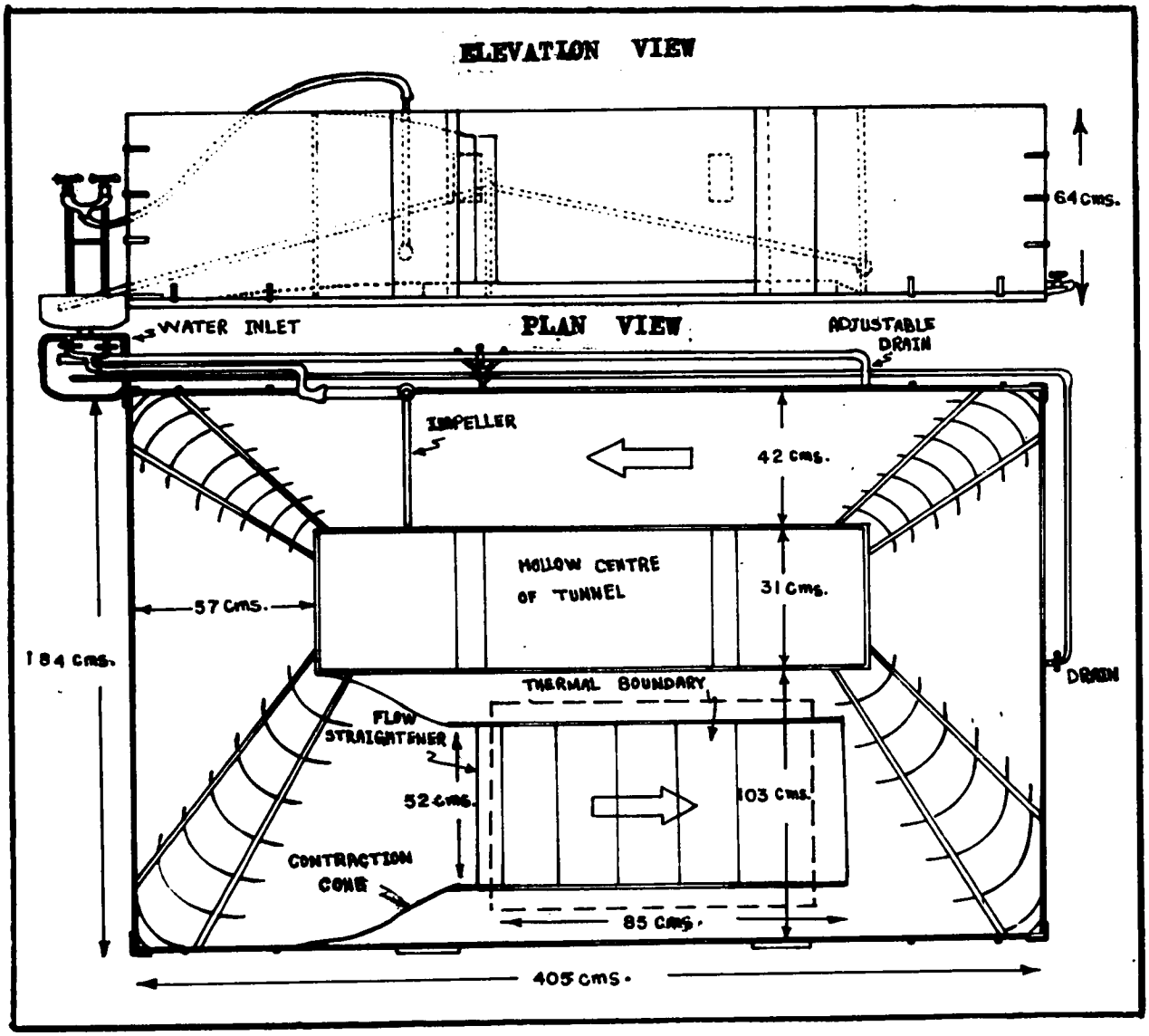

Figure 5.2 Construction Details of the Water Tunnel, Including the Provision for Control of Fluid Flow.

at the input to the test region all aid in maintaining laminar flow (Pope 1958, p.1).

Care is taken to prevent draft in the tunnel environment, so that spurious convection will not arise in the simulating fluid. For this purpose, the laboratory windows and the section of the laboratory containing the water tunnel are enclosed by draw-curtains. Insulation between the wooden framework and the laboratory table and a plastic cover above the tunnel also assist in controlling the fluid temperature.

Figure 5.1 also shows the related observing equipment adjacent to the laboratory simulation. Details of these observing techniques will be given in the next chapter.

5.4 Control of the Flow

The fluid in the water tank is maintained at a depth of 25 cms. for experimental observations. According to the scaling criteria of Section 5.1, the region of interest in the troposphere (lowest kilometer) is represented by the first 10 cms. of the water above its underlying surface in this tank. The remaining 15 cms. of water above this is a buffer region under the free water surface.

The water controls, as illustrated in Figure 5.2, provide three functions. First, the maximum height of water in the tank is governed by the adjustable drain at the rear wall, Secondly, the water temperature is controlled by regulating the inputs from the separate sources of cool and warm water. And thirdly, horizontal flow of the water (to simulate general advection in the troposphere)

is governed by the inflow from the impeller in the back of the channel of the tank. This impeller is a pipe with a row of small holes along one side which act as jets for the inflow. Initial tests indicated that turbulence arising from these jets is attenuated to a negligible amount if the impeller is located sufficiently far up-stream at a distance of about 350 cms. from the test region, as in Figure 5.2 (see Appendix III). By means of this impeller, horizontal flow in the test section of the tunnel is controlled at rates between 0.3 cm. sec^{-1} and 3 cm. sec^{-1} corresponding to advection rates from 0.6 meters sec^{-1} to 6 meters sec^{-1} in the lower troposphere; laminar flow of water occurs throughout this range.

5.5 The Test Region of the Simulation

The test section is the jet of the water tunnel,as indicated by the broken lines in Figure 5.2. When general flow occurs, the water moves from left to right. A contraction cone at the entrance to the test region guides the flow through a flow straightener; the latter is an automobile radiator, chosen for expediency and effectiveness without a detailed study. The full horizontal depth of the water tunnel is resumed in the test region, following the constriction at the straightener; this arrangement reduces the effect of the walls upon the main stream motion. A plate glass window in the front wall of the test region is provided for visual inspection. This also permits observations on the isotherms in the water and the velocity profiles, as described in the next chapter.

Daytime residual heating of the air adjacent to the earth's surface in the prototype is simulated in the water tank by heaters at

the base of the test region. It will be recognized that this is a residual heating of the boundary, since the initial condition in either the simulation or the lower troposphere is due to equilibrium in the transfer of heat from other sources. Such residual heating in the troposphere may be attributed to an excess of heating from the ground beyond that required for the initial condition. Figure 5.3 gives details on the construction of this thermal boundary. Its leading and trailing edges are of varnished wood with curved contours and the upper surface is smooth, to aid in maintaining laminar flow in the water. The central section contains four electric heaters, each with a thick aluminum upper plate and a heating element embedded in wet sand. Three bead thermistors are mounted within each metal plate, at the surfaces, to indicate the surface temperature; these have shown that the plate temperature is uniform within $0.01^{\circ}C$ when the plate is heated $10^{\circ}C$ above room temperature.

Each heater compartment is lined with asbestos and wood to insulate it from the adjacent heaters. The plate temperature is adjusted by varying the heater supply, voltage, according to a procedure described in Chapter VII.

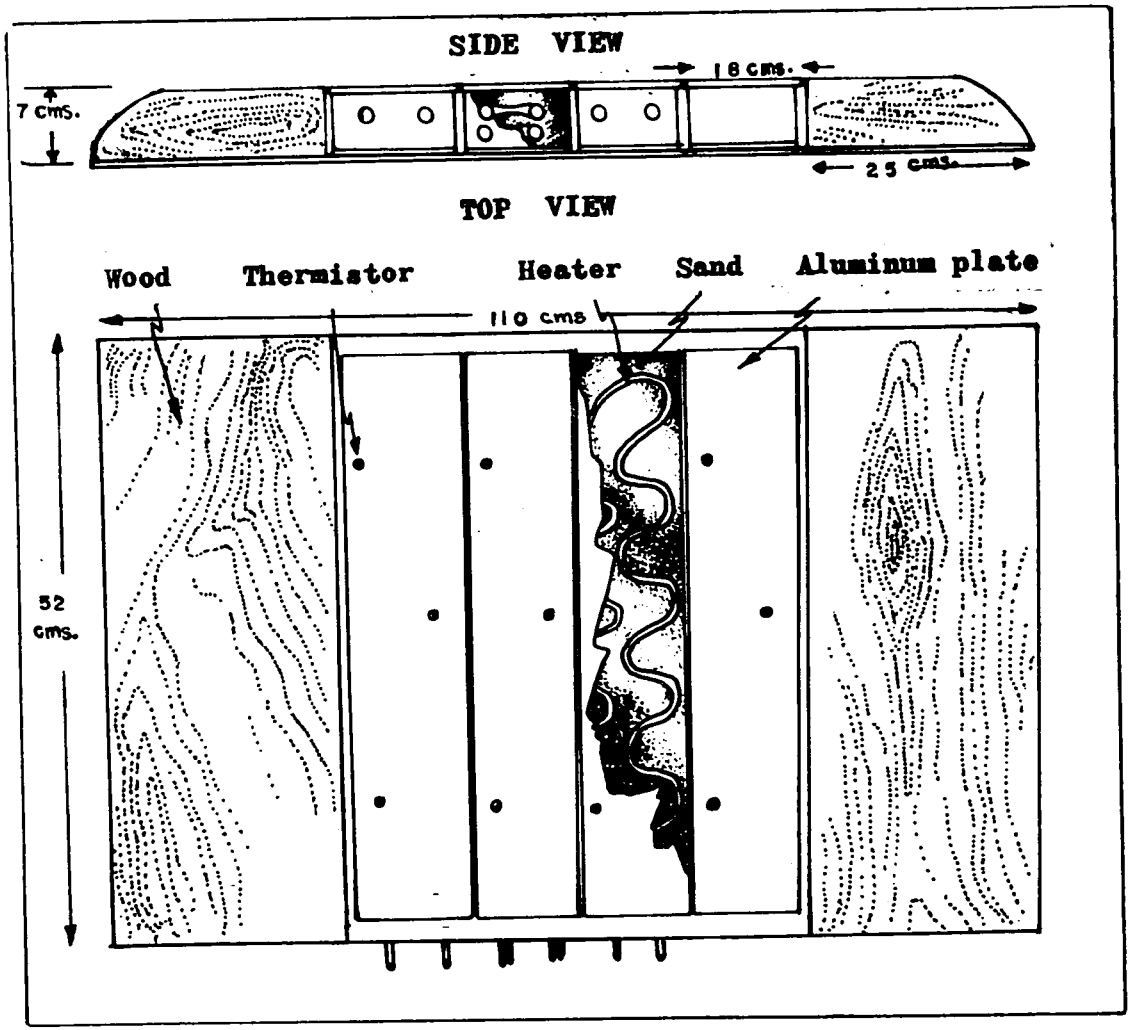

Figure 5.3 Thermal Boundary at the Base of the Test Region of the Water Tunnel.

CHAPTER VI

TECHNIQUES OF OBSERVATION

In this chapter, attention is confined to the test region of the laboratory simulation. A study of the patterns or models of convection in the lowest 10 cms. of the water above the thermal boundary is the main objective here. For this reason, observations are required on the temperature and velocity profiles, the isotherm contours and the organized motion within the water. Temperature of the underlying surface also must be recorded. Details on the observing techniques for each of these purposes are given in the following sections.

6.1 Fluid Velocity

The technique of streak photography is used to record the velocity profiles in the vertical plane of the water. Minute particles of metal suspended in the water are illuminated from above and the paths of these bright points of light are photographed over a specified time-interval.

The metal particles require special preparation before they are introduced into the water. Aluminum particles of diameter 10^{-3} cm. are used for this purpose. They first are wetted through vigorous

agitation in alcohol followed by repeated filtering and washing with water. Then, they are mixed with water and placed in the reservoir of the dispensing apparatus, upstream from the test region, as shown in Figure 6.1. This apparatus disperses the mixture into the moving water of the simulation at a rate which is controlled by a tap on the top of the reservoir.

A preliminary study has shown that the fall velocities of the aluminum particles are negligible in comparison with the horizontal water velocities during general flow (Appendix IV). Thus, the particle motion is a reliable indicator of the water motion.

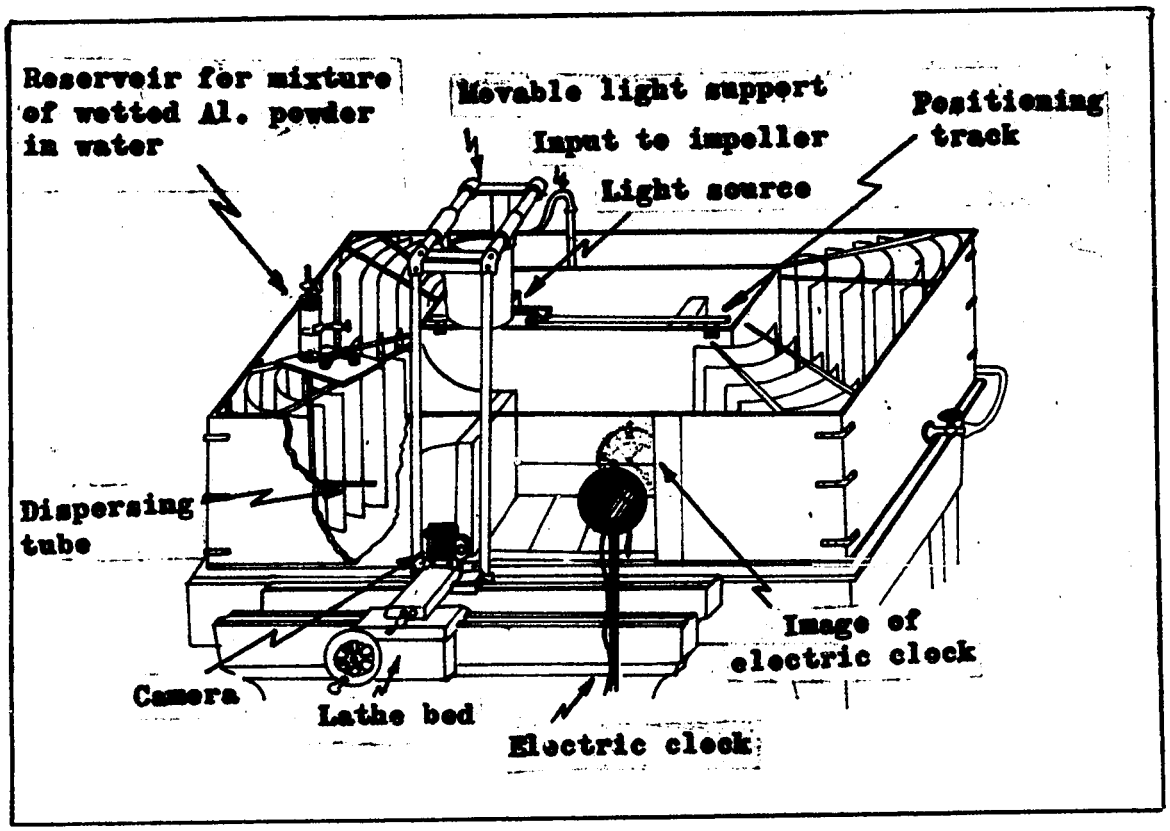

Figure 6.1 Apparatus for Observing Water Velocity Profile, through Streak Photography.

agitation in alcohol followed by repeated filtering and washing with water. Then, they are mixed with water and placed in the reservoir of the dispensing apparatus, upstream from the test region, as shown in Figure 6.1. This apparatus disperses the mixture into the moving water of the simulation at a rate which is controlled by a tap on the top of the reservoir.

A preliminary study has shown that the fall velocities of the aluminum particles are negligible in comparison with the horizontal water velocities during general flow (Appendix IV). Thus, the particle motion is a reliable indicator of the water motion.

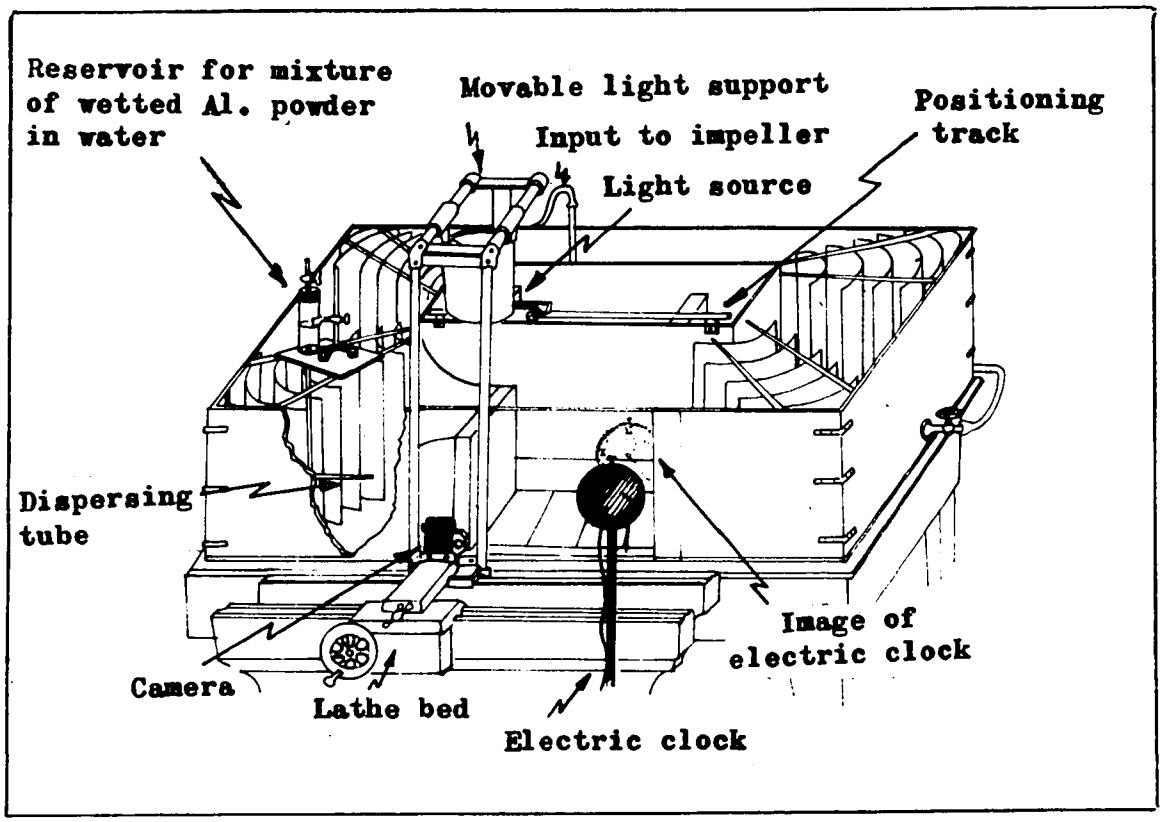

Figure 6.1 Apparatus for Observing Water Velocity Profile, through Streak Photography.

To ascertain the vertical profile of water velocity, a vertical "curtain" of light is projected from above into the desired section of the test region. This illumination extends 10 cms. along the direction of flow, 2 cms. lateral to the flow and throughout the full height of the water. A 35 mm. camera mounted on the movable carriage of a lathe was used to photograph the particle streaks, with Tri-x film. The length of the exposure is indicated by the sweep second hand of an electric clock, whose image is reflected in the glass front of the test region. The light "curtain" may be transferred to any desired part of the test region with the aid of the same lathe carriage. A scale and position index is provided for the photographs, by mounting a short wire of known length at a specified location on the thermal boundary, in the field of view. Figure 6.2 shows a sample photograph as taken by this method. The analysis of this was carried out by projecting the original negative through an enlarger lens of good quality. Through averaging of velocities from numerous adjacent streaks, local velocities are ascertained with an accuracy of 20%.

6.2 Temperature of the Underlying Boundary

Thermistor probes* are used to indicate the surface temperature of each section in the underlying thermal boundary. Each thermistor is embedded in a threaded aluminum plug of plate material as shown in Figure 6.3. In this way, the underlying thermal boundary presents a smooth surface to the adjacent water; the thermistor connections are

---

* Fenwall thermistors, type GC32J5 (Fenwall Electronics, Inc. Framingham, Mass. U.S.A.)

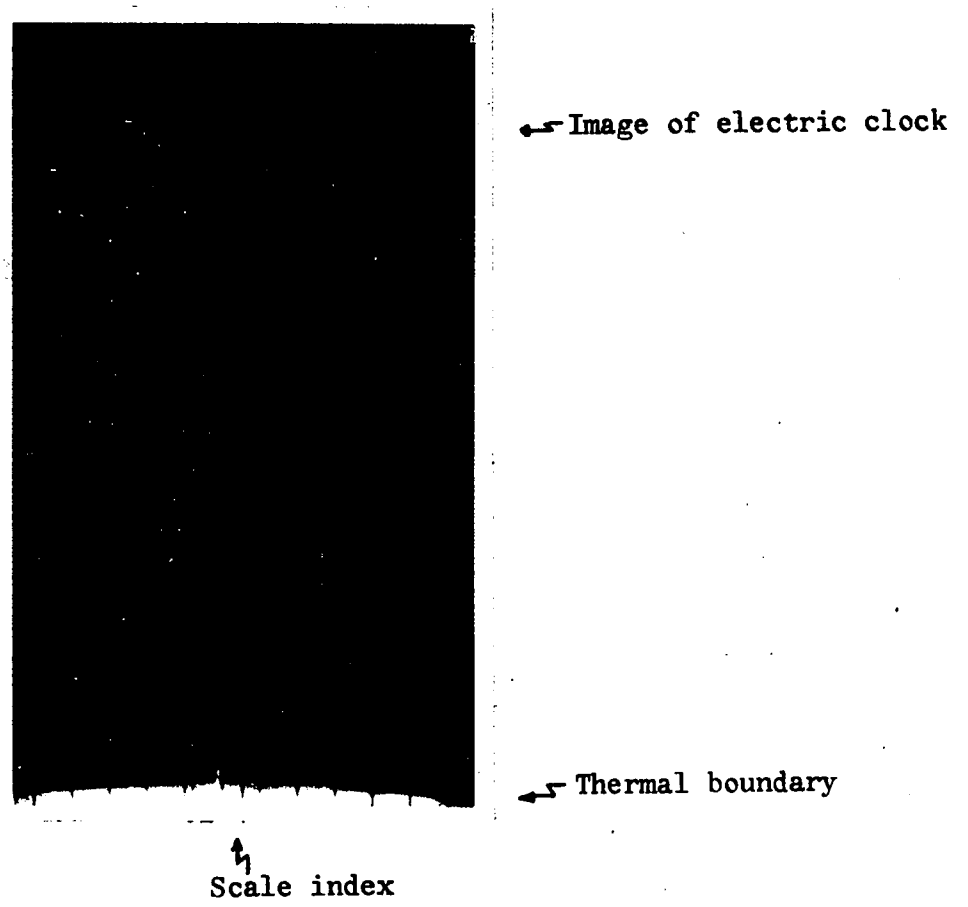

Figure 6.2 Photograph of Path Followed by Al. Particles in Curtain of Light.

continued through the sand beneath the plate and out the side of the boundary case where they do not interfere with the main flow in the test region.

Calibration of the thermistor probes has followed standard procedure (Middleton and Spilhaus 1953, p. 82). Prior to calibration, the thermistors were stabilized by artificial aging (Railstone 1954). For temperature measurements, the thermistor is connected into one arm of a precision Wheatstone bridge* through a low-resistance switch

---

* H.W. Sullivan Ltd., London, Serial No. 2239 List No. T.1080. The accuracy of the bridge is $\pm$ 0.02%.

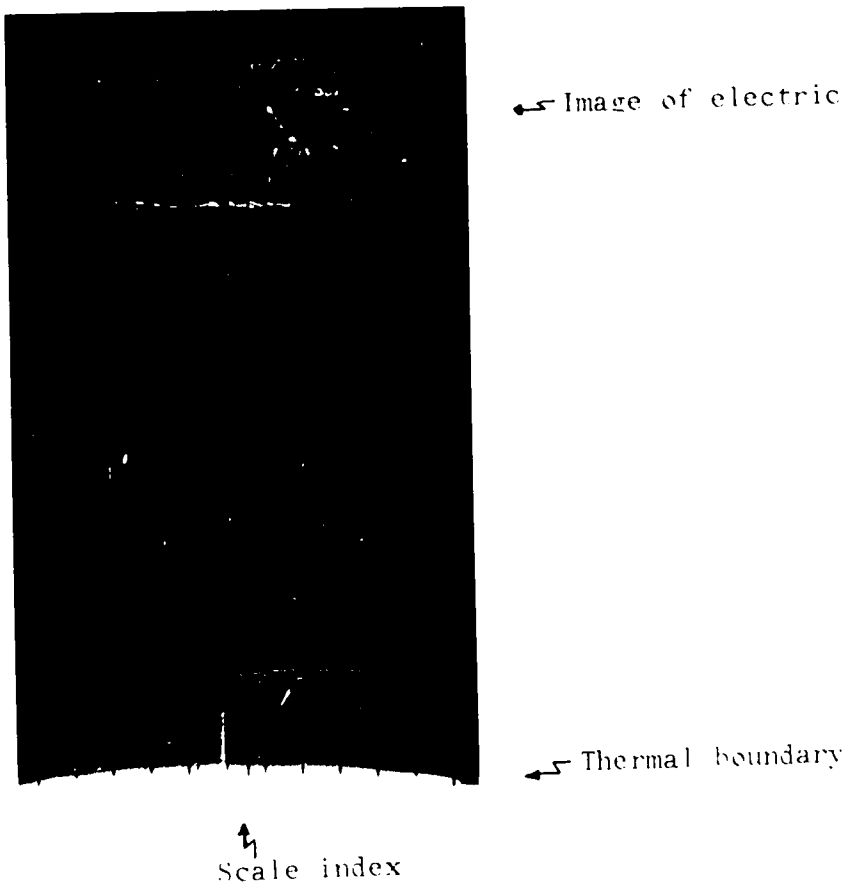

Figure 6.2 Photograph of Path Followed by Al. Particles in Curtain of Light.

continued through the sand beneath the plate and out the side of the boundary case where they do not interfere with the main flow in the test region.

Calibration of the thermistor probes has followed standard procedure (Middleton and Spilhaus 1953, p. 52). Prior to calibration, the thermistors were stabilized by artificial aging (Railstone 1954). For temperature measurements, the thermistor is connected into one arm of a precision Wheatstone bridge* through a low-resistance switch

---

* H.W. Sullivan Ltd., London, Serial No. 2239 List No. T.10-0. The accuracy of the bridge is ± 0.02 °.

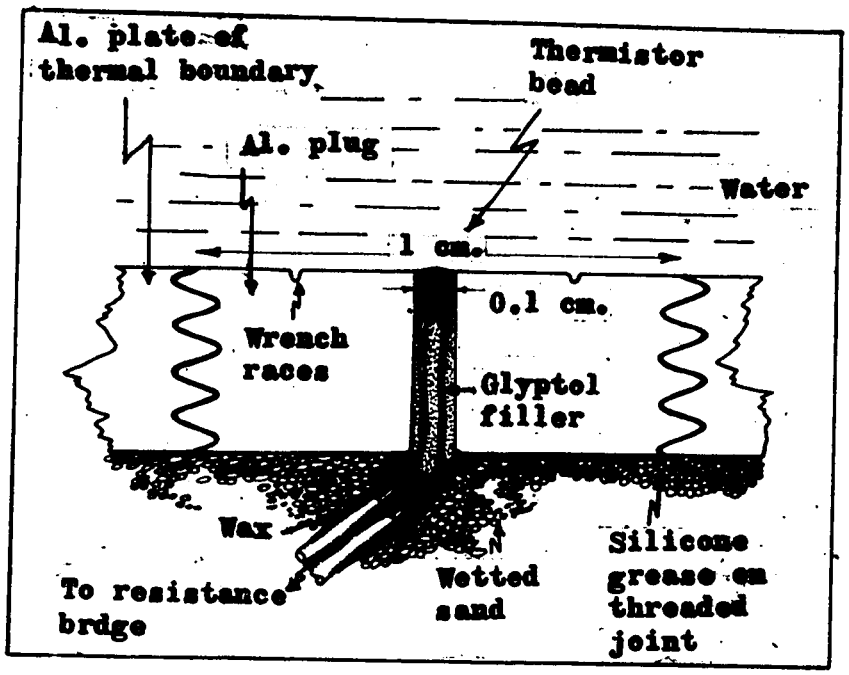

Figure 6.3 Temperature Probe for Thermal Boundary.

which permits selection of any of the probes in the thermal boundary. Appendix V describes the method of ascertaining the bridge supply voltage to eliminate anemometer effect in the probe. The actual calibration compares the thermistor resistance with the temperature of a commercial water bath as indicated by a precision mercury thermometer (see Appendix VI). Accuracy in measurement of water temperature is $\pm$ 0.2°C for the range of water temperature +10 to +30°C.

6.3 Isotherms in the Fluid

Information on the patterns of heat transfer in the water is provided by a study of the isotherms. Local regions of constant temperature will indicate either stagnation or rapid transport of heat, depending upon the environment. A convenient method of observing the isotherm patterns uses the shadowgraph technique; this

has been described in detail by Landenburg et al (1954, p. 26), Lewis and von Elbe (1961, p. 567) and Goldstein (1965, p. 288).

The principle of the shadowgraph technique may be explained by referring to Figure 6.4. According to Washburn (1930, p. 13), the

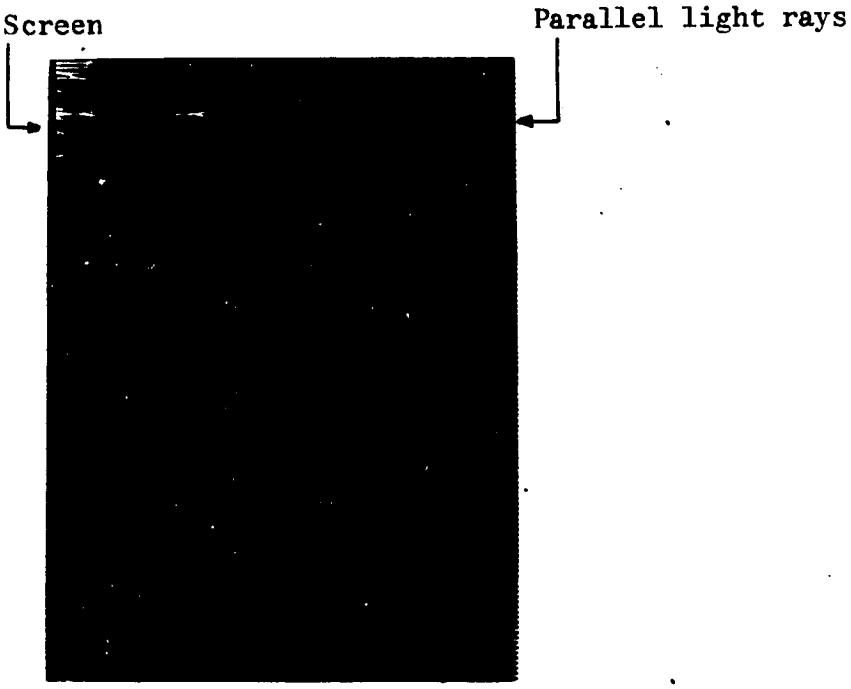

Figure 6.4 Refraction of Light Rays Due to Temperature Inhomogeneities.

refractive index (n) of water at optical wave lengths and for temperatures around 20°C is

$$n = 1.33299 - 10^{-5}\left[0.124\ (T-20) + 0.1993\ (T^2 - 400) - 0.000005\ (T^4 - 160000)\right] \qquad 6.1$$

Thus a local change in water temperature of 0.5°C results in a local inhomogeneity of water refractivity of magnitude 3.3×10^{-5}.

has been described in detail by Landenburg et al (1954, p. 26), Lewis and von Elbe (1961, p. 567) and Goldstein (1965, p. 288).

The principle of the shadowgraph technique may be explained by referring to Figure 6.4. According to Washburn (1930, p. 13), the

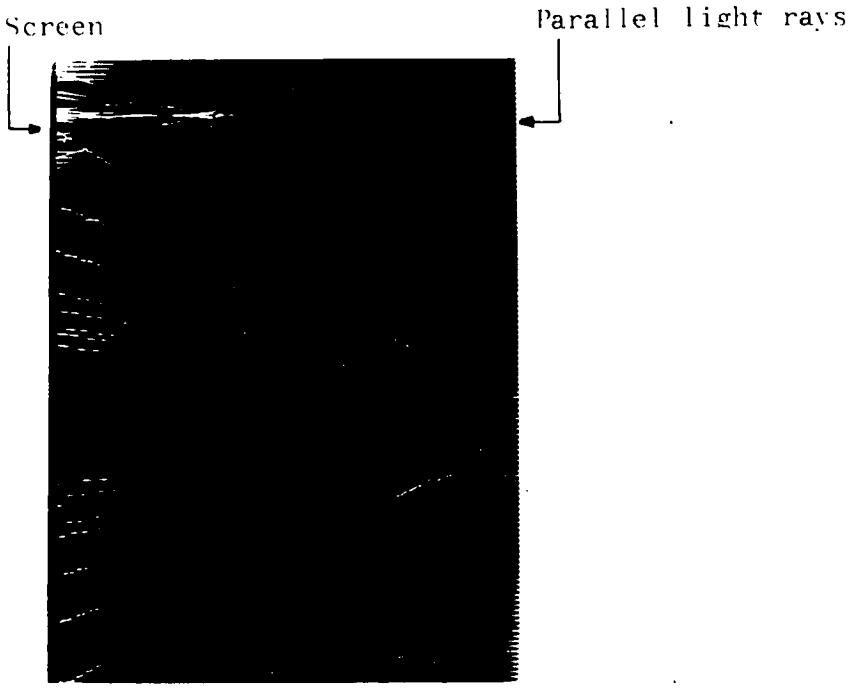

Figure 6.4 Refraction of Light Rays Due to Temperature Inhomogeneities.

refractive index (n) of water at optical wave lengths and for temperatures around 20°C is

$$n = 1.33299 - 10^{-5}\left[0.124\ (T-20) + 0.1993\ (T^2 - 400) - 0.000005\ (T^4 - 160000)\right] \quad 6.1$$

Thus a local change in water temperature of 0.5°C results in a local inhomogeneity of water refractivity of magnitude 3.3×10^{-5}.

Light rays passing through the water will be refracted according to Snell's law, and the interference pattern created by interaction of the deviated and undeviated rays at a detector will indicate the geometry of the temperature inhomogeneity. In Figure 6.4, parallel rays of white light are incident from the right, upon two circular inhomogeneities of refractive index in an otherwise uniform medium. The two patterns of ray deviation are due to a refractivity decrease (local heating, lower circle) and a refractivity increase (local cooling, upper circle) relative to that of the environment. A detector on the left which is sensitive to variations in light intensity will display the patterns of light shading that result from constructive and destructive interference of rays*.

Two additional features of this ray diagram should be emphasized. First it will be noted that, in the absence of magnification, the interference pattern at the detector delineates approximately the size and geometry of the temperature inhomogeneity in the water. Secondly, by placing a focusing lens at the detector on the left the interference pattern may be indicated for a selected plane (normal to the diagram) within the water; in general, the intensity variations will be greatest when this selected plane passes through

---

* The techniques of physical optics are required for calculation of light intensity in the interference pattern.

the inhomogeneity*. For the present application, the inhomogeneities in water refractivity are very weak and hence the variations in light intensity at the detector will be significant in practice only when this selected plane is at the inhomogeneity. Hence, this technique is a good indicator of the geometry of the temperature inhomogeneity as it is position - selective within the water.

Two experimental arrangements are used to observe shadowgraphs of the test region. In each, light from a point source (6 volt automobile head lamp) passes through the full depth of the water to the back wall of the test region, where it is reflected from a plate-glass mirror (back surface silvered and waterproofed by wax) through the test region to be observed at a location outside of the water near the light source. If a small part of the test region is to be examined and the geometry of the isotherm patterns is to be displayed accurately, the image is focussed on a photographic film in a 35 mm. camera. Since the cross-section of the disturbance in the test region is limited by the cross-section of the lens, the camera lens is removed and is replaced by a larger one (focal length 53 cms. and 7.5 cms. in diameter). Another lens is placed in front of the light source for parallel rays through the water.

The second experimental arrangement provides for observation of an expanded field of isotherm contours in the test region. The two lenses are eliminated and the image is received on a large beaded

---

* This is illustrated by the common experience of changing clarity of the lines in an optical image, as the object is moved away from the focal plane of a lens.

screen; this image may be photographed in the normal way.

The explanation given above applies to a focusing system where inhomogeneities in a given plane are recorded. On the other hand, the wide field system is not space-selective within the water and hence the recording screen indicates the "shadows" cast by temperature inhomogeneities throughout the depth of the test region. In this case the geometry of these inhomogeneities is distorted through variable magnification.

Figure 6.5 gives an example of the shadowgraphs as observed by each of these experimental arrangements. The upper photograph was taken with the confined - field system and it represents a vertical section of the water of about 7 cms. in diameter. Details of two or three isotherm patterns are readily distinguishable. The lower photograph was taken with the wide field system, showing the patterns through the full height of the water and extending laterally some 54 cms. The envelopes of the isotherms above the thermal boundary, in which the brighter contours represent fluid which is warmer than the environment, is clearly visible.

6.4 Organized Motion

Measurements of velocity in Section 6.1 provide information on local movement within the fluid. A sensitive indicate of systematic movements in a larger volume of the test region is helpful in studying convective structure. A simple technique for this purpose is illustrated in Figure 6.6 a. Here, white precipitate (skimmed milk diluted with water) is introduced slowly onto the underlying thermal boundary of the test region which is illuminated by a thin "curtain" of light from an external source.

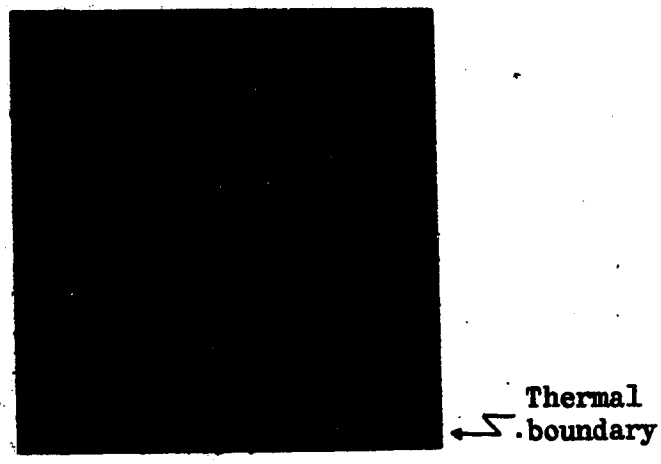

(a) Confined Field

(b) Wide Field

Figure 6.5 Examples of Isothermal Patterns in the Laboratory Simulation as Observed with the Two Arrangements of the Shadowgraph System.

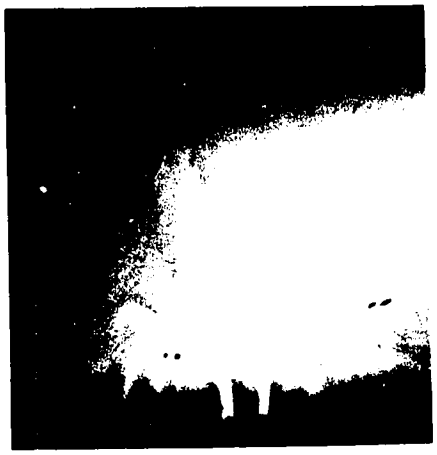

(a) Confined Field

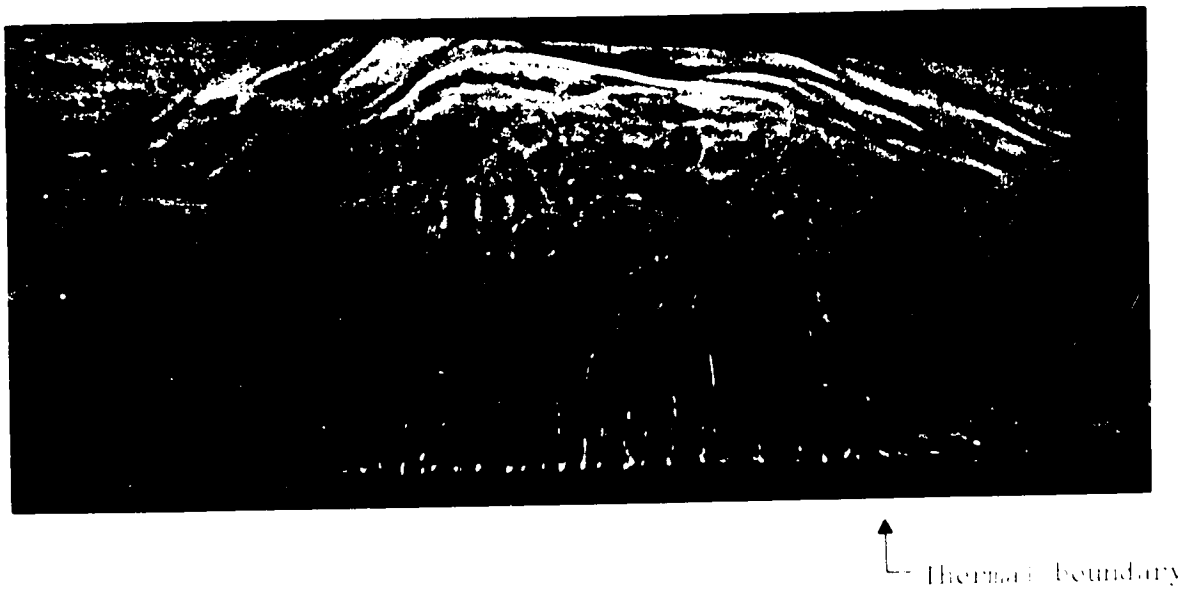

(b) Wide Field

Figure 5.2 Examples of Isothermal Patterns in the Laboratory Simulations as Viewed with the Two Arrangements of the Shadowgraph System.

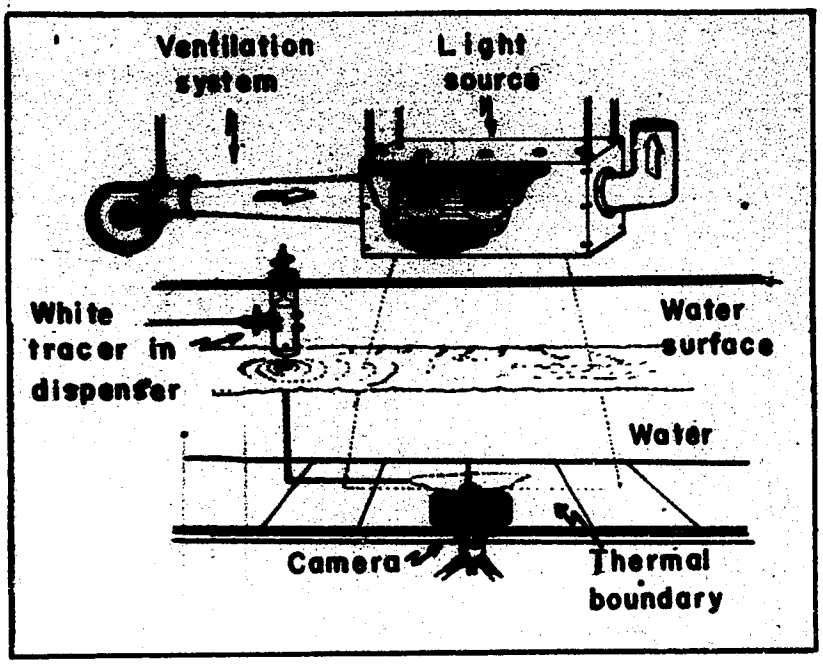

(a) Apparatus for observing the patterns of organized motion in the laboratory simulation.

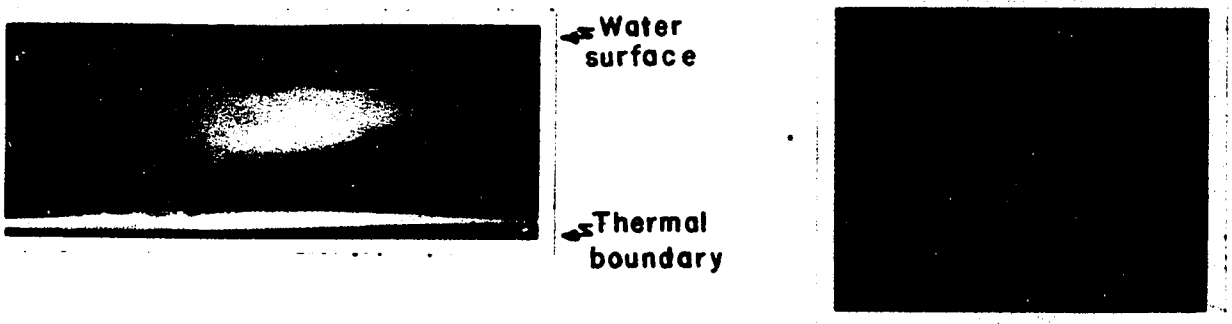

(b) Photographs of flow patterns above the heated boundary, in the water.

Figure 6.6 Technique for Observing Systematic Movements within a Large Region of the Test Section (Simulation).

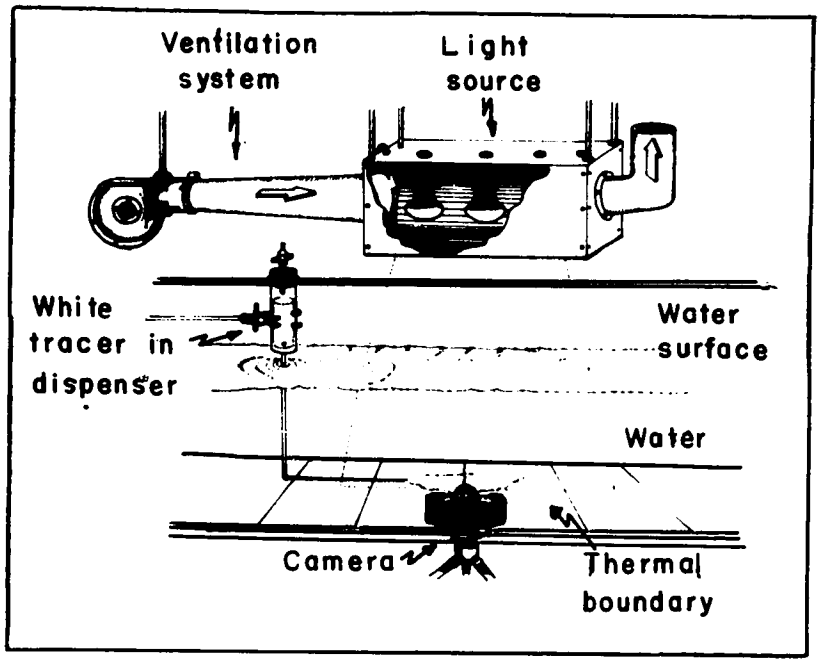

(a) Apparatus for observing the patterns of organized motion in the laboratory simulation.

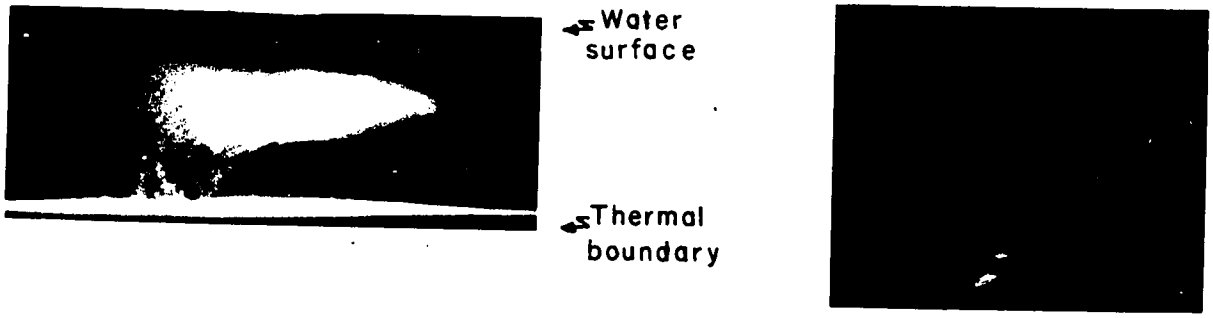

(b) Photographs of flow patterns above the heated boundary, in the water.

Figure 6.6 Technique for Observing Systematic Movements within a Large Region of the Test Section (Simulation).

The dispersal pattern of the white indicator then, is recorded photographically. Both horizontal and vertical sections of the test region are observed, by appropriate orientation of the illumination and the camera. Figure 6.6 b shows two sample photographs obtained by this procedure.

6.5 Fluid Temperature

Measurement of water temperature in the laboratory simulation is carried out with thermistor probes of rapid response and good spatial resolution. Figure 6.7 shows the details of the probe mounting and water tight seal*. For the present study, it is desirable to observe temperatures in the water simultaneously at several locations. Figure 6.8 shows two probe arrays for this purpose, one with fixed

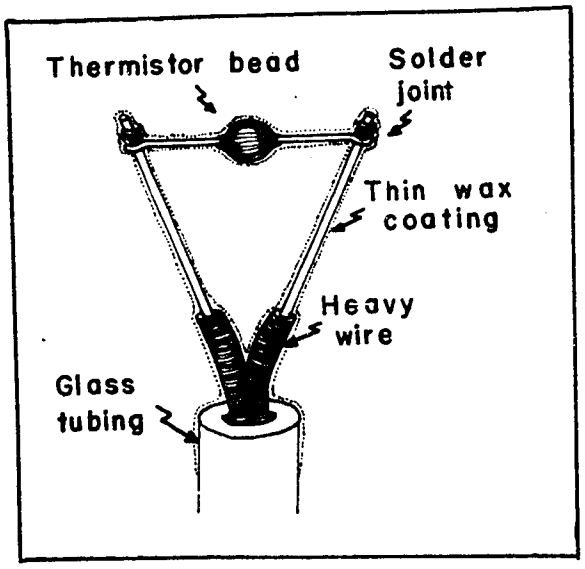

Figure 6.7 Details of the Temperature Probe Mounting.

---

* The thermistor is described in Section 6.2. Its measured thermal lag in moving water is 0.17 sec. (See Appendix V). The wax coating provides a good seal against water for period exceeding 160 hours.

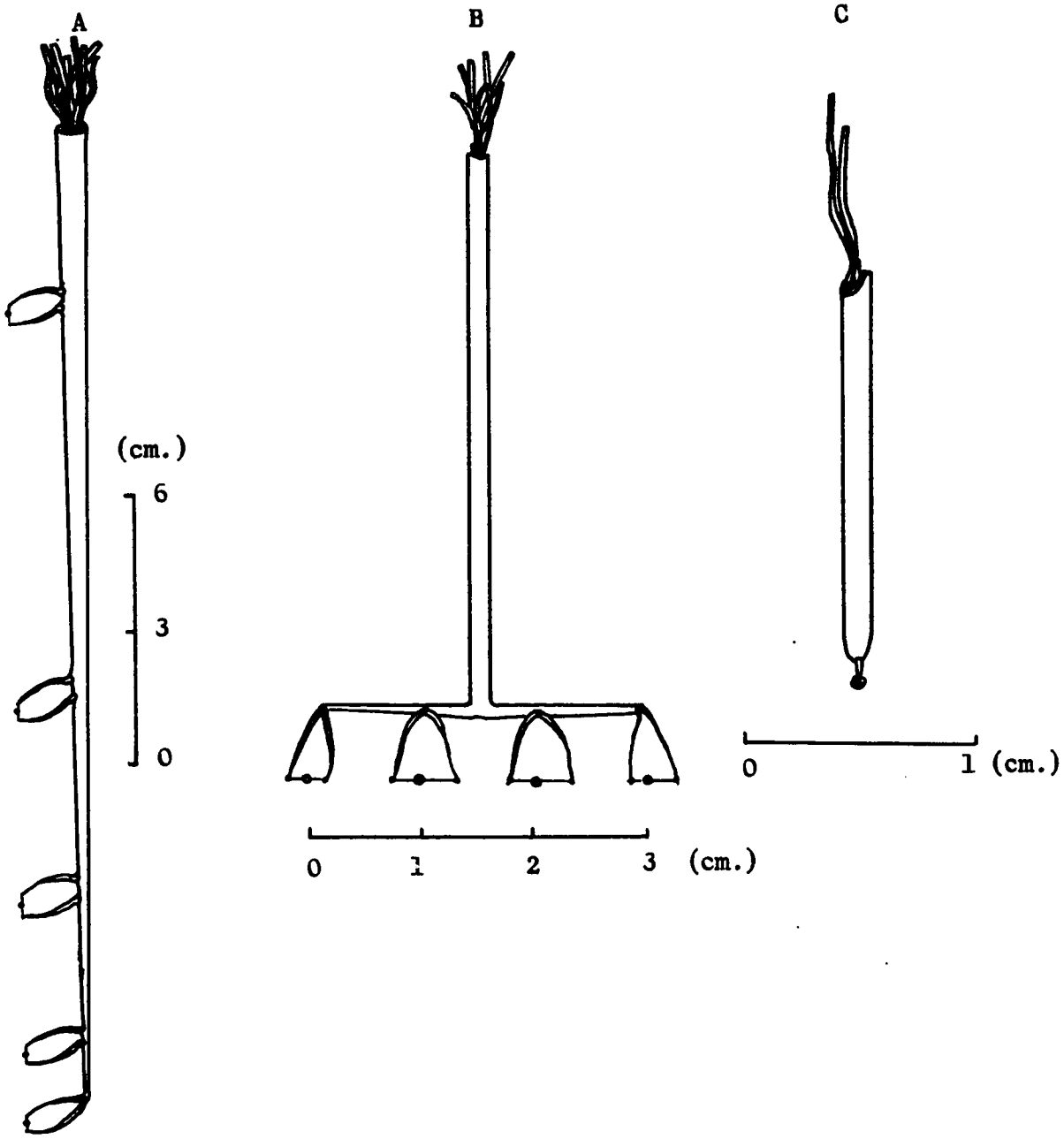

Figure 6.8 Three Types of Mounting for Thermistor Probes.

vertical spacing and the other with fixed horizontal spacing. A third mounting contains a single probe. Each of these mountings has been designed for negligible disturbance of the water as the probes are moved through the water, by the technique described below.

The method of moving the probes systematically through the water is illustrated in Figure 6.9. Here, provision is made for transport of the probe array in any selected vertical plane. A motor drive controls the uniform movements of one probe in the vertical and another in the horizontal, at a speed of 0.2 cm sec^{-1}. The direction of motion is reversed automatically at the end of each transit. The position of the probe in the water is indicated by a series of electrical contacts which provide voltage impulses for an external recorder. A photographic study of the probe motion has shown that these contacts locate the probe position with an accuracy of $\pm$ 0.1 cm. in the vertical and $\pm$ 0.3 cm. in the horizontal. The time required for a full horizontal transit of the test region is about 7 minutes.

Each thermistor probe is connected through flexible leads to a Wheatstone bridge and chart recorder system. Separate bridge networks are used for each thermistor and the unbalance voltages of the bridges are measured with a 6 - channel Sanborn Recorder*. The methods of aging and calibrating these probes have been described in Section 6.2.

A sample chart recording of the temperature variations in the water above the heated boundary is shown in Figure 6.10. It will be noted that changes in temperature as small as 0.1°C are readily

---

* Sanborn Model 67-300 recorder amplifier and Model 152-100A Recorder.

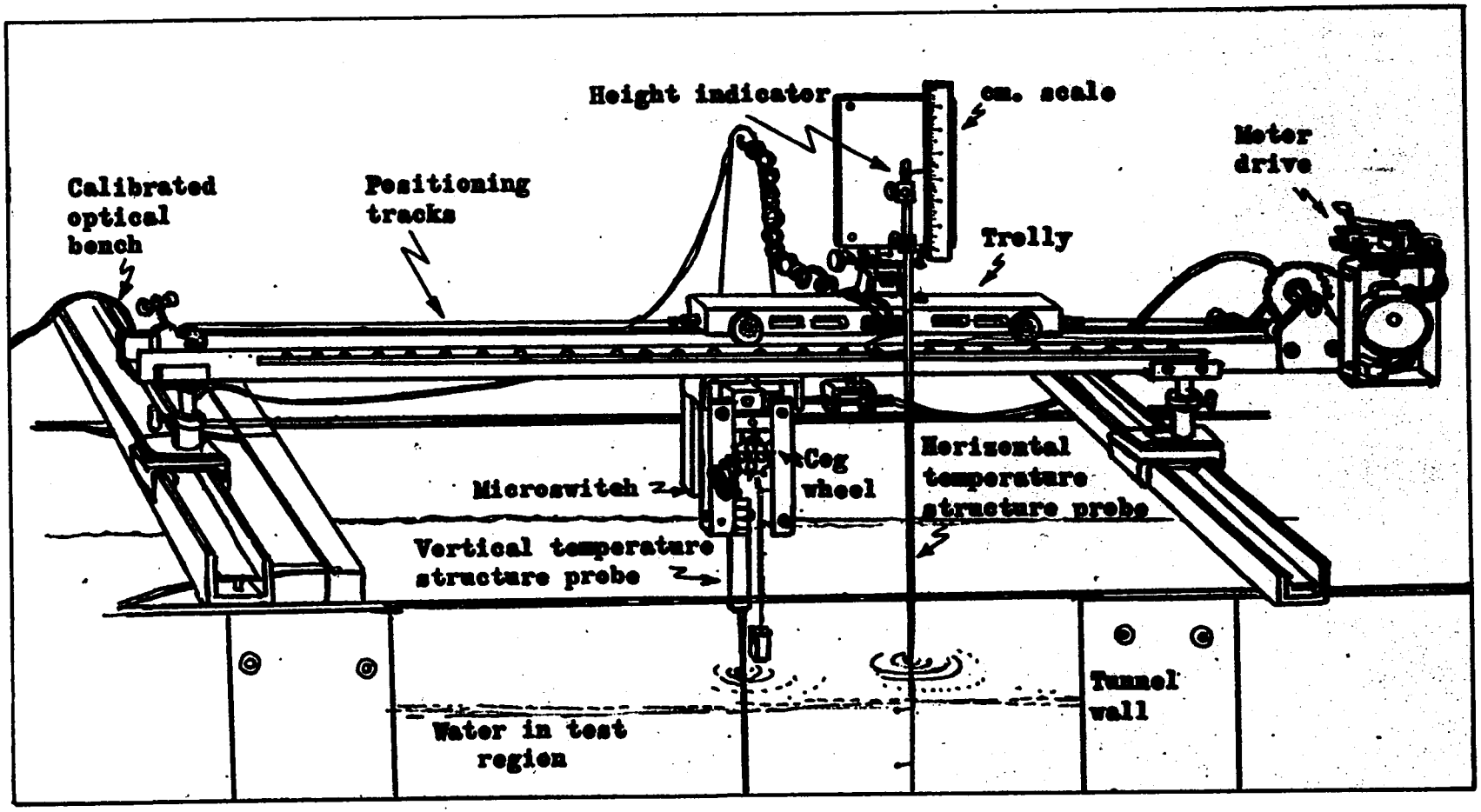

Figure 6.9 Mechanical System for Moving the Temperature Probes through the Test Region of the Simulation.

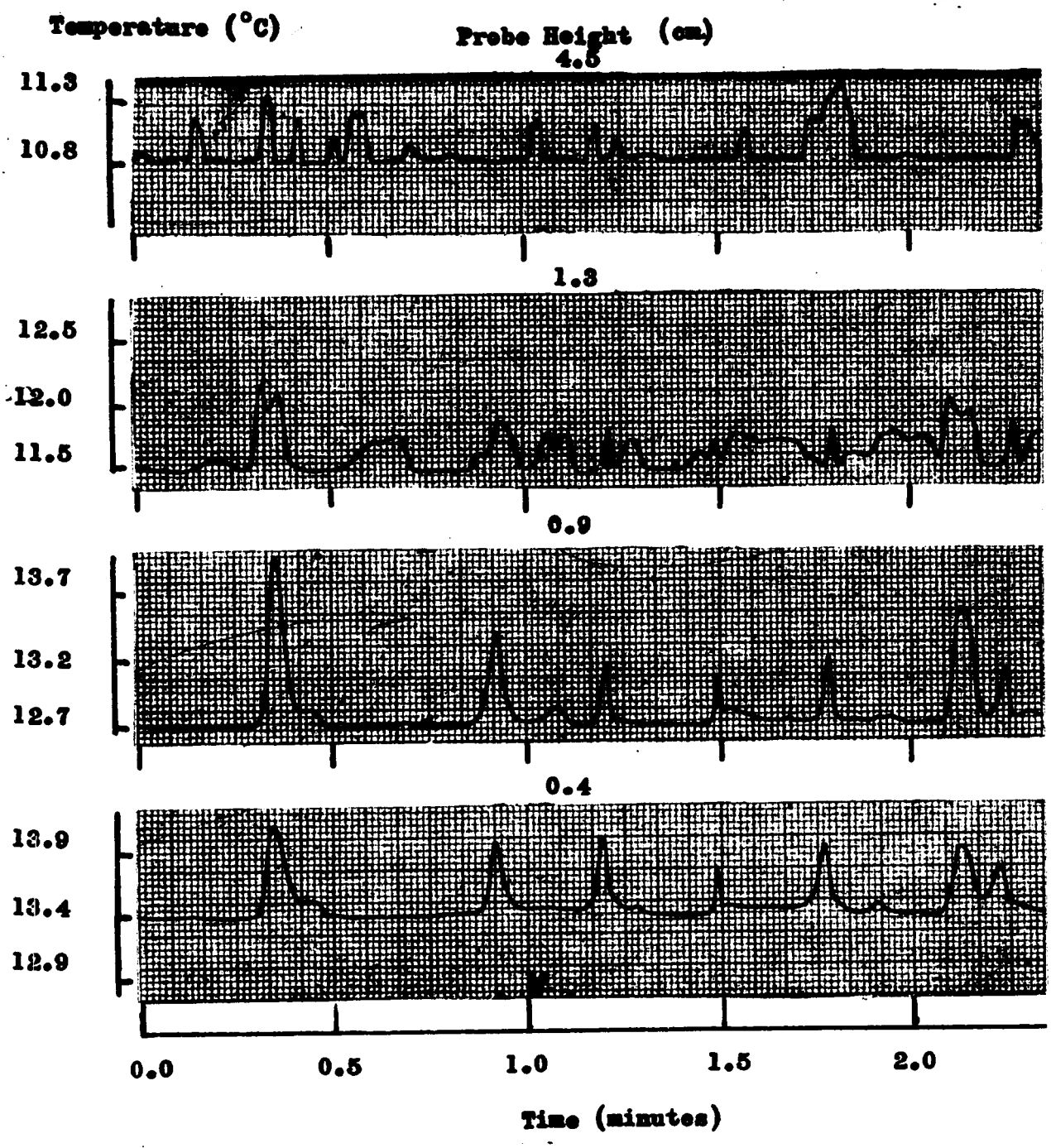

Figure 6.10 Sample Recording of Temperatures in the Vertical Plane, at the Indicated Heights above the Lower Boundary. Probe A of Figure 6.8 was Used in a Horizontal Transit through the Water.

observed. Examination of the bridge and recorder stability was made by changing the room temperature 10°C for an interval of 47 minutes; drift in the indicated temperature, due to circuit components other than the thermistor probe, was less than 0.05°C.

CHAPTER VII

OBSERVED PROFILES OF TEMPERATURE AND FLOW IN THE SIMULATION

The observing techniques of the previous chapter have been used to examine the distributions of temperature and velocity within the test region of the laboratory simulation. The initial condition in the simulation represents the lower troposphere in which the vertical gradient of temperature is in the range from isothermal to adiabatic. Some residual heating of the lower boundary is introduced and the resultant patterns of convection are examined for the absence of general horizontal flow (natural convection) and for moderate horizontal flow (free convection).

Laboratory dimensions are used throughout the present chapter. The conversion to the scale of the lower troposphere (prototype) will be included in the discussion of later chapters.

The experimental observations are presented under three general headings. The first will clarify the coordinate system and setting up of the boundary conditions in the test region, During the initial heating of the lower boundary, the simulation is in a transitional stage and the observed temperature and flow patterns describe the approach to stationarity, in the second division. In the third division, the temperature of the lower boundary has become constant and the processes of convection are stable; detailed mapping of temperature throughout the test region is possible only during this

stable condition, because of the prolonged interval (20 minutes) needed to move the probes without disturbing the convective patterns.

7.1 The Boundary Conditions

The coordinate reference system for the experimental observations is shown in Figure 7.1. It will be seen that the origin is located at

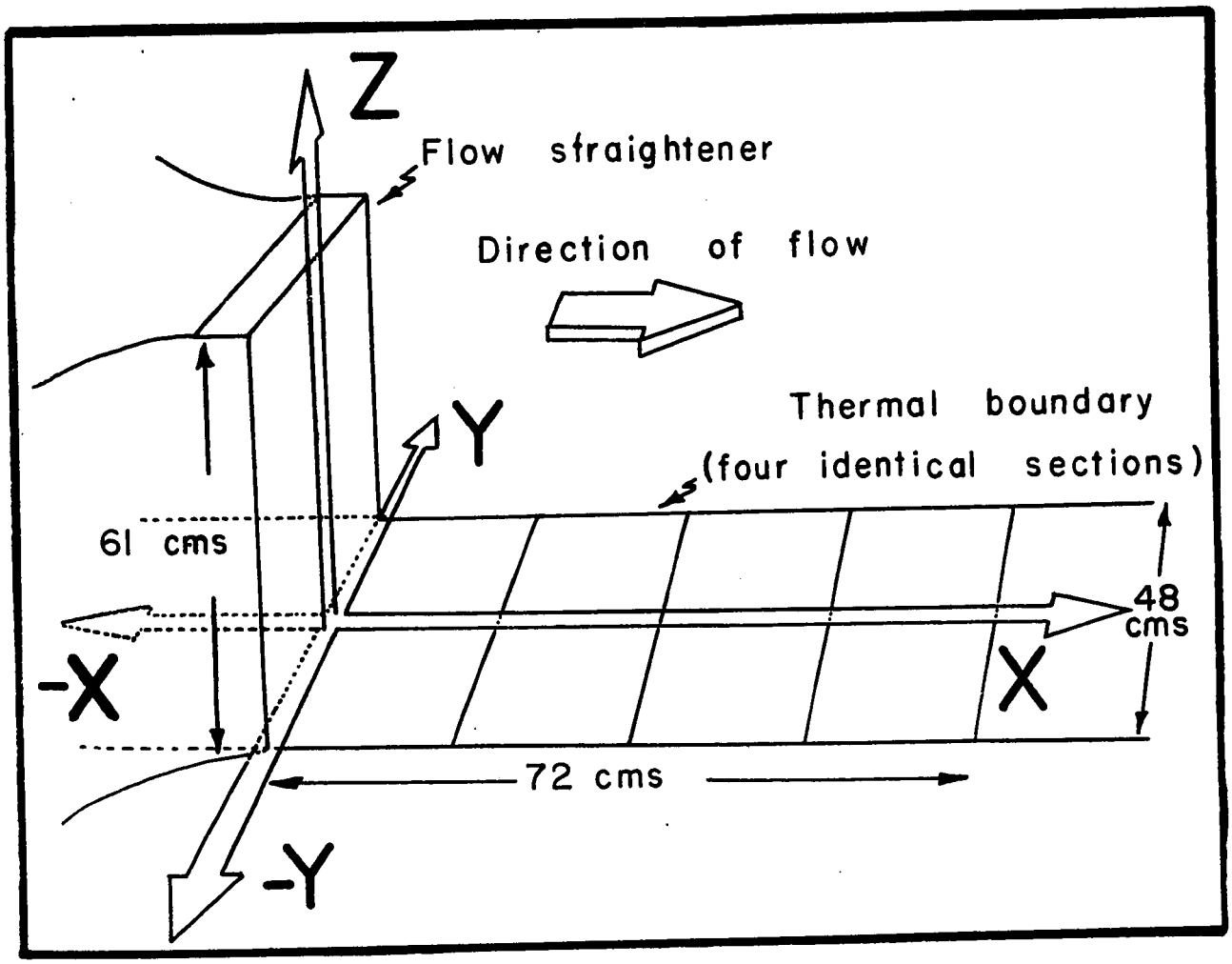

Figure 7.1 Coordinate Reference Axes in the Test Region of the Laboratory Simulation

the intersection of the thermal boundary axis and the face of the flow straightener. Only the first three sections of the lower boundary are heated ($0 < x \leq 54$ cms.; $-24 < y \leq 24$ cms.). For the special case of natural convection, in which general flow is absent, the flow straightener is removed and the lower boundary is continued smoothly

in the negative x-direction by the addition of a varnished wooden slab to preserve symmetry about the heaters.

The effect of discontinuities in the boundaries upon the models of convection will be considered below. These occur in the (x = 0) plane for natural convection and for both natural, and free convection in the (y = $\pm$ 24) planes, the (x = 54) plane and the (z = 25) plane of the upper surface of the water.

Most of the observations described in later sections were made in the centre of the test region to avoid edge effects. Unless stated otherwise, these are at coordinates (27, 0, z).

7.1a General Horizontal Flow

The initial step in preparing the simulation requires the introduction of water into the tank to a height of 25 cms. above the thermal boundary at a temperature 10°C below room temperature. During this time the water is mixed thoroughly by circulation. Subsequently, the rate of flow is adjusted to the desired value by controlling the input to the impeller.

The boundary conditions for this initial setting are stated readily from the vertical profiles of temperature (T) and horizontal velocity (U). Figure 7.2 shows typical profiles, as observed above the centre of the test region. It will be seen that the lower boundary and water are in thermal equilibrium and that temperature is constant with height. The horizontal velocity (along x-axis) increases with height above the boundary until it reaches a limiting maximum. It is this maximum or "free stream" value (U_f) which will be used to specify the general horizontal flow. The physical significance of the velocity gradient at the lower surface, as it applies to the surface in the

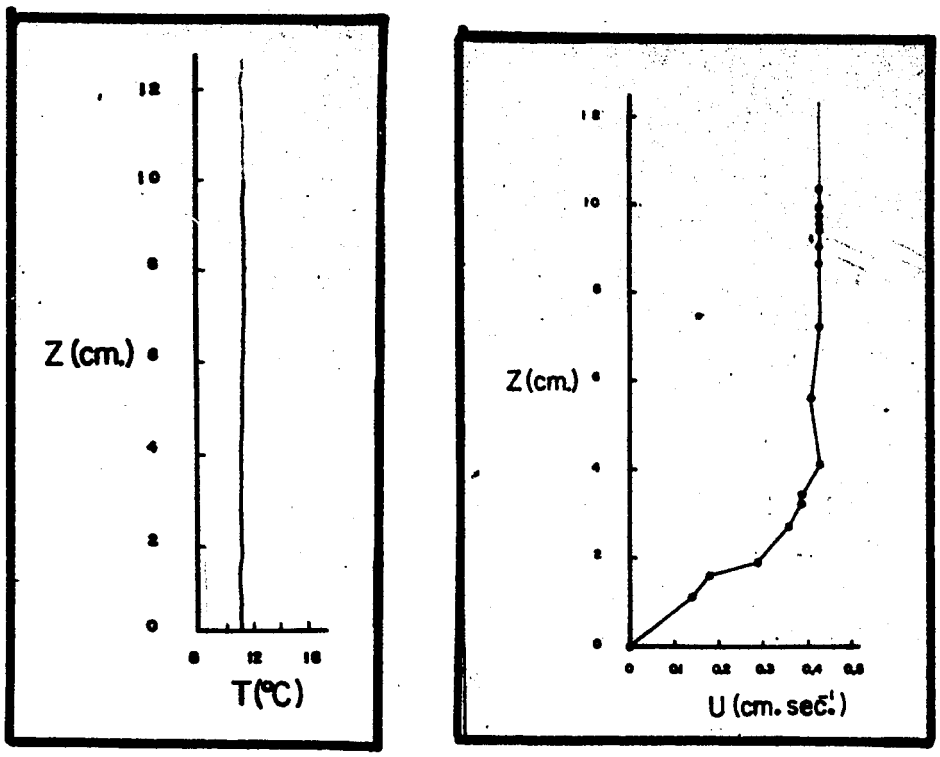

(a) (b)

Figure 7.2 Vertical Profiles of Water Temperature and Horizontal Velocity, during the Initial Setting of the Simulation.

prototype, will be examined in the next chapter.

7.1.b Vertical Profile of Temperature

The isothermal profile of temperature in Figure 7.2 represents a condition that may occur in the lower troposphere during the transition between daytime and nighttime and also when the air is well mixed below an overcast sky.

The important feature of the mean temperature profile for the present study is its vertical gradient. It is this gradient which determines the rate of heat transfer, in conjunction with the diffusion coefficient. Hence, the actual fluid temperature will not be considered further here, and temperature profiles will be described by their gradients.

All vertical profiles of mean temperature in the present study will have gradients that are close to the zero-gradients of Figure 7.2. Small departure will be due to residual heating of the underlying

boundary as described below*.

7.1.c Heating of the Lower (Thermal) Boundary

After the initial preparation of the laboratory simulation, the heaters in the lower boundary are energized to provide heat for perturbation of the stably-stratified fluid.

The change in temperature of the thermal boundary has been examined during the progress of heating. Figure 7.3 shows how the boundary temperature increases with time, for different heating rates; separate graphs are given for the maximum and minimum flow speeds of water above the boundary. For all settings, thebboundary temperature becomes constant about 200 minutes after heating is initiated. Then, experimental observations on fluid convection during the first 200 minutes of heating will be described under the heading "Approach to Stationarity"; observations following this period are given in the section headed "Stationary Boundary Temperature". This division is primarily for experimental convenience.

An estimate may be made of the residual heat flux from the

---

* Two approximations in the governing equations, which led to the conditions for laboratory simulation in Chapter III, require that the vertical gradient of mean temperature in the troposphere be less than $0.1^{\circ}C$ per meter and that this gradient change by less than $0.01^{\circ}C$ meter^{-2}. These requirements are restated in the simulation units as $5^{\circ}C$ per millimeter and $5^{\circ}C$ mm^{-2}, respectively. All temperature gradients in the observations of this chapter satisfy these requirements.

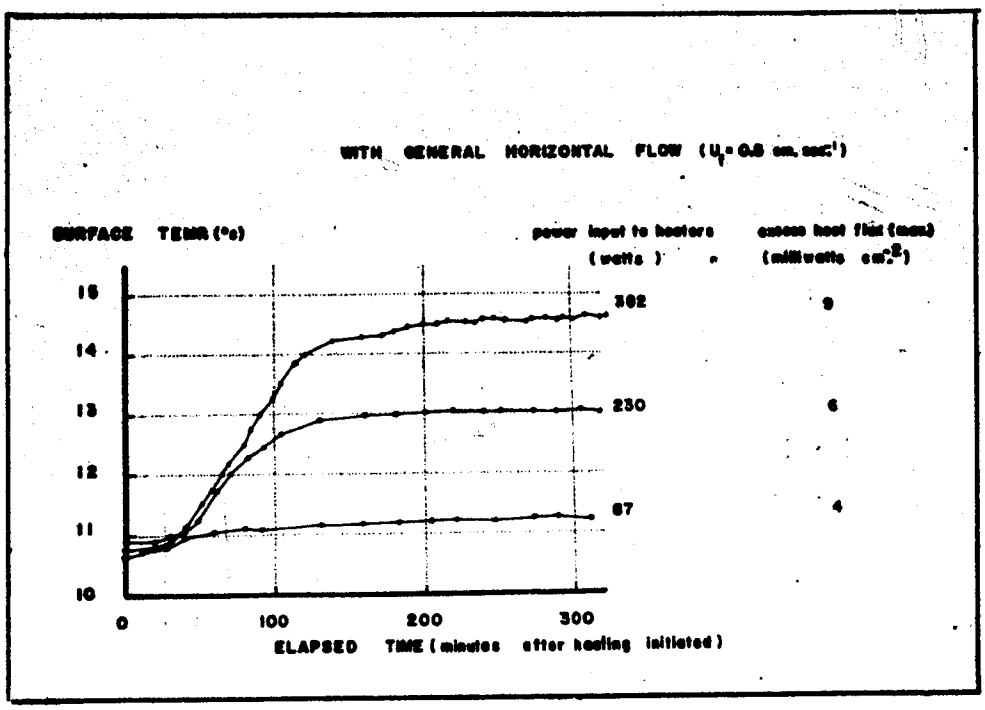

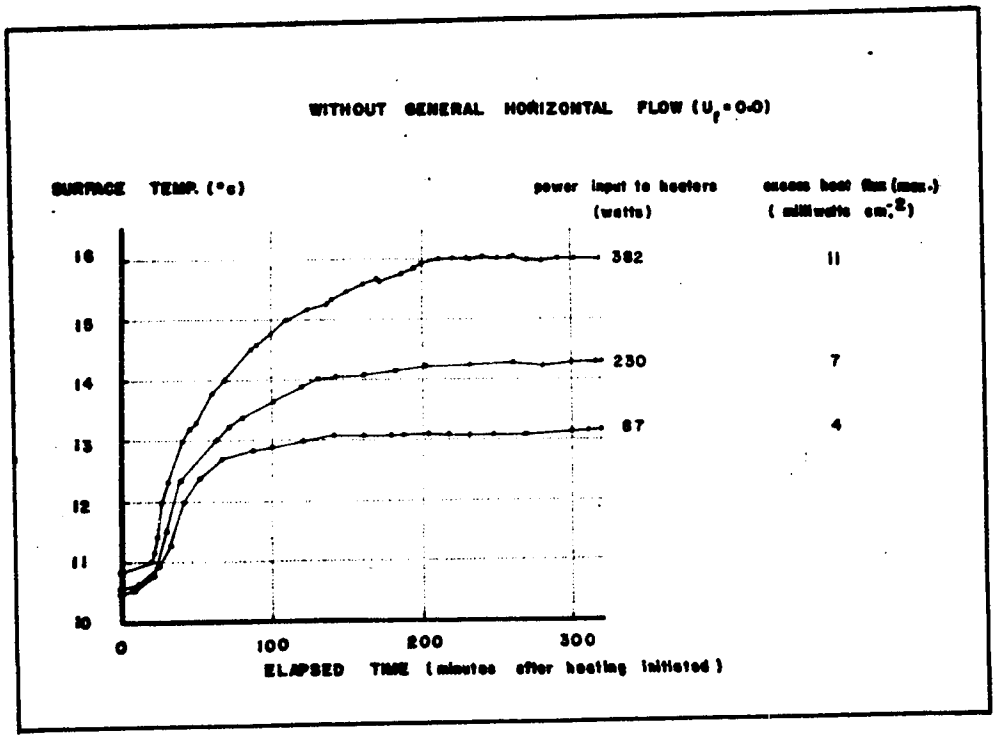

Figure 7.3 Approach to Stationarity of the Surface Temperature of the Underlying Boundary.

lower boundary into the water for each heating rate. For one-dimensional heat flow, the flux H_s (cal. cm^{-2} sec^{-1})* is (see, e.g. Munn 1966, p. 33),

$$H_s = -K \frac{\partial T}{\partial z} \qquad 7.1$$

where K is the molecular thermal conductivity (0.0014 cal. cm^{-1} $sec^{-1}{}^{o}C^{-1}$). The temperature gradients at the surface for each heating rate are obtained from temperature profiles reported in later sections. Then the residual heat fluxes at stationary boundary temperature are deduced from the above equation and noted on the curves in Figure 7.3.

7.1.d Edge Effects

A preliminary examination of the extremities of the test region has been made in order to assess the edge effects upon the simulation of convection. This includes observations of the temperature profiles, isotherm contours and flow patterns. Of special importance are the regions above the edges of the lower boundary and below the water surface for natural convection ($U_f = 0$) and the vertical profiles of horizontal flow at various distances away from the flow axis for free convection ($U_f \neq 0$).

Figure 7.4 illustrates several features of temperature fluctuations above the edge of the lower boundary for natural convection. The shadowgraph shows that complex isotherm patterns begin about 3 cms. in from the edge of the boundary. Between these and the edge of the

---

* The residual heat flux in the prototype (H_p) is related to H_s by the following relation $H_p = 3\ 10^{-2} H_s$.

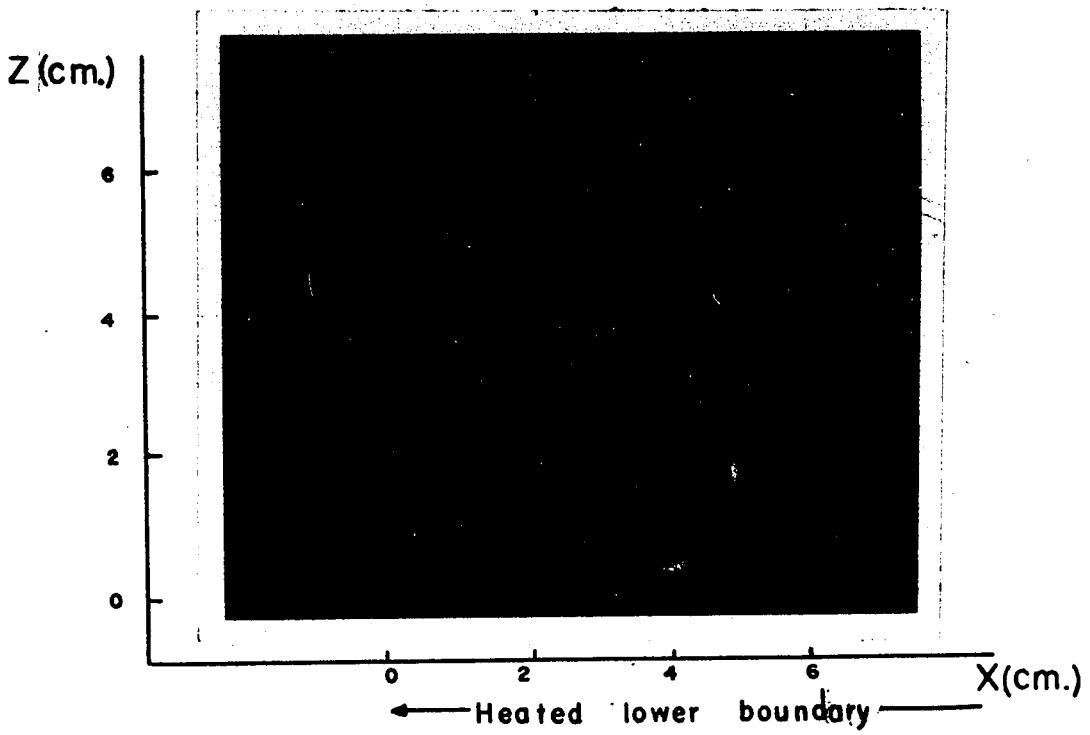

(a) Isotherms contours above the edge of the thermal boundary.

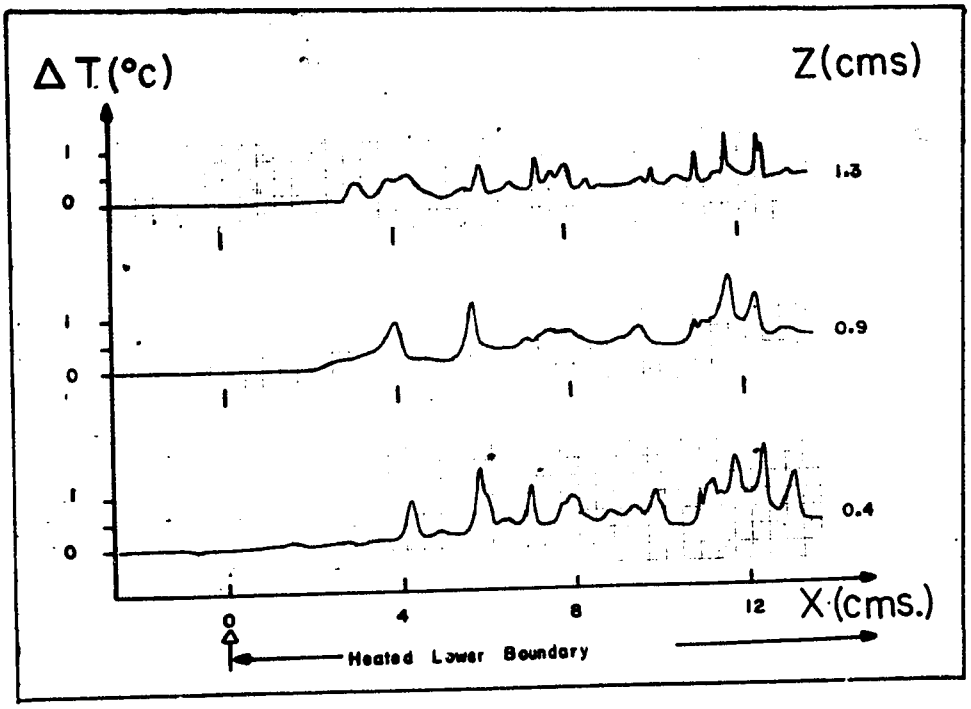

(b) Temperature perturbations taken simultaneously at three heights above the edge of the thermal boundary.

Figure 7.4 Isotherms and Temperature Profiles in the Y=0 Plane near the Edge of a Thermal Boundary for Natural Convection (U_f=0) and Maximum Heating of the Boundary (Excess Flux = 11 milliwatts cm^{-2}).

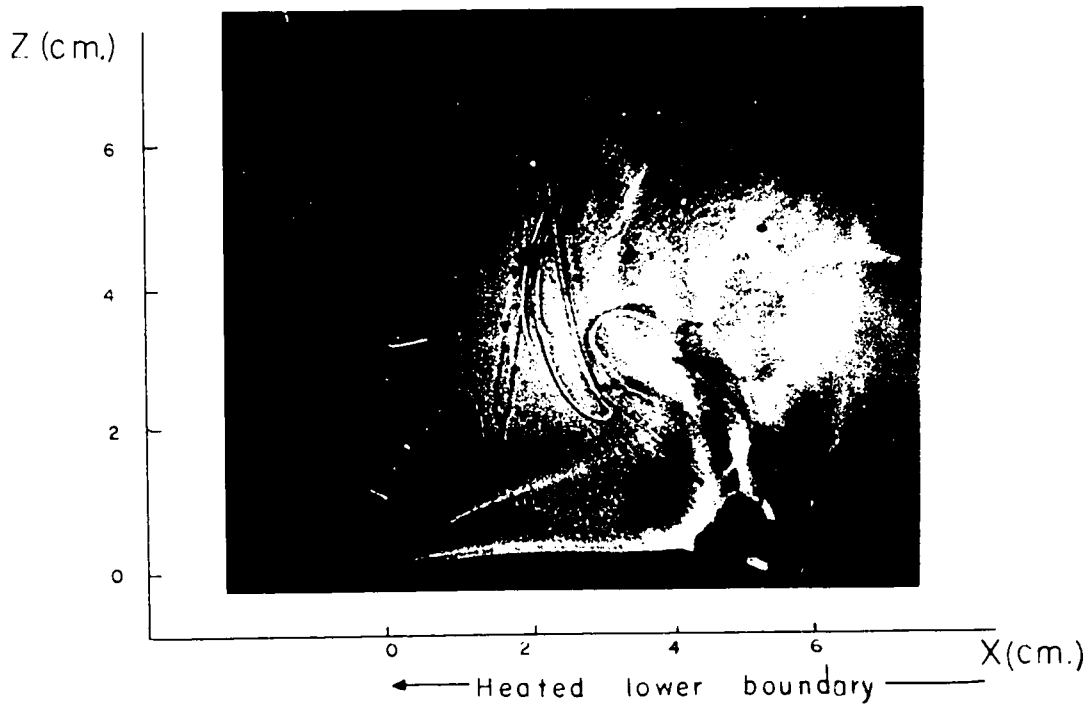

(a) Isotherms contours above the edge of the thermal boundary.

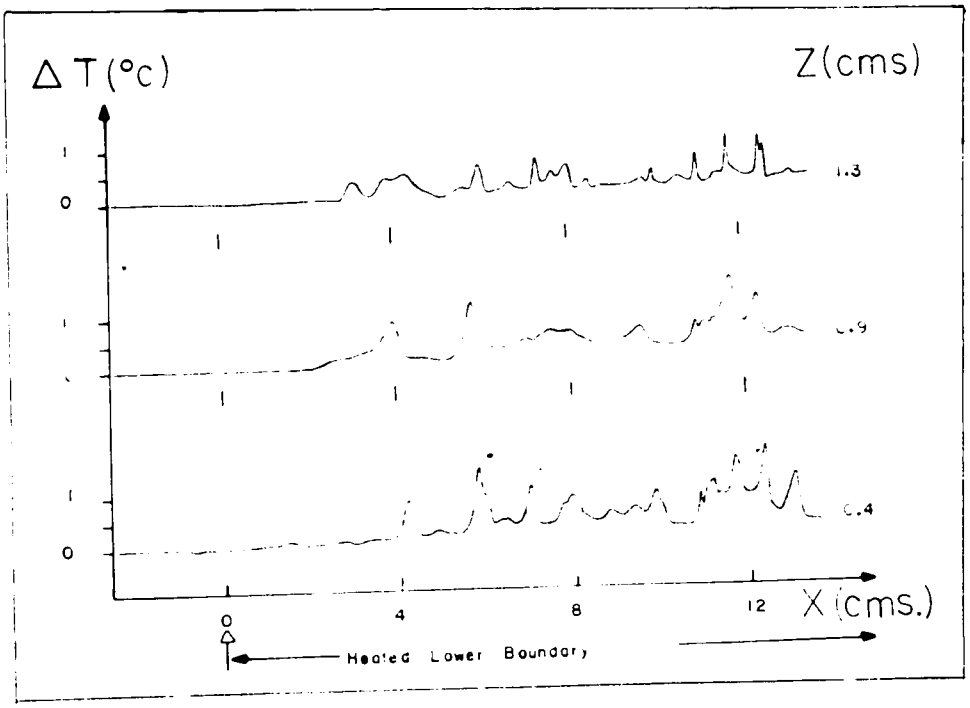

(b) Temperature perturbations taken simultaneously at three heights above the edge of the thermal boundary.

Figure 7.4 Isotherms and Temperature Profiles in the Y 0 Plane near the Edge of a Thermal Boundary for Natural Convection (U_f 0) and Maximum Heating of the Boundary (Excess Flux 11 milliwatts cm^{-2}).

boundary, the shading suggests that the warmer fluid just above the boundary and the cooler fluid beyond the edge of the boundary merge in more regular fashion. The temperature profiles indicate that the temperature perturbations of the isotherm profiles are about 1°C relative to the ambient temperature. At distances greater than about 5 cms. in from the boundary edge, the perturbations appear to be well established.

Vertical profiles of horizontal velocity of the type shown in Figure 7.2 have been observed at various positions above the thermal boundary. At all positions, the "free stream" velocity (U_f) is maintained to heights of 16 cms. or more. Above this, the velocity decreases irregularly towards a minimum at the upper surface of the water. For a given setting of the flow impeller, maximum U_f is measured near the centre of the flow straightener; the decrease in U_f along the central flow axis is about 30 percent and lateral to the flow is about 15 percent, to the edges of the boundary. Hence, the vertical profiles of horizontal flow are well behaved at heights less than 16 cms. in the simulation, although adjustment of the impeller may be required for a specific value of U_f over a given part of the lower surface.

How the upper surface of the water limits vertical motion for natural convection is considered next. Figure 7.5 shows the velocity field in the vertical plane above the boundary with one heated section. Inspection of the central portion suggests that vertical motion is affected significantly by the upper surface only at heights greater than 16 cms. It is not clear to what extent the large scale circulation is modified by the water surface, but it

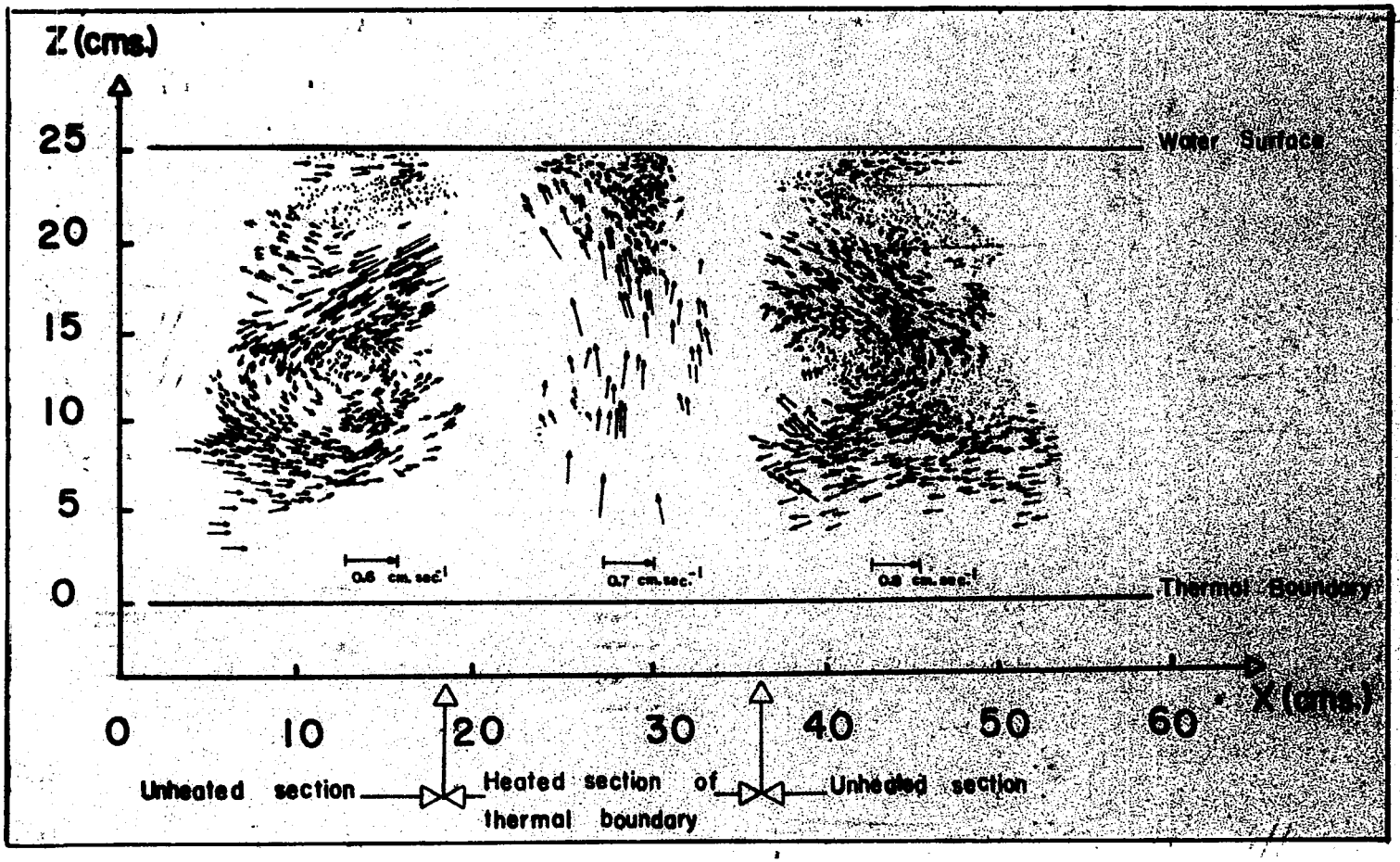

Figure 7.5 The Velocity Field in the Central Vertical Plane (Y=0) above the Thermal Boundary, for Natural Convection (U_f=0), with only One Section Heated (Excess Heat Flux = 11 milliwatts $cm.^{-2}$).

appears that local convection is not changed appreciably within the heights of interest in the present work.

The preceding observations suggest that edge effects in patterns of convection should be small if measurements are confined to the lower 10 or 15 cms. of the fluid and at least 5 cms. from the sides of the thermal boundary. All further observations have been made close to the central (Y = 0) plane of the thermal boundary for this reason and regions have been avoided for which asymmetrical convection patterns occur that may be attributed to edge effects.

7.2 Approach to Stationarity

Vertical profiles of water temperature, horizontal flow and the isotherms in the water have been recorded during the initial heating period of the lower boundary. Because of the slow scanning speed of the temperature probes, the temperature records are used here only to indicate the approximate magnitude of temperature fluctuations. However, rapid changes in the isotherm patterns may be detected readily in a succession of shadowgraphs.

7.2.a For Natural Convection ($U_f = 0$)

Figure 7.6 illustrates the growth of the temperature perturbations in the water as heating of the thermal boundary progresses. Initially, the water is at uniform temperature throughout the depth of interest and no detail is apparent in the shading of the shadowgraph. 44 minutes later a relatively strong gradient in temperature has developed at the lower boundary, corresponding to a brightening of the gray background in the shadowgraph; at the same time, temperature

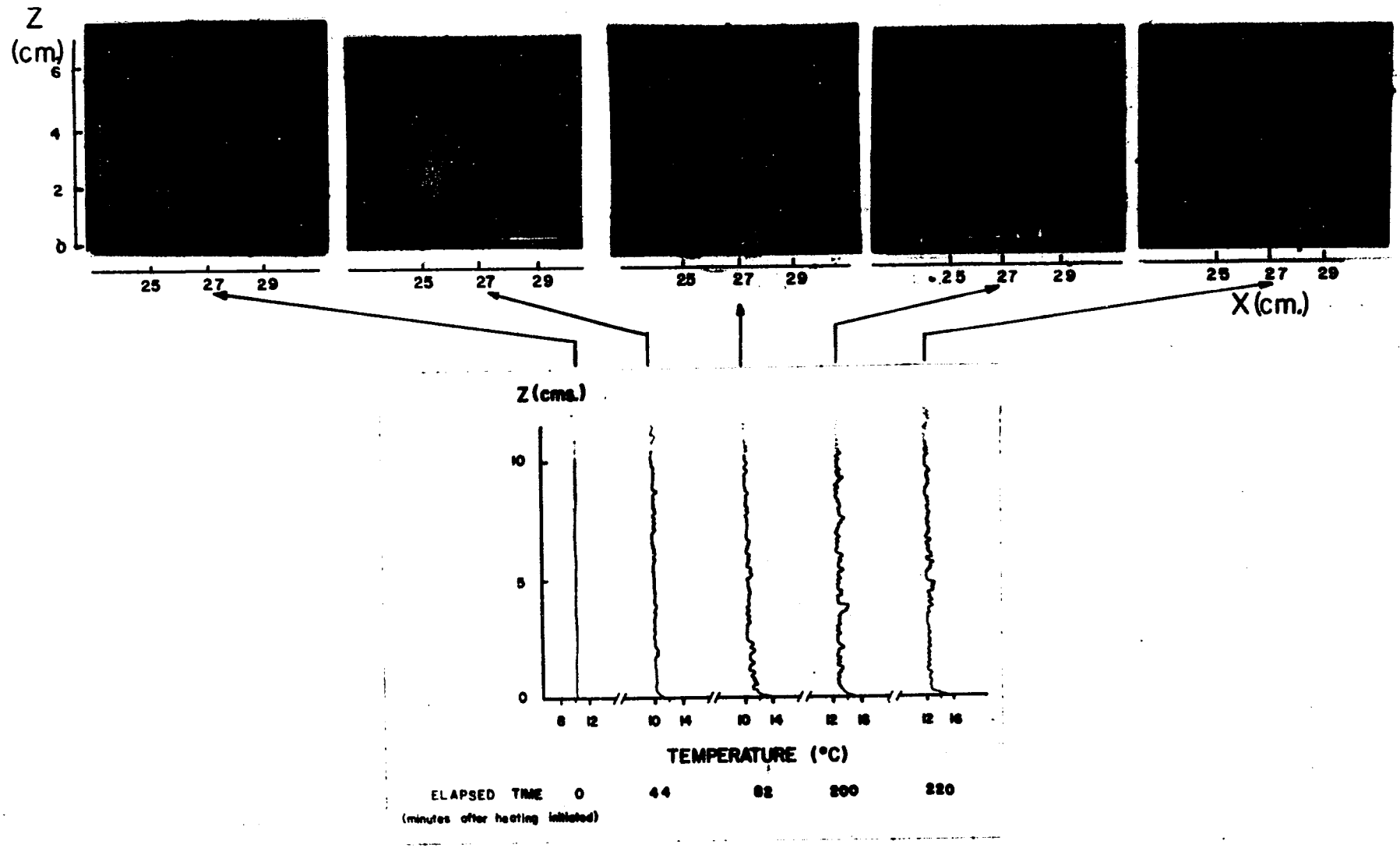

Figure 7.6 Growth of Temperature Perturbations and Isotherm Contours above the Thermal Boundary during the Initial Heating Period (U_f=0; Power Input to Heaters = 382 watts).

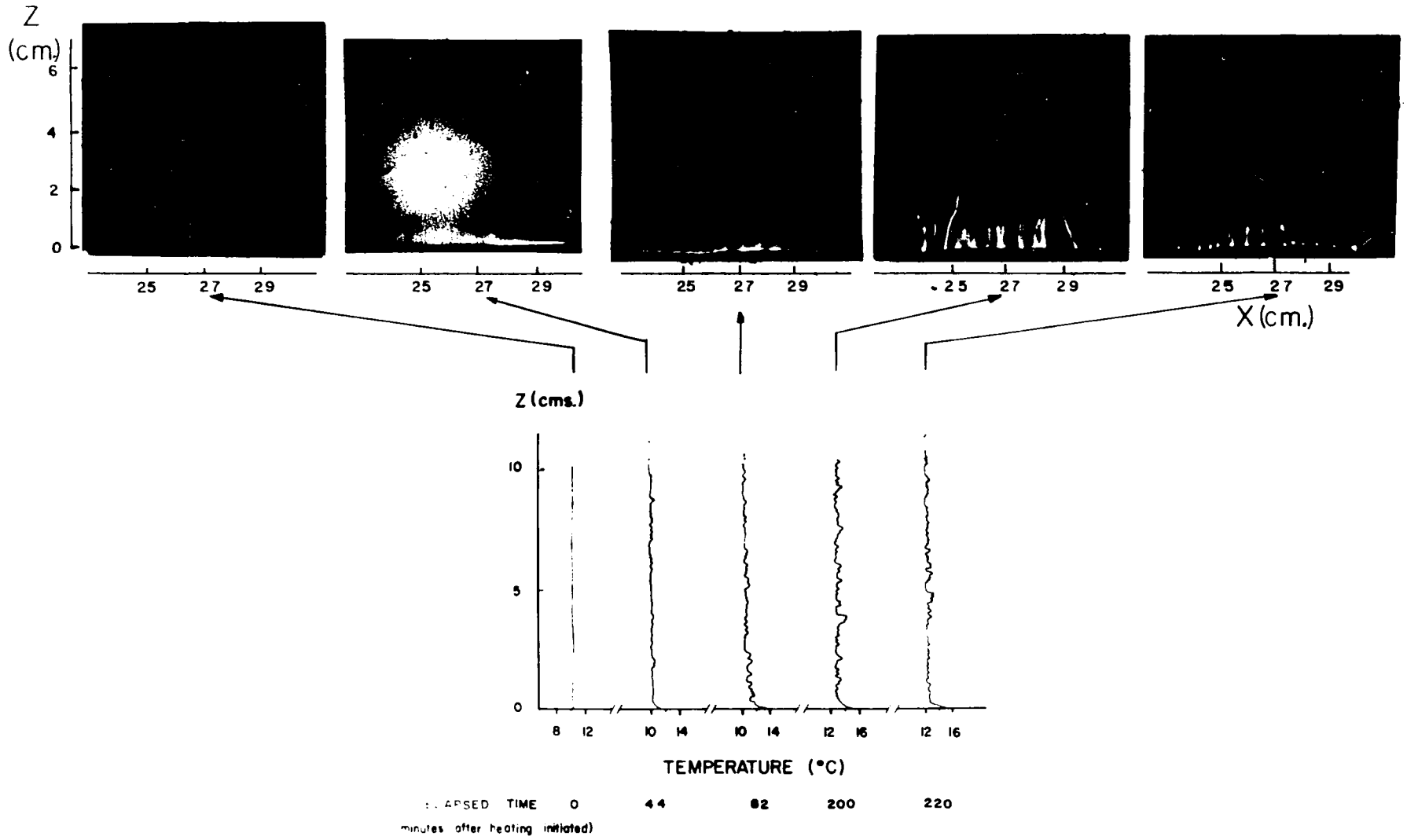

Figure 7.6 Growth of Temperature Perturbations and Isotherm Contours above the Thermal Boundary during the Initial Heating Period (U_f=0; Power Input to Heaters = 382 watts).

fluctuations of the order 0.5°C are superimposed upon the isothermal profile to heights exceeding 10 cms. and few streaks or columns of shallow contrast extend upwards from the surface in the shadowgraph. After 82 minutes, the temperature fluctuations on the isothermal background are about 1°C near the surface, decreasing to 0.5°C at a height of 10 cms.; the shadowgraph patterns have become more complex and more contrasted just above the surface, with a suggestion of cap-like contours (concave downwards) in the upper region. The last two sets of contours, observed more than 200 minutes after heating of the lower boundary began, have similar features. This suggests that stationarity in the convective process has been reached, at least for a period of about 20 minutes. There, the temperature fluctuations on the isothermal background exceed 1°C at lower levels and the bright streaks in the shadowgraphs show high contrast within 2 cms. of the boundary. The horizontal separation of these columns at the boundary is irregular, with a mean of about 0.7 cm.

Details on the growth of the bright streaks or columns in the shadowgraphs are shown in Figure 7.7. This series of photographs was obtained at intervals of 1 second. Two columns are of special interest, as indicated at (a) and (b). These appear to rise approximately vertically out of the boundary interface, upwards towards concave "caps". It will be seen that the "cap" of (a) rises at a rate of about 0.6 cm.sec^{-1}. Above column (b), the "cap" seems to disintegrate eventually or to join with an adjacent column in extending further aloft. In Chapter VI it was pointed out that a bright region in the shadowgraph results from fluid which is warmer

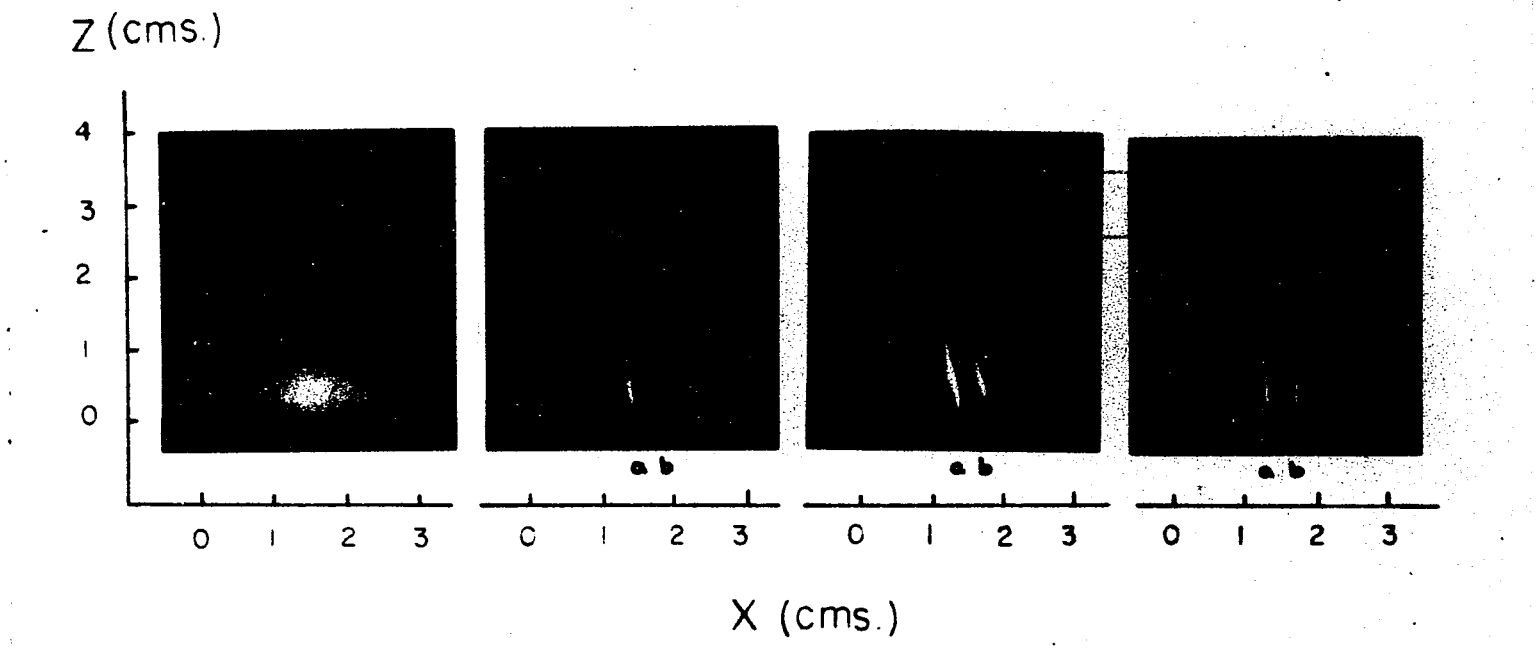

t (Seconds)	Before heating	0	1	2

Figure 7.7 Shadowgraph Detail of the Growth of Convective Patterns above the Lower Boundary (U_f=0; Power Input to Heaters = 382 watts). These photographs were taken during the approach to equilibrium.

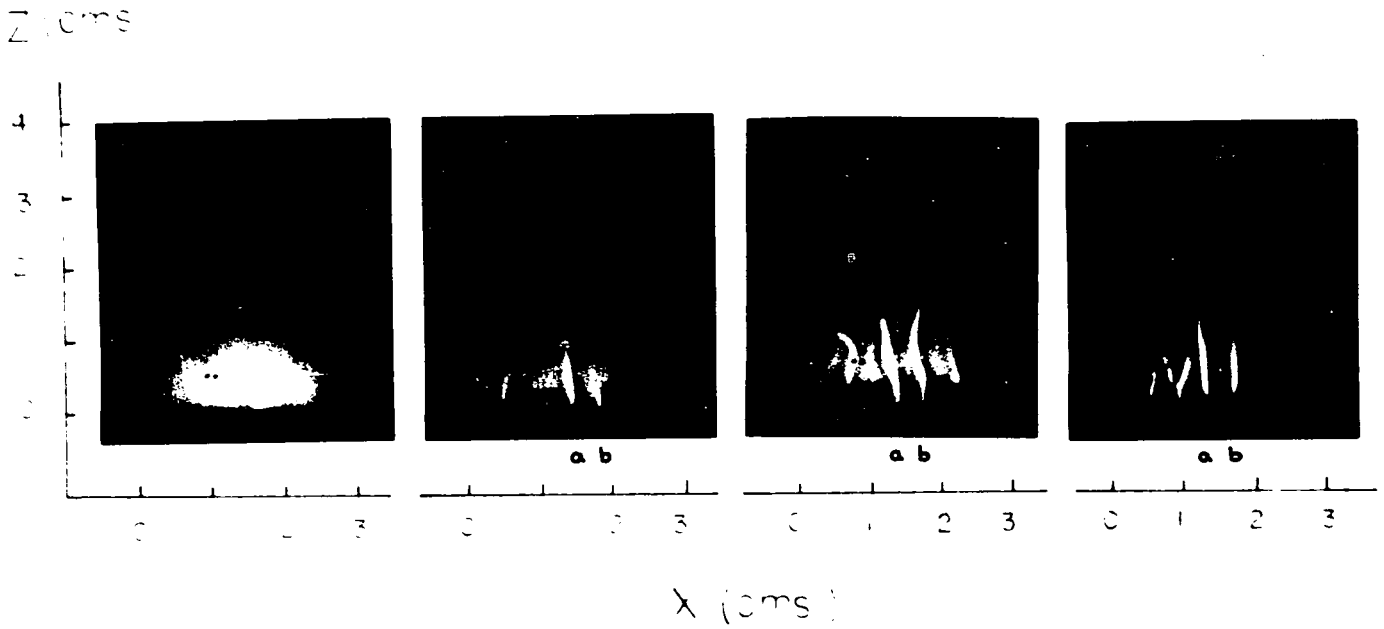

t (Seconds)	Before heating	0	1	2

Figure 7.7 Shadowgraph Detail of the Growth of Convective Patterns above the Lower Boundary (U_f=0; Power Input to Heaters = 382 watts). These photographs were taken during the approach to equilibrium.

than its environment; consequently, these growing columns appear to convey heat aloft from the warm underlying surface to an umbrella-like region which may maintain its shape as it rises or may disintegrate into a vertical extension of the lower column.

7.2.b For Free Convection (U_f = 0.4 cm. sec.$^{-1}$)

The effect of general horizontal flow on the temperature and velocity contours is illustrated in Figure 7.8. The power dissipation of the heaters in the lower boundary is the same here as in Figure 7.6. It will be seen that there are four principal interactions between the flow and the convection: the free stream velocity (U_f) increases about 20 percent as the heating of the water progresses (for fixed setting of the impeller); the fluctuations of the temperature are confined to the lowest 4 cms. of the water; the mean temperature gradient is slightly negative in the region of the fluctuations but slightly positive at levels above this; and the shadowgraph columns or streaks generally are inclined to the vertical with their upper extremities tending towards the horizontal in a wave-like tail. Again, the bright band at the surface corresponding to a relatively strong temperature gradient is apparent in the shadowgraphs. Stationarity in the general nature of the temperature patterns has been reached here, also, in the last two sets of records.

Further detail on the isotherm contours is shown in the sequence of Figure 7.9. Examination of many contours has indicated that the umbrella-like caps found in the isotherms for natural convection are distorted when general horizontal flow occurs. However,

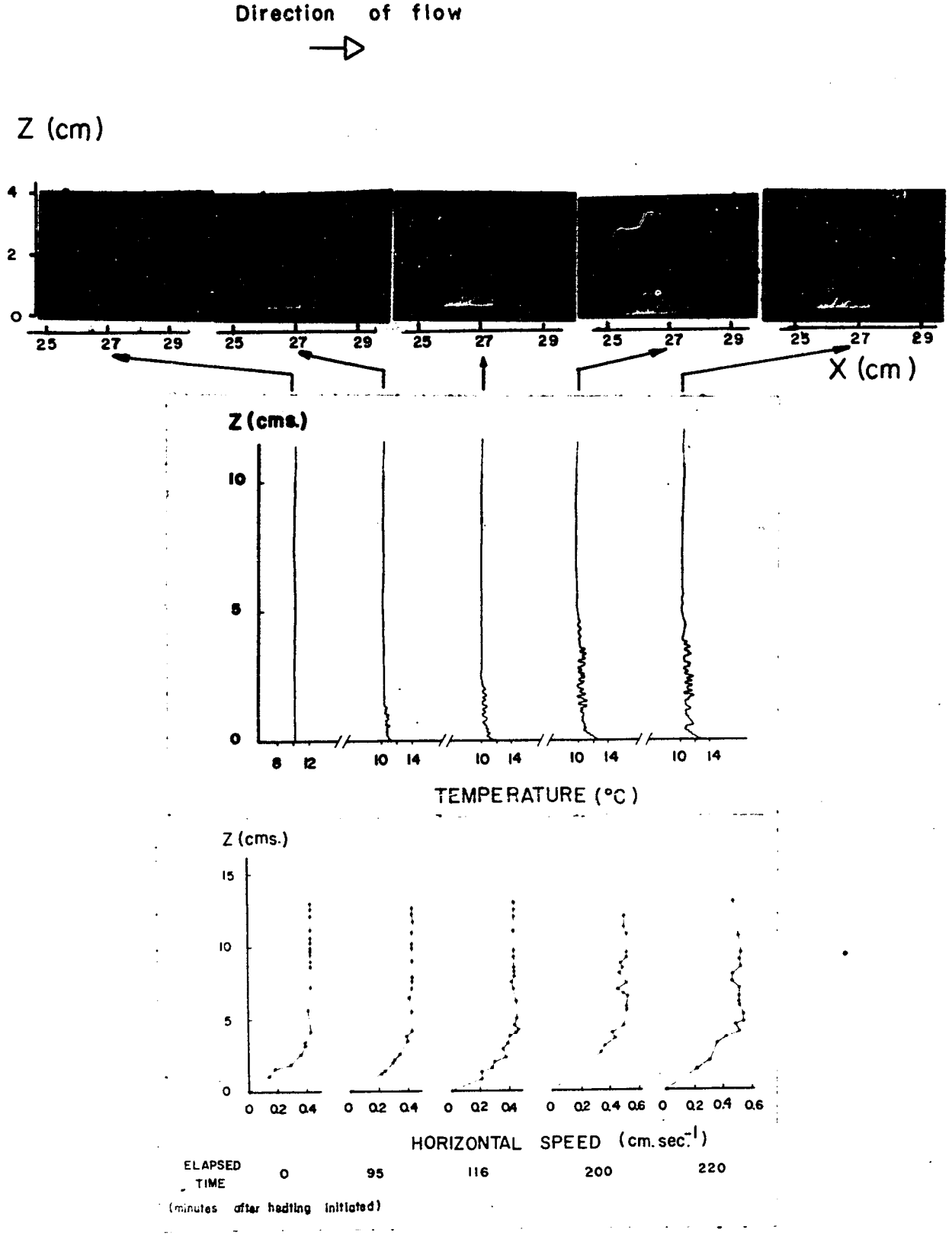

Figure 7.8 Growth of Temperature Perturbations and Isotherm Contours above the Thermal Boundary During the Initial Heating Period (U_f=0.4 cm. sec^{-1}; Power Input to Heaters = 382 Watts).

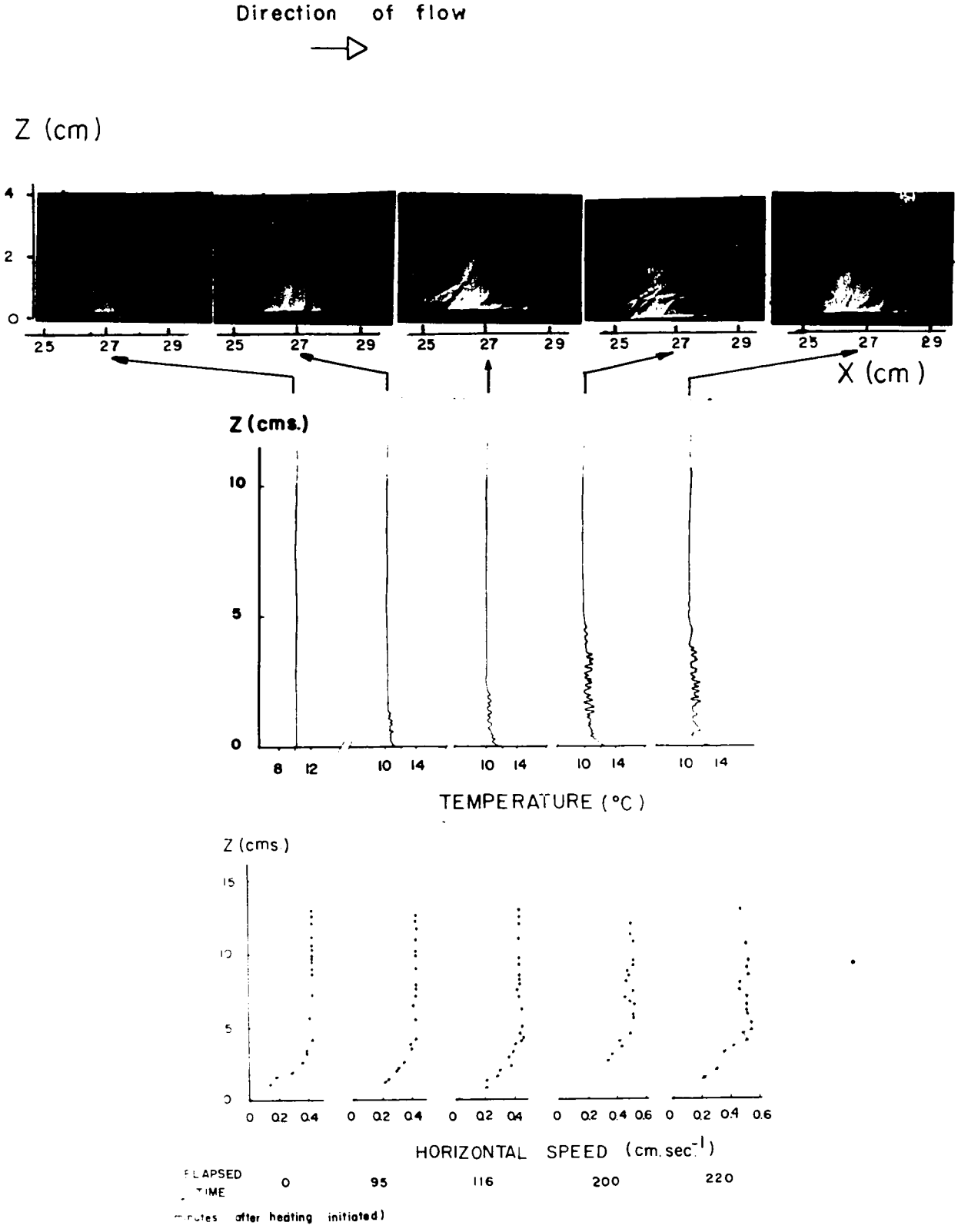

Figure 7.8 Growth of Temperature Perturbations and Isotherm Contours above the Thermal Boundary During the Initial Heating Period (U_f=0.4 cm. sec^{-1}; Power Input to Heaters = 382 Watts).

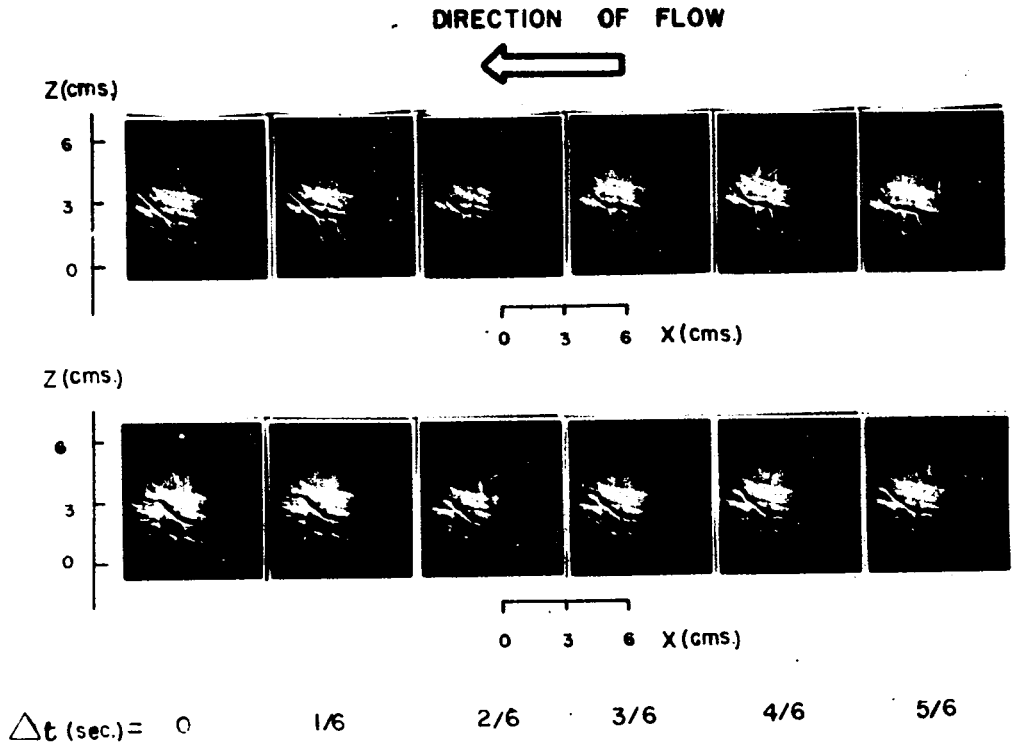

Figure 7.9 Two Shadowgraph Sequences Showing Details of the Isotherm Patterns in General Horizontal Flow (U_f=0.4 cm.sec^{-1}; Power Input to Heaters = 382 watts). The two sequences are separated in time by one second.

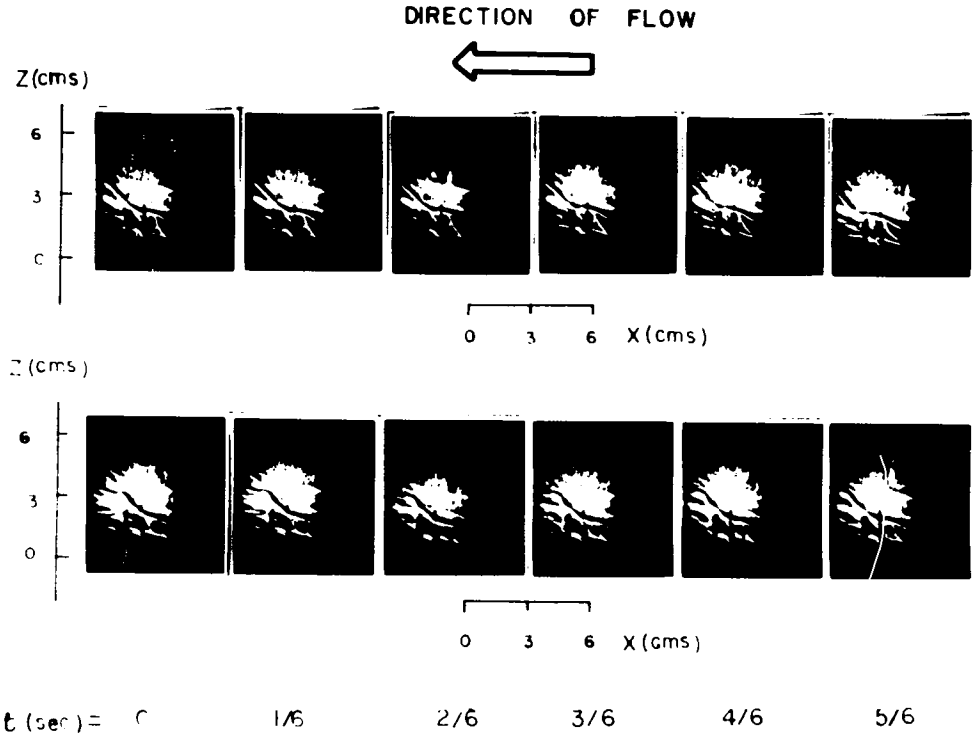

Figure 7.9 Two Shadowgraph Sequences Showing Details of the Isotherm Patterns in General Horizontal Flow (U_f=0.4 cm.sec^{-1}; Power Input to Heaters = 382 watts). The two sequences are separated in time by one second.

wavy perturbations of the inclined columns frequently appear, as in the illustration. It will be seen that such perturbations may move horizontally at a speed of about 0.8 cm. sec^{-1} (twice that of U_f). When it is recalled that temperature profiles are obtained by moving the probe through the fluid at a speed of 0.2 cm. sec^{-1}, it will be apparent that the probe will appear almost stationary to many of these perturbations. Hence, the probe will reproduce faithfully the temperature profiles of many of the perturbations.

7.3 Stationary Boundary Temperature

Stationarity in the patterns of convection is achieved 200 minutes after heating begins in the thermal boundary. This permits extensive study of the temperature probes. The following sections summarize this information.

7.3.a Mean Horizontal Flow

Evidence of increase in velocity fluctuations with residual heating of the lower boundary is found in the mean horizontal flow. Figure 7.10 shows two sets of velocity profiles, each for different positions along the central x-axis. The set on the left is for an isothermal fluid; only small irregularities appear in the profiles. In the set on the right, a residual heat flux of 9 milliwatts cm^{-2} is provided by the lower boundary; here, the velocity perturbations have grown to some 0.1 cm. sec^{-1}, at heights which increase with distance downstream.

7.3.b Vertical Gradient of Mean Temperature

Recording of fluid temperature simultaneously at each of

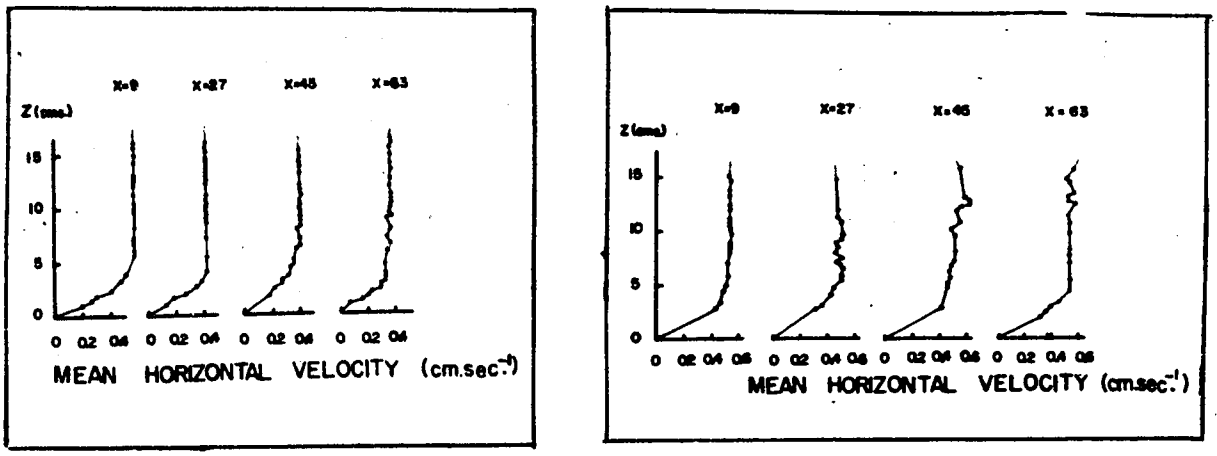

(a) Without residual heating of lower boundary.

(b) Residual heat flux from lower boundary = 9 mw.cm.$^{-2}$

Figure 7.10 Vertical Profiles of Mean Horizontal Velocity in the Y=0 Plane, Showing the Effect of Boundary Residual Heating upon the Profile.

several heights above the lower boundary for a 20 minute interval permits the local mean temperatures to be calculated accurately. Figure 7.11 gives two graphs of mean temperature profiles in the vertical, as derived in this way. One is for natural convection ($U_f = 0$), and the other for free convection ($U_f = 0.4$ cm. sec^{-1}). The same residual heat flux is provided in each case. Inspection shows that the vertical temperature gradient is large and negative in the lowest centimeter of height. Above this, the magnitude of the gradient decreases substantially, remaining negative in some instances and changing to positive in others.

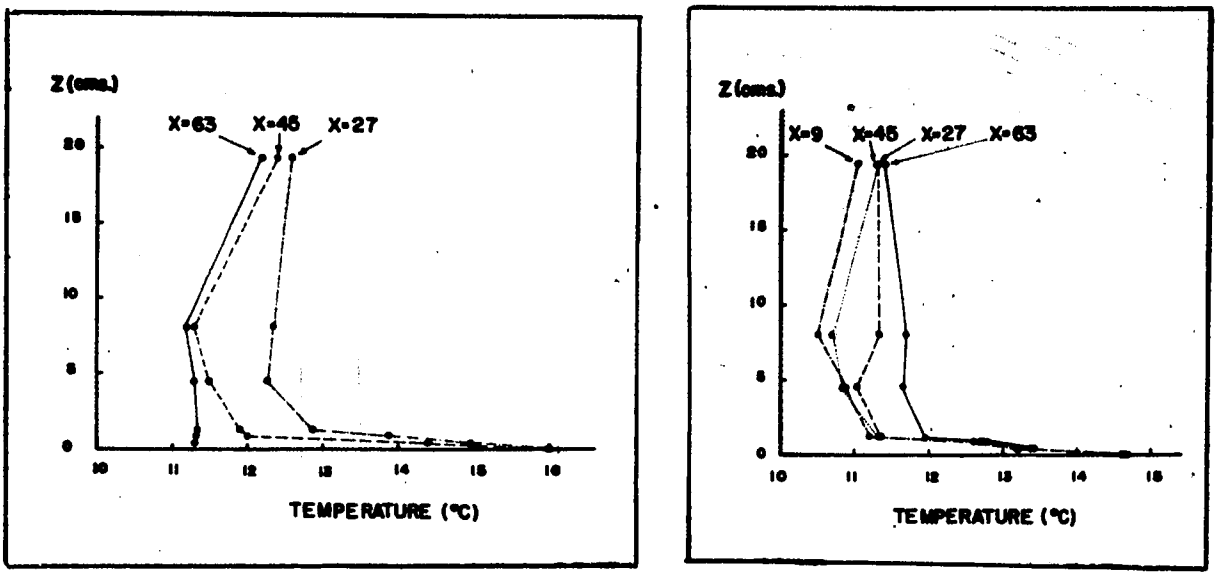

U_f=0

U_f=0.4 cm. sec^{-1}

Figure 7.11 Vertical Profiles of Mean Temperature in the Central Vertical Plane (Y=0) for Natural and Free Convection, at Various Positions Downstream. Residual Heat Flux from Lower Boundary = 9 milliwatts cm^{-2}

7.3.c Temperature Perturbations and the Temperature Gradient

Vertical profiles of fluid temperature which were presented earlier have suggested a possible relation between the local temperature gradient and the amplitude of temperature fluctuations. In order to study this possibility further, all recordings of temperature in the Y = 0 plane have been analyzed for the mean and standard deviation at each point, over a 20 minute interval. Appendix VI gives the IBM 7040 computer program for this calculation. The multiple-probe array in the vertical was used for these recordings, with U_f = 0 and 0.4 cm. sec^{-1}, and several values of residual heat flux from the lower

boundary, while the array was located at each of 8 positions along the X-axis. Figure 7.12 shows the results of this analysis. It will be seen that for both free and natural convection the trend appears to pass through the origin. For natural convection there is a general increase in σ as $-\frac{\partial \bar{T}}{\partial z}$ increases. The correlation between σ and $-\frac{\partial T}{\partial z}$ for free convection is less clear.

7.3.d Temperature Perturbations and the Environment

Temperature fluctuations are related also to the boundary conditions of the fluid. Again, the multiple-probe array in the vertical has been used here; the temperature has been recorded above the centre of one heater section of the lower boundary, for forced and free convection and for one rate of residual heating. Figure 7.13 gives three sample recordings; in (a) the probes are located only near the lower boundary, while in (b) and (c) they extend upwards to 19.3 cms.

A review of recordings of this type shows several trends. For a given heat flux, the magnitude of the temperature fluctuations decreases with increasing height; however, the fluctuation amplitude at all heights increases with heat flux. The major temperature perturbations extend to greater heights towards the centre of the heated region for natural convection; but in free convection their upward extension increases with distance down-flow over the heated region. Fluctuations near the lower surface are well correlated over the lowest centimeter of height, but the correlation deteriorates

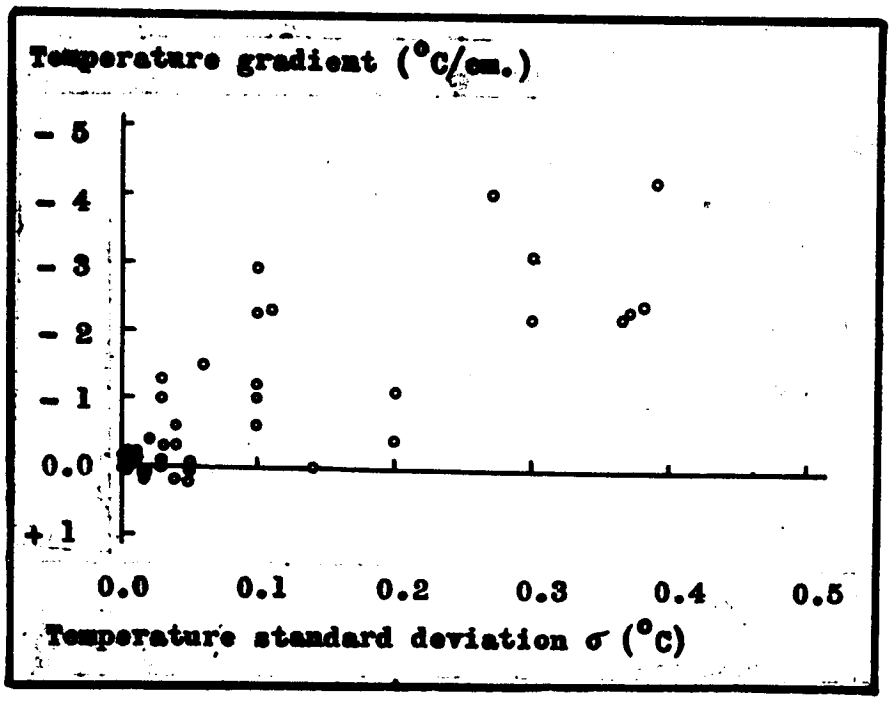

$U_f = 0.0$

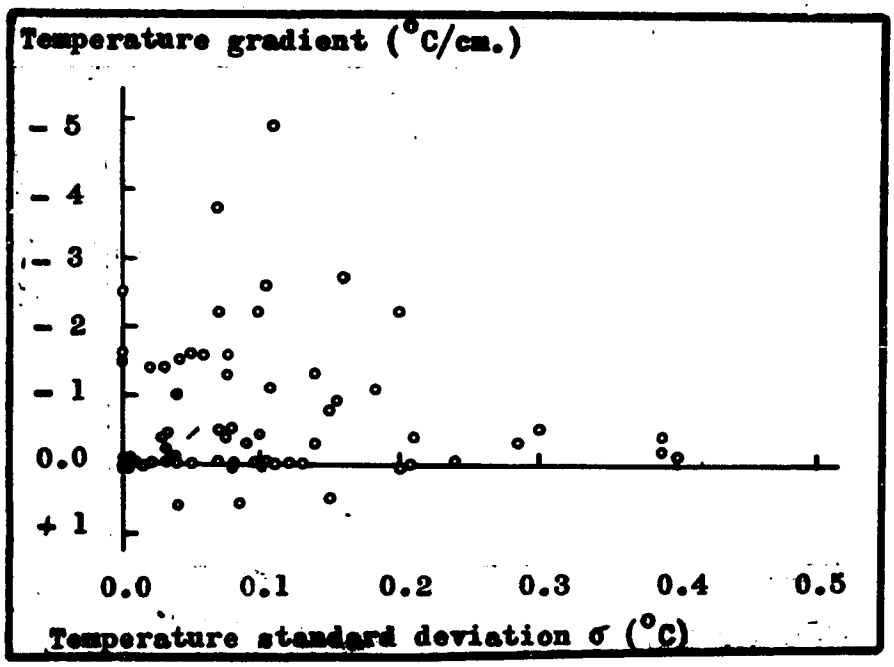

$U_f = 0.4$ cm.sec.$^{-1}$

Figure 7.12 Relationship between Local Gradient of Temperature and Magnitude of Temperature Fluctuations.

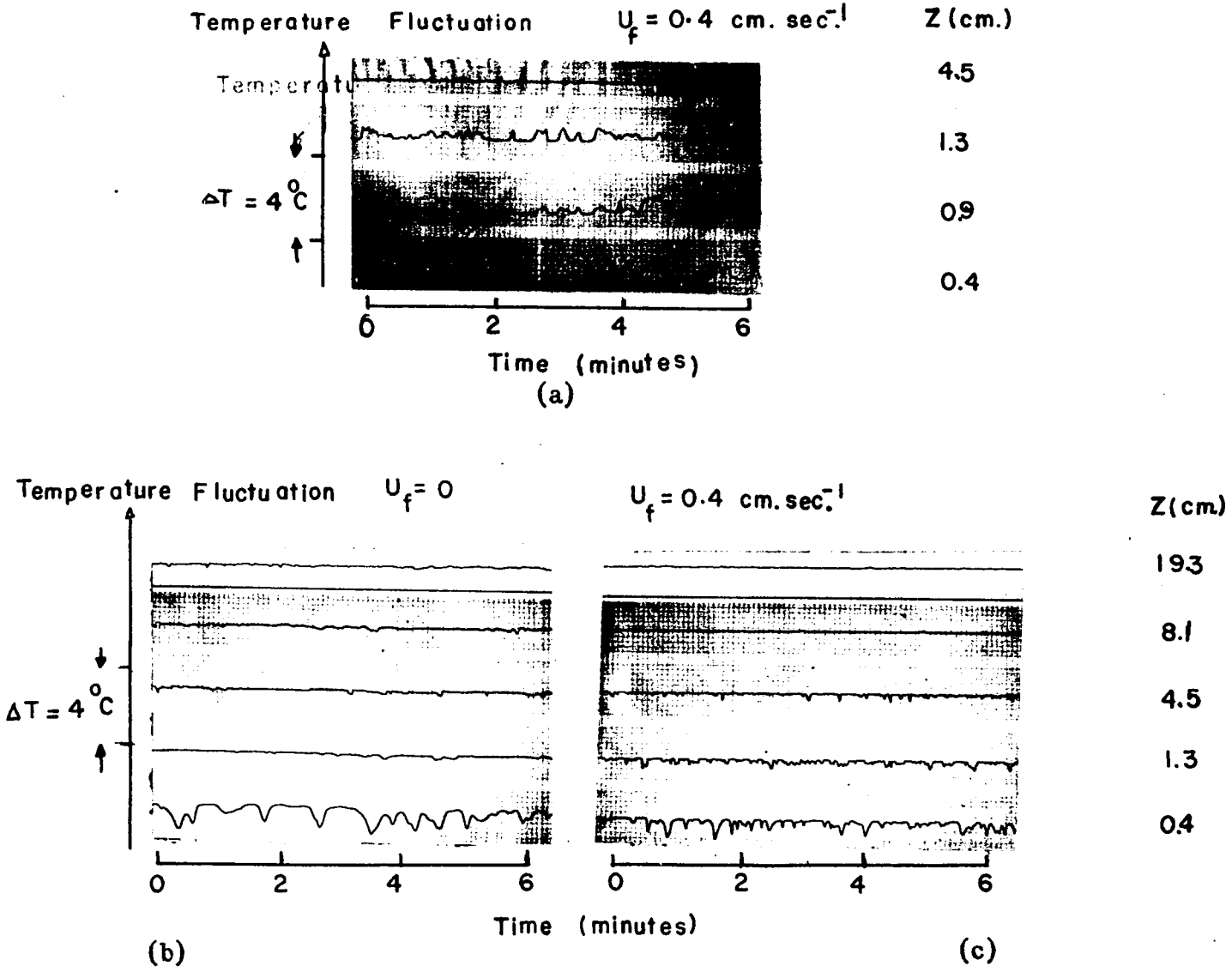

Figure 7.13 Sample Recordings of Water Temperature as Observed Simultaneously at Several Heights for Natural Convection (U_f=0) and Free Convection (U_f=0.4 cm.sec^{-1}). Probe Position (27,0,Z). Residual Heat Flux at the Boundary 11 and 9 milliwatts cm.$^{-2}$

above this level. The duration of each fluctuation tends to be shorter for free convection than for natural convection and to become increasingly shorter in free convection with distance down-flow over the lower thermal boundary.

7.3.e Isothermal Contours in the Horizontal

Further information on the temperature perturbations is obtained by moving the horizontal array of probes along the central X-axis at different heights above the lower boundary. These probes are 1 cm. apart, extending in the Y-direction. Isotherm contours have been derived from these observations and presented in Figure 7.14. Relative motion of the probe array and the fluid may result in distortion of these contours along the X-direction; but alternate traverses up-flow and down-flow indicate that the distortion is not significant.

For free convection, the isotherm contours are irregular with general elongation in the Y-direction. The central core is warmer than the periphery and the core temperature decreases with increasing height above the thermal boundary. Relatively few of these perturbations extend upwards above 10 cms. for U_f = 0.4 cm. sec^{-1}. The down-flow dimension of the contours decreases by a factor of at least two, with increasing distance in the X-direction; the separation of adjacent contours also follows this trend.

The isotherm contours in natural convection close to the centre of the thermal boundary are generally similar to those for free convection, but with wider separation.

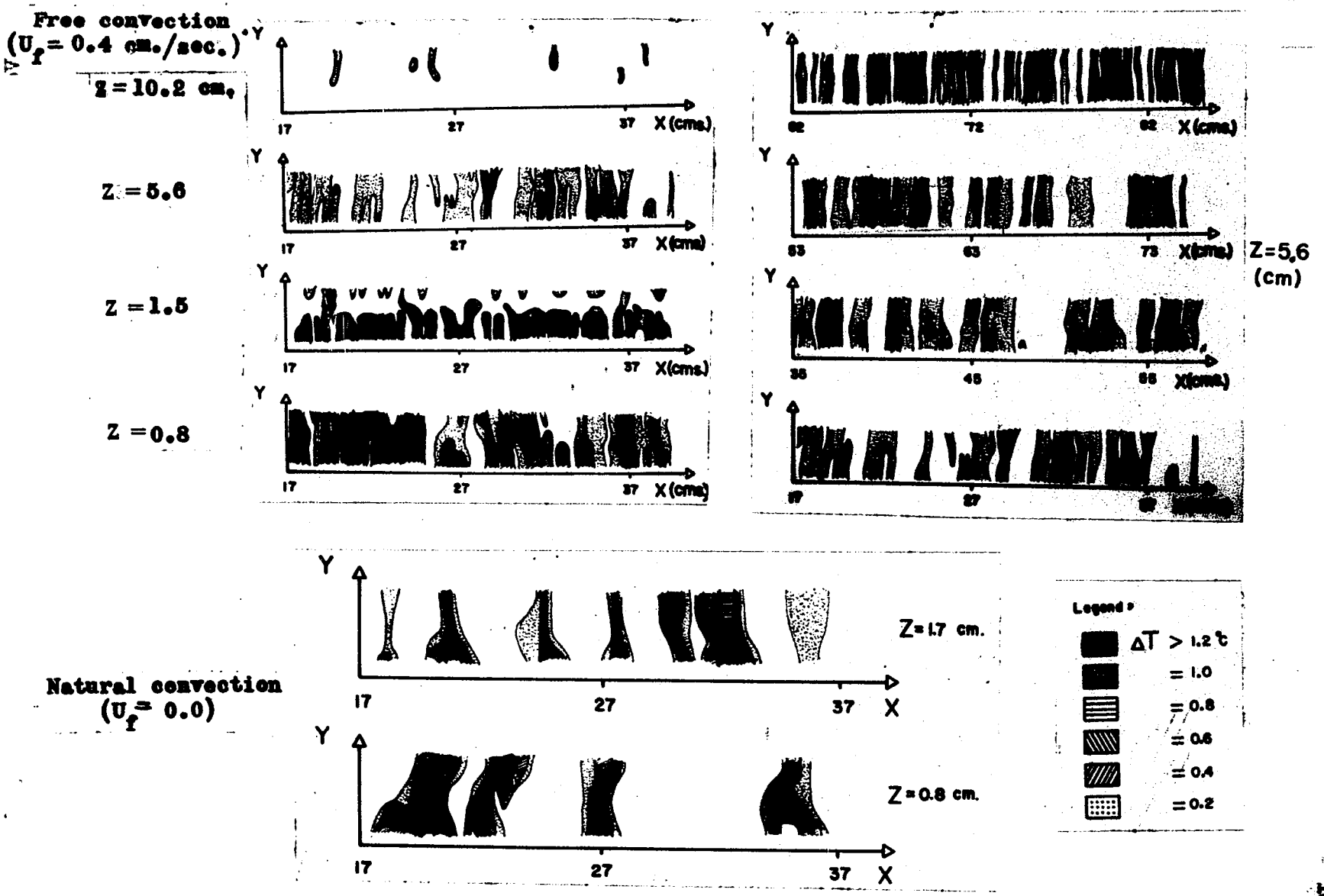

Figure 7.14 Isotherm Contours in Horizontal Planes at the Indicated Heights above the Lower Boundary. Each Plane is 3 cms. Wide, Directly above the X-axis. Residual Heat Flux for Free and Natural Convection = 9 and 11 milliwatts $cm.^{-2}$ respectively.

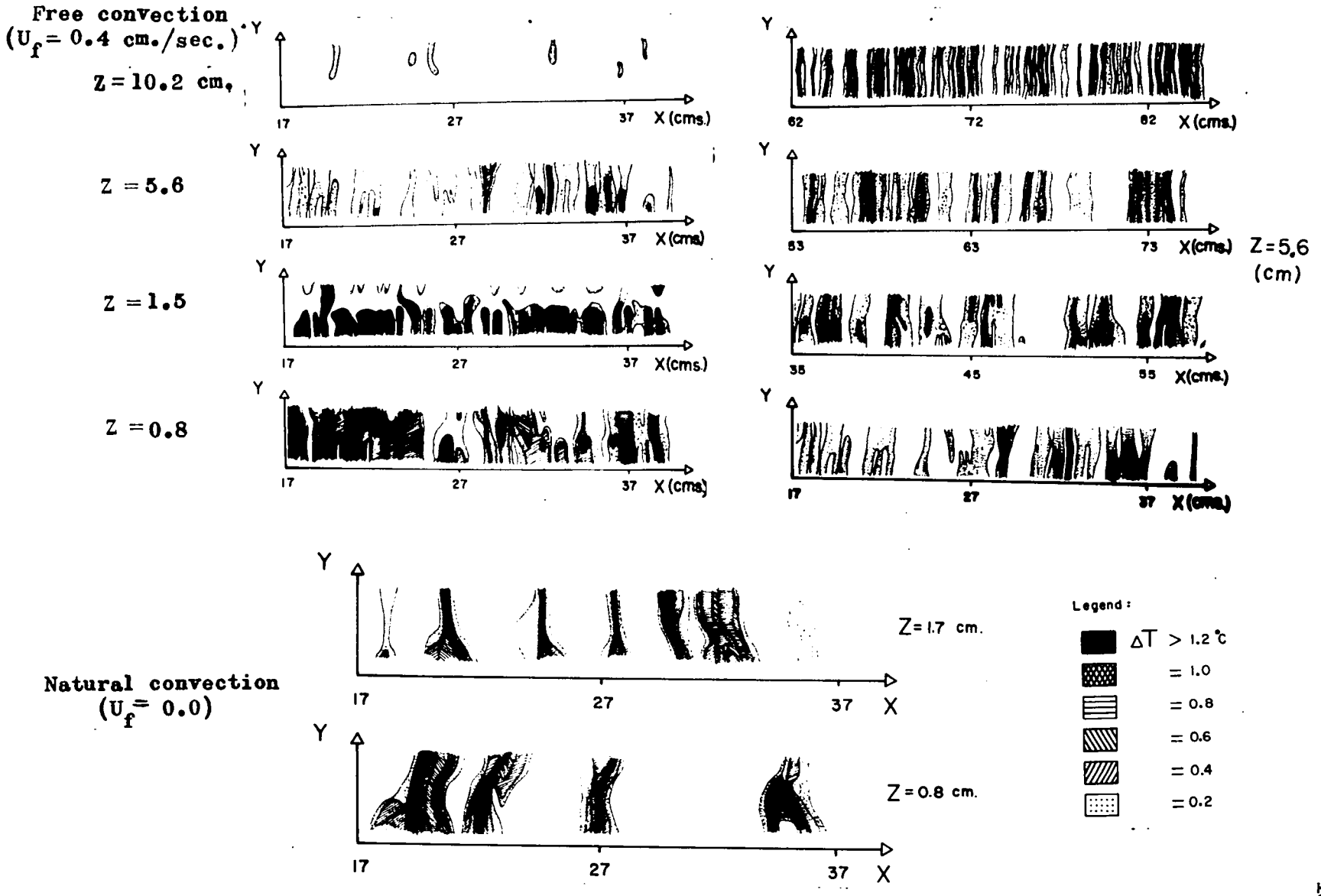

Figure 7.14 Isotherm Contours in Horizontal Planes at the Indicated Heights above the Lower Boundary. Each Plane is 3 cms. Wide, Directly above the X-axis. Residual Heat Flux for Free and Natural Convection = 9 and 11 milliwatts $cm.^{-2}$ respectively.

7.3.f Buoyancy Within Convective Columns

The isotherms within the vertical (Y = 0) plane have been examined for various rates of general horizontal flow (U_f), through the shadowgraph technique. As noted earlier, the convective columns incline to the vertical in the presence of general flow and their upper extremities become almost horizontal in wave-like extensions. The whole field of the simulation presents a very complex pattern of contours at heights more than 1 or 2 cms. above the thermal boundary, where the multiplicity of column extensions merges with the environment. However, if attention is confined to the lowest 2 cms. of the simulation, the inclination of separate contours to the vertical may be deduced from the shadowgraphs.

Figure 7.15 a shows the lower sections of four shadowgraphs for different rates of general flow. For each, the inclinations of several convective columns to the horizontal (Ψ) have been measured and the means plotted in the graph of Figure 7.15 b. The range of inclinations about each mean also is indicated. It will be seen that tan Ψ varies in a regular manner with U_f.

The vertical (buoyant) flow (w) within the convective columns may be estimated readily from these observations. Earlier, it was noted that the horizontal flow rate increased with height until it attained the free-stream value U_f; at a height of 2 cms. above the boundary, the horizontal flow of the environment (U_2) is about 0.5 U_f. Then, the column inclination results from the two velocity components, such that

$$\tan \Psi = \frac{w}{U_2} = \frac{2w}{U_f} \qquad 7.2$$

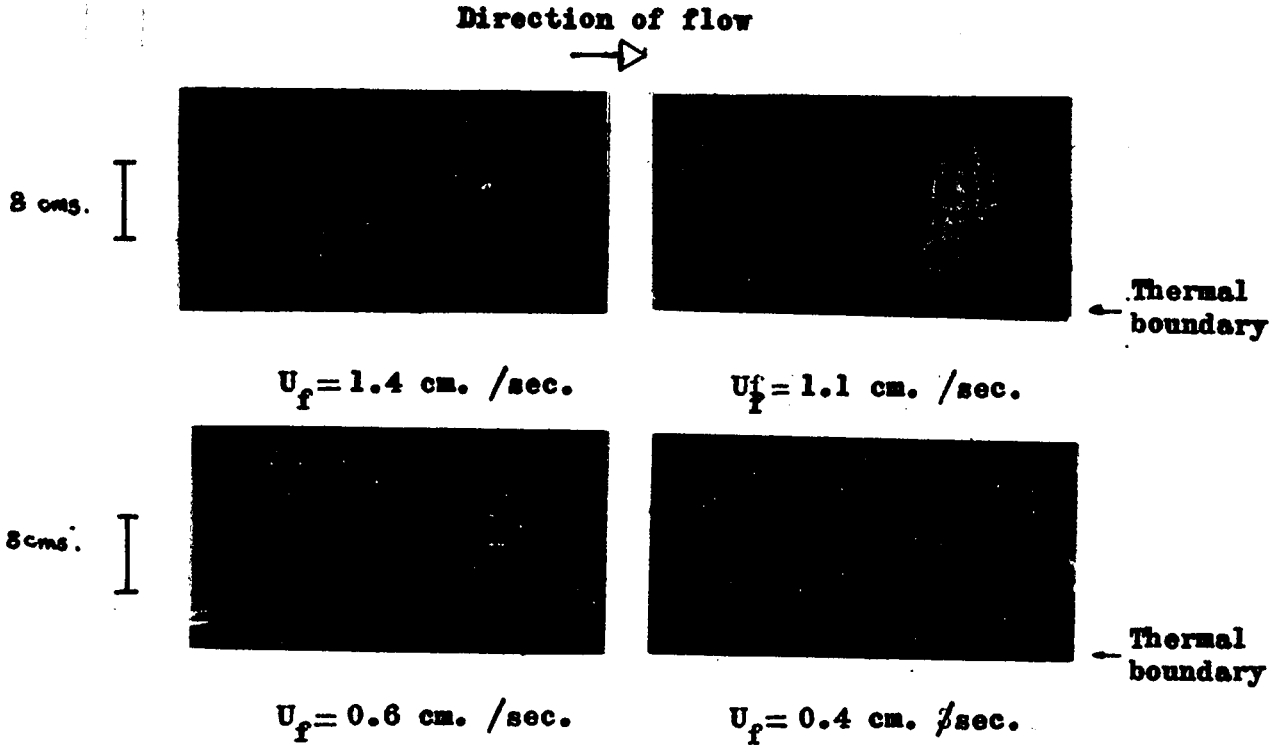

(a) Shadowgraphs in the Y=0 plane, for various "free stream" velocities.

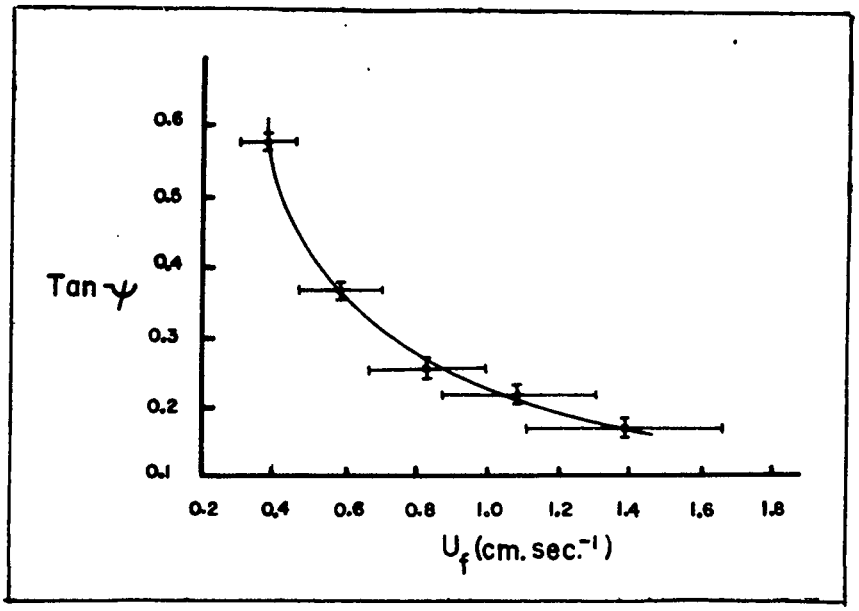

(b) Tangent of the mean angle of inclination (Ψ) of convective columns, for various flow rates (U_f).

Figure 7.15 The Effect of General Flow upon the Inclination of Convective Columns above a Heated Boundary (Residual Heat Flux ≈ 9 milli-watts cm^{-2}).

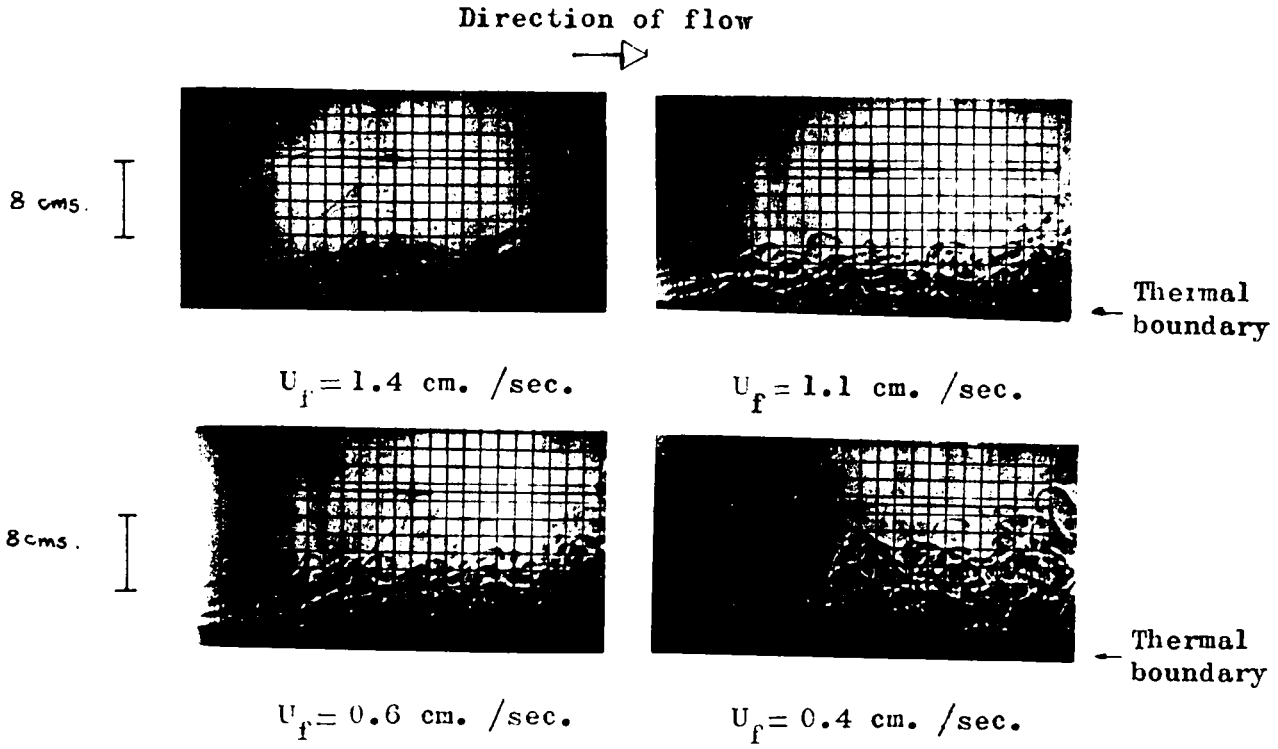

(a) Shadowgraphs in the Y O plane, for various "free stream" velocities.

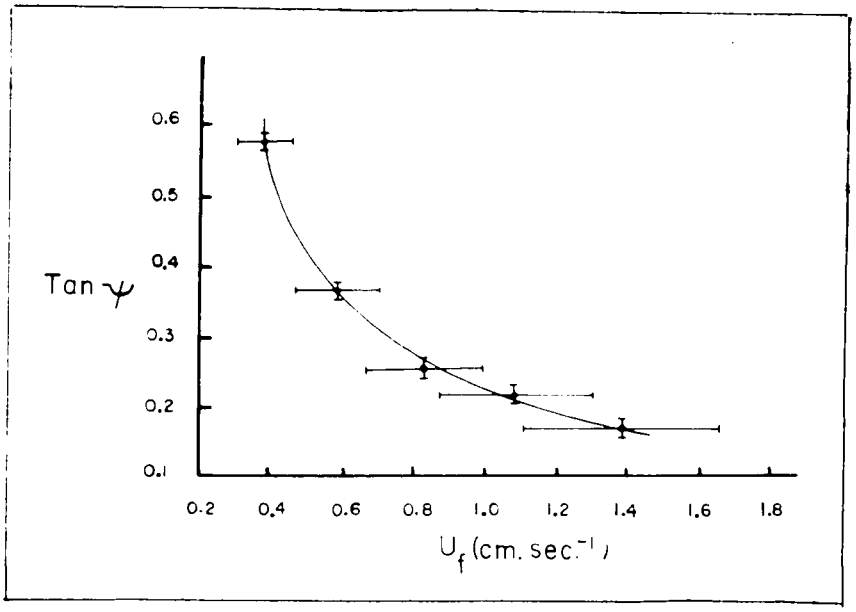

(b) Tangent of the mean angle of inclination (Ψ) of convective columns, for various flow rates (U_f).

Figure 7.15 The Effect of General Flow upon the Inclination of Convective Columns above a Heated Boundary (Residual Heat Flux ~ 9 milli-watts cm^{-2}).

When Equation (7.2) is applied to the points in Figure 7.15 b it is found that w in all cases is 0.11 cm. sec^{-1}. Hence, the residual heat flux of 9.0 milliwatts cm^{-2} at the lower boundary produces a constant buoyant velocity within the convective columns near the surface, for a wide range of horizontal flow.

7.3.g Temperature Asymmetry in Convective Columns

Another effect of general flow upon convective columns is observed in the horizontal temperature profiles through them. For this purpose, the fluid temperature is recorded as the multiple-probe arrays are moved both down-flow and up-flow in the X-direction. Figure 7.16 gives several examples of the temperature recordings. These examples show that the more prominent temperature perturbations are asymmetrical along the direction of general flow, with a rapid rise on the up-flow side and a slow decrease on the down-flow side

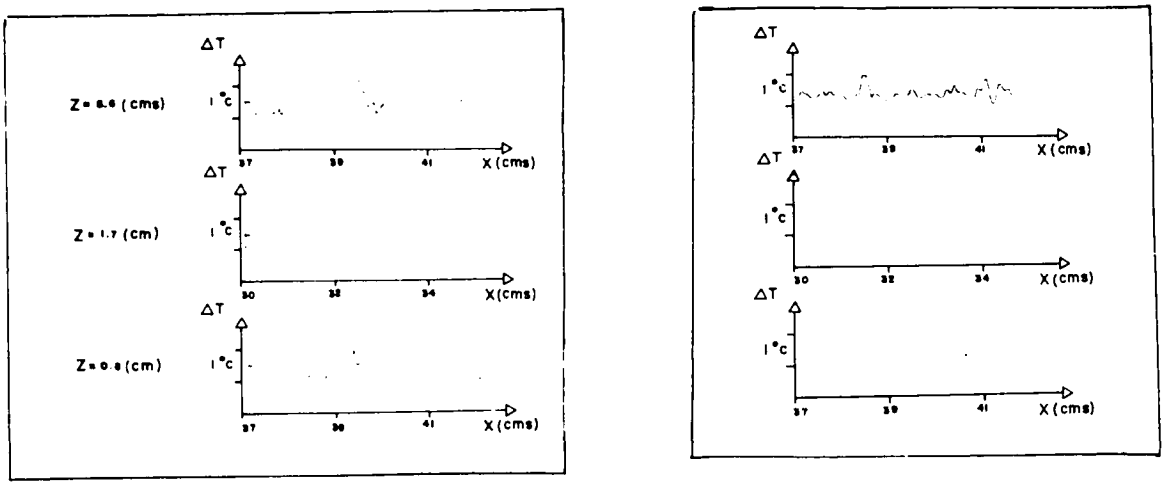

(a) Probes moving in direction opposite to that of mean flow.

(b) Probes moving in the direction of mean flow.

Figure 7.16 Cross-Sections of Temperature Variation Through the Convective Structure at Several Heights above the Boundary in the Y=0 Plane. (U_f = 0.4 cm. sec^{-1}; Residual Heat Flux from Boundary = 9 milliwatts cm^{-2}

When Equation (7.2) is applied to the points in Figure 7.15 b it is found that w in all cases is 0.11 cm. sec^{-1}. Hence, the residual heat flux of 9.0 milliwatts cm^{-2} at the lower boundary produces a constant buoyant velocity within the convective columns near the surface, for a wide range of horizontal flow.

7.3.g Temperature Asymmetry in Convective Columns

Another effect of general flow upon convective columns is observed in the horizontal temperature profiles through them. For this purpose, the fluid temperature is recorded as the multiple-probe arrays are moved both down-flow and up-flow in the X-direction. Figure 7.16 gives several examples of the temperature recordings. These examples show that the more prominent temperature perturbations are asymmetrical along the direction of general flow, with a rapid rise on the up-flow side and a slow decrease on the down-flow side

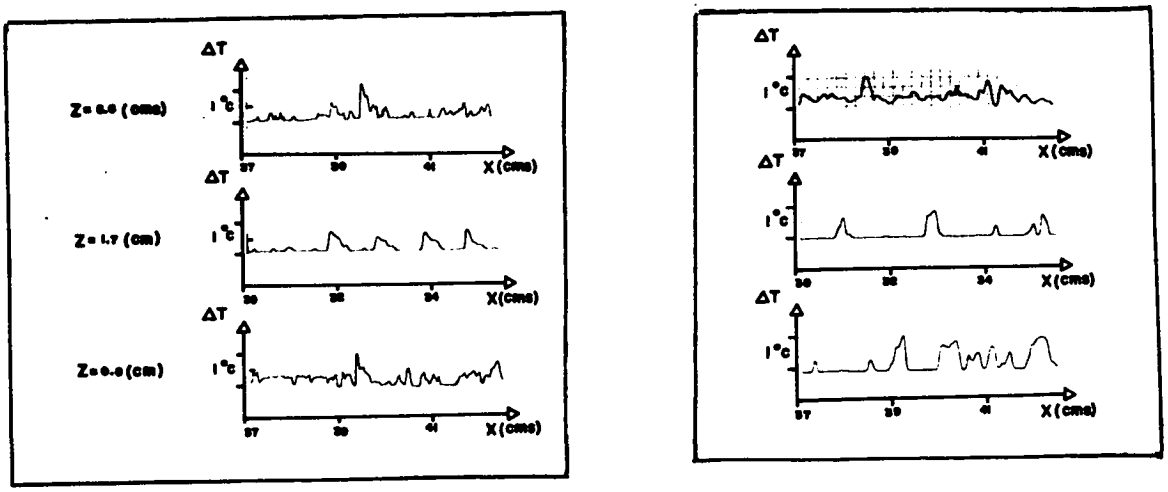

(a) Probes moving in direction opposite to that of mean flow.

(b) Probes moving in the direction of mean flow.

Figure 7.16 Cross-Sections of Temperature Variation Through the Convective Structure at Several Heights above the Boundary in the Y=0 Plane. (U_f = 0.4 cm. sec^{-1}; Residual Heat Flux from Boundary = 9 milliwatts cm^{-2}

of the convective columns. The temperature gradient on the up-flow side is at least 10°C cm^{-1} in the horizontal. This asymmetry suggests that the general flow erodes the warm periphery from the leading edge of the column to expose the more rapidly rising hot core on the up-flow side; erosion of the periphery on the down-flow side appears negligible.

7.3.h Penetration of an Elevated Inversion

Information on the upward extension of convective columns towards a temperature inversion layer has been obtained also from shadowgraph recordings, for natural convection. The initial setting of the environment is obtained by a special procedure. The laboratory simulation is exposed to the room temperature (22°C)without residual heating of the lower boundary, for a period of 5 hours. At the end of this time, the fluid temperature is constant at 11°C for heights below 12 cms; above this, the vertical gradient is positive at 0.2°C cm^{-1}. Then, the lower boundary is heated, at a rate which approaches 11 milliwatts cm^{-2} of heat flux when its temperature becomes stationary at 15.7°C. As a result, a relatively stationary temperature perturbation of 0.5°C over a height interval of 1 cm. appears at the top of the isothermal region; the position of this perturbation (and the top of the isothermal region) rises as heating of the lower boundary progresses, at a rate of 3.5 cms in 54 minutes.

The formation of isotherm patterns (convective columns) is observed during this heating interval. Figure 7.17 illustrates several stages. Initially, the field shows no convective columns. Then, the

T_b=10.7 °C

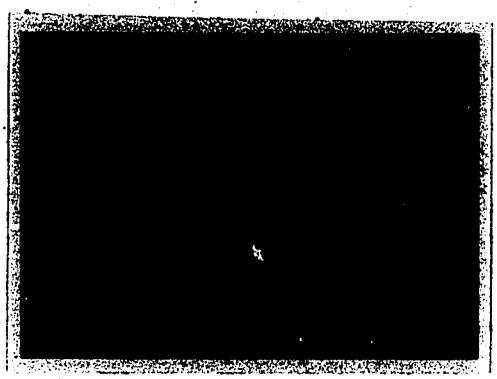

T_b= 14.8 °C

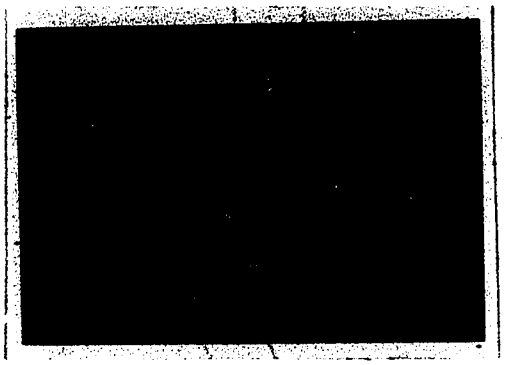

T_b= 15.0 °C

T_b= 15.2 °C

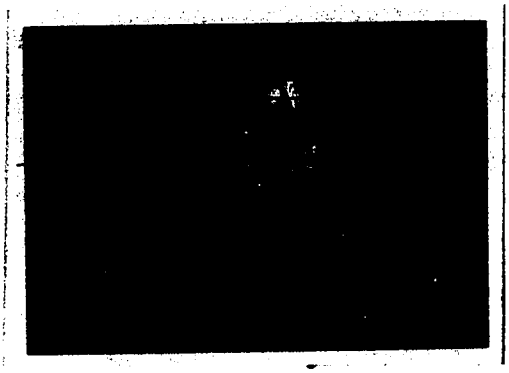

T_b= 15.5 °C

T_b= 15.7 °C

Figure 7.17 Shadowgraphs showing Progress in Development of Convective Columns and Perturbation of the Elevated Inversion as Boundary Temperature (T_b) Increases (U_f=0; Residual Heat Flux from Boundary Increasing to 11 milliwatts $cm.^{-2}$).

T_b= 10.7 °C

T_b= 14.8 °C

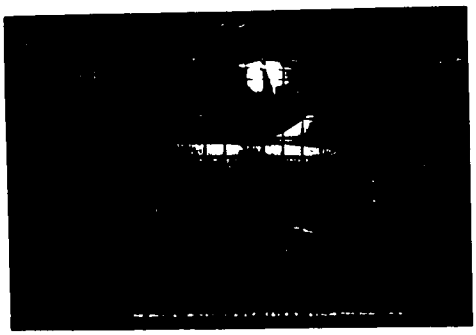

T_b= 15.0 °C

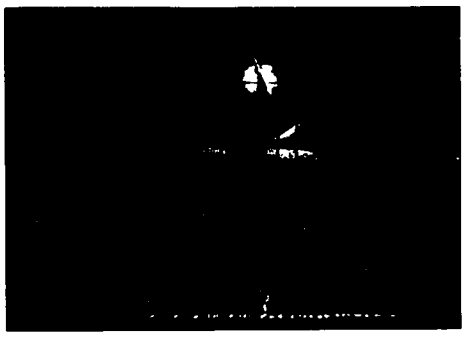

T_b= 15.2 °C

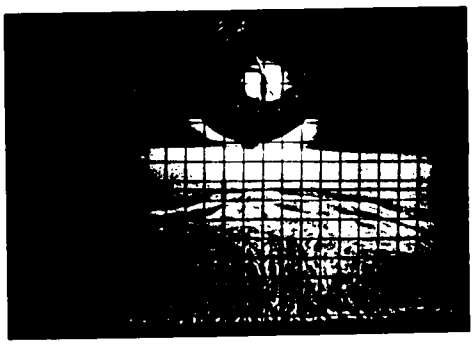

T_b= 15.5 °C

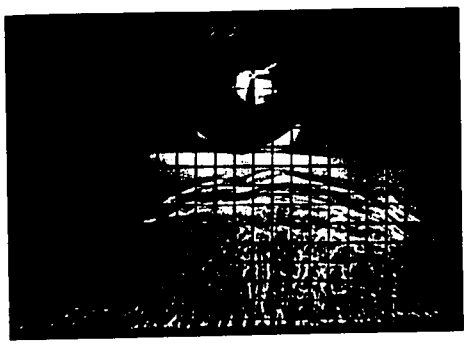

T_b= 15.7 °C

Figure 7.17 Shadowgraphs showing Progress in Development of Convective Columns and Perturbation of the Elevated Inversion as Boundary Temperature (T_b) Increases (U_f=0; Residual Heat Flux from Boundary Increasing to 11 milliwatts cm^{-2}).

columns begin to appear, together with an indication of the inversion layer at 12 cms. above the surface. With further heating from below, the convective columns rise to the inversion as the latter moves upward; at the same time, the inversion layer becomes more distinct and broken by wave-like perturbations. Some of these waves appear to move laterally, with velocities around 0.3 cm. sec^{-1}. The above observations suggest that the convective columns convey heat to the elevated inversion in a manner which both creates oscillations in the layer and also raises its mean position. Although the inversion rises to heights which probably are beyond the valid simulation region of the present study, yet the trend appears to be a continuous and reasonable extension of conditions within the region of valid simulation.

CHAPTER VIII

COMPARISON WITH FLOW AND TEMPERATURE IN THE LOWER TROPOSPHERE

The laboratory simulation has been designed with a number of assumptions regarding the lower troposphere. Although the requirements of the governing equations have been followed closely, as outlined in Chapter III, practical considerations have led to the following conditions: heat transfer by radiative flux divergence in the troposphere is important only within the lowest few meters (the simulation assumes an effective air temperature at the top of this level); the air in the troposphere is dry; turbulent heat transfer occurs throughout the region between a few meters and 1 kilometer above the ground, as described by a mean thermal diffusivity of 10^4 cm^2 sec^{-1}, and the earth's surface is a uniformly heated horizontal plane.

Limitations which these conditions may impose upon the usefulness of the simulation will now be examined. Various aspects of heat transfer in the lower troposphere will be compared with the observations of the previous chapter for this purpose. This comparison involves characteristics of the associated temperature perturbation and flow.

The appropriate scaling factors will be introduced in this chapter so that all of the laboratory observations are transformed

into tropospheric dimensions. Four features of the troposphere will be considered: the vertical profile of mean horizontal flow, the vertical gradient of air temperature, air stability, and temperature perturbations.

8.1 The Vertical Profile of Mean Horizontal Flow

Several empirical equations have been developed by various authors to describe the wind profile in the lower troposphere (Munn 1966, p. 53). One useful form was suggested by Deacon (1949) and supported later by Rider (1954). The mean wind speed ($\bar{U}$) is related to height (z) by

$$\bar{U} = \frac{U^*}{0.4(1-\beta)} \left[\left(\frac{z}{z_o}\right)^{1-\beta} - 1 \right] \qquad 8.1$$

where z_o is the roughness length, U* is the friction velocity and β is a function of height that depends on the stability of the lower troposphere. The roughness length, which depends upon the physical surface of the ground, is the height at which the velocity vanishes; the friction velocity is a convenient coefficient which depends upon the local shearing stress and the air density. It is believed generally that Eq. 8.1 is valid only at heights below 100 meters, although Theullier and Lappe (1964) have succeeded in applying it to observed wind profiles at heights up to 450 meters with appropriate constants for β and U*.

The writer has used the convenient form of Equation (8.1) to provide analytical expressions for the observed flow profiles in the laboratory simulation. These expressions will be used later in the development of plume theory. It is recognized that this application may extend beyond the limits of validity in the troposphere as suggested

by other authors, and consequently no attempt will be made here to imply a strict interpretation of β, U* and z_o in the analytical expression. Figure 8.1 gives two examples of the fitted profiles; values of z_o, U*

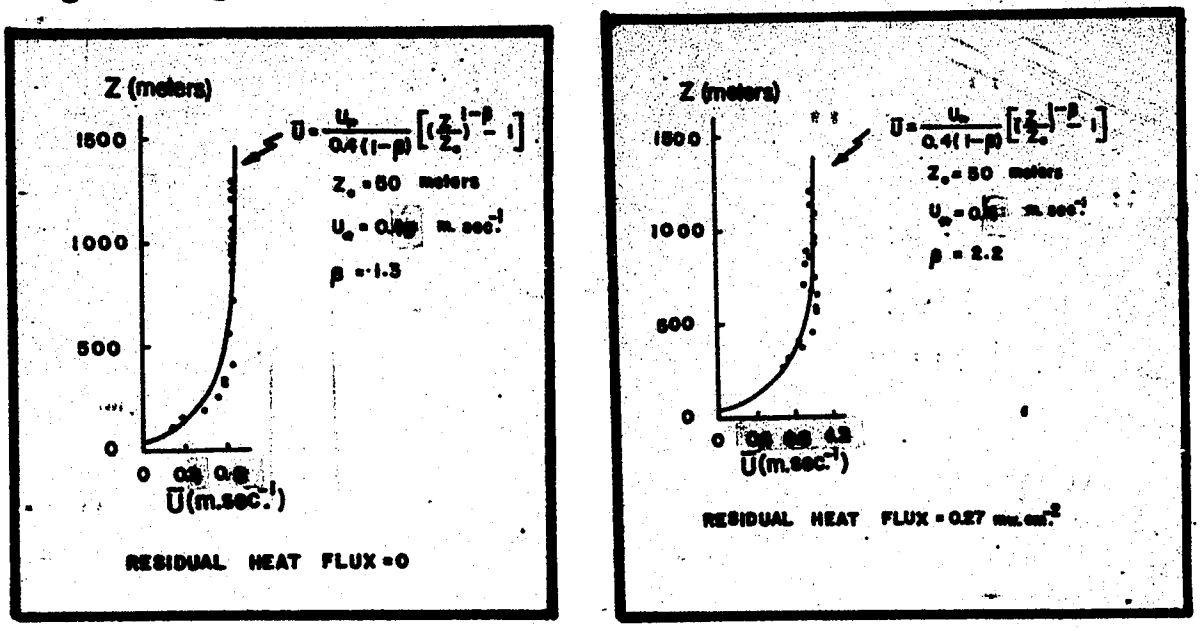

(a) (b)

Figure 8.1 Modified Deacon Wind Profiles Fitted to the Observed Flow in the Laboratory Simulation (U_f=0.8 and 1.0 meter sec^{-1}; Coordinates 27,0,Z in Simulation).

and β are 50 meters, 0.18 to 0.4 m. sec^{-1} and 1.3 to 2.2 respectively. In the simulation the value of z_o is due to a slight elevation of the lower edge of the flow straightener above the thermal boundary. This shallow stagnation layer continues across most of the lower boundary.

An interesting feature of the vertical profile of horizontal flow in the lower troposphere has been reported by several workers (see, e.g. Theullier and Lappe 1964, Mashkova 1965 and Klinov and Poltavskii 1965). They have found that horizontal flow tends to increase with increased heating from below. A similar trend has been noted in the present study.

8.2 Vertical Gradient of Air Temperature

Priestley (1954, 1959) has considered convective transfer of heat in the lower troposphere and compared his theoretical prediction

with experimental observations. He demonstrated that the mean potential temperature ($\bar{\theta}$) is related to height above the ground (z) during free convection by

$$\frac{\partial \bar{\theta}}{\partial z} = -c\, z^{-4/3}$$

$$= \frac{\partial \bar{T}}{\partial z} + \Gamma \qquad 8.2$$

where $\bar{T}$ is the average absolute temperature, Γ is the adiabatic lapse rate of temperature (-0.98°C per 100 meters) and c is a constant which depends upon the heat flux.

The experimentally observed temperature gradients of Chapter VII are compared with the tropospheric gradients of Priestley in Figure 8.2. The prediction of Eq. (8.2) is represented by the solid line with slope (- 4/3), while the broken lines follow the observations for natural and free convection. Several features of interest should be noted. In free convection, the slope is approximately (- 4/3) for heights between 175 and 1,000 meters, but notably different outside of this region. Further, although Eq. (8.2) has not been applied to natural convection (true natural convection rarely occurs in the troposphere), the range of slope (- 4/3) extends between heights of 150 and 370 meters. Thus, the gradients of mean temperature in the simulation follow those in the troposphere over most of the range of interest, in free convection. A range of application of Eq. (8.2) is suggested for natural convection, but the significance of this requires further study.

8.3 Air Stability

A well-known criterion for atmospheric stability is the Richardson number (Ri) (see, e.g. Munn 1966, p. 82):

$$Ri = \frac{g}{T} \frac{\partial \bar{\theta}/\partial z}{(\partial \bar{u}/\partial z)^2} \qquad 8.3$$

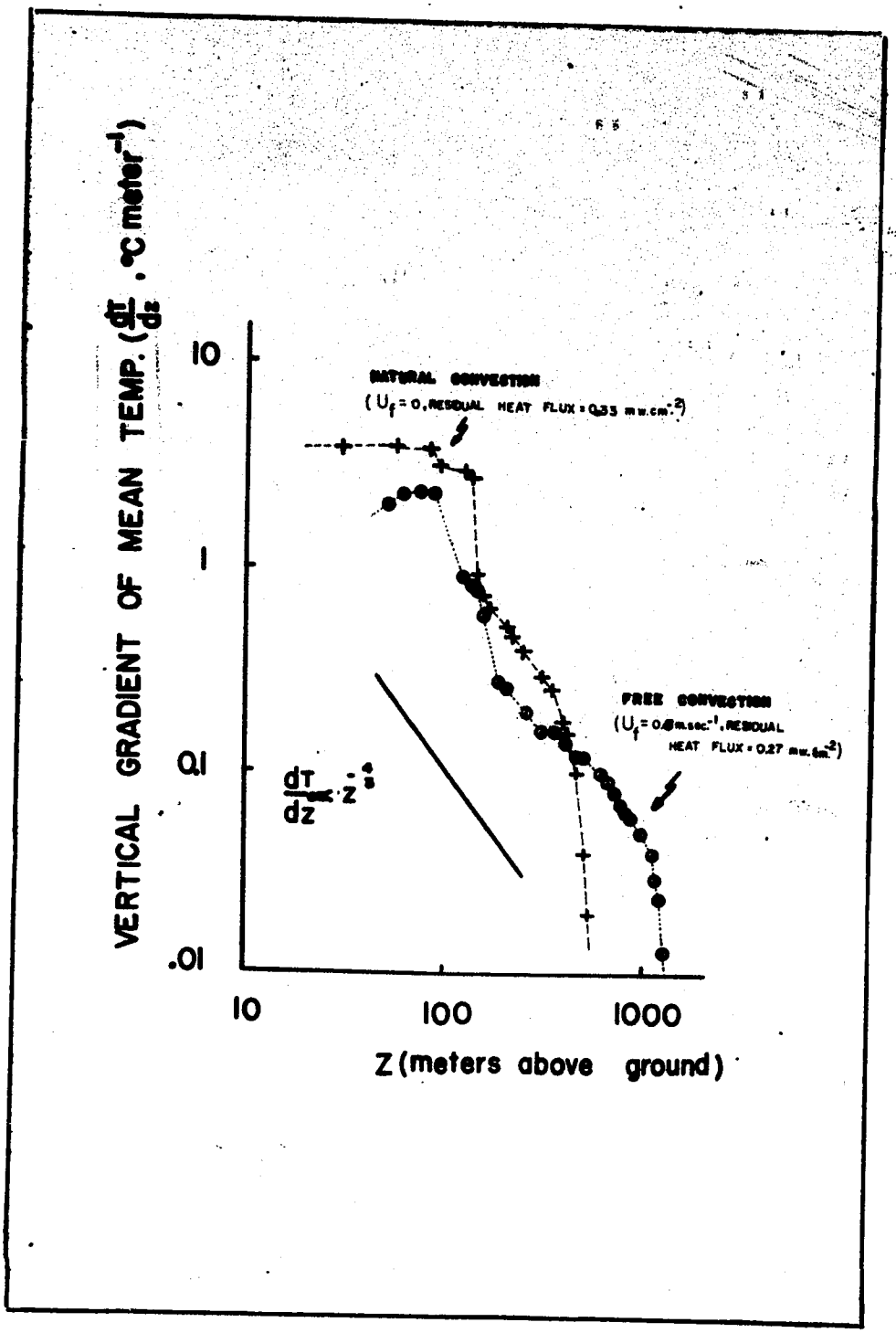

Figure 8.2 Vertical Gradients of Temperature in the Simulation for Natural and Free Convection, Compared with the "$-\frac{4}{3}$ Power Law" of Priestley.

Here, g is the gravitational acceleration. This number indicates the ratio of buoyancy to shearing forces; in general, increasing -Ri represents increasing instability, and an approximate division between stable and unstable air occurs at -Ri = 0.03. Lumley and Panofsky (1964, p. 104) introduce a non-dimensional wind shear, S, which is related to vertical wind shear by

$$S = \frac{kz}{u^*} \cdot \frac{\partial \bar{u}}{\partial z} \qquad 8.4$$

where k is the von Karman constant (=0.4). Then, they derive the following relation between S and Ri:

$$S = (1 - 18\ Ri)^{-\frac{1}{4}} \qquad 8.5$$

which provides a non-dimensional equation applicable in the troposphere and in the laboratory simulation. Figure 8.3 shows a comparison between Eq. (8.5) and experimental observations in both the troposphere and the laboratory simulation. The upper graph is taken from Figure 1 of Swinbank (1966); the experimental points were derived from Swinbank's measurements at heights up to 16 meters in the troposphere under a wide range of environmental conditions, and analyzed by Panofsky (1966). The lower graph is calculated from the observations of Chapter VII; a much wider range of -Ri is available from the laboratory work than from the tropospheric observations. It will be seen that there is generally good agreement between the Lumley-Panofsky curve and the tropospheric observations on the one hand, and the Lumley-Panofsky curve and the simulation observations on the other (over an extended range of -Ri). The points in Figure 8.3 b about -Ri = 20 that are remote

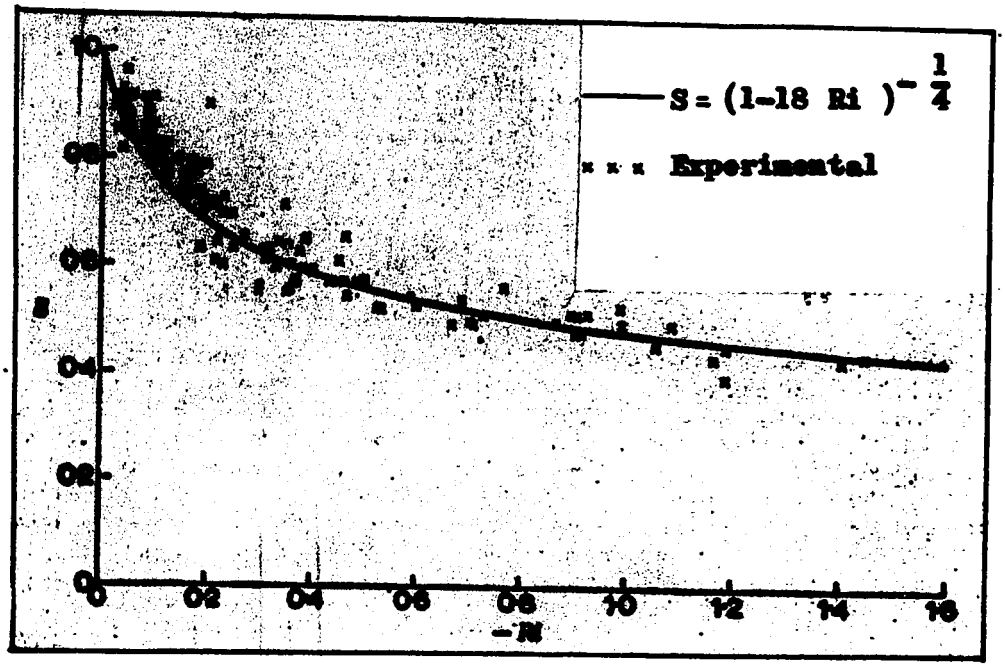

(a) From tropospheric observations (Swinbank 1965 and 1966).

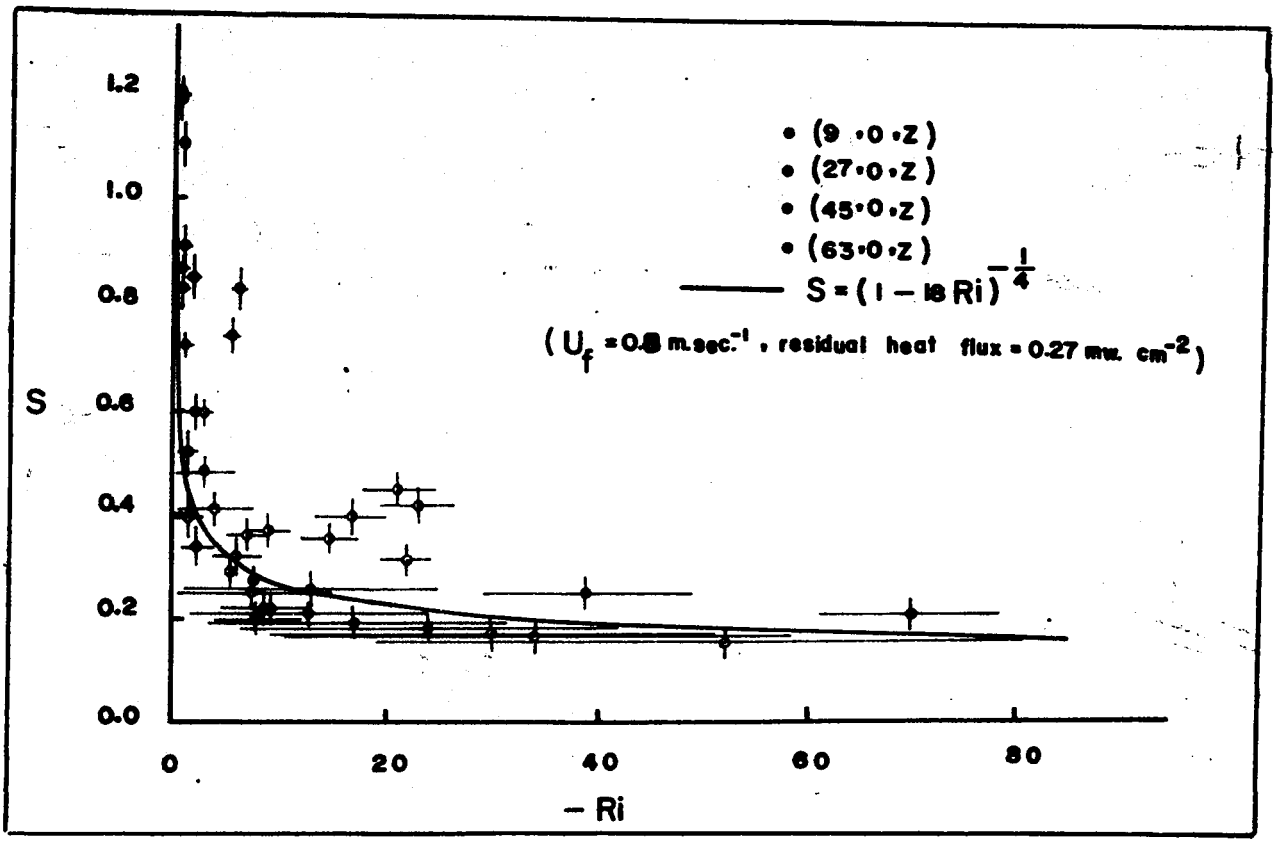

(b) From observations in the laboratory simulation.

Figure 8.3 Comparison between the Stability Function of Lumley and Panofsky and the Observation of the Laboratory Simulation.

from the solid curve are derived from observations downflow from the heated boundary, above an unheated (isothermal) region.

8.4 Temperature Perturbations

Small fluctuations in temperature are a normal feature of the lower troposphere. Measurements by Turner and Hay (1963) with a rapid-response thermometer give a direct indication that temperature changes of about 0.2°C occur over height intervals as small as a decimeter.

Several of the special features of temperature fluctuation that were noted in the laboratory simulation (Chapter VII) also have been observed in the lower troposphere. Although the boundary conditions for the latter were not fully specified, James (1953), Warner and Telford (1963) and Grant (1965) have recorded temperature fluctuations of the order 0.1°C, whose incidence decreased with increasing height; their aircraft observations showed that these temperature inhomogeneities extended some 120-1200 meters horizontally. The same authors, and Vasil'chemko and Ledokhovitz (1968), noted that the temperature perturbations at heights up to several hundred meters were asymmetrical in free convection as illustrated in Figure 7.16. Martin (1966) found similar fluctuations about 1 meter above ground. Martin, and Vasil'chemko and Ledohkovits have suggested that the perturbations are associated with convective columns some 100-200 meters in diameter (similar to those described in Chapter VII), and that the asymmetry in temperature profile is due to erosion of the columns on the windward side and down-wind extension on the lee side. Vasil'chemko and Ledokhovits noted that the region above 400 meters was thermally stable; below this, the

temperature lapse was thermally unstable and hence the convective columns arise within the unstable region to penetrate aloft into the stable layer.

A set of isotherm contours in the horizontal has been derived by Warner and Telford (1963) from their aircraft measurements; again, specification of the boundary conditions is incomplete. Figure 8.4 is a reproduction of one set of their contours; it will be seen that details of these contours are not unlike those presented in Chapter VII with appropriate scaling of dimensions.

8.5 Penetration of Inversion Layer

Observations by Neiburger (1960) on a temperature inversion off the Southern California Coast show vertical displacements at some 70 meters hr^{-1}, rising in one region and sinking in another. The boundary conditions in this case have not been specified. Ball (1960) on the other hand has estimated from observations of the diurnal variation of inversion height in Central Australia, that an inversion will rise at a rate of 150 meters hr^{-1} above a heat flux of 20 mw cm^{-2}. The rate of rise in this case is large compared to the one observed in the simulation (8 meters hr^{-1}). This may be due to the fact that the heat flux in the prototype is larger than that in the simulation. However, some of the features of the inversion layer, as described by Ball, agree with those observed in the simulation (see Chapter VII).

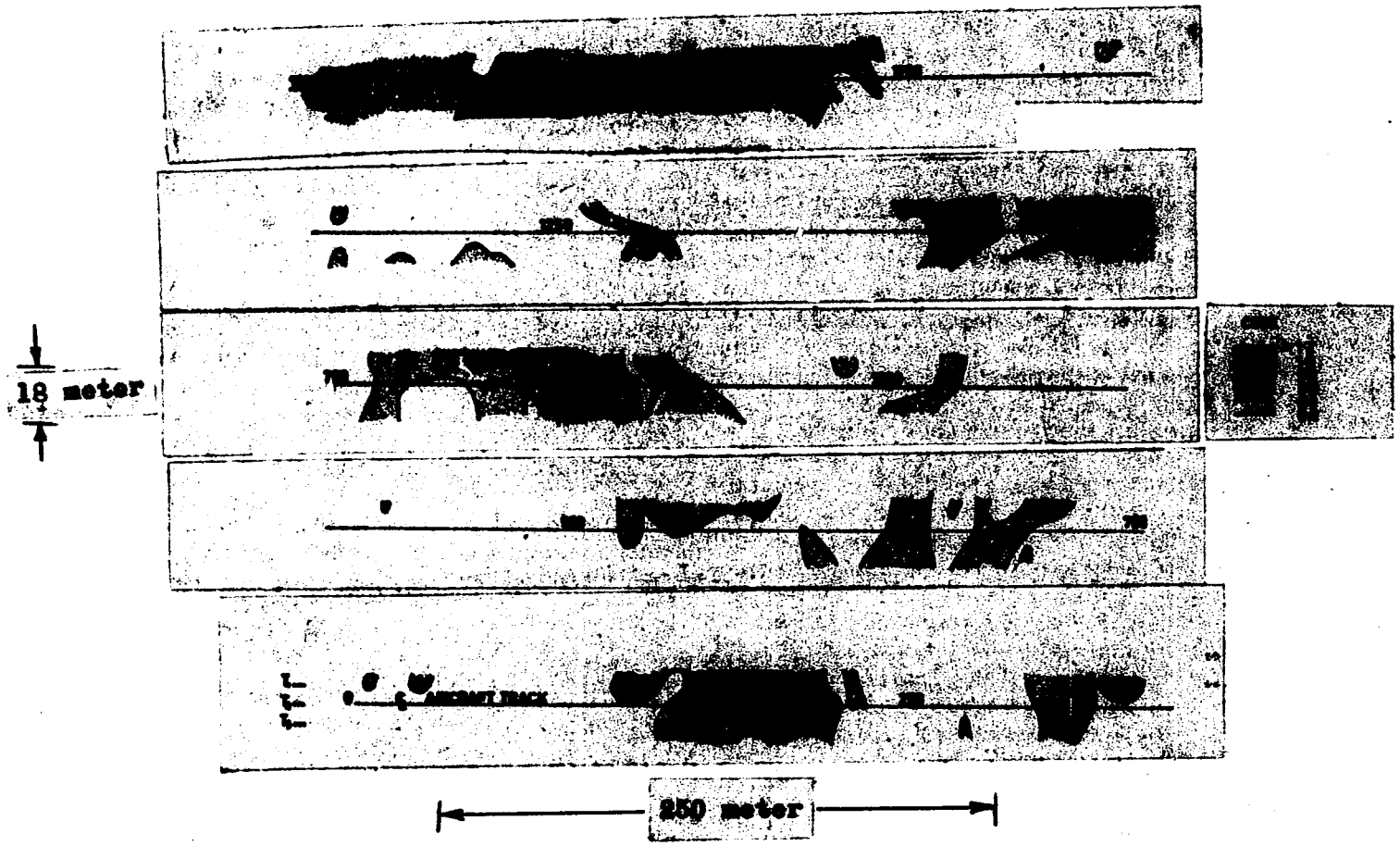

Figure 8.4 Isotherm Contours in the Horizontal as Obtained by Warner and Telford (1963) at Height 30 Meters, through Aircraft Soundings.

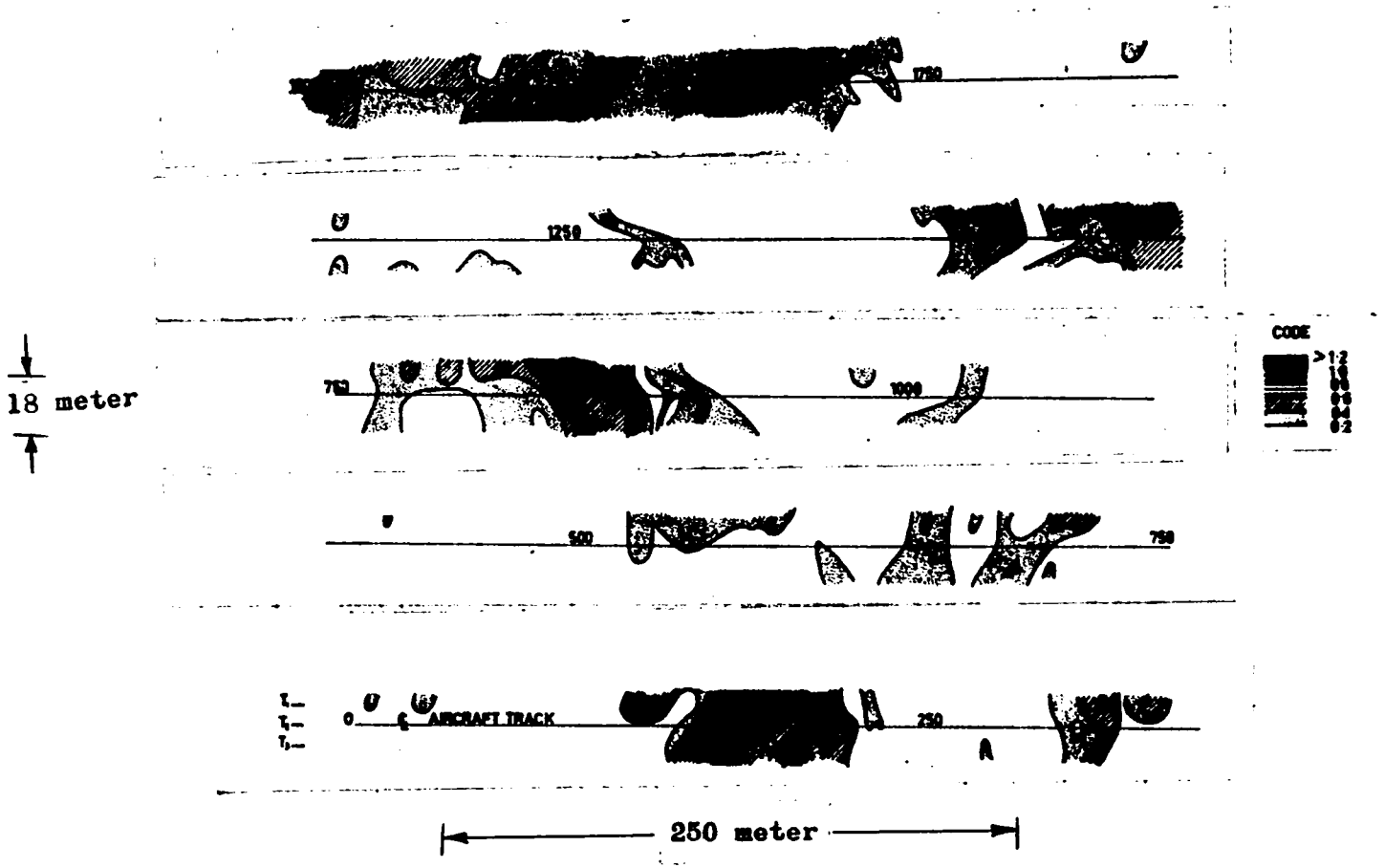

Figure 8.4 Isotherm Contours in the Horizontal as Obtained by Warner and Telford (1963) at Height 30 Meters, through Aircraft Soundings.

CHAPTER IX

REMARKS

The present study has provided a detailed investigation of thermal convection in the lower troposphere, through a dynamic simulation. The review of Chapter II showed that the current understanding of convective models is incomplete and controversial. Although various authors have described the models as convective cells or thermals, bubbles, mushrooms, vortex rings, turbulent eddies, and columns or plumes, there is little direct evidence to assist either in clarifying these suggestions or in establishing the conditions under which the models exist. Most of their studies have treated these models as pre-existing convective elements which have a given shape. In this thesis no such assumption has been made.

This work has proceeded with a number of simplifying limitations. It is well known that full dynamic similitude requires preservation of the geometry, the boundary conditions, and the governing equations in transferring from the full-scale prototype (lower troposphere) to the laboratory simulation. Complete simulation for thermal convection requires invariance of the Reynolds number, Froude number, Grashof number, Peclet number, Prandtl number and Rossby number in transferring from atmosphere (prototype) to laboratory (simulation). The writer has neglected Coriolis forces

in the simulation, and hence not preserved the invariance of the Rossby number; however, account of this factor has been taken in the analysis of Appendix VII. Two other compromises have been made here: eddy diffusion in the atmosphere has been represented by molecular diffusion in the simulation (and hence mechanical turbulence is not apparent in the simulation), and the Prandtl number has been preserved only within order-of-magnitude (1 in the prototype and 7 in the simulation).

These requirements have been met in the present work if attention is confined to the lowest kilometer of the troposphere. The precision of temperature measurement in the simulation does not permit distinction between atmospheres that are initially isothermal or adiabatic; hence the present work implies that the patterns of convection arising from residual heating from below, as observed in the simulation, are similar for both of these initial conditions. The simulation provides for general horizontal flow that is either absent (natural convection) or limited to 0.5 meters sec^{-1} (free convection). The troposphere is assumed dry. Residual heat transfer from the underlying surface into the troposphere is introduced as a perturbation, at rates up to 0.33 milliwatts $cm.^{2}$; this is a small fraction of the normal daytime heat flux (19.2 milliwatts $cm.^{-2}$). The accompanying transfer of heat is assumed by an unspecified mode of turbulence, as may be represented by a mean thermal diffusivity of 5,000 $cm.^{2}$ sec^{-1} throughout the lower troposphere.

The observed flow and temperature perturbations in the laboratory simulation have shown general agreement with the available observations in the prototype. The Richardson number varies with local wind shear

in free convection, in a similar manner in both the prototype and the simulation. Further, the profiles of temperature follow the same trends in the two systems, although the boundary conditions in the prototype have not been fully specified. The scarcity of additional details on the lower troposphere does not provide for other comparisons.

A description of convection in the lower troposphere will be presented in the following two sections. These will be based upon the experimental observations in the simulation, beyond those used in Chapter VIII. The result of neglecting Coriolis forces in the simulation, upon the model of convection, will also be reviewed. Several questions arise directly from this study; an investigation of these will require refinements of the present simulation. These questions are discussed in the last section.

9.1 Model of Natural Convection in the Lower Troposphere

Figure 9.1 (a) illustrates the model of natural convection as deduced from the laboratory simulation. After the lower troposphere has become isothermal, residual heating of the surface will initiate an upward flux into the air. A strong, negative gradient of temperature builds up within the lowest few meters, and vertical columns surmounted by caps break through this layer to grow upwards. These caps may rise at some 0.6 meters per second as the columns beneath them convey heated air upwards. The caps resemble thermals in the form of spherical vortices. These columns deform laterally with time, in an irregular manner; two adjacent columns may merge aloft and the cap may change into a vertical extension of the column to heights as great as 700 meters.

The density of columns emerging from the heated surface layer increases with surface heating. As the residual heat flux approaches 0.33 milliwatts cm^{-2}, the horizontal separation of the convective columns

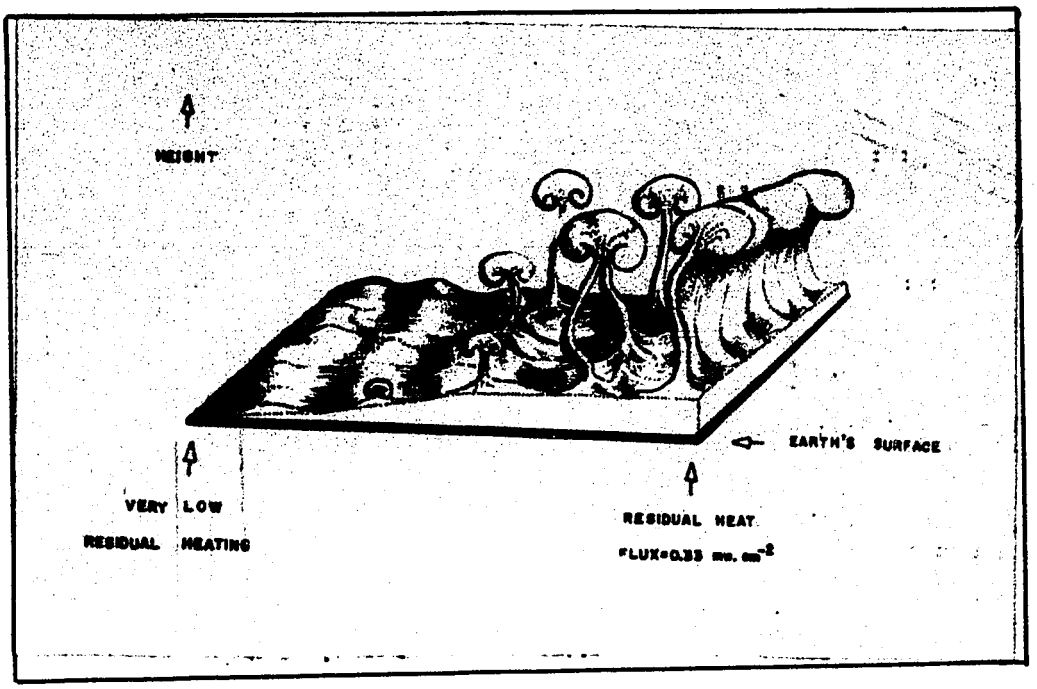

(a) Convective columns above the heated surface.

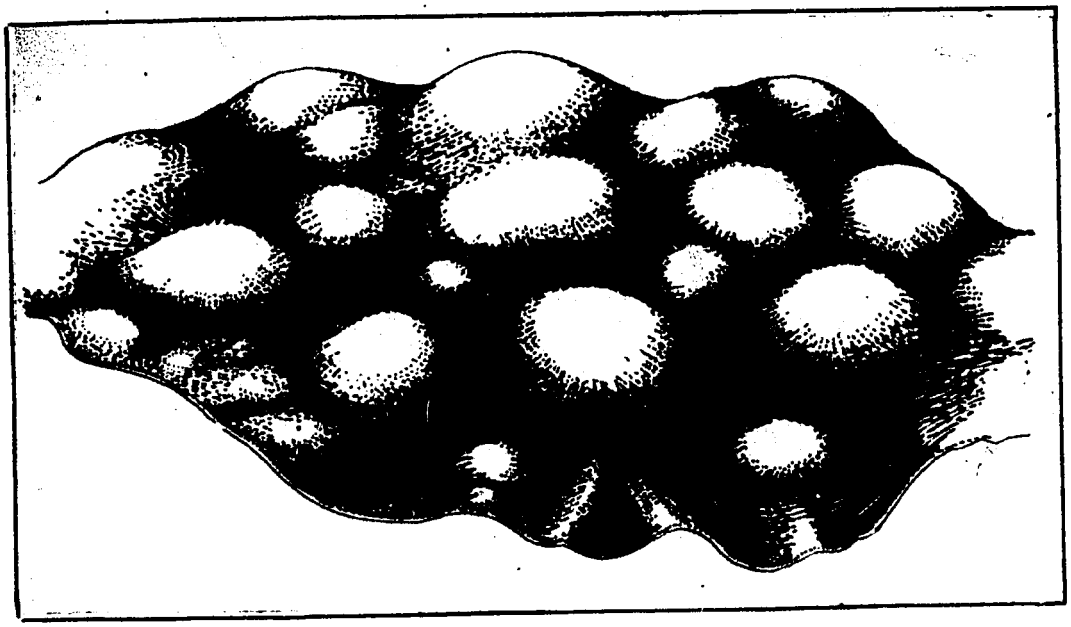

(b) Perturbation of an elevated temperature inversion.

Figure 9.1 Models of Thermal Convection in the Lower Troposphere, for Residual Heating of Isothermal, Dry Air from Below. Natural Convection.

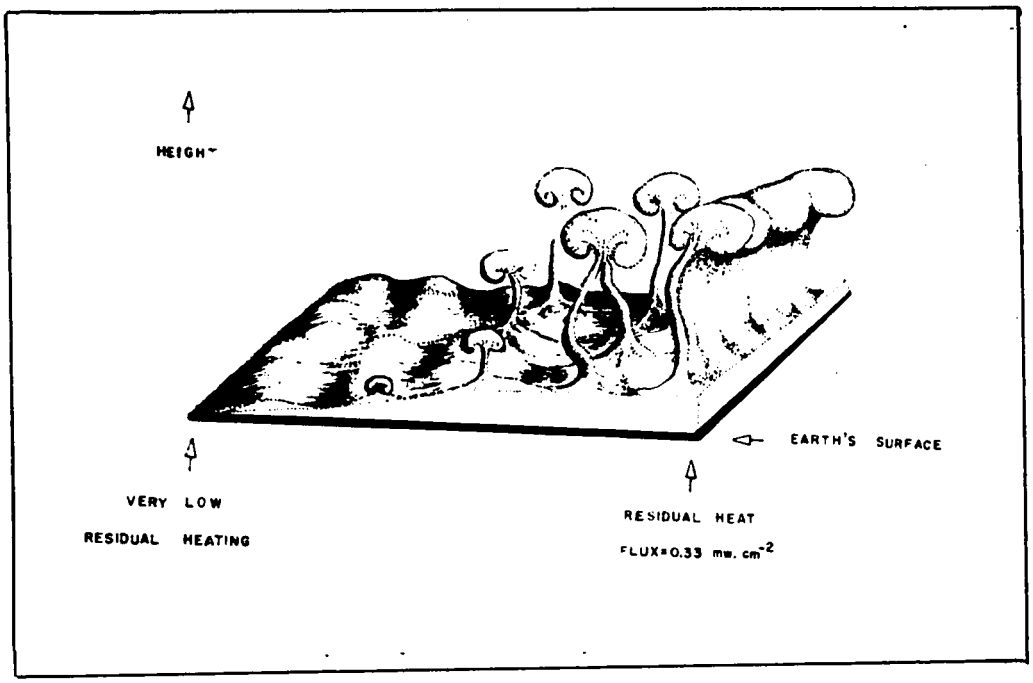

(a) Convective columns above the heated surface.

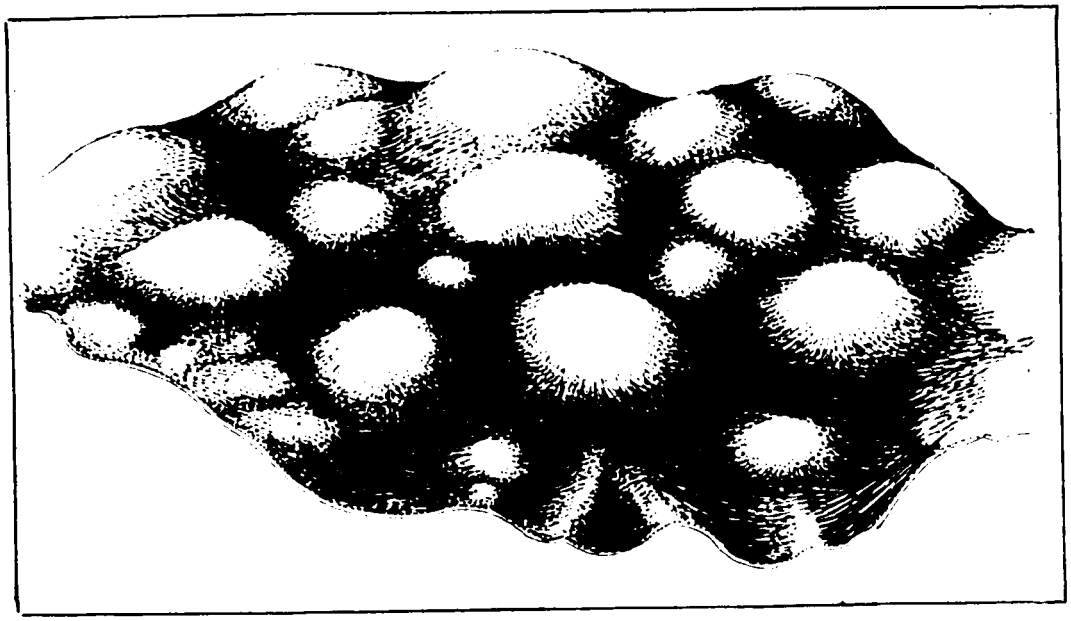

(b) Perturbation of an elevated temperature inversion.

Figure 9.1 Models of Thermal Convection in the Lower Troposphere, for Residual Heating of Isothermal, Dry Air from Below. Natural Convection.

becomes roughly 100 - 200 meters; there is a tendency for adjacent columns to join laterally, thus forming a convective wall. Each column contains a warm central core with a cooler periphery. For the maximum residual heating mentioned above, the core temperature just above the lower boundary is about 0.2°C above that of the environment; this temperature difference decreases with height. In total, the temperature field of the lower troposphere above the first one or two hundred meters is a complex pattern of convective columns surmounted by concave caps. It will be noted that the patterns formed by these convective columns are clearly different from the cells described by Bénard. It is of interest to note further that a convective column may, in some cases, carry heat upwards along a positive temperature gradient.

The effect of these convective columns upon an elevated temperature inversion is shown in Figure 9.1 (b). As residual heating of the lower surface continues, the convective columns convey warm air upwards until it penetrates the inversion and ceases to rise in the stable air above. Each penetration produces a dome-like perturbation of the inversion layer; the subsequent oscillation of the perturbation in the stable air initiates an internal gravity-shear wave that moves laterally along the inversion at about 0.6 meters sec^{-1}. In addition, the general accumulation of warm air at the level of the inversion causes the whole inversion to rise at a rate of some 8 meters hr^{-1}.

9.2 Model of Free Convection in the Lower Troposphere (U_f = 0.8 $m.sec^{-1}$)

Introduction of horizontal flow (wind) modifies the model of heat convection in several ways (Figure 9.2). The incipient caps which would form above the column are quickly distorted into quasi-horizontal

extensions of the columns. Increased heating of the lower surface again extends the columns farther upwards, but the maximum height is only about half that for natural convection. Here, the columns are inclined with the wind by an amount which increases with height, until the upper extremity is almost horizontal in a wave-like tail; at times, this tail may break away from the rest of the column and move as a wave section with the wind for a short time. Within the lower part of the column, heated air is lifted upwards by buoyancy at a speed of some 0.22 meters sec^{-1} for residual heat flux 0.27 milliwatts $cm.^{-2}$; the speed is reduced considerably with cooling of the core at higher levels. The more buoyant columns with warmer cores are eroded by the wind, so that the periphery is stripped away on the windward side to expose the warm core. Horizontal temperature gradients of $0.02^{o}C$/meter may occur at the eroded cores. The

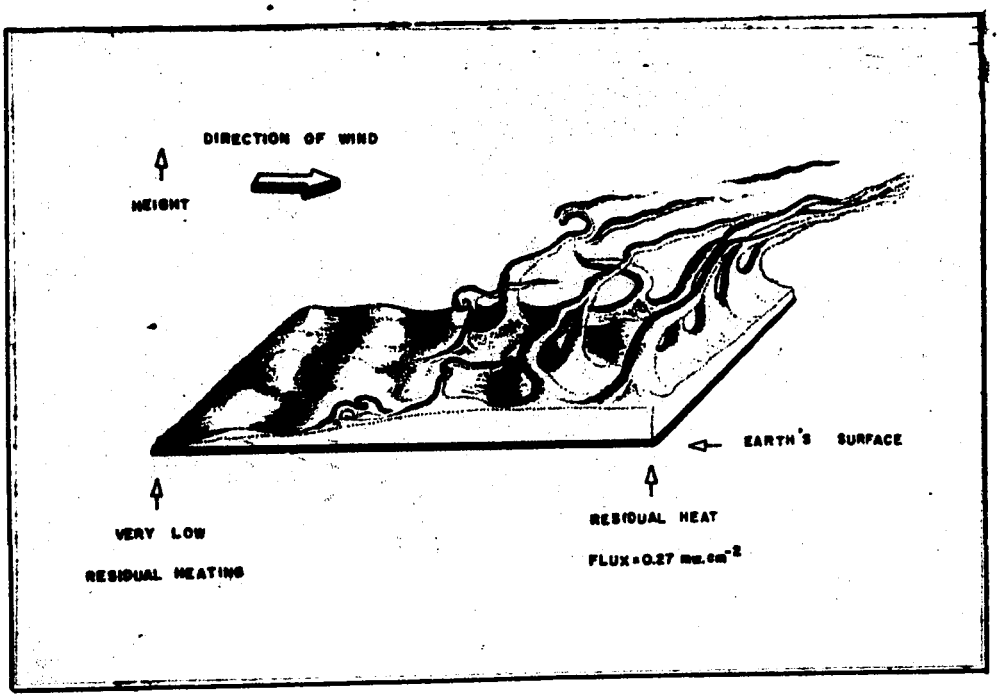

Figure 9.2 Model of Thermal Convection in the Lower Troposphere, for Residual Heating of Isothermal, Dry Air, from Below. Free Convection (U_f = 0.8 meter sec^{-1}).

leeward side of the column is not altered and there is a lesser tendency for the columns to merge into a lateral wall than there is in the case of natural convection.

Two further implications of the column indications should be noted. If a section of the earth's surface with lower albedo is located downwind from a section with higher albedo, the latter may provide the desired residual heating for convection while the former supports an isothermal troposphere with no appreciable convection. In this case, the horizontal tails of the upwind columns may continue at an elevated-level for one or two kilometers into the isothermal region without residual heating. Furthermore, the velocity perturbations that are associated with the inclined columns cause a notable increase in the averaging time that is required to obtain the mean velocity aloft.

9.3 Effect of Coriolis Forces upon the Convective Column

The neglect of Coriolis forces and the Rossby number in the present simulation has assumed that the simulation is in a non-rotating reference system. In reality, rotation of the earth subjects moving air to these Coriolis forces which result is the well-known Ekman spiral of wind direction at heights between a few tens of meters and a kilometer above ground.

The writer has examined the possible effects of Coriolis forces upon the convective columns observed in the simulation. For this purpose, the theories of smoke columns from stacks in the absence of wind (Morton et al, 1956) and in the presence of very strong wind (Briggs, 1968) have been generalized by the writer, to permit the inclusion of Coriolis forces and moderate winds in the environment. The vertical profile of wind is

assumed non-linear, according to common observation. Details of this analysis are given in Appendix VII.

This analysis has shown several features of interest. For columns of moderate inclination to the vertical (i.e. in moderate winds), the presence of Coriolis forces reduces the maximum height of the columns by only some 20 percent. Further, the column becomes weakly deformed into a shallow spiral, with total rotation less than 90^{o}, because of the Coriolis forces. Entrainment of environmental air by peripheral turbulence at the column is included in the theory of buoyant plumes through the use of an entrainment constant, although the physical process associated with this constant is not clear. It is of interest to note that the calculated entrainment constants as deduced for the columns observed in the present simulation are very close to the constants derived from observations on smoke columns in the atmosphere.

9.4 For Further Study

Several extensions of the present work are readily suggested. It is desirable, for example, to examine the models of convection when the vertical profile of air temperature is neither isothermal nor adiabatic. Stronger heating of the surface about mid-day causes a negative temperature gradient of about $1^{o}C$ per 100 m. To what extent can the concept of residual heating and the above models of convection be carried over into this different set of boundary conditions?

The relationship between the magnitude of temperature perturbations and the local vertical gradient of temperature as observed in the simulation is shown in Figure 9.3 for free and natural convection.

Figure 9.3 Relationship between Local Gradient of Temperature and Magnitude of Temperature Fluctuations for Free and Natural Convection (Observed in the Simulation, and Converted to the Prototype Scale).

It will be noted that the standard deviation of temperature tends to increase with the magnitude of the temperature gradient although the dispersal of points is wide. This trend should be examined further for larger lapse rates of temperature, as a means of studying the physical process of convection in detail.

Another topic which deserves consideration is the effect of the surface geometry upon the models of convection. The large value of roughness length z_o in the present work is due to a physical irregularity in the input flow straightener. z_o should be reduced by a flow straightener of different design and the observations repeated. Extension of the observations to heights closer to the surface would be permitted. The writer has examined many shadowgraphs for details of the origin of the convective columns. He suggests that Benard-type cells within the thermal boundary layer at the surface may perturb its upper level and cause eventual penetration by a

column, as illustrated in the sequence of Figure 9.4. This possibility

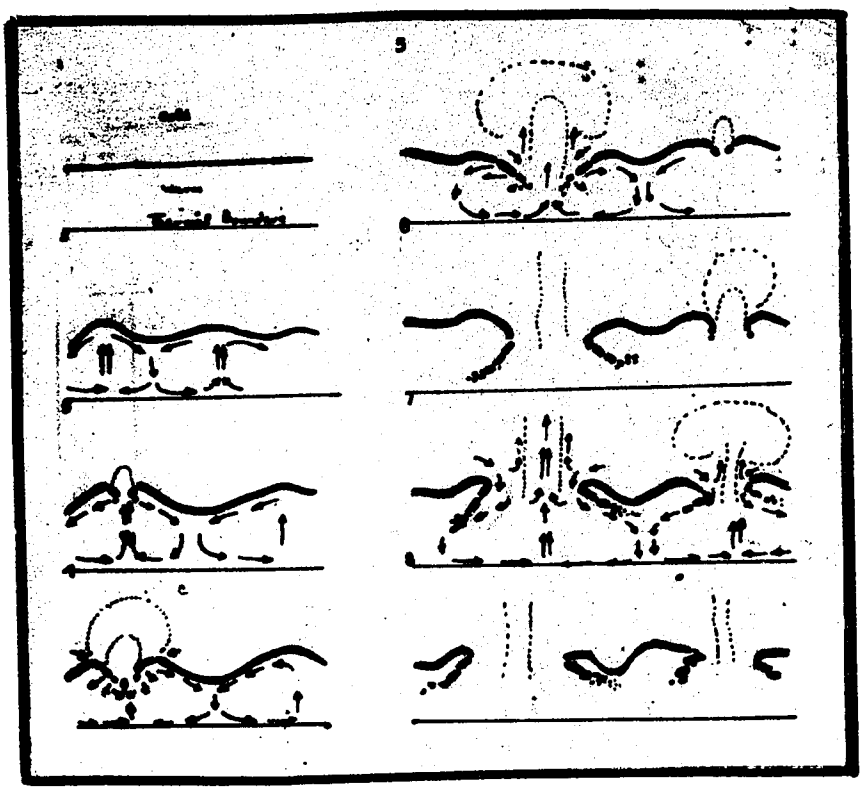

Figure 9.4 Suggested Sequence in the Generation of Convective Columns at the Thermal Boundary Layer (Region of Large Temperature Gradient at the Surface).

should be explored.

Yet another interesting extension is the study of convective models in forced convection. Here, it is necessary to increase the flow rate in the simulation, so that the surface friction effects predominate the buoyancy motion due to surface heating. It is noted that the horizontal flow (wind) increases with surface heating. Examination of the isotherm patterns suggests that this increase may be due to the rising of the convective columns. This suggestion should be investigated.

The theory of buoyant plumes also should be examined further. This would include consideration of the entrainment constant and its physical significance, and the effects of various rates of columnar convection upon the column geometry.

APPENDIX I

LIST OF SYMBOLS

$A_{i,p}$, $A_{i,s}$	Variables in the governing equations,
C	Specific heat,
c_p,c_v	Specific heats at constant pressure and constant volume, respectively,
Fr.	Froude number,
g	Acceleration of gravity,
Gr.	Grashof number,
H	Heat flux,
k	von Karman's constant,
L	Representative,
$\mathcal{L}$	Monin-Obukhov length,
P	Pressure force,
Pe	Peclet number,
Pr.	Prandtl number,
R	Gas constant of dry air; radius of the thermal leading edge; thermistor resistance,
Ra.	Rayleigh number,
Re.	Reynolds number,
Ri	Richardson's number,
T	Temperature,
Δ T	Representative temperature difference,

U	Representative velocity along the horizontal,
u,v,w	Components of fluid velocity,
$\vec{V}$	Fluid velocity,
x,y,z	Space coordinates,
z_o	Roughness length,
α	Coefficient of thermal expansion,
α_i	Scaling factor,
β	Temperature gradient,
γ	Ratio of specific heats,
Δ	Finite difference,
ρ	Density,
σ	Temperature standard deviation,
Ψ	Angle of inclination of plumes.

APPENDIX II

ORDERS OF MAGNITUDE OF THE TERMS IN THE GOVERNING EQUATIONS

Hydrodynamics texts generally indicate that Eqs. 3.1, 3.4 and 3.6 can be reduced to Eqs. 3.17, 3.24 and 3.26 respectively by the application of the Boussinesq approximation (see e.g. Chandrasakar, 1961, p. 61). This approximation has been discussed by Spiegel and Veronis (1960) and Mihalijan (1962). Essentially, it treats the density ρ as a constant except in the term describing gravitational force. The variation of ρ in the latter case is given by Eq. 3.20. Long (1965), however, points out that this approximation must be treated with caution when it is applied to some atmospheric phenomena. In his analysis of internal gravity waves, he notes that the Boussinesq approximation would lead to neglect of perturbation quantities which are important to this phenomenon.

In the present study, the physical implications of the Boussinesq approximation will be examined by considering the relative magnitudes of the terms of the governing equations. The following table presents the accepted constants of the dry air in the lower troposphere.

The following assumptions will be made which appear to be valid in the lower troposphere. The magnitude of the maximum average horizontal and vertical velocities are assumed to be $\bar{U} = 2\ 10^3$ cm. sec^{-1} and $w = 10$ cm. sec^{-1} respectively. (Brunt 1934, p. 162).

TABLE IIa

Properties of the Lower Troposphere

Physical Property	Symbol	Magnitude	Units	Reference
Air density	ρ	$1.3\ 10^{-3}$	gm cm^{-3}	Haltiner & Martin (1957) p. 248
Specific heat at constant pressure	c_p	1.003	Jouls gm^{-1} $^oK^{-1}$	Haltiner & Martin (1957) p. 12
Eddy kinematic viscosity	ν	10^4	cm^2 sec^{-1}	Haltiner & Martin (1957) p. 253
Eddy thermal diffusivity	κ	10^4	cm^2 sec^{-1}	Haltiner & Martin (1957) p. 253
Acceleration due to gravity	g	980	cm sec^{-2}	
Molecular viscosity	μ_m	$1.8\ 10^{-4}$	gm cm^{-1} sec^{-1}	Haltiner & Martin (1957) p. 216
Molecular thermal conductivity	K_m	$0.6\ 10^{-4}$	cal $cm^{-1}sec^{-1}$ $^{-1}$	Munn (1966) p. 34
Angular speed of the earth's rotation	Ω	$0.7\ 10^{-4}$	radians sec^{-1}	
Speed of sound	c	$353\ 10^2$	cm sec^{-1}	Schlichting (1960) p. 9
Coefficient of thermal expansion of air	α	$3\ 10^{-3}$	$^oK^{-1}$	Sutton (1953) p. 115

The eddy viscosity and eddy thermal diffusivity are assumed constant (see Chapters II and III) and because their magnitudes are large compared with those of their molecular counterparts the latter will be neglected. c_p is independent of temperature, of time and of position. It is also assumed that the temperature gradient (∇T) is of the order 10^{-3} $^{o}C\ cm^{-1}$. This includes adiabatic and subadiabatic conditions in a horizontally stratified troposphere. It will be assumed further that this gradient changes (i.e. $\nabla^2 T$) by less than 10^{-6} $^{o}C\ cm^{-1}$. The maximum velocity gradient is 1 sec^{-1}.

By virtue of the above assumptions the orders of magnitude of the various terms in the governing equation are given in Table IIb.

TABLE IIb

Orders of Magnitude of the Terms in the Governing Equations

Term	Order of Magnitude	Units
$\vec{\Omega} \times \vec{V}$	10^{-1}	$cm\ sec^{-2}$
∇P	1	$gm\ cm^{-2}\ sec^{-2}$
$(\nabla \mu_m)_{maximum}$	10^{-9}	$gm\ cm^{-2}\ sec^{-1}$
$(\nabla K_m)_{maximum}$	10^{-9}	$gm\ cm^{-2}\ sec^{-1}$
$\frac{DP}{Dt}$	10^{3}	$gm\ cm^{-1}\ sec^{-3}$
$\frac{D\rho}{Dt}$	10^{-6}	$gm\ cm^{-3}\ sec^{-1}$
Φ	1	sec^{-2}
$\nabla . \vec{V}$	10^{-3}	sec^{-1}
$\frac{DP'}{Dt}$	1	$gm\ cm^{-1}\ sec^{-3}$

Hence, for the Navier-Stokes equation:

$$\frac{\vec{DV}}{Dt} = 2\,\vec{\Omega} \times \vec{V} + \vec{g} - \frac{1}{\rho}\nabla P + \frac{1}{\rho}\vec{S} \qquad \text{II.1}$$

$$= -0\left[10^{-1}\right] + 0\left[10^{3}\right] - 0\left[10^{3}\right] + 0\left[?\right]$$

The order of magnitude of the last term in Eq. II.1 depends upon whether the motion is laminar or turbulent and also in the term $\nabla \cdot \nabla \vec{V}$. Since this term may be of the same order of magnitude as the second and third terms, only the first term will be neglected and Eq. II.1 can be written as:

$$\frac{\vec{DV}}{Dt} \approx \vec{g} - \frac{1}{\rho}\nabla P + \frac{1}{\rho}\vec{S} \qquad \text{II.2}$$

With regard to the term $\vec{S}$:

$$\vec{S} = \mu\,\nabla \cdot \nabla \vec{V} + \frac{1}{3}\mu\,\nabla\,(\nabla \cdot \vec{V}) \qquad \text{II.3}$$

The orders of magnitude of the first and second terms again are uncertain. It will be recalled that $\nabla \vec{V}$ is $0\left[1\right]$, and $\nabla \cdot \vec{V}$ is $0\left[10^{-3}\right]$; hence the magnitude of the fourth term generally will be small compared with that of the second. Then any significant contribution to $\vec{S}$ would depend upon the second term, and Eq. II.3 can be written:

$$\vec{S} \approx \nabla \cdot \nabla \vec{V} \qquad \text{II.4}$$

From Eq. 3.6

$$\rho\, c_p \frac{DT}{Dt} = K\,\nabla^2 T + \frac{DP}{Dt} + \mu\Phi \qquad \text{II.5}$$

$$= 0\left[10^{2}\right] + 0\left[10^{3}\right] + 0\left[10^{-4}\right]$$

Hence,

$$\rho c_p \frac{DT}{Dt} \approx K \nabla^2 T + \frac{DP}{Dt} \qquad \text{II.6}$$

Applying the method of perturbations to Eq. II.6 (see Chapter III) one obtains

$$\frac{DT'}{Dt} = - \vec{V}.\nabla T_o + \kappa \nabla^2 T' + \kappa \nabla^2 T_o + \frac{1}{c_p \rho_o} \frac{DP'}{Dt} - \frac{1}{c_p} \vec{V}.\vec{g} \qquad \text{II.7}$$

since ∇T_o may be either equal to $- \frac{g}{c_p}$ for an adiabatic atmosphere ($\nabla^2 T_o = 0$) or to zero for an isothermal atmosphere. For an initially adiabatic atmosphere, Eq. II.7 may be written as

$$\frac{DT'}{Dt} = \kappa \nabla^2 T' + \frac{1}{c_p \rho_o} \frac{DP'}{Dt} \qquad \text{II.8}$$

$$= 0\left[10^2\right] + 0\left[10^{-4}\right]$$

For an initially isothermal atmosphere, Eq. II.7 may be written as

$$\frac{DT'}{Dt} = \kappa \nabla^2 T' + \frac{1}{c_p \rho_o} \frac{DP'}{Dt} - \frac{1}{c_p} \vec{V}.\vec{g}$$

$$= 0\left[10^2\right] + 0\left[10^{-4}\right] - 0\left[10^{-4}\right]$$

It will be noted that in both cases Eq. II.7 may be written as

$$\frac{DT'}{Dt} \approx \kappa \nabla^2 T' \quad \text{to a good approximation.}$$

APPENDIX III

IMPELLER FLOW EXAMINATION

An impeller, having a sufficiently high outlet velocity, may introduce irregular eddying motion to the ambient fluid. Since laminar flow in the test region is essential, an examination of the impeller outlet flow at different output velocities was needed.

The impeller was placed in the centre of the test section and the flow was investigated using the shadowgraph technique discussed in Section 6.3. The arrangement is shown in Figure III.1. The water tunnel was filled to a depth of about 25 cms. A shadowgraph was taken of the outlet of the impeller (Fig.III.2a) which indicated refractivity inhomogeneities due to the contrasting water temperature within the ambient fluid. The water was allowed to flow through the impeller with a very small outlet velocity. Pressure difference through the manometer was recorded and shadowgraph picture of the outlet of the impeller was taken. This process was repeated for different outlet velocities. It was noted that at first (Fig. III.2 b, c, d) the outlet flow formed a straight filament with laminar characteristics. With increase in the velocity, greater than 3 cm./sec. the laminar filament broke off gradually changing to a turbulent motion some distance away from the outlet (Fig. III.2 e, f). The outlet flow became turbulent with further increase in the velocity (Fig. III.2

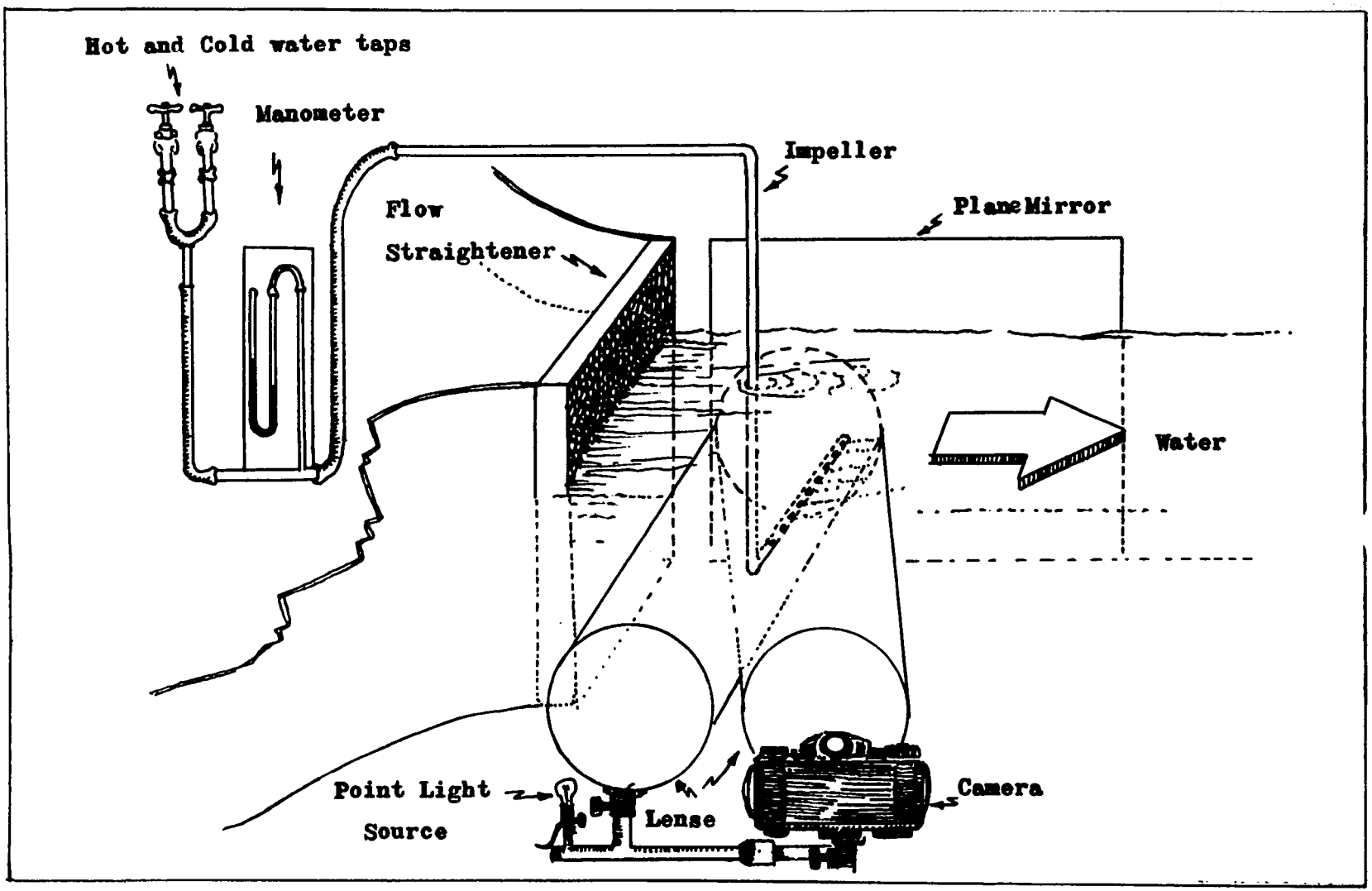

Figure III.1 Impeller Flow Examination.

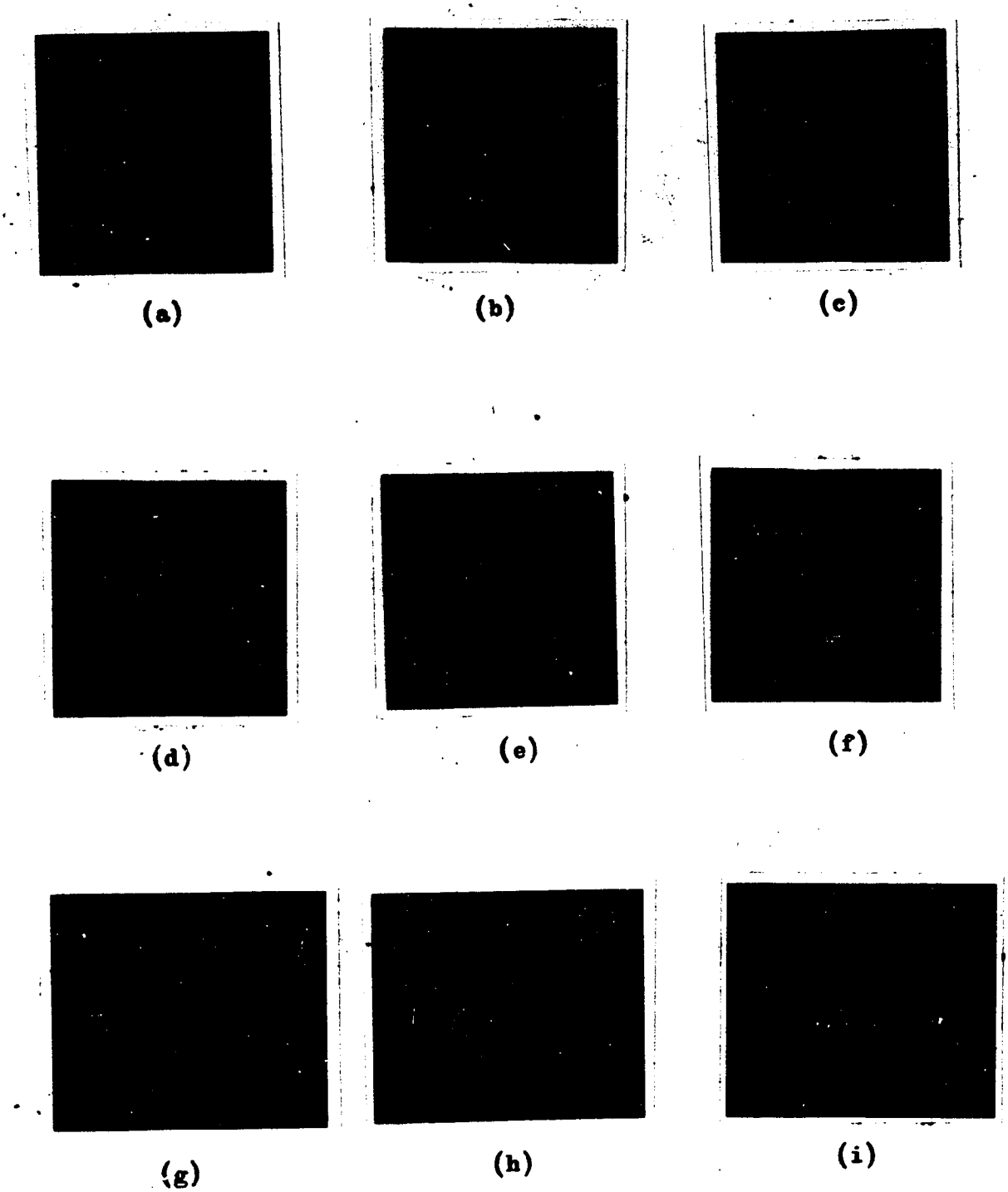

Figure III.2 Shadowgraph of Water Flow from the Impeller.

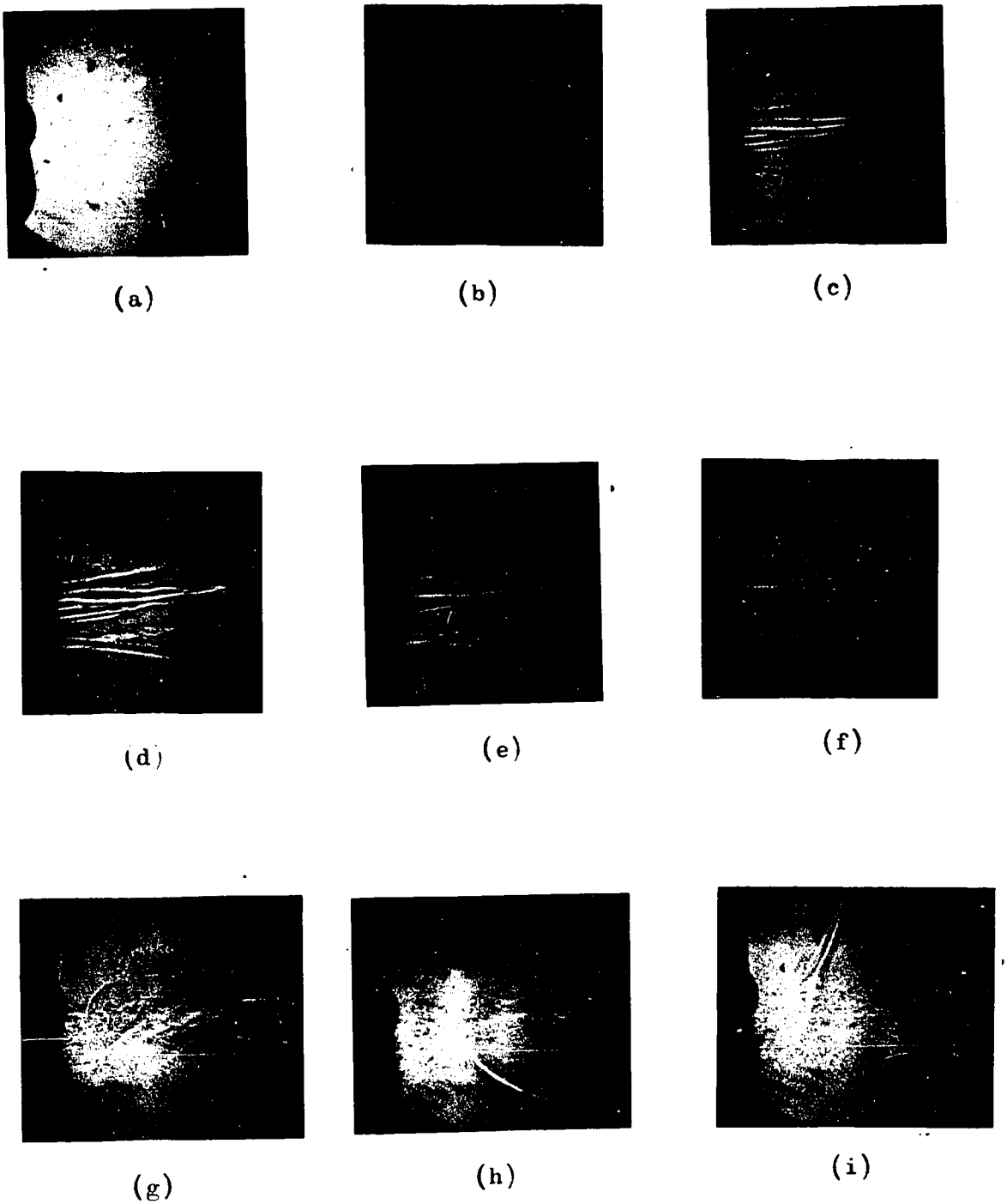

Figure III.2 Shadowgraph of Water Flow from the Impeller.

g, h, i). It was therefore seen that the outlet of the impeller must be limited to give a velocity of not more than 3 cm. sec^{-1} and it should be located far up stream from the test region in order to prevent turbulence in the latter.

Examination of the flow pattern close to the flow straightener indicated that for low velocity the height of the fluid in motion decreases with a decrease in the velocity. Figure III.3 shows the flow pattern close to the flowstraightener at different stream velocities. The number at the bottom of each picture indicates the magnitude of the velocity. It can be seen from this study that the outlet velocity of the impeller should be adjusted to give a general horizontal flow of not less than 0.3 cm. sec^{-1} and not more than 3 cms. sec^{-1} close to the flow straightener.

0.1 cm./sec.

0.2 cm./sec.

0.3 cm./sec.

0.35 cm./sec.

Figure III.3 Velocity Distribution at Different Stream Velocities.

0.1 cm./sec.

0.2 cm./sec.

0.3 cm./sec.

0.35 cm./sec.

Figure III.3 Velocity Distribution at Different Stream Velocities.

APPENDIX IV

RELATIONSHIP BETWEEN Al. PARTICLES AND WATER MOVEMENTS

The motion of the Al. particles is governed by the patterns of flow. An isolated particle will be carried upwards where the upward vertical components exceed the fall velocity (0.02 cm. sec^{-1}). It will be also carried downwards when the fall velocity exceeds the flow components. There is thus, a continual change in the position of the particle and, in general, it does not duplicate the exact movements of water. The difference in the movements is important in interpreting the result of the velocity measurements. This can be treated analytically.

As the flow passes the particle, the stream lines deflect around it and form a wake down the stream. As a result, forces are developed on the particle which might be decomposed into a drag force in the direction of the mean flow and a lift force perpendicular to the mean horizontal flow. Here, the lift force is the resultant of the pressure difference between the upper and lower sides of the particle. Since on both sides of the particle the pressure is reduced by nearly the same amount, the lift force may be neglected.

The force which resists the motion is the submerged weight of the particle along the vertical. A diagram showing forces on a typical particle is shown in Figure IV.1 a.

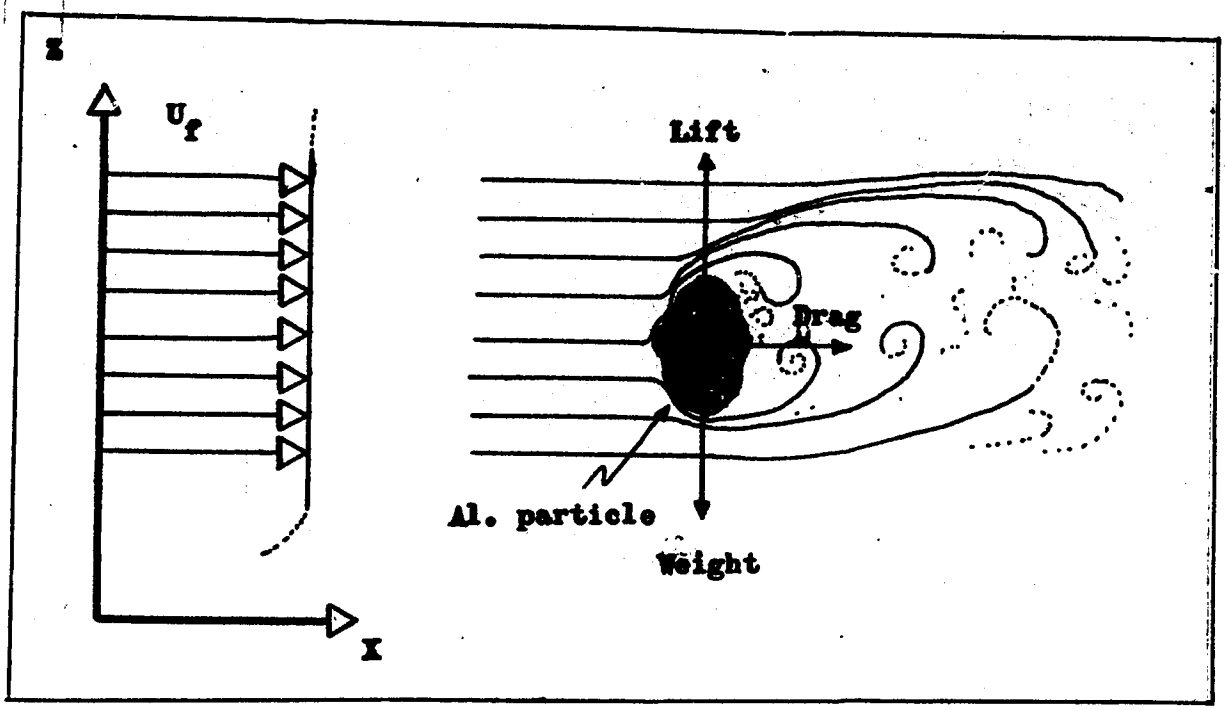

(a)

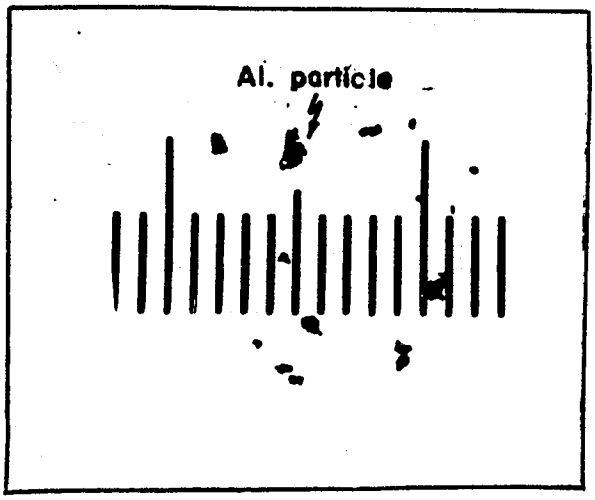

(b)

Figure IV.1 Examination of the Relationship between Al. Particles and Water Movements.

The movement of the particle depends upon the magnitudes of these forces.

For simplicity, consider that the general horizontal flow has a constant velocity U_f and the Al. particle has a spherical shape with radius $r = 0.5\ 10^{-3}$ cm. (Fig. IV.1 b). The equation of motion along the horizontal can be written

$$M \frac{dU_p}{dt} = F \qquad \text{IV.1}$$

The quantities involved are: M, mass of the particle; U_p, velocity of the particle; t, time; F, the drag force.

Of the quantities involved, only F poses a special consideration. F is a function of the velocity difference between the Al. particle and the water. For a laminar flow and for a Reynolds number <1, by Stokes' formula (Lamb 1945, p. 597), F may be given as

$$F = 6 \pi \mu r (U_f - U_p) \qquad \text{IV.2}$$

Here, μ is the viscosity of water ($\approx 10^{-2}$). Substituting in Eq.(IV.1) from Eq. (IV.2) and integrating, one gets

$$U_p = U_f(1 - \exp(-6 \pi \mu rt/M)) \qquad \text{IV.3}$$

Assuming that at $t = 0$ $U_p = 0$. It will be seen that

$$U_p \approx U_f$$

Since $\exp(-6 \pi \mu rt/M) \approx 0$, as $6 \pi \mu rt/M$ is of the order 10^5 for $t > 0$. The drag force on the particle will then tend to carry it along the horizontal with a velocity equal to that of the water.

The combination of the horizontal motion due to the drag and the downward vertical motion due to the weight of the particle will result in a trajectory to a point where the particle reaches the bottom of the water tunnel. This, however, will depend on the magnitude of the general horizontal velocity. The angle θ that the resultant velocity U of the particle makes with the horizontal is given by

$$\tan \theta = \frac{w}{U_f}$$

where w is the falling velocity. The magnitude of U is given by

$$U = \sqrt{U_f^2 + w^2} \qquad \text{IV.4}$$

The fall velocity of the Al. particles (Fig. IV.2) in a fluid at rest is determined by the buoyancy force B

$$B = \frac{4}{3} \pi r^3 g (\rho_p - \rho_w) \qquad \text{IV.5}$$

where r is the radius of the particle, g is the acceleration of gravity, ρ_p is the density of the particle and ρ_w is the density of water.

The force B is opposed by the viscous force η of the water and will let the particle settle with a small velocity w. For laminar flow conditions and for Re $<$ 1 by Stokes' formula

$$\eta = 6 \pi \mu rw \qquad \text{IV.6}$$

where μ is the viscosity of water.

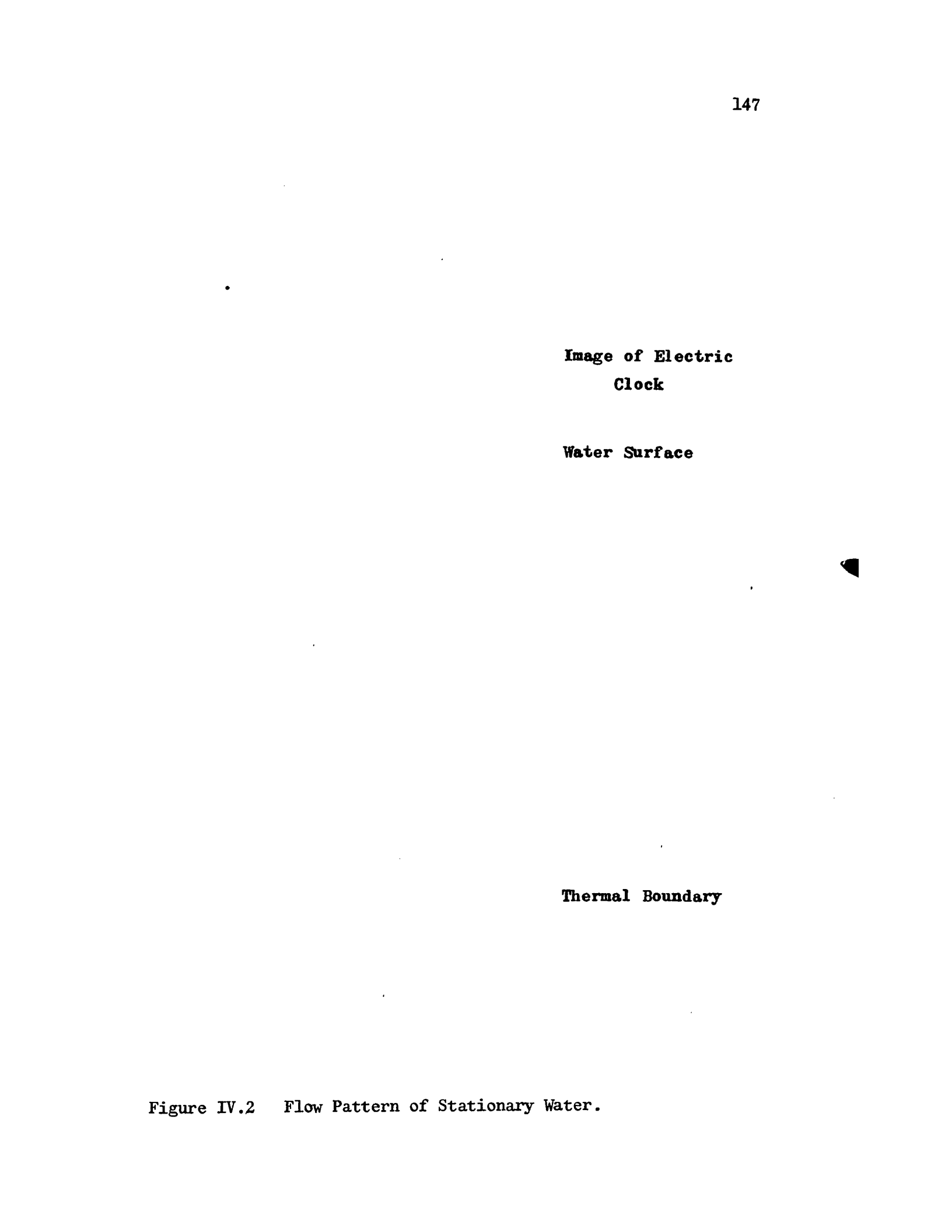

Figure IV.2 Flow Pattern of Stationary Water.

Since the fall of the Al. particle is uniform,

$$\eta = F \qquad \text{IV.7}$$

Hence,

$$w = \frac{2}{9} g \frac{r^2}{\mu} (\rho_p - \rho_w) \qquad \text{IV.8}$$

For $r = \frac{10^{-3}}{2}$, $\mu = 10^{-2}$, $g = 980$, $\rho_p = 7.7$, $\rho_w = 1$

$$w \approx 0.02 \text{ cm.sec}^{-1}$$

From Eq. (IV.5) the magnitude of U is then given by

$$U \approx U_f$$

Since $w^2 < U_f^2$.

APPENDIX V

ANEMOMETER EFFECT AND TIME CONSTANT OF TEMPERATURE SENSOR

A. Anemometer Effect

Large dissipated power, within the thermistor, may heat the sensor above the ambient temperature. Consequently,in a moving fluid, the sensor would act as a hot wire anemometer and in still fluid, this causes an erroneously high temperature. This effect is highly undesirable. It was reported by the manufacturer that the dissipation constant, which will raise the temperature of the thermistor $1^{o}C$ above its surrounding (air), is 0.1 milliwatt. An attempt was made to measure the power dissipation through the thermistor during the motion of the ambient water. Figure V.1 shows the apparatus which was used for this investigation. The bridge was balanced while the water was kept at constant temperature. Nine values of current were applied which raised the dissipated power through the thermistor. Due to this increase, the probe acted as a hot wire anemometer and due to the cooling of the probe, the scope trace started to measure variations in the fluid velocity. Consequently, the bridge should supply a power not more than 0.01 mw.

Dissipated power	Scope trace	Dissipated power	Scope trace	Dissipated power	Scope trace

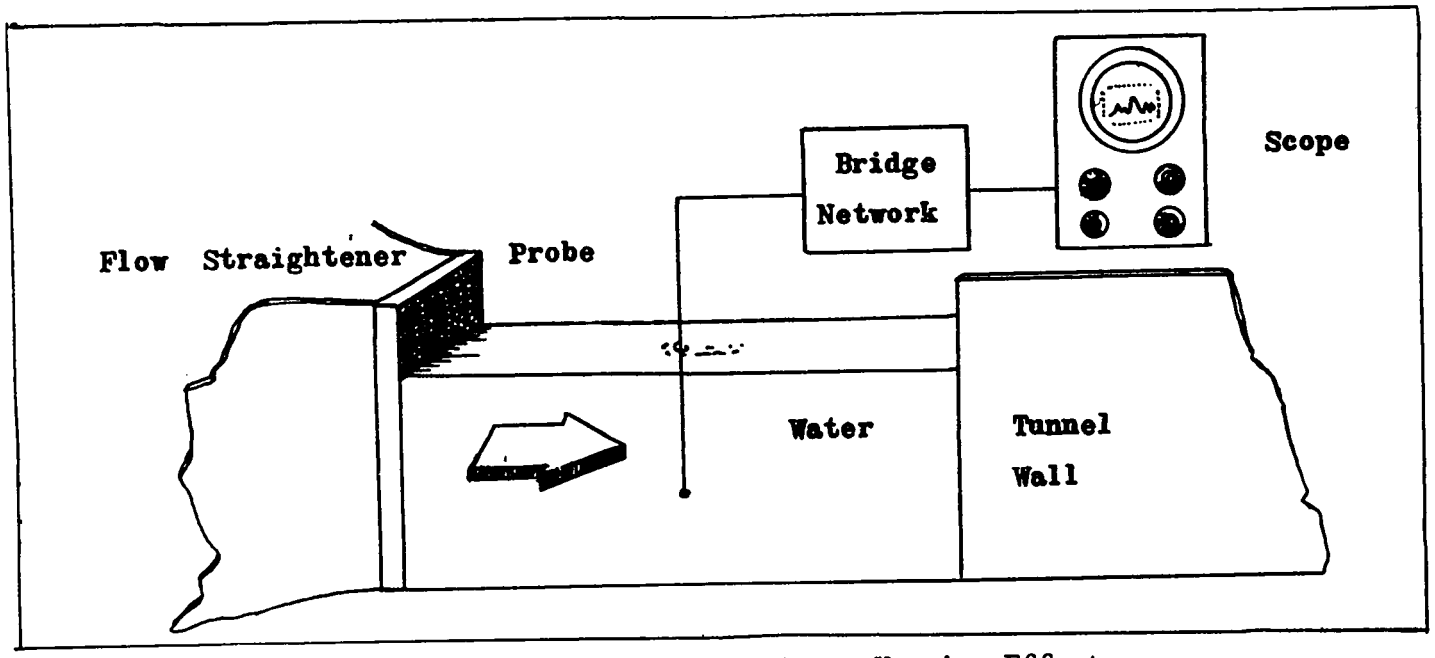

Figure V.1 Examination of Thermistor Heating Effect

B. Time Constant

When the thermistor bead is placed in a medium of a different temperature, the bead will take up the new temperature asymptotically. The rate of its approach to the new temperature depends on the material, dimensions and insulation of the thermistor and on the properties of the ambient medium (see e.g. Middleton and Spilhaus 1953, p. 63). This rate is described by the time constant of the thermistor, which is the time, in seconds, required for the bead to change its temperature from 63% of its original value to its new value. This new temperature is impressed upon the thermistor in a step change.

Specially designed equipment was used to measure the time constant of the wax and glass coated thermistors. The arrangement of this equipment is shown diagramatically in Figure V.II

Two laminar streams of tap water with a temperature difference of $4^{o}C$ were allowed to flow through rubber hoses of radius (r) 1.3 cms. with an average velocity ($\bar{V}$) equal to 63 cm/sec. $\bar{V}$ is given by (see e.g. Streeter 1961, p. 3-6)

$$\bar{V} = \frac{Q/t}{\pi r^2}$$

where Q = 77 milliliter, is the amount of water collected at a given time t = 0.23 second. The probe was placed on a circular disc fastened to the bench through a ball bearing. With this mechanism the probe was allowed to oscillate from one stream to the other at the point of convergence of the two streams. The disc had a proturberance to trigger a microswitch which in turn was used to trigger an oscilloscope

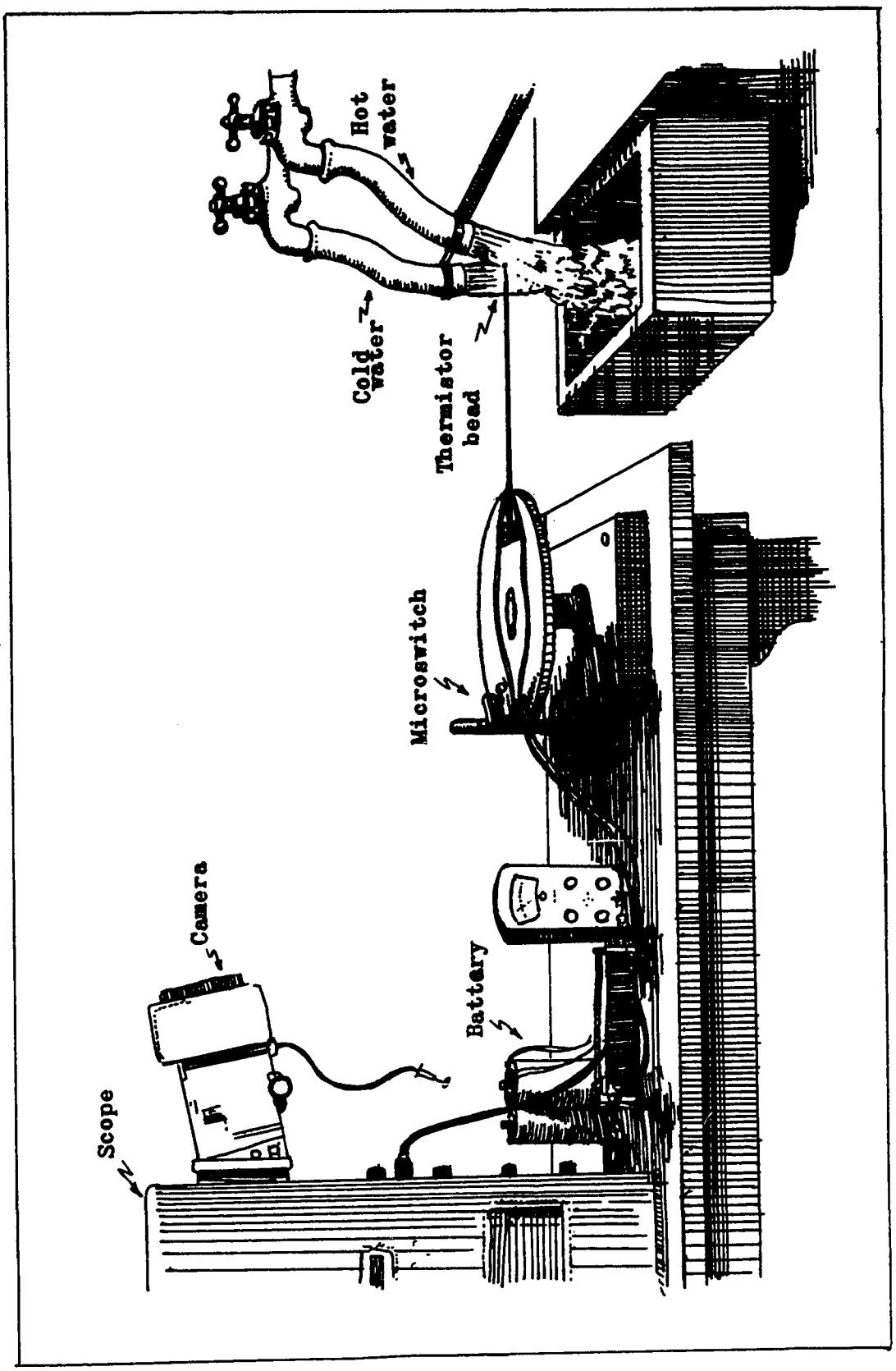

Figure V.2 Arrangement for Probe Time Constant.

with recording poloroid camera. A very small D.C. current was supplied to the probe raising the temperature of the bead not more than 0.008°C above the ambient medium. A diagram of the electrical circuit used in these investigations is shown at the top of Figure V.II. The change in the resistance of the thermistor was traced on the scope screen and photographed while the sensor was crossing the two streams at the point of convergence. Figure V.III is a pair of photographs of the scope trace taken of the wax coated and the glass coated probes. It was found that the time constants for the wax coated and for the glass coated thermistor were 0.17 and 0.12 second respectively.

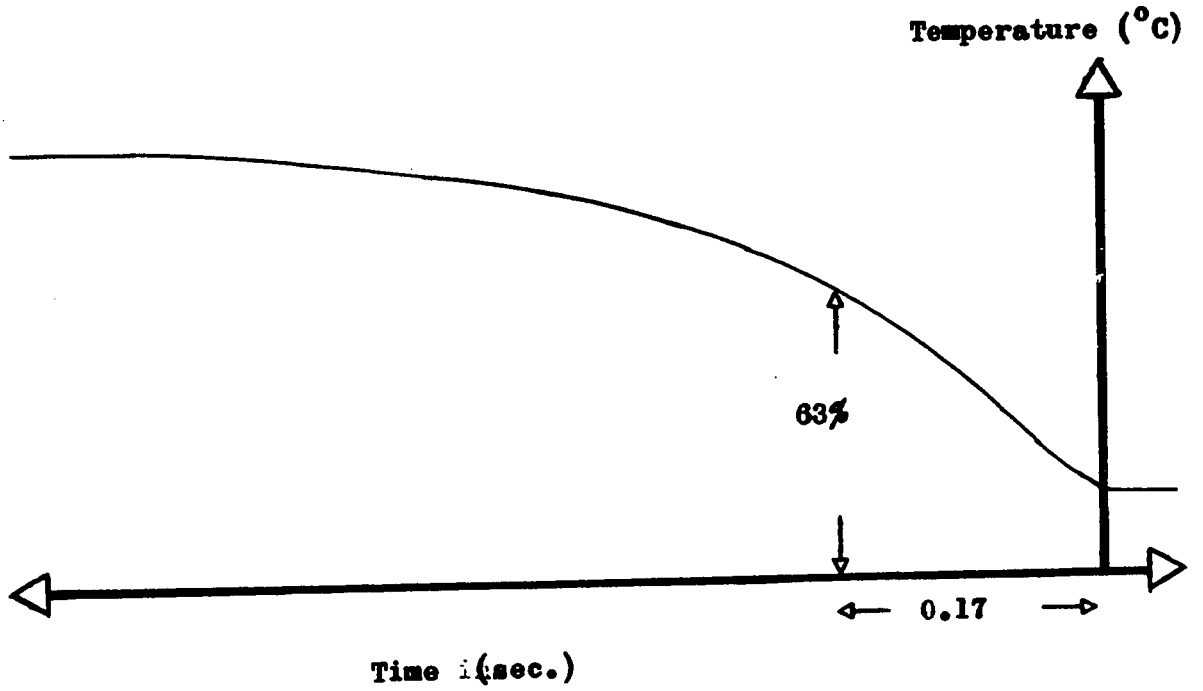

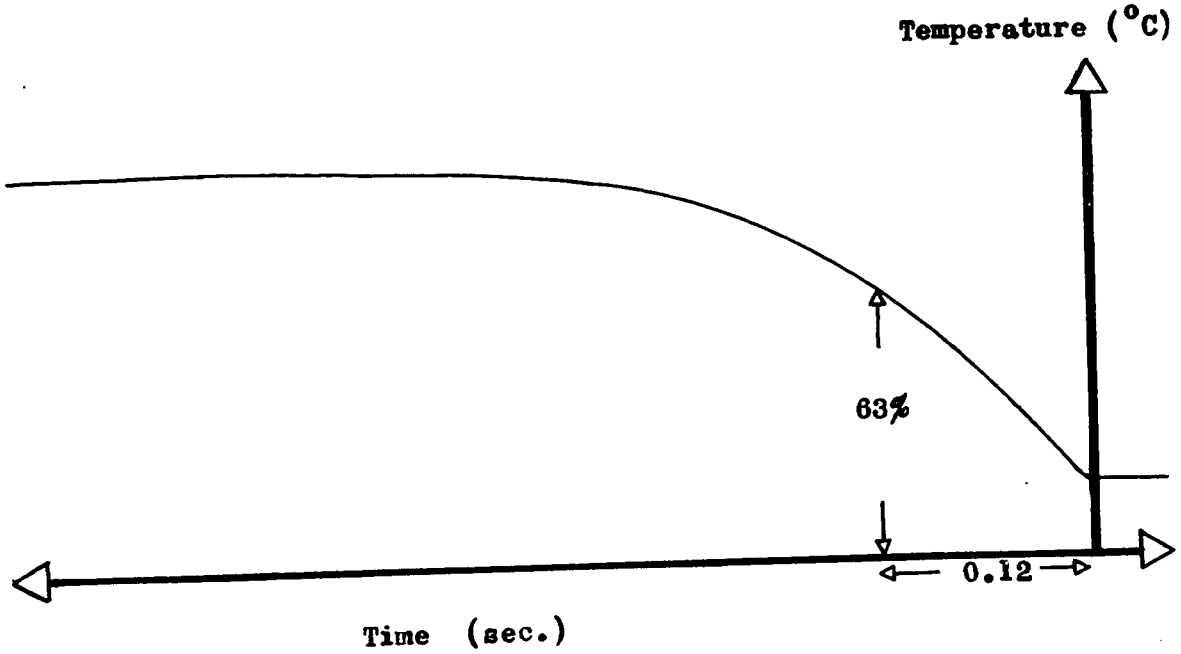

Figure V.3 Time Constant Measurements.

APPENDIX VI

THERMISTOR CALIBRATION

Each thermistor probe was calibrated by immersing the probe in a water bath which was electrically heated, with an accuracy of 0.01°C, and stirred continuously. The calibration took place throughout the required temperature +10°C to +30°C against a standard N.P.L. certified mercury-in-glass thermometer. The temperature of the water bath was changed, in steps of about 1°C for each change, and the resistance of the thermistor was measured.

The mathematical expression relating the temperature to the resistance may take many forms (see e.g. Becker et al 1947). For simplicity the relation

$$\log R = a + \frac{b}{T} \qquad \text{VI.1}$$

where R is the thermistor's resistance a and b are constants and T is the absolute temperature, was fitted to the data of calibration. A typical calibration curve is given in Figure VI.1. It will be noted that due to the artificial heating the shift in the calibration is relatively small. Therefore, all the probes were recalibrated from time to time. It was necessary to estimate the value of the parameters a and b of Eq. (VI.1). The method of least squares was used for this investigation (see e.g. Worthing and Geffner 1960) and the values

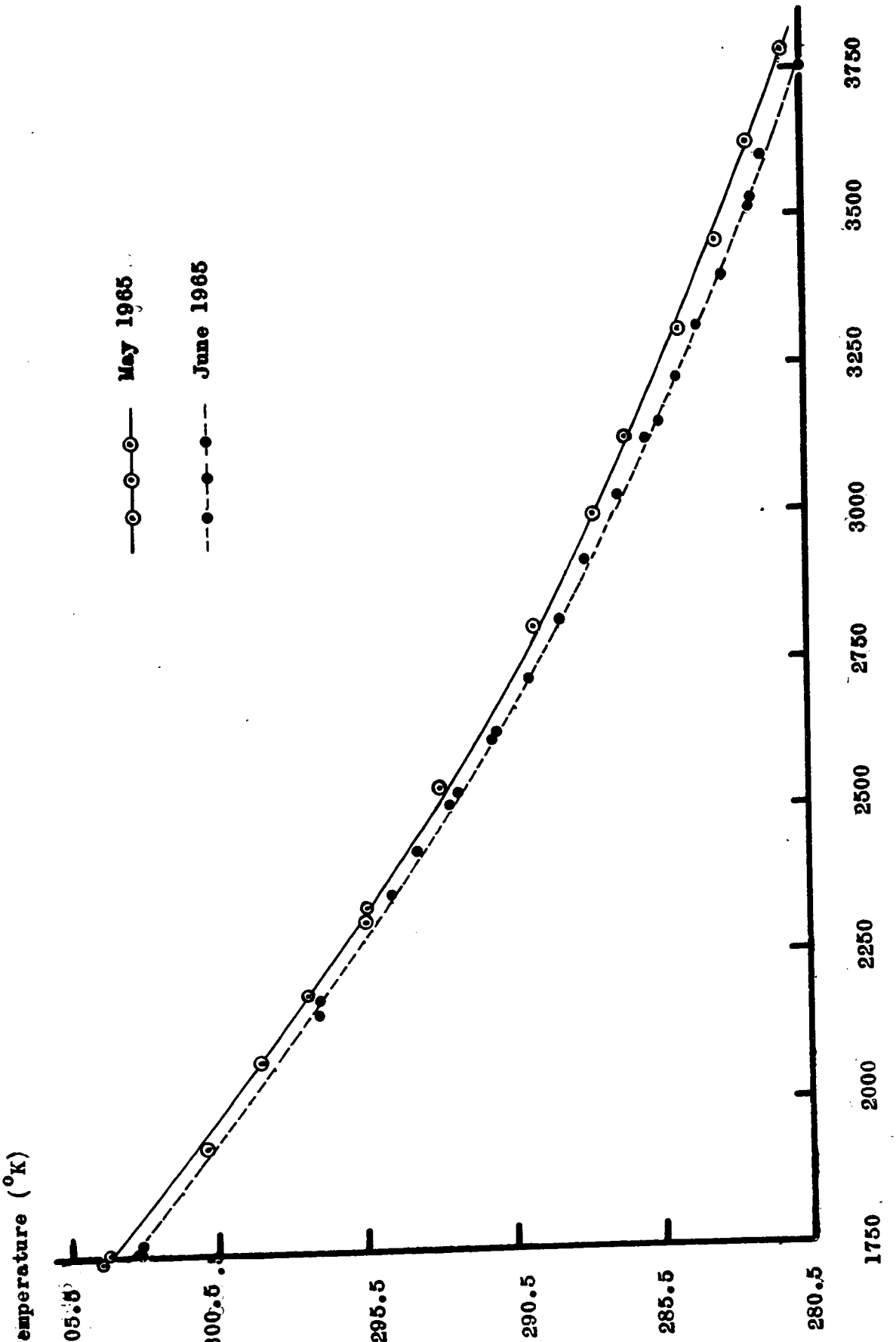

Figure VI.1 Calibration Curve for Thermistor Probe.

of a and b were computed for each thermistor.

Examination of the fit of Eq. VI.1 was undertaken and a typical result is shown in table VI.a. It will be noted that the deviation between the temperature, calculated by Eq. VI.1, and the observed quantity differ by 0.06%. The calibration data, being represented by Eq. VI.1 is, then, within the experimental error. Fitting a linear equation (Eq. VI.1) by the method of least squares, to the data of calibration, enables one to calculate error in calibration. The calibration error coupled with the data evaluation in determining the thermistor resistance is $\pm$ 0.2°C in the range +10°C to +30°C.

To convert the probe resistance at the null balance of the bridge to temperature using Eq. VI.1, a program of computation has been drawn up, making use of the IBM 7040 Electronic Computor. The program for this computation is given in table VI.b.

TABLE VI.a

Regression Analysis of Equation VI.1

Resistance (ohms)	Observed Temp. (^oK) T_o	Residuals (^oK) $T - T_o$	Percentage Discrepancy $(T - T_o)100$
3757	277.62	-0.03	-0.01
3516	279.63	-0.13	-0.04
3151	282.85	-0.14	-0.05
2625	288.31	-0.15	-0.05
2501	289.82	-0.16	-0.05
2347	291.84	-0.18	-0.06
2185	294.03	-0.12	-0.04
1802	300.17	+0.05	+0.01
1583	304.40	+0.11	+0.03
1616	303.61	+0.19	+0.06
1800	300.28	-0.02	-0.00
2182	294.02	-0.08	-0.03
2426	290.77	-0.12	-0.04
2526	289.23	+0.10	+0.03
2626	288.10	+0.04	+0.01
2724	286.95	+0.07	+0.02
2823	286.00	-0.06	-0.02
2924	285.01	-0.12	-0.04
3026	283.78	+0.08	+0.03
3125	282.93	-0.02	-0.00
3225	282.10	-0.12	-0.04
3313	281.14	+0.05	+0.02
3410	280.40	-0.04	-0.01
3506	279.49	+0.07	+0.03
3605	278.85	-0.09	-0.03

```
0 $IBFTC TEMP
  C      AVERAGE TEMP. MEASUREMENTS
 1       DIMENSION LA(4000),ALF(4000),S(4000),T(4000)
 2     1 READ(5,2) OPD,A,B,R,N,NOS,IRA,(LA(I),I=1,N)
12     2 FORMAT (4F10.5,2I5,I30/(40I2))
13       DO 10 I=1,N
14    10 ALF(I)=LA(I)
16       DO 3 I=1,N
17       S(I)=R-ALF(I)*OPD
20     3 T(I)=B/(ALOG10(S(I))+A)-273.2
22       WRITE(6,4)NOS,A,B,R
23     4 FORMAT(1H1 50X 24HTEMPERATURE MEASUREMENTS//58X 7HSET NO.I3//
        138X 2HA=F10.5,5X 2HB=F10.5,10X 2HR=F10.5//34X 1HI,14X1HS,16X
        24HALFA ,19X1HT/)
24       WRITE(6,5) (I,S(I), ALF(I),T(I),I=1,N)
31     5 FORMAT(30X I5,10X F8.2,10X F8.2,10X E14.4)
32       FN=N
33       AVER=0.0
34       DO 20 I=1,N
35    20 AVER=AVER+T(I)
37       AVER=AVER/FN
40       DO 21 I=1,N
41    21 T(I)=T(I)-AVER
43       WRITE(6,23) (I,T(I),I=1,N)
50    23 FORMAT(40X I5,10X E14.4)
51       SIGMA=0.0
52       DO 40 I=1,N
53    40 SIGMA=SIGMA+T(I)*T(I)
55       FN=FLOAT (N)
56       SIGMA=SQRT(SIGMA/FN)
57       WRITE (6,22)AVER,SIGMA
60    22 FORMAT(1H0// 30X 8HAVERAGE=E16.6,10X 6HSIGMA=E16.6)
61       IF (IRA.EQ.0) GO TO 1
64       STOP
65       END
```

Table VIb Fortran (7040) Program for Resistance to Temperature Conversion.

APPENDIX VII

EFFECT OF CORIOLIS FORCES ON BUOYANT PLUMES

To examine the effect of Coriolis forces on buoyant plumes, an approximate mathematical model is developed with the aid of the experimental observations described in this thesis. Accordingly, this study projects the interpretation of the laboratory simulation into the prototype which involves the Ekman layer.

The ascension of smoke plumes from steadily maintained sources, in the absence of wind and Coriolis forces, has been studied by Priestley and Ball (1955), Morton et al (1956), Telford (1966), Morton (1967 and 1968) and Briggs (1968). Briggs has extended the work of the other authors to take into account the effect of a horizontal wind. The latter work neglects the bending of the plume at the source, and assumes that the plume is quasi-horizontal while moving with the speed of the wind. The predictions of these models show reasonable agreement with the observed behaviour of smoke columns from stacks.

The present analysis extends the work of these authors by including the effects of Coriolis forces on the buoyant plume.

1. Assumptions

Following Morton et al (1955), the following assumptions are made regarding the buoyant plume rising through its atmospheric

environment:

(a) A steady state condition has been reached.

(b) The axis of the buoyant plume follows a trajectory which is determined by the horizontal velocity components of the natural wind (u,v), the vertical velocity (w) of the buoyant air within the plume, and turbulent mixing of the buoyant air with its environment by entrainment at the plume edges.

(c) During ascent of the plume, environmental air flows laterally into the plume with an effective entrainment velocity W due to the turbulent mixing such that

$$W = \alpha w \qquad (1)$$

where α is an entrainment constant. Little is known about the physical process which is represented by this entrainment constant.

(d) The horizontal profiles of velocity and buoyancy within the plume are similar, at all heights.

One may add to the above assumptions that wind speed increases from zero at the roughness height to a constant, maximum value (the geostrophic wind) in the geostrophic region aloft.

2. Governing Equations

Equations governing the motion of the rising plume are derived by considering the conservation of volume, of mass, and of momentum. Figure VII.1 illustrates the notation. The plume rises from a point source at the origin which is located at the roughness length above the ground, and it is inclined at an angle Ψ to the horizontal. S is the

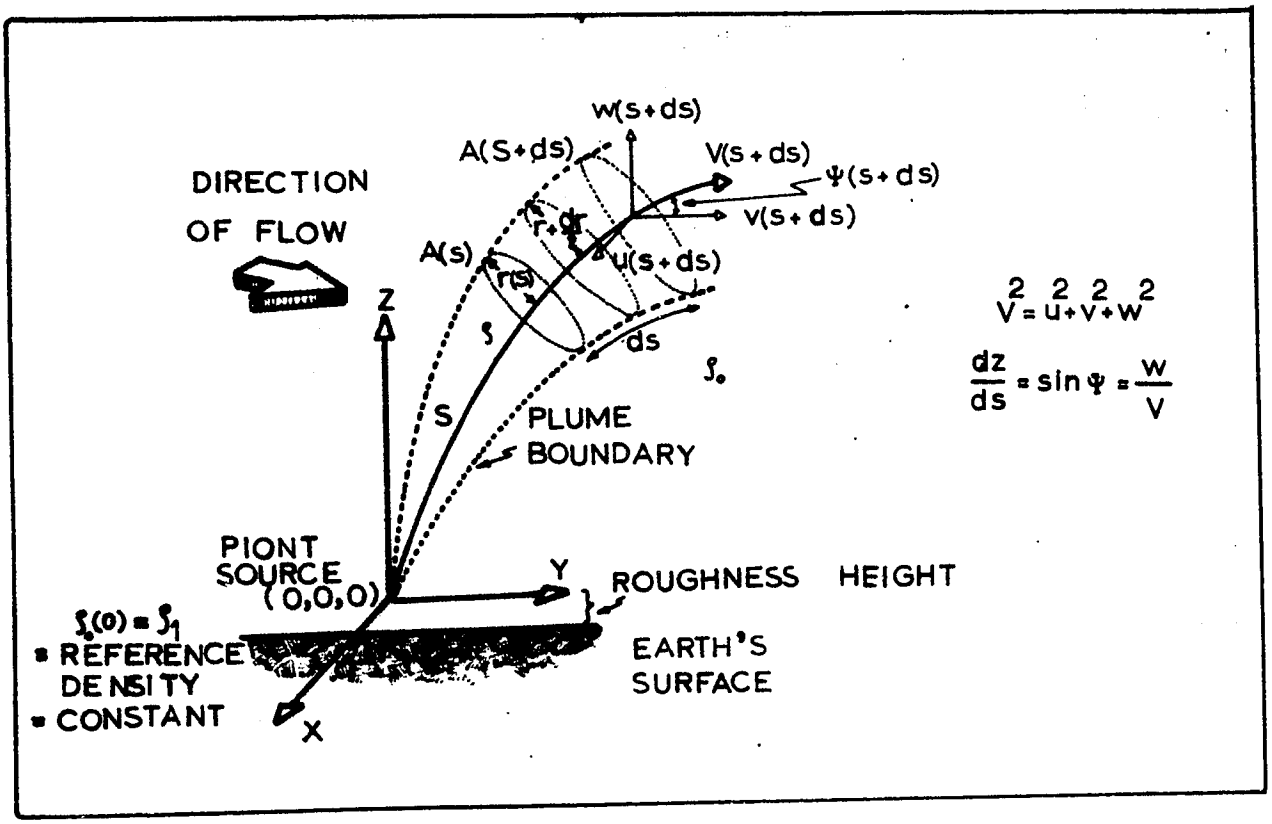

Figure VII.1 Geometry of an Inclined Plume.

axial distance along the plume, and the axial velocity, V, is given by

$$V^2 = u^2 + v^2 + w^2 \qquad (2)$$

Let A(S) and A(S + dS) be the cross-sectional areas of the plume at position S and S + dS. Note that A(S) is given by

$$A(S) = \pi r^2(S)$$

where r(S) is the radius of the plume at that position. Assuming constant

density of the air over a small height increment,

$$V(S+dS)\ A(S+dS) = A(S)\ V(S) + 2\pi\left(r + \frac{dr}{2}\right) dS \alpha w \tag{3}$$

where use has been made of assumption (C).

$$\text{Now} \qquad V(S+dS) = V(S) + \frac{dV}{dS} dS \tag{4}$$

$$A(S+dS) = A(S) + \frac{dA}{dS} dS = \pi\ r^2(S) + \frac{d\pi r^2}{dS} dS \tag{5}$$

Substituting Eqs. (4) and (5) into Eq. (3), and neglecting higher order differentials, gives

$$\frac{d}{dS} \pi r^2 V = 2\pi r \alpha w \tag{6}$$

Consider next the conservation of mass during entrainment in the rising plume.

$$\rho(S+dS)\ V(S+dS)\ A(S+dS) = \rho(S)\ A(S)\ V(S) + 2\pi\left(r + \frac{dr}{2}\right) dS\ \rho_o \alpha w \tag{7}$$

Here ρ and ρ_o are the density of the plume and the environment respectively. By neglecting higher order differentials, this becomes:

$$\frac{d}{dS} \pi\ r^2 V \rho = 2\pi \alpha r w \rho_o \tag{8}$$

Combining Eqs. (6) and (8):

$$\frac{d}{dS} \pi\ r^2 V(\rho_o - \rho) = r^2 V \frac{d\rho_o}{dS} \tag{9}$$

Since the rate of change of momentum is equal to the buoyancy force along the trajectory, one obtains

$$\frac{d}{dt} r^2V^2 = \frac{g(\rho_o - \rho)}{\rho} \sin\Psi \, r^2V\rho \qquad (10)$$

where t is the time required for a plume element to move a distance S. Making use of the relation

$$\frac{d}{dt} = \frac{dS}{dt}\frac{d}{dS} = V\frac{d}{dS}$$

Eq. (10) may be rewritten as,

$$\frac{d}{dS} r^2V^2 = g(\rho_o - \rho) \sin\Psi \, r^2 \qquad (11)$$

Finally, Eqs. (6), (9) and (11) may be rewritten for convenience in terms of height Z:

$$\frac{d}{dZ} r^2V = 2\alpha rV \qquad (12)$$

$$\frac{d}{dZ} r^2V g \frac{(\rho_o - \rho)}{\rho_1} = r^2V \frac{g}{\rho_1} \frac{d\rho_o}{dZ} \qquad (13)$$

$$\frac{d}{dZ} r^2V^2 = r^2g \frac{(\rho_o - \rho)}{\rho_1} \qquad (14)$$

The above equations can be solved numerically for an arbitrary density profile in the atmosphere. It is of interest to note that, Eqs. (12), (13) and (14) can be reduced to the equations given by Morton et al (1956) for a vertical plume.

3. Effect of Wind and Coriolis Forces on the Plume

The equations of the previous section will be applied here to buoyant plumes having characteristics indicated by the writer's laboratory investigation.

3.1 Plume Parameters

Some of the parameters in Eqs. (12), (13) and (14) may be evaluated from the experimental study in the laboratory. First it will be noted that the fluid density is constant (approximately) in the simulation, Eq. (13) gives for a point source

$$r^2 V g \frac{(\rho_o - \rho)}{\rho_1} = \text{constant} = F \qquad (15)$$

or

$$F = r^2 V g \beta T \qquad (16)$$

since

$$\frac{\rho_o - \rho}{\rho_1} = \beta \Delta T$$

where β is the coefficient of cubical expansion (for air $\beta \approx 3\ 10^{-3}$ $^oK^{-1}$) and ΔT is the temperature difference between the plume and its environment ($\Delta T = 0.2\ ^oK$, see Fig. 7.4, Chapter VII). Taking $r \approx 50$ meters (see Fig. 7.14, Chapter VII). Also Warner and Telford (1963), and $V \approx 0.2$ meter sec^{-1} (see Sec. 7.3f, Chapter VII), F assumes the value 3 $meter^4$ sec^{-3}.

For a point source, the exact solution of Eqs. (12) and (14) applying Eq. (16), gives

$$r = \frac{6\alpha}{5} Z \qquad V = \frac{5}{6\alpha} \left(\frac{9}{10} \alpha F\right)^{\frac{1}{3}} Z^{-\frac{1}{3}} \qquad g\frac{(\rho_o - \rho)}{\rho_1} = \frac{5F}{6\alpha}\left(\frac{9}{10}\alpha F\right)^{-\frac{1}{3}} Z^{-\frac{5}{3}}$$

..... (17)

3.2 Horizontal Wind

Assignment of a value to the entrainment constant (α) is

considered next. Morton et al (1956) assumed $\alpha \approx 0.1$ for a vertically rising plume, through comparison of their theoretical predictions with observations on smoke columns. But, for a horizontal plume in a strong wind, Briggs (1968) deduced $\alpha \approx 0.5$, again by comparing his predictions with observed plume behaviour. The writer has derived an estimate of α by alternative means.

The predicted height at which a plume ceases to rise is dependent on the entrainment constant, α . The present investigation suggests that plumes may rise to some 700 meters in the troposphere. In this case the wind speed follows the Deacon profile (see Chapter VIII). A workable approximation to this profile is given by

$$u = 10^{-2} z^{\frac{2}{3}} \quad \text{meter sec}^{-1}$$

and

$$v = 0 \tag{18}$$

The vertical velocity of the plume is found through reference to Fig. 1, and by combining the second part of Eq. (17) and Eq. (18).

$$w = \left[\left(\frac{5}{6\alpha}\right)^2 \left(\frac{9}{10}\alpha F\right)^{\frac{2}{3}} - a^2 z^2 \right]^{\frac{1}{2}} . z^{-\frac{1}{3}} \tag{19}$$

Taking $w \approx V \approx 0.2$ meter sec^{-1}, and $F \approx 3$ meter^4 sec^{-3}, the values of α for plumes rising to various terminal heights are given by Eq. (19) as listed in Table VII.a. It will be noted that these values lie close to those suggested by Morton et al (1956) for vertical plumes (0.1), and Briggs (1968) for horizontal plumes (0.5).

TABLE VII.a

Entrainment Constant (α) for Plumes Rising to Various Terminal Heights

Entrainment Constant	Maximum Heights of Plumes (meters)
0.86	100
0.38	200
0.20	300
0.16	400
0.11	500
0.09	600
0.07	700

3.3 Coriolis Forces

The introduction of Coriolis forces results in rotation of the horizontal wind vector with increasing height through the transition layer (see, e.g. Haurwitz 1941, p. 201). Thus, the simple wind profile of the previous section does not apply. Haurwitz shows that the horizontal components of wind in this Ekman layer are given by

$$u = - v_g e^{-fZ} \sin fZ \tag{20}$$

$$v = v_g (1 - e^{-fZ} \cos fZ) \tag{21}$$

where v_g is the geostrophic wind speed = 1 meter sec^{-1}, $f = \sqrt{\frac{\rho \omega \sin \phi}{\mu}} = 2\ 10^{-3}$, ρ is the air density = 1.1 10^{-3} gm. cm^{-3}, ω is the angular velocity of the earth's rotation = 0.7 10^{-4} sec^{-1}, ϕ latitude angle assumed = 45° and μ is the eddy viscosity $\approx$ 110 gm. cm^{-1} sec^{-1}.

u and v as computed from Eqs. (20) and (21) are shown in Fig. (VII.2). The curve in Fig.(VII.2) represents the locus of the wind vector, where the numbers indicate height along this locus. This is the well-known Ekman spiral.

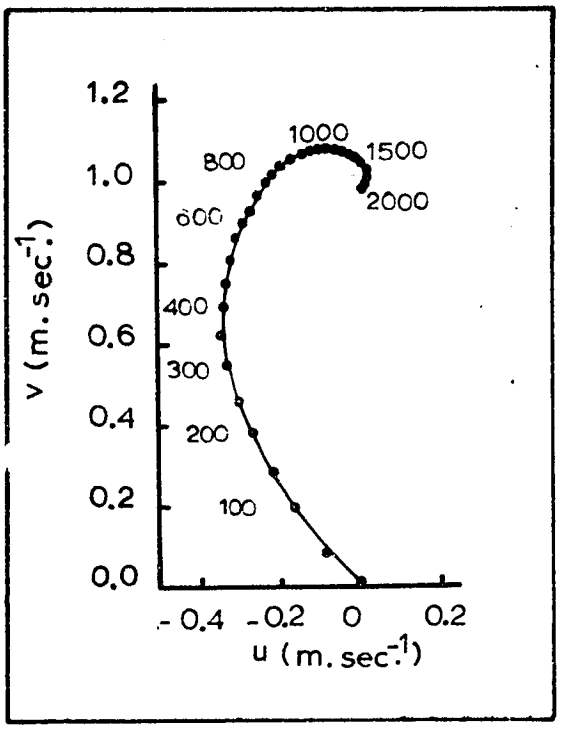

Figure VII.2 The Ekman Spiral of Horizontal Wind in the Transition Region.

In this environment, the vertical speed of the buoyant plume is found by combining Eqs. (19), (20) and (21):

$$w = \left[\left(\frac{5}{6\alpha}\right)^2 \left(\frac{9}{10}\alpha F\right)^{\frac{2}{3}} - v_g^2 \left(e^{-2fZ} \sin^2 fZ + \left(1 - e^{-fZ}\cos fZ\right)^2\right) Z^{\frac{2}{3}}\right] \cdot Z^{-\frac{1}{3}} \quad \ldots\ldots\ldots \quad (22)$$

The contours of a buoyant plume with and without the influence of Coriolis forces are found with the aid of Eqs. (19) and (22). Figs. VII.3 and VII.4 show the results of this calculation. In each case, the inclination of

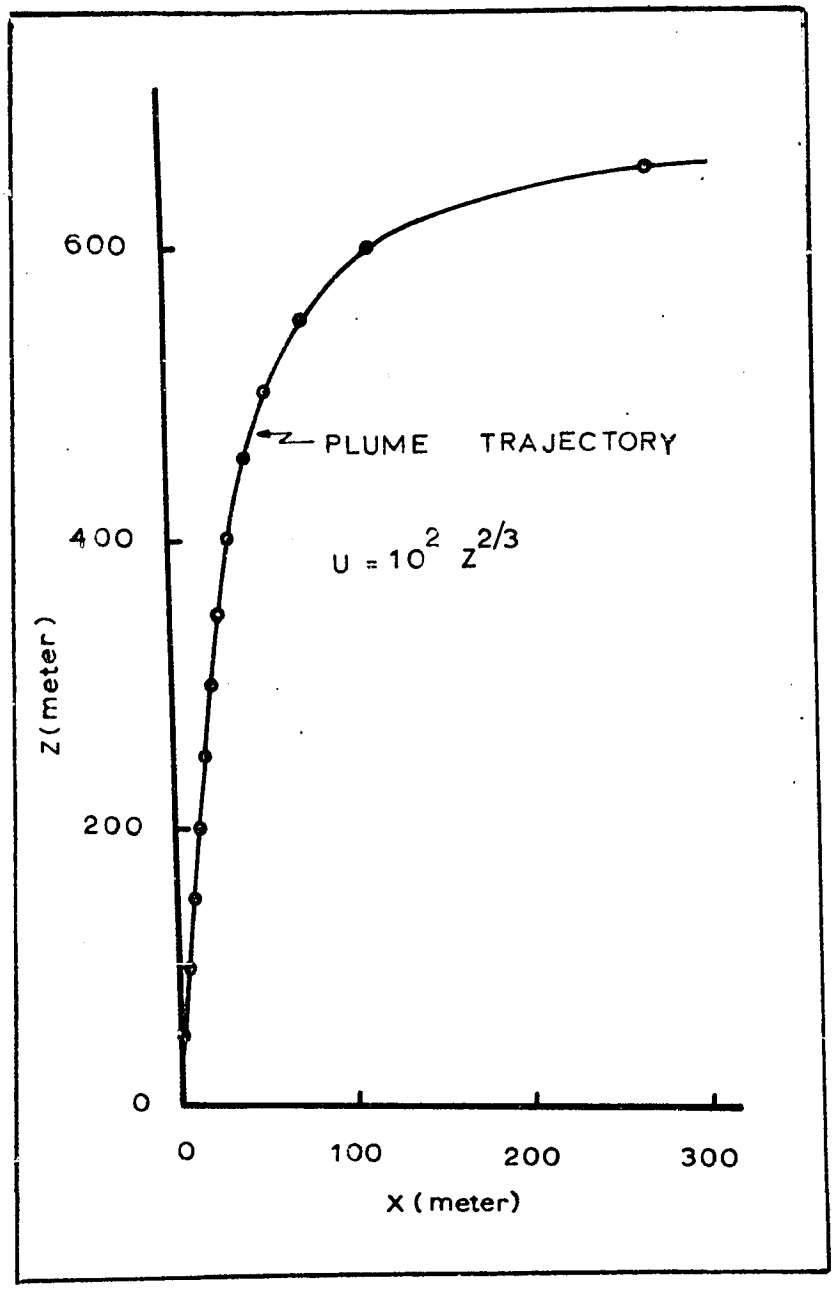

Figure VII.3 Contour of a Buoyant Plume in the Absence of Coriolis Forces.

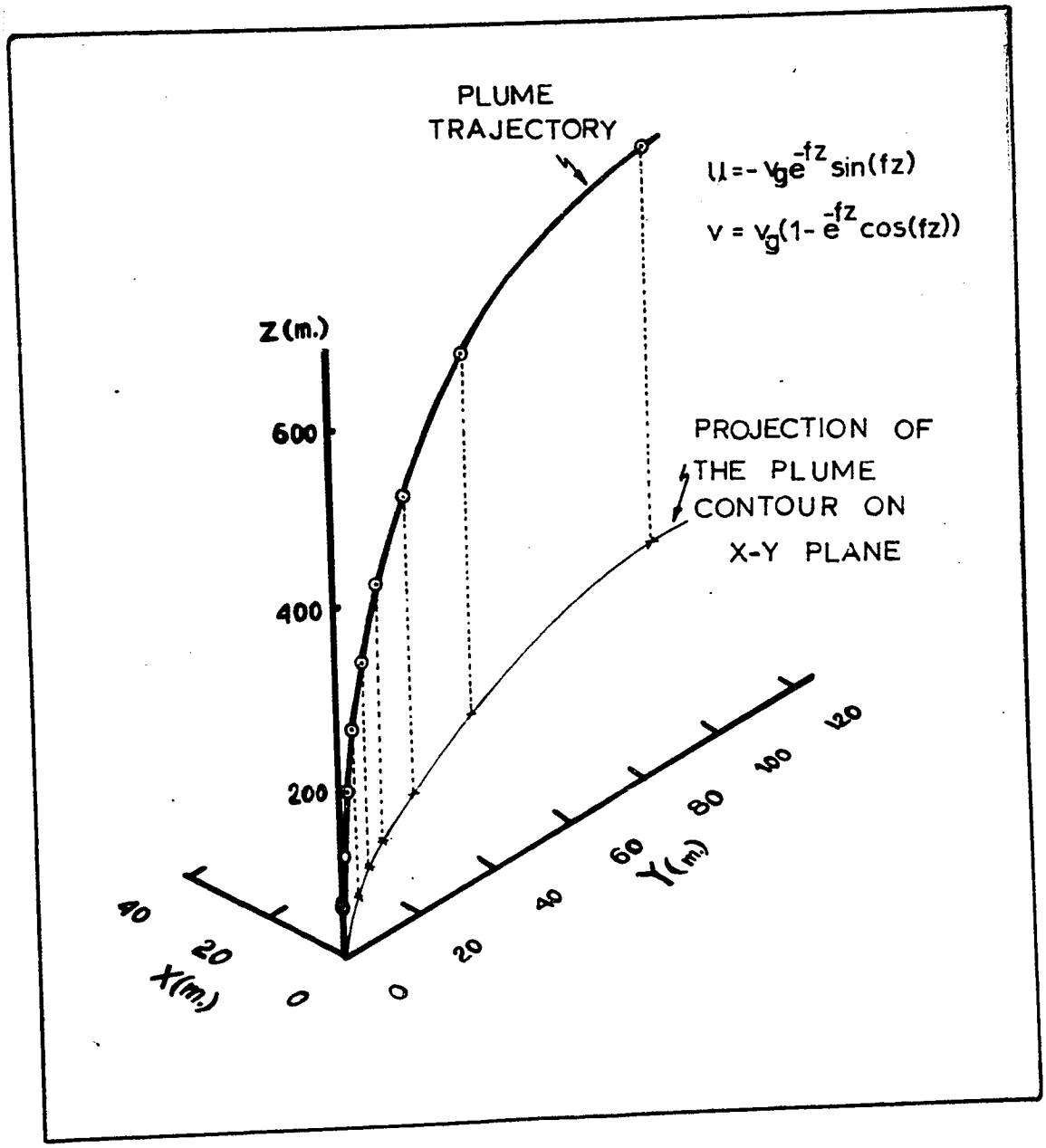

Figure VII.4 Contour of Buoyant Plume under the Effect of Coriolis Forces.

the plume to the vertical increases with height. In the absence of Coriolis forces, the plume becomes approximately horizontal at a height of 600 meters; the introduction of Coriolis forces reduced this maximum height to some 500 meters, and deforms the plume contour into a shallow spiral with a horizontal

rotation of some 90 degrees.

The slope of the rising plume at any height is deduced from the ratio of its vertical and horizontal velocities at that level.

Then for $U = 10^{-2} z^{\frac{2}{3}}$

$$\text{slope} = \tan \Psi = \left[\left(\frac{5}{6\alpha}\right)^2 \left(\frac{9}{10}\alpha F\right)^{\frac{2}{3}} - 10^{-4} z^2 \right]^{\frac{1}{2}} 10^{-2} z^{-1} \qquad (23)$$

and for $U = (V_g^2 e^{-2fZ} \sin fZ + V_g^2 (1 - e^{-fZ} \cos fZ)^2)^{\frac{1}{2}}$

$$\text{slope} = \tan\Psi = \frac{\left[\left(\frac{5}{6\alpha}\right)^2 \left(\frac{9}{10}\alpha F\right)^{\frac{2}{3}} - V_g^2 (1 + e^{-2fZ} - 2e^{-fZ} \cos fZ) z^{\frac{2}{3}} \right]}{V_g (1 + e^{-2fZ} - 2e^{-fZ} \cos fZ)^{\frac{1}{2}} z^{\frac{1}{3}}} \qquad (24)$$

Fig. 5 compares the plume slopes for these two cases. It will be seen that the slope increases somewhat more rapidly in the absence of Coriolis forces.

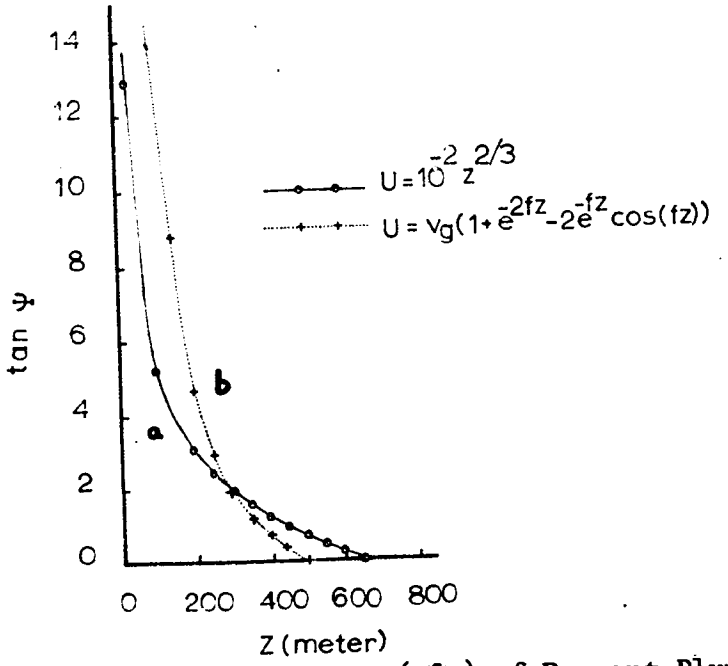

Figure VII.5 Tangent of Inclination (Ψ) of Buoyant Plume as a Function of Height , (a) in the Absence of Coriolis Forces, and (b) under the Effect of Coriolis Forces.

REFERENCES

Abe, M. (1941), Bull. Centr. Meteorol. Soc., 7, 3 (Japan).

Aitken, J. (1884), Trans. Roy. Soc. Edinburgh, 32, 239.

Ball, F.K. (1958), Q.J. Roy. Meteorol. Soc., 84, 61.

_____ (1960), Q.J. Roy. Meteorol. Soc., 86, 483.

Batchelor, G.K. (1954), Q.J. Roy. Meteorol. Soc., 79, 224.

Becker, J.A., Green, C.B. and Pearson, G.L. (1947), Bell Syst. Tech. J. 76, 170.

Bell, M.B., Hay, D.R. and Johnston, R.W. (1964), Can. J. Phys., 42, 273.

Bird, R.B., Stewart, W.E. and Lightfoot, E.N. (1960), "Transport Phenomena", John Wiley & Sons, Inc., New York, U.S.A.

Birkhoff, G. (1950), "Hydrodynamics: A Study in Logic, Fact and Similitude", Princeton Univ. Press, Princeton, New Jersey.

Briggs, G.A. (1968), "Penetration of Inversion by Plumes", National Conference of Am. Meteorol. Soc., San Francisco, U.S.A.

Brunt, D. (1929), Proc. Roy. Soc., A 124, 201.

_____ (1934), "Physical and Dynamical Meteorology", Cambridge University Press, London.

_____ (1951), "Compendium of Meteorology", Edited by T.F. Malone. Am. Meteorol. Soc., Boston, p. 1255.

Budyko, M.I. and Yudin, M.I. (1948), Meteorology and Hydrology, No. 1.

Bunker, A.F. (1956), Aust. J. Phys., 9, 133.

Cermak, J.E., Sandborn, V.A., Plate, E.J., Binder, G.H., Chuang, H., Meroney, R.N. and Ito, S. (1966), "Simulation of Atmospheric Motion by Wind-tunnel Flows", Technical Report, CER66JEC-VAS-EJP-GHB-CH-RNM-SI117, Fluid Dynamics and Diffusion Laboratory, Colorado State University, Fort Collins, Colorado.

Chandrasakar, S. (1961), "Hydrodynamic and Hydromagnetic Stability", Oxford University Press.

Croft, J.F. (1958), Q.J. Roy. Meteorol. Soc., 84, 418.

Davenport, A.G. (1961), Q.J. Roy. Meteorol. Soc., 87, 194.

Davis, R.M. and Taylor, G.I. (1950), Proc. Roy. Soc. A200, 375.

Deacon, E.L. (1949), Q.J. Roy. Meteorol. Soc., 75, 89.

Deardorf, J.W. and Willis, G.E., (1967a), Q.J. Roy. Meteorol. Soc., 93, 166.

_____ (1967b), J. Fluid Mech., 28, 675.

Defant, F. (1951), "Compendium of Meteorology", Edited by T.F. Malone. Am. Meteorol. Soc., Boston, p. 655.

Deissler, R.G. (1968), The Physics of Fluid, 11, 432.

Eckart, C. (1960), "Hydrodynamics of Oceans and Atmospheres", Pergamon Press, New York.

Elder, J.W. (1965a), J. Fluid Mech., 23, 77.

_____ (1965b), J. Fluid Mech., 23, 99.

_____ (1967a), J. Fluid Mech., 27, 29.

_____ (1967b), J. Fluid Mech., 27, 609.

Faller, A. (1963), J. Fluid Mech. 15, 560.

_____ (1964), J. Atmos. Science, 22, 176.

Fanaki, F.H. (1962), M.Sc. Thesis, Department of Physics, University of Western Ontario, London, Canada.

Fritz, S. (1951), "Compendium of Meteorology", Edited by T.F. Malone. Am. Meteorol. Soc., Boston, p. 13.

Fultz, D. (1949), J. Meteorol. 6, 17.

_____ (1952), J. Meteorol. 9, 379.

_____(1961), Advances in Geophysics 7, 1. Edited by H.E. Landsberg and J.V. Mieghem, Academic Press, New York.

Funk, J.P. (1960), Q.J. Roy. Meteorol. Soc. 86, p. 382.

Geiger, R. (1959), "The Climate Near the Ground", (English Translation from the German by Harvard University Press), Cambridge, Massachusetts.

Gjessing, D.T. and Irgens, F. (1964). IEEE Transaction on Antennas and Propagation, AP-12, 703.

Goldstein, S. (1965), "Modern Developments in Fluid Dynamics, Dover Publication, Inc. New York, (originally published by Oxford University Press, 1938).

Grant, D.R. (1965), Q.J. Roy. Meteorol. Soc. 91, 268.

Haller, G.L. (1942), Proc. I.R.E., 30, 357.

Haltiner, G.J. and Martin, F.L. (1957), "Dynamical and Physical Meteorology", McGraw-Hill Book Company, Inc., New York.

Haurwitz, B. (1941), "Dynamic Meteorology", McGraw-Hill Book Company Inc., New York, U.S.A.

Hay, D.R. and Reid, W.M. (1962), Can. J. Phys. 40, 128.

_____ and Fanaki, F.H. (1963), Can. J. Phys. 41, 563.

_____ and Naito, K. (1965), Radio, Sci. J. Res. N.B.S. 69D, 877.

Hidy, G.M. (1967), Bull, Am. Meteorol. Soc. 48, 143, No. 3.

Ingersoll, A.P. (1966), J. Fluid Mech. 25, 209.

James, D.G. (1953), Q.J. Roy. Meteorol. Soc. 79, 425.

Jeans, Sir J. (1954), "The Dynamical Theory of Gases", Fourth Edition, Dover Publication Inc.

Jeffreys, H. (1926), Phil. Mag., 2, 833.

_____ (1928), Proc. Roy. Soc. (London) A118, 195.

Klinov, F. Ya and Poltvskii, V.V. (1965), "Investigation of the Bottom 300-Meter Layer of the Atmosphere", Edited by N.L. Byzova, Isreal Program for Scientific Translations, Jerusalem, p. 57.

Krueger, A.F. and Fritz, S. (1961), Tellus, 13, 1.

Kuettner, J. (1959), Tellus, 11, 267.

Kuo, H.L. (1961), Tellus, 13, 441.

_____ (1963), The Physics of Fluid, 6, 195.

Lamb, H. (1945), "Hydrodynamics" Sixth Edition, Dover Publications, New York, U.S.A. (Originally published by Cambridge University Press, 1932).

Landau, L.D. and Lifshitz, E.M. (1959), "Fluid Mechanics", 6, Course of Theoretical Physics. English Edition. Pergamon Press.

Landenburg, R.W., Lewis, B., Pease, R.N. and Taylor, H.S. (1954), "Physical Measurements in Gas Dynamics and Combustion", Princeton Univ. Press, Princeton, New Jersey.

Lester, E. and von Elbe, G. (1961), Second Edition. Academic Press Inc., New York.

Lilly, D.K. (1964), J. Atmosph. Science, 21, 83.

Lodge, O.J. and Clark, J.W. (1884), Proc. Roy. Soc. (London), 6,1.

Long, R.R. (1959), "Laboratory Model of Air Flow over the Sirra Nevada Mountains", The Atmosphere and the Sea in Motion, Rockefeller Institute Press, New York, U.S.A.

_____ (1965), Tellus, 1, 46.

Low, A.R. (1929), Proc. Roy. Soc. (London), A125, 180.

Ludlam, F.H. and Scorer, R.S. (1953), Q.J. Roy. Meteorol. Soc. 79, 317.

Lumley, J.H. and Panofsky, H.A. (1964), "The Structure of the Atmospheric Turbulence", Interscience monographs and tests in Phys. and Astronomy, 12, John Wiley & Sons, New York.

Malkus, J.S. and Scorer, R.S. (1954), Woods Hole Ocean. Inst. Tech. Pap. No. 26, 68.

Malurkar, S.L. and Ramadas, L.A. (1931), Indian J. Phys. 6, 495.

Martin, H.C. (1966), Ph.D. Thesis, Department of Physics, University of Western Ontario, London, Canada.

Mashkova, G.B. (1965), "Investigation of the Bottom 300-Meter Layer of the Atmosphere", Edited by N.L. Byzova. Isreal Program for Scientific Translations, Jerusalem, p. 43.

Middleton, W.E.K. and Spilhaus, A.F. (1953), "Meteorological Instruments, University of Toronto Press, Toronto, Canada.

Mihalijan, J.M. (1962), Astrophysical J. 136, 1126.

Moller, F. (1951), "Compendium of Meteorology", Edited by T.F. Malone, Am. Meteorol. Soc. Boston, p. 34.

Monin, A.S. (1965), Bull. (Izv.) Acad. Sci. USSR. Atmospheric and Oceanic Physics, 1, No. 6, 375.

Morton, B.R., Taylor, G.I. and Turner, J.S. (1956), Proc. Roy. Soc. London, A234, 1.

_____ (1959), J. Fluid Mech., 2, 127.

_____ (1967), J. Atmos. Science, 24, 135.

_____ (1968), J. Atmos. Science, 25, 135.

Munn, R.E. (1966), "Descriptive Micrometeorology", Advances in Geophysics, Supplement 1, Academic Press, New York.

Neiburger, M. (1960), Tellus, 12, 31.

Nemoto, S. (1961a), Pap. Meteorol. Geophys., 12, 30, Part 1.

_____ (1961b), Pap. Meteorol. Geophys., 12, 117, Part 2.

_____ (1961c), Pap. Meteorol. Geophys., 12, 129, Part 3.

Nield, D.A. (1964), J. Fluid Mech., 19, 341.

Orlenko, L.R. (1967), Bull. (Izv.) Acad. Sci. USSR, Atmospheric and Oceanic Physics, 3, No. 7, 449.

Pearson, J.R. (1958), J. Fluid Mech., 4, 489.

Pellow, A. and Southwell, R.V. (1940), Proc. Roy. Soc. A176, 312.

Plank, V.G. (1956), Geophys. Res. Papers, No. 50, A.F.C.R.C.

Plate, E.J. (1966), "On Atmospheric Simulation: A Colloquium" NCAR-TN-22 App. 14. Boulder, Colorado.

Pope, A. (1954), "Wind Tunnel Testing", Second Edition, John Wiley and Sons, Inc. New York.

Priestley, C.H.B. and Swinbank, W.C. (1947), Proc. Roy. Soc., A189, 543.

_____ (1953), Austr. J. Phys., 6, 279.

_____ (1954), Austr. J. Phys., 7, 176.

_____ and Ball, F.K. (1955), Q.J. Roy. Meteorol. Soc., 81, 144.

_____ (1956), Q.J. Roy. Meteorol. Soc., 82, 165.

Priestley, C.H.B., McCormick, R.A. and Pasquill, F. (1958), "Turbulent Diffusion in the Atmosphere", W.M.O. Tech. Note No. 24, Geneva, Switzerland.

_____ (1959), "Turbulent Transfer in the Lower Atmosphere", University of Chicago Press.

_____ (1960), J. Fluid Mech., 7, 375.

_____ (1962), Tellus, 14, 123.

_____ (1962), Q.J. Roy. Meteorol. Soc., 88, 100.

Railston, W. (1954), Proc. Phys. Soc. B67, 42.

Ramadas, L.A. and Malurkar, S.L. (1932), Indian J. Phys., 7, 1.

_____ (1953), Indian J. Phys., 28, 304.

Rayleigh, J.W.S., Lord, (1882), Nature 28, 139.

_____ (1916), Phil. Mag. 32, 529.

Reynold, O. (1883), Phil. Trans., 164, 935.

Rider, N.E. (1954), Q.J. Roy. Meteorol. Soc., 80, 198.

Robinson, G.D. (1950), Centenary Proc. Roy. Meteorol. Soc. p. 26.

Rouse, H. (1951), "Compendium of Meteorology", Edited by T.F. Malone. Am. Meteorol. Soc., Boston, Massachusetts, p. 1249.

Schlichting, H. (1960), "Boundary Layer Theory", Translated by J. Kestin, McGraw-Hill Book Company, Fourth Edition.

Scorer, R.S. and Ludlam, F.H. (1953), Q.J. Roy. Meteorol. Soc. 79, 94.

_____ (1954), Q.J. Roy. Meteorol. Soc., 91, 60.

_____ and Ronne, C. (1956), Wheather, 11, 151.

_____ (1957), J. Fluid Mech., 2, 583.

Sinclair, G., Jordan, E.C. and Vaughan, E.W. (1947), Proc. I.R.E., 35, 1451.

_____ (1948), Proc. I.R.E., 36, 1364.

Spiegel, E.A. and Veronis, G. (1960), Astrophysical J., 131, 442.

Stommel, H. (1947), "Summary of the Theory of Convective Cells", Ann. N.Y. Acad. Science, 48, 715.

Streeter, V.L. (1961), "Handbook of Fluid Dynamics", McGraw-Hill Book Company Inc., First Edition.

Sutton, O.G. (1951), "Compendium of Meteorology", Edited by T.F. Malone. Am. Meteorol. Soc., Boston, p. 492.

_____(1953),"Micrometeorology", McFraw-Hill Book Company, Inc., New York.

Swinbank, W.C. (1955), Technical Paper No. 2, C.S.I.R.O., Div. Meteorol. Phys. Melbourne.

_____ (1966), Q.J. Roy. Meteorol., 92, 416.

Taylor, G.I. (1915), Phil. Trans. Roy. Soc. A215, 1.

_____ (1917), Proc. Roy. Soc. (London) A93, 99.

Telford, J.W. and Warner, J. (1964), J. Atmosph. Science, 21, 539.

_____ (1966), J. Atmosph. Science, 23, 652.

Theullier, R.H. and Lappe, U.O. (1964), J. App. Meteorol. 3, 299.

Townsend, A.A. (1956), "The Structure of the Turbulent Shear Flow", Cambridge University Press.

_____ (1962), Q.J. Roy. Meteorol. Soc. 88, 51.

_____ (1964), Q.J. Roy. Meteorol. Soc. 90, 248.

Turner, J.S. (1963a), Q.J. Roy. Meteorol. Soc., 89, 62.

_____ (1963b), J. Fluid Mech., 16, 1.

_____ (1964), J. Fluid Mech., 18, 195.

Walker, Sir G.T. (1931), Q.J. Roy. Meteorol. Soc., 57, 314.

_____(1932), Q.J. Roy. Meteorol. Soc., 58, 23.

Warner, J. and Telford, J.W. (1963), J. Atmos. Science, 20, 313.

_____ (1967), J. Atmos. Science, 24, 374.

Washburn, E.W. (1930), "International Critical Tables of Numerical Data, Physics, Chemistry and Technology", 7, 13, First Edition, McGraw-Hill Book Company, Inc. New York, U.S.A.

Webb, E.K. (1958), Q.J. Roy. Meteorol. Soc., 84, 118.

_____ (1962), Nature, 193, 840.

Webb, E.K. (1964), App. Optics, 3, 1329, No. 12.

Willis, G.E. and Deardorf, J.W. (1965), The Physics of Fluid, 8, 2225.

Woodcock, A.H. (1940), J. Mar. Res., 3, 248.

_____ and Wyman, J. (1947), "Convection Motion in Air Over the Sea", Ann. N.Y. Acad. Science, 48, 749.

Woodward, B. (1959), Q.J. Roy. Meteorol. Soc. 85, 144.

_____ (1960), "Cumulus Dynamics", Proc. of the First Conf. on Cumulus Convections, Edited by C.E. Anderson, Pergamon Press, New York, U.S.A.

Worthing, A.G. and Geffner, J. (1960), "Treatment of Experimental Data", John Wiley and Sons, Inc. New York.

Yates, A.H. (1953), Q.J. Roy. Meteorol. Soc., 79, 420.

Yudin, M.I. (1966), Bull, (Izv.) Acad. Sci. USSR, Atmospheric and Oceanic Physics, 2, No. 2, 124.

Vasil'chemko, I.V. and Ledokhovits, A.A. (1968), Meteorol. Translations, No. 13, p. 24, Canada Dept. of Transport, Toronto.

Vul'fson, N.I. (1961), "Studies of Clouds, Precipitation and Thunderstorm Electricity", Amer. Meteorol. Soc., 119, Boston.